A FINITE ELEMENT ANALYSIS OF RESIDUAL STRESS IN BRAZING OF SAPPHIRE AND INCONEL

CHAN CHOW KHUEN

FACULTY OF ENGINEERING
UNIVERSITY OF MALAYA
KUALA LUMPUR

2011

A FINITE ELEMENT ANALYSIS OF RESIDUAL STRESS IN BRAZING OF SAPPHIRE AND INCONEL

CHAN CHOW KHUEN

**RESEARCH PROJECT SUBMITTED
IN PARTIAL FULFILMENT OF THE REQUIREMENTS FOR
THE DEGREE OF MASTER OF ENGINEERING**

**FACULTY OF ENGINEERING
UNIVERSITY OF MALAYA
KUALA LUMPUR**

2011

UNIVERSITI MALAYA

ORIGINAL LITERARY WORK DECLARATION

Name of Candidate: CHAN CHOW KHUEN (I.C/Passport No: 840205-08-5223)

Registration/Matric No: KGC090024

Name of Degree: MASTER OF ENGINEERING (M.Eng.) MANUFACTURING

Title of Project Paper/Research Report/Dissertation/Thesis ("this Work"):

A FINITE ELEMENT ANALYSIS OF RESIDUAL STRESS IN BRAZING OF SAPPHIRE AND INCONEL

Field of Study:

I do solemnly and sincerely declare that:

(1) I am the sole author/writer of this Work;
(2) This Work is original;
(3) Any use of any work in which copyright exists was done by way of fair dealing and for permitted purposes and any excerpt or extract from, or reference to or reproduction of any copyright work has been disclosed expressly and sufficiently and the title of the Work and its authorship have been acknowledged in this Work;
(4) I do not have any actual knowledge nor do I ought reasonably to know that the making of this work constitutes an infringement of any copyright work;
(5) I hereby assign all and every rights in the copyright to this Work to the University of Malaya ("UM"), who henceforth shall be owner of the copyright in this Work and that any reproduction or use in any form or by any means whatsoever is prohibited without the written consent of UM having been first had and obtained;
(6) I am fully aware that if in the course of making this Work I have infringed any copyright whether intentionally or otherwise, I may be subject to legal action or any other action as may be determined by UM.

Candidate's Signature Date

Subscribed and solemnly declared before,

Witness's Signature Date

Name:
Designation:

ABSTRACT

A research cum study project has been done on the finite element analysis of residual stress in brazing sapphire and Inconel. The Inconel covered in this research study is Inconel 600. The materials used in this research project are sapphire, Inconel 600, brazing filler BAg-8-Ti, copper and nickel. The sample model is modelled in Ansys Mechanical APDL simulation software. In this the simulation, the thermal mechanical analysis is performed. In this thermal mechanical analysis, there are two main categories of simulation, which are transient thermal analysis and thermal-structural analysis. In the transient thermal analysis, the heat conduction between interlayer is discovered and studied. Subsequently, the thermal-structural analysis is performed in order to obtain the Von Mises stress distribution. The stress distribution is then compared with the yield strength of each type of material used. The stress which exceeds the yield strength is the cause of residual stress. In this research project, it is discovered that sample 3 with brazing temperature 865^0C is the optimum parameter as it has less residual stress impact.

ABSTRAK

Satu projek kajian telah dijalankan ke atas analisis unsur terhinggaan untuk tegasan baki dalam pemanasan sapphire dan Inconel. Inconel yang dikaji dalam kajian ini ialah Inconel 600. Bahan yang digunakan ialah sapphire, Inconel 600, pengisi pemanas BAg-8-Ti, kuprum dan nikel. Model sampel dipermodalkan dalam pengisian simulasi Ansys Mechanical APDL. Dalam simulasi ini, analisis mekanikal terma dikaji. Dalam analisis mekanikal terma, terdapat dua kategori utama, iaitu analisis terma transian dan analisis struktur terma. Dalam analisis terma transien, terdapat konduksi haba di antara lapisan dan dikaji secara menyeluruh. Selepas itu, analisis struktur terma dijalankan untuk memperoleh tekanan *Von Mises*. Distribusi tekanan kemudian dibanding dengan kekuatan alah untuk setiap bahan yang digunakan. Tekanan yang melebihi kekuatan alah untuk setiap bahan menyebabkan tegasan baki berlaku. Untuk projek kajian ini, sampel 3 dengan suhu pemanasan 865^0C ialah parameter yang optimum kerana mempunyai tegasan baki yang paling kurang.

ACKNOWLEDGEMENT

First and foremost, a very much thanks to the Great God Almighty in order for me to complete this research dissertation though there might a lot of difficulties experienced in the process of completion in both the project simulation completion and also the report writing completion.

On top of that, I am deeply indebted to my project supervisors Prof. Dr. Mohd Hamdi bin Abdul Shukor and Associate Prof. Dr. Judha Purbolaksono from University Malaya, Kuala Lumpur whose assistance, stimulating ideas, suggestions and encouragement assisted me in all time of research purposes and also thesis writing purpose. I would like to state my gratitude to Associate Prof. Dr. Judha Purbolaksono in assisting me in the process of Ansys simulation configurations. He has guided in this research project with great effort, patience, effort and support in order for the success of this project. Furthermore, I would like to express my gratitude to Prof. Dr. Mohd Hamdi bin Abdul Shukor for his essential information on the theory part of the project especially the theory on residual stress and also the brazing process. Nevertheless, the mentorship of both the supervisors has been tremendous help towards the completion of the research dissertation.

Besides that, I would like to express my gratitude to Tuan Zaharinie binti Tuan Zahari for sharing her knowledge and valuable information either experimentally or theoretically with regards to this research project. Nevertheless, it must be mentioned that many constants value or experimental parameters used in this research project are based on her project as she is currently performing the brazing experimental study while this project consist of her simulation that is based on her experimental project parameter settings.

Also, a special thanks to Prof Ariga for spending his effort and time in providing information of the project especially the details of brazing filler for this project. Without his assistance, more time were required in order to discover the best value and information for Bag-8-Ti brazing filler used.

Members of AMMP Research Center, my colleagues, Mr Ehsan Amiri and my friends were constant sources of support and encouragement throughout the project. Their curiosity, insight and suggestions kept me both on track of the project besides exploring and discovering new methods and ideas in making this project a success. A bunch of thanks to them all for their time and support in making and expanding the simulation brazing project.

Last but not least, I would like to express my special thanks to my family members whose patient love and care have lead to the success and completion this research project.

TABLE OF CONTENTS

LIST OF FIGURES

LIST OF TABLES

LIST OF APPENDICES

CHAPTER 1

INTRODUCTION

1.1 BACKGROUND

Pressure sensor is device to measure pressure typically gases and liquids. It will act as a transducer to convert energy to electrical signal. Pressure sensors are utilized to measure the intake manifold pressure, atmospheric pressure especially in the fuel tank. The operation principles of a pressure sensor will remain the same or similar although there is a different in location of application. Pressure sensors can be used to monitor the level of a tank by measuring and monitoring the pressure while the information of volume and liquid density are known. It is also used in hydraulic systems, gas compressors and it is commonly found in petrol station whereby the tyre pressure pump is available.

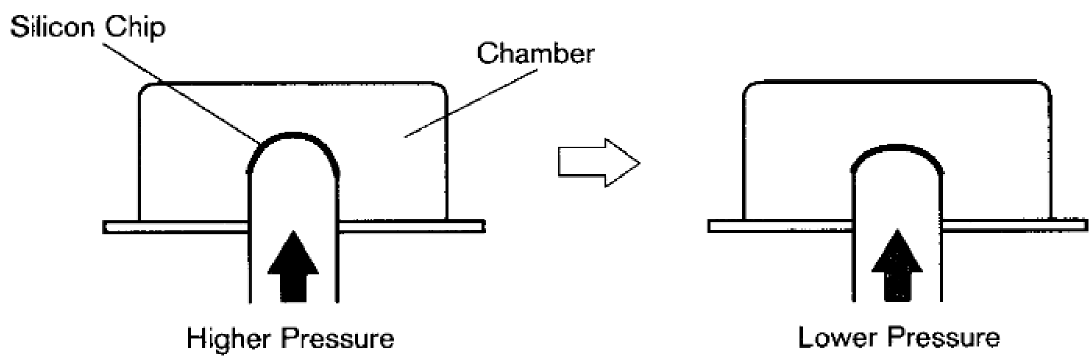

Figure 1.1: Pressure Sensing Element whereby the Flexion of Silicon Chip Varies as Pressure Changes

Source: ("Pressure Sensors," 2011)

Besides that, the pressure sensor has been widely applicable in the building automation, process automation and also the factory automation (Shigeo Kimura, 2006). Oil filled silicon piezoresistive pressure sensor element has been widely adopted and applied in many applications. Example of an oil-filled type pressure sensor product is Yamatake DSTJ3000Ace which consists of sensor chip to provide the sensing element. The sensing element of piezo-resistive pressure sensor chip is about the size of several millimetres square. In the new generation of sensor's requirements, there is a strong need for high temperature sensors so that the pressure sensor is functioning in the hot environment. There is also a strong requirement that the sensor is of corrosion resistant to maintain the accuracy of readings. There is of course the need for product miniaturization. Therefore, according to the findings from Yamatake, the best solution is making the requirements a success is to implement entirely sapphire-based sensor chip and also oil-free structure (Shigeo Kimura, 2006). The pressure sensor that are available in the market of oil-filled pressure sensor rather than oil-free structure sensor. With this type of oil-filled type pressure sensor, there is a tendency corrosion to occur. Furthermore, there is a tendency provide a dirty environment while handling the oil-filled type pressure sensor. Nevertheless, the fully sapphire-based sensor chip will cause the production of the sensor to be expensive. Instead of producing an entirely sapphire-based sensor chip, there is another alternative whereby it can be said that the combination of sapphire and Inconel 600 will produce almost the same effect as the fully sapphire-based sensor chip. On the other hand, there is requirement to check whether the combination of sapphire and Inconel 600 is reliable.

According to Yamatake Properties, sapphire is a type of non-coloured (colourless), transparent mineral named corundum which consists of aluminium oxide (Al_2O_3). With impurities in the sapphire, it is the impurities that provide colours in the corundum. Artificially grown sapphire is normally non-colored and transparent due to the extremely low impurities. Also, the purpose of Yamatake selecting the sapphire as the single crystal sapphire has the characteristics of excellent elastic properties, excellent heat resistance and also good in corrosion resistance. It is said that the sapphire is the most reliable material to produce the sensor chip as it is not prone to corrosion whether it is in the acidic or alkali environment. Moreover, the sapphire has very high heat resistance and Young's modulus, 1950^0C and $3.8X10^{11}$Pa respectively. Also, it has moderate bend strength of 275-700 MPa and a Poisson's ration of 0.25 (Lay, 2006).

From the findings by Yamatake, the new generation of pressure sensor will be sapphire-based capacitive pressure sensor (Shigeo Kimura, 2006).

1.2 PROBLEM STATEMENT

Sapphire gas pressure sensor consists of three (3) important parts. There are sapphire sensor chip (diaphragm and substrate), sapphire disk as sensor support and Inconel as the metal support (connected to the metal body of the sensor).

In manufacturing of pressure sensor today, the sapphire sensor chip was fabricated by various stages which include sapphire etching, direct bonding and other sapphire processing techniques. Joining of sapphire by direct bonding method is difficult and expensive. Therefore, the cost of producing pressure sensor by applying this method is expensive.

Another point that needs to be in consideration during design of a pressure sensor is that whether the joints of the sapphire sensor chip is capable to withstand the thermal stress during the operation of the pressure sensor. This is because of the different coefficient of thermal expansion which leads to the breakage of the sapphire disk. From the calculation by using mathematical interpolation, the coefficient of thermal expansion for

Inconel 600 are 16.19 μm/m.^{0}C (at 830^{0}C), 16.295 μm/m.^{0}C (at 865^{0}C) and 16.40 μm/m.^{0}C (at 900^{0}C) while for sapphire (α-Al_2O_3) are 9.3575 μm/m.^{0}C (at 830^{0}C), 9.445 μm/m.^{0}C (at 865^{0}C) and 9.5325 μm/m.^{0}C (at 900^{0}C). By referring to the values, it can be noticed that the difference of coefficient of thermal expansion at different temperatures will cause residual stress to occur as the both the materials are not expanding or retracting in the same rate.

1.3 OBJECTIVES

Based on the problem highlighted above in the problem statement, the main objectives of this research project are as below:

1) To develop the heat transfer distribution (conduction) plot from layer to layer of different types of material during the simulated brazing of Inconel 600 and sapphire.
2) To determine the optimum parameters in order to provide the least residual stress and optimum brazing result of Inconel 600 and sapphire.

1.4 SCOPE AND LIMITATIONS

The scope and limitations of this research project are as below:

1) Original width and depth of sample model is not applicable due to the constraint of the processor of the computer. Instead, a smaller dimension of the width and depth was applied in order to generate the simulation results in a timely manner and also to reduce the number of warnings of errors which will lead to inaccurate results. For this research project.

2) Residual stress can be measured and studied when the sample is cool down to room temperature. Therefore, the cooling process from brazing temperature to room temperature cycle is observed and studied. The heating and brazing process and time will not be included in this research project.
3) This research project is limited to the scope of Inconel 600, sapphire, nickel, copper and brazing filler of BAg-8-Ti.
4) The nickel and copper are assumed to be non-porous in this simulation research study.
5) The sample is clamped to a fix jig during the brazing process.

1.5 THESIS ARRANGEMENT

In Chapter 2, the basic concept of brazing is highlighted. There will be an introduction on brazing method. Furthermore, there will be literature study on the different brazing samples which consists of different types of material that have been performed.

In Chapter 3, the material selection used for the sample model in this research project will be discussed. Also, the material properties of the different types of material will be discovered and listed down to ease the study especially in the configuration of the Ansys Mechanical APDL simulation software. The properties are Young's Modulus, Poisson's ratio, coefficient of thermal expansion, thermal conductivity, density, specific heat capacity and also the yield strength. The methodology in modelling of the sample model by using Ansys Mechanical APDL simulation software, the thermal mechanical analysis which consists of transient thermal analysis and thermal-structural analysis will be discussed thoroughly.

In Chapter 4 which consists of the results and discussion of this research project. The results of heat conduction from layer to layer of material will be observed by studying the nodal plot of the transient thermal analysis result. The most important results are that the Von Mises stress plot. In this plot, there will a number of colour plots of different stresses at different part of the sample model. The colours are then compared with the yield strength of each of the material to determine the residual stress.

In Chapter 5, the optimum sample model with the optimum parameters will be discovered and summarized by comparing the data in the results. Also, the heat conduction or heat distribution plot will be observed. Last but not least, there will recommendation or further work in order to provide suggestion for better improvement in the results.

CHAPTER 2

LITERATURE REVIEW

2.1 IMPORTANT TEMINOLOGIES DEFINITIONS

2.1.1 Heat Transfer

Heat transfer (or heat) is defined as thermal energy in transit (medium) due to a spatial difference in temperature. Therefore, heat transfer occurs whenever there is a temperature difference in a medium or between media or medium (P.Incropera, Dewitt, Dewitt, & Lavine, 2007).

In heat transfer, there are basically three modes whereby the heat is transferred. There are conduction, convection and radiation heat transfer modes. When a temperature gradients occurs in a stationary or static (non-moving) medium, medium can be either a solid or fluid, then the term of conduction refers to heat transfer that will occur between across (in) the medium itself. On the other hand, the term convection means that the heat transfer occur between a surface of a medium and a moving fluid when they are at different temperatures. Radiation in heat transfer can also be labelled as thermal radiation. In thermal radiation, all surfaces of finite temperature emit or distribute energy in the form of electromagnetic waves. Thus, although there is no intervening medium, there is still net heat transfer by radiation between two surfaces at different temperatures (P.Incropera, et al., 2007).

2.1.2 Residual Stress

Residual stress is a type of stress induced due to a condition during processing. The residual stress will occur in the molded part itself. Not only that, the residual stress will occur when there is a difference of coefficient of thermal expansion (CTE). Residual stress can be categorized into two categories which are flow-induced or thermal-induced. Also, this stress will affect a part of sample material which is similarly like being applied with external stresses. If the residual stresses are way too strong that it is enough to overcome the structural of the sample model, the model will have a tendency to warp upon removal from the stress of upon ejection. There can be a possibility that crack will occur when external load is applied onto the sample model. Residual stress is the main factor that causes a material or a sample model with different types of material to warp or shrink in size. In order to overcome this residual stress, the conditions during processing and also the design elements have to be taken into consideration. This is important because this process will help to lower or reduce the residual stress, especially the flow-induced residual stress. On the other hand, the thermal-induced residual stresses can be reduced if there is enough packing and uniform in mold cooling. As for the fiber-filled material sample, the conditions during processing can promote uniform mechanical properties which will further reduce the thermal-induced residual stress (Center, 2011).

2.2 INTRODUCTION TO BRAZING

Brazing can be said to be included comprehensively in the group of welding processes as the brazing process produce the combination or coalescence of different types of material by heating them to the desired brazing temperature in the presence of filler metal. The brazing filler metal must have the properties of liquidus or melting point temperature above 450^0C or 840^0F and below the solidus or solid state point of the base metal. The brazing filler will act by providing distribution or wetting between the adjacent fitted surfaces of the joint by the process of capillary action (Schwartz, 2003).

It is a practice that the sample model used is heated to a temperature around 56^0C higher than the temperature of the brazing filler metal used. The filler metal can be preplaced, plated or applied from an external source.

In the process of selecting a suitable joining method, a consideration of requirements must take into consideration. The considerations include the service temperature and environment, reliability of the joining process, fatigue resistance, impact resistance and also other cyclic conditions just to name a few. Not only that, manufacturing cost, time to assembly, equipment used and other details assembly must be taken into consideration.

Brazing involves high temperature of 540^0C to 1620^0C and that is the reason this process is not applicable for the plastic material. It is instead applicable for the metal-matrix composites and also ceramic-matrix composites.

The most practiced and common type of brazing is lap joints. This type of lap joints has the same or similar strength or stronger that the base material used in this type of joining process. This is because the faying surfaces overlap for a distance equal to at least there (3) times the thickness of the thinner material of the same sample. The clearance between two adjacent parts is to be remained to around 0.075 mm (0.003 in) or less at brazing temperature.

2.2.1 Comparison between Brazing and Soldering

The main difference between brazing and soldering is that the temperature used in the brazing process is higher than any temperatures of other soldering process which involve filler metal of a liquidus state not exceeding 450^0C (Schwartz, 2003).

Brazing and soldering require the application of a number of scientific and engineering skills to produce joints with quality and reliability. Brazing process requires higher temperatures than in the soldering process. Nevertheless, the basic concept of the brazing process and soldering process is similar. This comparison can be seen in Table 2.1. Nevertheless, the characteristics such as the joint design, materials to be joined, filler-metal and flux selection, heating methods and joint preparation can be differ between the two joining processes. Also, the economic consideration in a joining process is also differing between these two types of processes. The economic considerations can be in terms of automated techniques, inspection and testing method. However, both these joining process of brazing and soldering are used in many industries like electrical and electronics applications, aerospace application or plumbing practices just to name a few.

Table 2.1: Comparison of Soldering, Brazing and Welding

Parameter	Process		
	Soldering	Brazing	Welding
Joint formed	Mechanical	Metallurgical	Metallurgical
Filler-metal melt temperature, $^0C(^0F)$	<450 (<840)	>450 (>840)(a)	>450 (>840)(b)
Base metal	Does not melt	Does not melt	-
Fluxes used to protect and to assist in wetting of base-metal surfaces	Required	Optional	Optional
Typical heat sources	Soldering item; ultrasonic; resistance; oven	Furnace; chemical reaction; induction; torch; infrared	Plasma; electron beam; tungsten and submerged arc; resistance; laser
Tendency to warp or burn	Atypical	Atypical	Potential distortion and warpage of base metal likely
Residual stresses	-	-	Likely around weld area
(a) Less than melting point of base metal. (b) Less than or equal to melting point of base metal			

(Source: Schwartz, 2003)

The type of metallurgical reaction between a filler and the main material will be used in order to differentiate the both the processes, brazing and soldering. Solders are usually reacting to create an intermetallic layer or phases. This intermetallic phase means that the compounds of the material used in the sample model have difference in terms of atomic arrangements than the elements in solid manner.

Soldering and brazing processes involve the same bonding or attaching mechanism. The mechanism is the reaction with the main material, usually alloying, I order to form metallic bonds at the interface. In both the processes, the wetting increases the formation of fillets which will increase the strength of the joints. Also, these two processes will produce joining samples with good adherence and corrosion resistance.

2.2.2 Benefits of Brazing Joining Process

According to Schwartz (Schwartz, 2003), there are many benefits of brazing which will be discovered in the following :

(a) Economical joining process of complex and multi-component assemblies
(b) Easy to obtain an extensive joint area and joint length
(c) Good in stress distribution and also properties in heat transfer in interlayer sample model
(d) The temperature of joining process is capable in approaching the temperature of the base metal
(e) Able to maintain the protective metal cladding or coating.
(f) Capable in joining cast materials to wrought metals.
(g) Able to produce a joining process between non-metals and metals.
(h) Capable in performing joining process regardless the thickness of the material used in the sample model
(i) Capable to perform joining process of dissimilar metals
(j) Capable to perform joining process of porous and non-porous metals
(k) Able to produce large assemblies in a stress-free condition
(l) Capable in preserving the metal special metallurgical characteristics
(m) Capable in joining fiber- and dispersion-strengthened composites
(n) Capable in maintaining precision production tolerance
(o) Produce reliable quality control braze sample
(p) Reproducible technique
(q) Produce less thermally induced distortion or warping compared to other joining process such as fusion welding. The rest of the part can be brought up to the same brazing temperature.

2.2.3 Disadvantages of Brazing Joining Process

A brazed joint is not a homologous body but is heterogeneous, composed of different phases with differing physical and chemical properties. A very simple sample braze model consist of base-metal part and also the filler metal. Nevertheless, partial dissolution of the base metal with the combination of diffusion processes is able to alter the composition. Thus, the chemical and physical properties of the boundary zone formed at the interface area between the base metal and filler metal and often of the entire joint. Therefore, in addition to the two different materials present in the example of braze sample model mentioned, a complicated or complex transitional or even completely different zone must be taken into consideration (Schwartz, 2003).

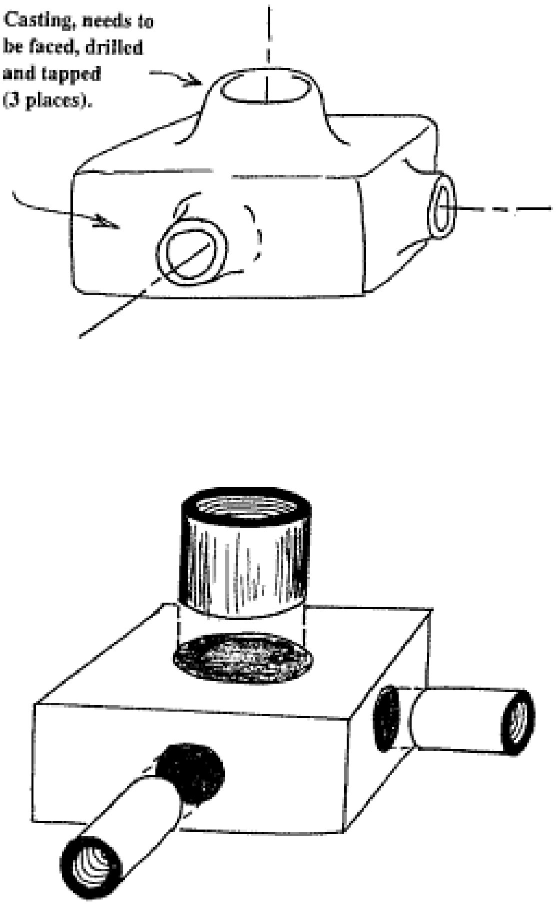

Figure 2.1: The Brazing Technique used to Perform Complex Model with Assemblies of Basic Components

(Source: Kay, 2000)

With refer to Figure 2.1, the casting shown on top is needed to be faced, drilled and in three places as illustrated by the arrows. On the other hand, it is rather easier to braze three threaded couplings tubes into a machined block as shown in the bottom sample model (Kay, 2000).

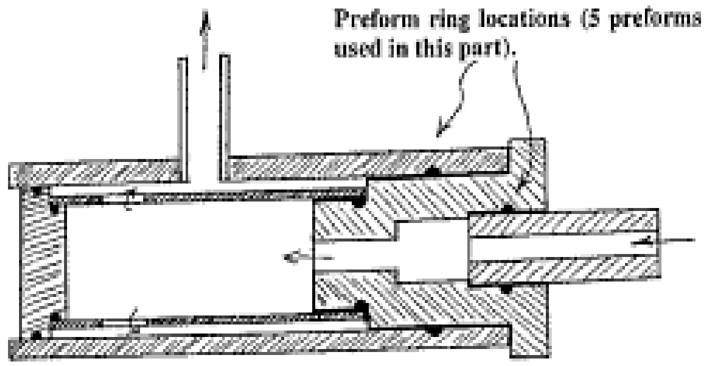

Figure 2.2: An Assembly of Several Internal Brazed Joints Accomplished at the Same Time in a Brazing Furnace

(Source: Kay, 2000)

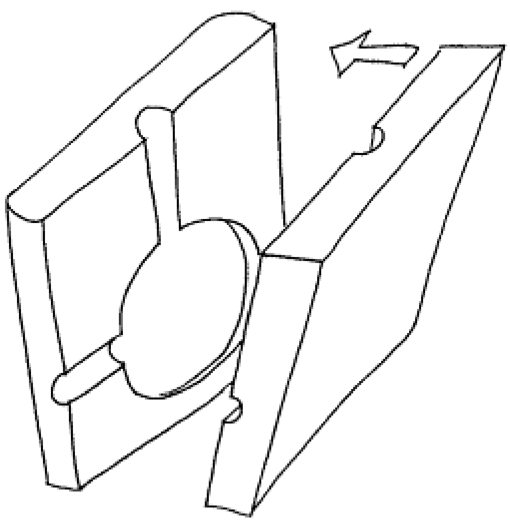

Figure 2.3: Joining of Large Covered Areas

(Source: Kay, 2000)

2.2.4 The Mechanism of Brazing Technique

According to E. Lieberman (E-Lieberman, 1988), the brazing involves a very small extent of dissolution, or another words called plastic deformation, of the base metal used in a brazed sample model. The brazing process undergoes four different steps. The steps are mentioned as below:

- The assembly or the region of the parts to be brazed-joined is heated to a temperature of minimum 450^0C.
- The temperature provided for the assembled parts and brazing filler metal is high in order to melt the brazing filler metal. The brazing filler metal can be in foil, wire, paste, platting) but not the parts.
- The function of molten brazing filler metal is to be held in the joint by surface tension which will spread into the joint and provide wetting to the surfaces of the base-metals.
- The brazing model sample part is cooled to the solidify state. The filler metal will be held in the joint by capillary attraction and joined the parts with the help of metallurgical reaction and also atomic bonding.

2.3 RECENT STUDY ON BRAZING AND RESIDUAL STRESS

A study on brazing of carbon fibre reinforced SiC composite and TC4 by using the active brazing alloy of Ag-Cu-Ti has been carried out by Jin Hui Xiong et.al. In this research study, the material used to be brazed are carbon fibre reinforced SiC (Cf/SiC) and TC4. This brazing research used the active brazing filler of Ag-Cu-Ti alloy powder. In order to check whether this project is as success or not, several testings have been done whereby the microstructures of the brazed joints were checked with the help of

SEM (Scanning Electron Microscope) machine, EDS (dispersive spectrometer) and also the X-ray diffraction (XRD) method. On the other hand, the mechanical properties of the brazed joints were checked and measured with the help of mechanical testing machine. In this research study done, titanium element in the alloy powder was discovered to react with Cf/SiC composite. Eventually, a combination of Ti_3SiC_2, TiC and Ti_5Si_3 had formed the reaction layers between Cf/SiC composite and interlayer. The formation of the diffusion reaction layers between interlayer and TC4 was due to the constantly dissolve of TC4 and the diffusion of Cu into TC4. Also, in this research study, the interface of the dissolve process can be separated into four stages which are: (i) the effect of Ag-Cu-Ti alloy powder melting, (ii) atoms diffusion, (iii) formation of the reaction layers, and (iv) the effect of the thickness and solidification process in the reaction layers. Furthermore, the shear strength of the brazed joints had been discovered also. At room temperature and 500^0C, the shear strengths of the brazed joint were 103 MPa and 51 MPa respectively after the process of brazing time 5 minutes and the brazing temperature is 900^0C (Xiong, Huang, Zhang, & Zhao, 2010).

Sudipta Mandal et.al. had investigated on the correlation between the mechanical properties and the microstructural behaviour of Al_2O_3-(Ag-Cu-Ti) brazed joints. In this investigation, the Al_2O_3 was the parental material while Ag-Cu-Ti was the brazing filler metal that was applied in this research. The technique of micro-indentation had been implemented in this research in order to obtain the strength of Al_2O_3-(Ag-Cu-Ti) brazed joints. Also, there were different compositions of alloy Ag-Cu-Ti utilized in this research and they were used at different temperatures of 800^0C, 900^0C, 1000^0C, 1100^0C and 1200^0C. The condition used in brazing research was that the process had been conducted under the vacuum with a constant load being applied. In order to obtain results, analyses were conducted with the technique of EPMA, SEM-EDX and XRD analyses. It was discovered that, from the three analyses mentioned, the adjacent of near to Al_2O_3, the diffused Ti amount was higher than copper (Cu). It was confirmed that the reaction layer was TiO and there was phase Ti_3Cu_3O was available between TiO and filler metal layer. A trial an error had been conducted to correlate the strength of the bond and also the microstructure of the brazing sample models. Also, an observation had been made that the higher amounts of element argentums (Ag) present in the brazing filler metal increases the reactivity of titanium (Ti), which consequently increase the strength of the bond. The results obtained were different for the filler metals with higher amounts of copper (Cu). This was because the higher composition of copper formed different Cu-Ti intermetallics. Nevertheless, these intermetallics did not react proportionally with ceramics. The alloys of $97(Ag_{28}Cu)_3Ti$ and $97(Ag_{40}Cu)_3Ti$ provide good performance in joining with the ceramics of Al_2O_3. In this research also, a small conclusion was made stating that the higher temperature and strength and resistivity to corrosion had promote the ceramic materials rather important for the use in electronic, nuclear industries, aerospace and automotive industries. Also, it was instead more preferred to perform joining of several layers rather than of the single piece ceramic component. The effect of brittleness associated with the ceramics limit the utilization of the brazing sample in the structural applications when the complicated ceramic component was manufactured. Joining the parts to shapes can expand the utilization of the ceramics and tolerance was achieved (Mandal, Ray, & Ray, 2004).

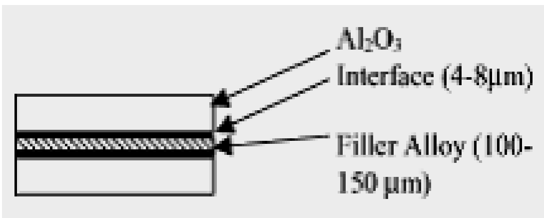

Figure 2.4: The Brazing Sample model of Interlayer of Al_2O_3-(Ag-Cu-Ti)

(Source: Mandal, et al., 2004)

Alexander E. Shapiro and Yury A. Flom had investigated on the brazing of titanium at temperatures below 800^0C. A review and suggested applications had been conducted as well. It was claimed that the brazing temperature of conventional Ti-Cu-Ni and Ti-Zr-Cu-Ni brazing filler metals was usually above the β-transus temperature of the titanium base metal which will affect the properties of the base metal. An experiment research was conducted by brazing the titanium with argentums based and aluminium based filler metals. The temperature implemented was below the β-transus temperature. Also, some new filler metal of Al-base was experimented in joining the structures of thin-wall titanium. A review and test was conducted in order to check on the effect of alloying the elements on the aluminium braze alloys, especially for the intermetallic formation in the brazed titanium joints. It was then reviewed that the brazed with Ti-based filler metals had higher strength than then titanium joints brazed with low-melting silver-based and Al-based brazing filler metal. Nevertheless, the titanium brazed structures were manufactured in Open Space as well which provide another opportunity in low-melting aluminium temperature and silver metal based filler metal. This was because the applications did not require an extreme high static or dynamic strength of joints. Furthermore, corrosion condition was not a problem or issue in Space. With that, the reactivity of the aluminium was prohibited by the extremely short in brazing thermal cycle. Another small conclusion discovered in this research is that the strength of titanium joints which had been brazed with silver filler metals were improved by the fast heating-cooling brazing cycle. 173 MPa was the shear strength when Ti-6Al-4V was brazed with silver based filler metal. On the other hand, the shear strength was 117.5 MPa when the furnace-brazed joints (Flom, 1997).

X.G. Songa et.al. investigated on the effects of Si_3N_4 particles in addition to the Ag-Cu-Ti filler alloy on Si_3N_4/TiAl brazed joint. In this research study, the composite filler alloy was implemented where the Si_3N_4p (p stands for particles) into the Ag-Cu-Ti filler alloy. The filler metal mentioned was utilized in the brazing of Si_3N_4 ceramics and TiAl intermetallics. The normal interfacial microstructure of the brazed joint consist of the reaction of $TiAl/AlCu_2TI$ + Al_4Cu_9 + Ti_5Si_3p + $TiNp/TiN$ +Ti_5Si_3 layers. There was an investigation on the effects of Si_3N_4p content in-composite filler alloy on the interfacial microstructure. It was said that the distribution of Ti_5Si_3p and TiNp compounds in Ag-based solid solution led to the decrease of them is similar with the coefficient of thermal expansion (CTE) and the Young's modulus between Si_3N_4 and TiAl material base. The maximum shear strength of 115 MPA was achieved when 3wt.% Si_3N_4p was an addition into the composite filler alloy. A fracture analysis had been conducted proving that the additional of Si_3N_4p was able to improve the mechanical properties of the joint (Song, Cao, Wang, & Feng, 2011).

Y.M He et.al. had investigated on the microstructure and mechanical properties of Si_3N_4/42CrMo steel joints when brazing with brazing filler metal Ag-Cu-Ti + Mo. In this research study, the Ag-Cu-Ti + Mo composite filler was used as brazing filler in brazing the joint of 42CrMo steel with Si_3N_4. Upon completion of the brazing process, the sample model was checked into the microstructure and also the mechanical properties of the joints formed. It was noticed that there were no defects when Si_3N_4 / 42CrMo steel joints and Ag-Cu-Ti + Mo composite filler were brazed together. A reaction layer was discovered was claimed to be formed near the Si_3N_4 ceramic. The reaction layer was later checked that it contained TiN and Ti_5Si_3. On top of that, a double reaction layer of Fe_2Ti and FeTi was formed near to the 42CrMo steel. Another layer of Fe_2Ti was formed and it was adjacent to the steel instead. It was noticed that the central part of the joint consists of Ag based solid solution, copper based solid solution, Mo particles and some Cu-Ti intermetallic compounds. Bending strength test was also been conducted. The maximum bending strength of 587.3 MPA with 10 vol.% Mo particles in the joint, whereby the strength of the joint 414.3% higher than the average strength if the Mo particles were not added. A small conclusion was made from this research stating that the Si_3N_4 ceramic was brazed successfully to 42CrMo steel by implementing the brazing filler metal Ag-Cu-Ti + Mo at temperature of 1173K while the brazing time is 10 minutes (He, Zhang, Sun, & Liu, 2010).

H.Matsumoto et.al. had investigated in the usage of low temperature brazing technique for accelerators. The research was conducted at KEK, National Laboratory for high energy Physics, Tsukuba, 305 Japan and Laboratory of nuclear Science, Tohoku University, Sendai, 982 Japan (H. Matsumoto, 1996). In this research study, the purpose of this research project is to implement the joining process of SiC (silicon carbide) – ceramic to copper. The objective was to observe the reducing deformation of the resultant structures. It was said that the low temperature brazing alloys like Sn (90%) – Au (10%) had been used successfully. The melting temperature for brazing alloys like Sn (90%) – Au (10%) was 309^0C. it was suggested that the technique used was of Shintake type (choke mode) HOM (Higher order mode) with frequency of 5712 MHz. Sn-Au with low temperature was brazed at 325^0C in a vacuum furnace was successfully joined SiC-ceramic to OFHC copper bars. The brazed sampled are then checked for the tensile strength and the results were of 260 kgf/cm^2 for the Cu-Cu and 80 kgf/cm^2 for the SiC ceramic-Cu joints. Hence, it was concluded that the low temperature brazing technique was able to fabricate choke mode structures with ample tensile strength. Furthermore, the structural defomation would reduce as well (T.Shintake, 1996).

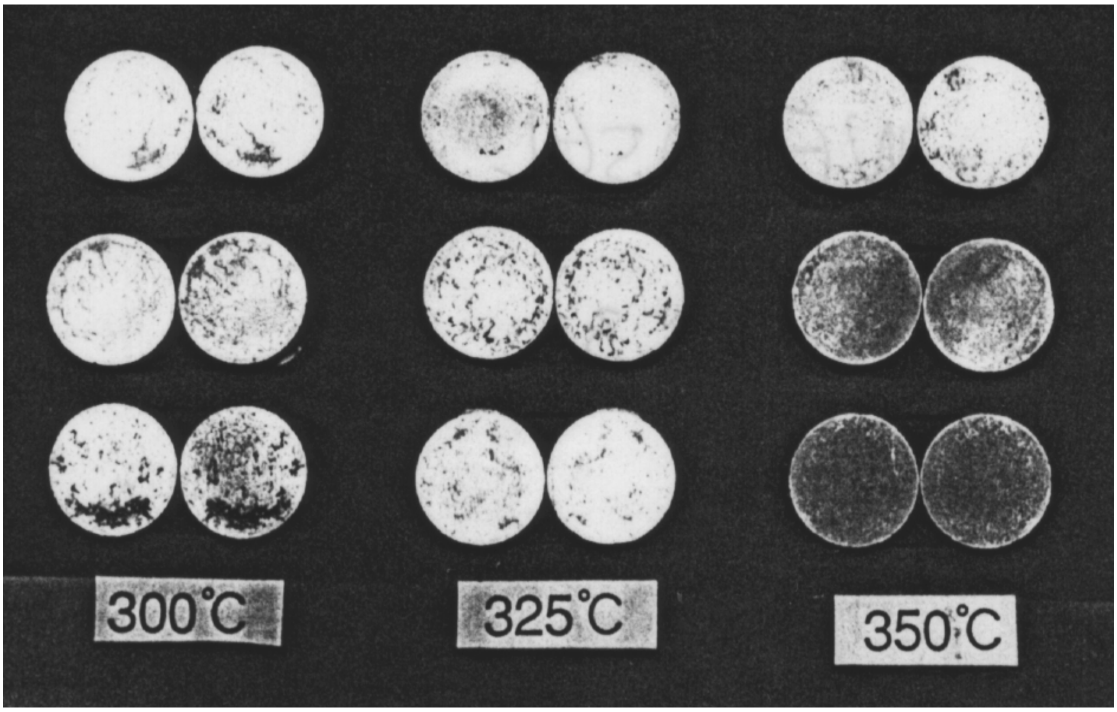

Figure 2.5: Fractured Cross Sectional View of the Copper-Copper Joint

(Source: H. Matsumoto, 1996)

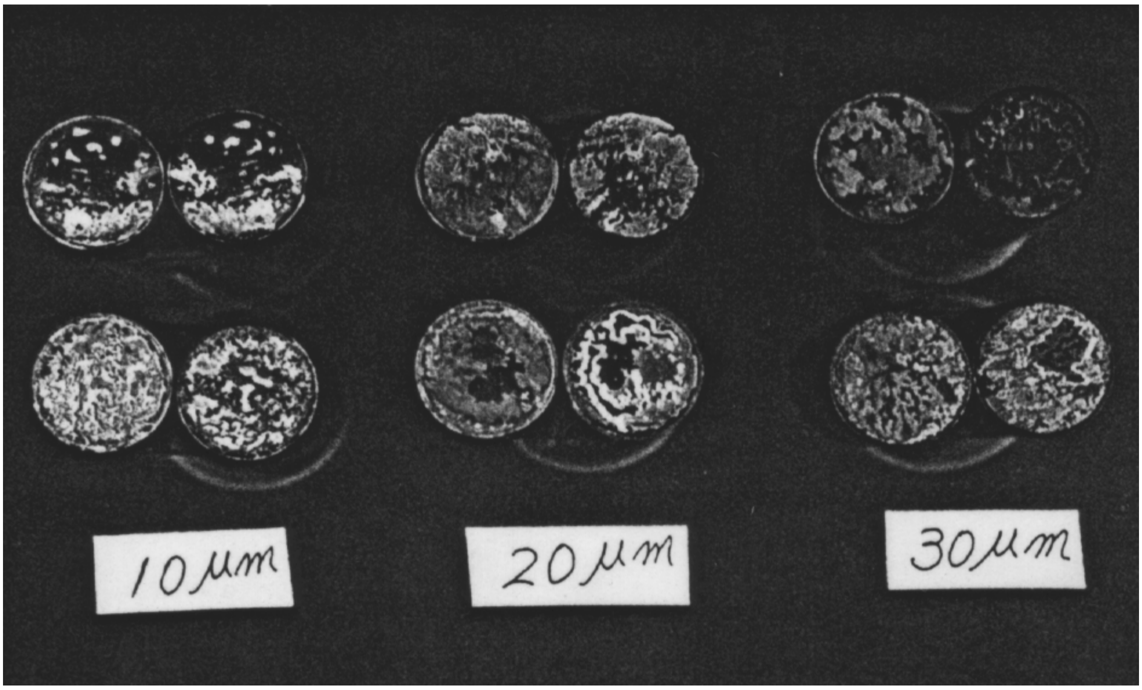

Figure 2.6: Fractured Cross Sectional View of the Cu-SiC-Cu Joint

(Source: H. Matsumoto, 1996)

LiYaJiang et.al. had investigated on the finite element analysis of residual stress in the welded zone of high strength steel. In this study, the weld joint of HQ130 grade high strength steel was simulated and analyzed in order to obtain the distribution of the residual stress. The software used was the Finite Element Analysis Ansys software. The simulation was based on the welding process which was conducted on the gas shielded arc welding with a input heat of 16 kJ/cm. The simulation results proved that there was a stress gradient around the fusion zone of the weld joint. The residual stress at a particular time increased to 800-1000MPa and 500-600MPa at below the weld. It was noticed also that the stress gradient adjacent to the fusion zone was higher than any other location in the surrounding area. This was prone to the reason for the formation of cold cracks at the fusion zone in the high strength steel. The thermal stress in the weld joint has to be decreased by controlling the welding heat input so that the welding crack defects could be reduced (LiYaJiang, 2004).

Ravikumar S.Kurhade et.al. had investigated on the finite element analysis of effects of strain hardening rate on cold expansion of fastener holes. It was claimed that the residual stress will cause a devastating effect on the fatigue lives of the parts especially in the aerospace application based industry. Process of mandrelizing was introduced in this research as the process expanded the hold diameter by methods of radial interference pressure to permit the radial plastic flow of material and some elastic recovery after the mandrel was removed. Hence, a stretch of residual compressive zone was formed around and near to the hole. It was this zone that acted as a barrier to promote crack growth which was able to promote and increase the service life of the structural components. By using Ansys software simulation, there was an analysis on the critical effects of material properties variation residual stress. Upon realizing that the hole cold expansion mandrelizing contributing to limitation, the hole was the removed and thereby providing almost uniform residual stress around the hole. The method of removal the hole cold expansion was rather reliable and increased the life span of the material compared to the mandrelizing method (Ravikumar S. Kurhade, 2004).

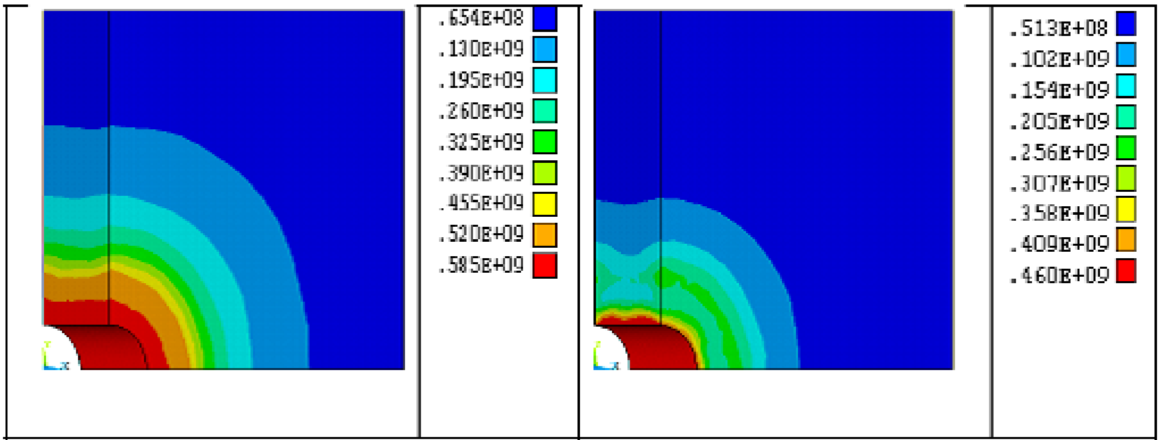

(a) von Mises stress contour when mandrel is inserted into the hole	(b) von Mises stress contour when mandrel is removed from the hole

Figure 2.7: Von Mises Stress Contours due to Cold Expansion (Et = 200MPa)

(Source: Ravikumar S. Kurhade, 2004)

Hwisouck Chang et.al. had investigated on the effects of residual stress on fracture strength of Si_3N_4 / stainless steel joints with a copper interlayer. A comparison of the change in fracture strength of a Si_3N_4 / Cu / steel joint with the change in residual stress as a function of the copper-interlayer thickness that was applied had been performed. It was claimed that the higher the residual stress and the lesser measured fracture strength of the joint will cause the overall dissolution of the Cu-interlayer into the brazing alloy. A finite element analysis of the residual stress was conducted and studied. The residual stress covered the measurement changes in the joint interface's microstructure. This was proportionally reflected the inverse changes in the measured fracture strength with respect to the thickness of the copper interlayer (Hwisouck Chang, 2002).

CHAPTER 3

METHODOLOGY

3.1 INTRODUCTION

In this research project, a research and confirmation whether the brazing of sapphire and Inconel 600 is a success or failure is conducted with the help of brazing filler BAg-8-Ti cum nickel and copper interlayer. The purpose of nickel and copper is to relieve the residual stress accumulated by sapphire and Inconel 600 during the brazing process as both of the main materials consist of different CTEs (coefficient of thermal expansion). The purpose of using filler BAg-8-Ti is to act as brazing filler for sapphire and Inconel 600. In another words, the purpose of BAg-8-Ti is to join both the material more firmly. Also, the use of this brazing filler is to provide wetting for the material to stick together.

In order to determine whether this brazing process of Inconel 600 and sapphire is a success or not, the residual stress of the samples are being simulated and studied. With the help of Ansys Mechanical APDL software, the samples are being checked and simulated for thermal mechanical transient analysis. In this thermal mechanical transient analysis, there are basically two analyses; there are transient thermal analysis and thermal-structural analysis. From the transient thermal analysis, the plot obtained will be the heat flow or heat transfer (conduction) from one layer to another. In the thermal-structural analysis, the plot obtained will display the Von Mises stress distribution which will determine the residual stress when compared with the yield strength of the material type.

Figure 3.1 displays the definition, position and terminology of width, depth and thickness of a sample model used in this research project. In the modelling of the sample models, the original width and depth dimension is not used but it is instead stepped down to the ratio of 1:10 as shown in Table 3.1. The purpose of this reason is that the computer used is not able to support the extreme large ratio of thickness towards width and depth. Therefore, the width and depth were attempted to be stepped down into a size that will provide faster simulation results or simulation with less errors and warnings. On the other hand, the thicknesses of the interlayers were remaining the same. With this setting, the result of the simulated residual stress will still as accurate as the actual experimental results of residual stress though the width and depth dimensions are reduced according to ratio 1:10 (as shown in Table 3.2) while the thickness is still the same.

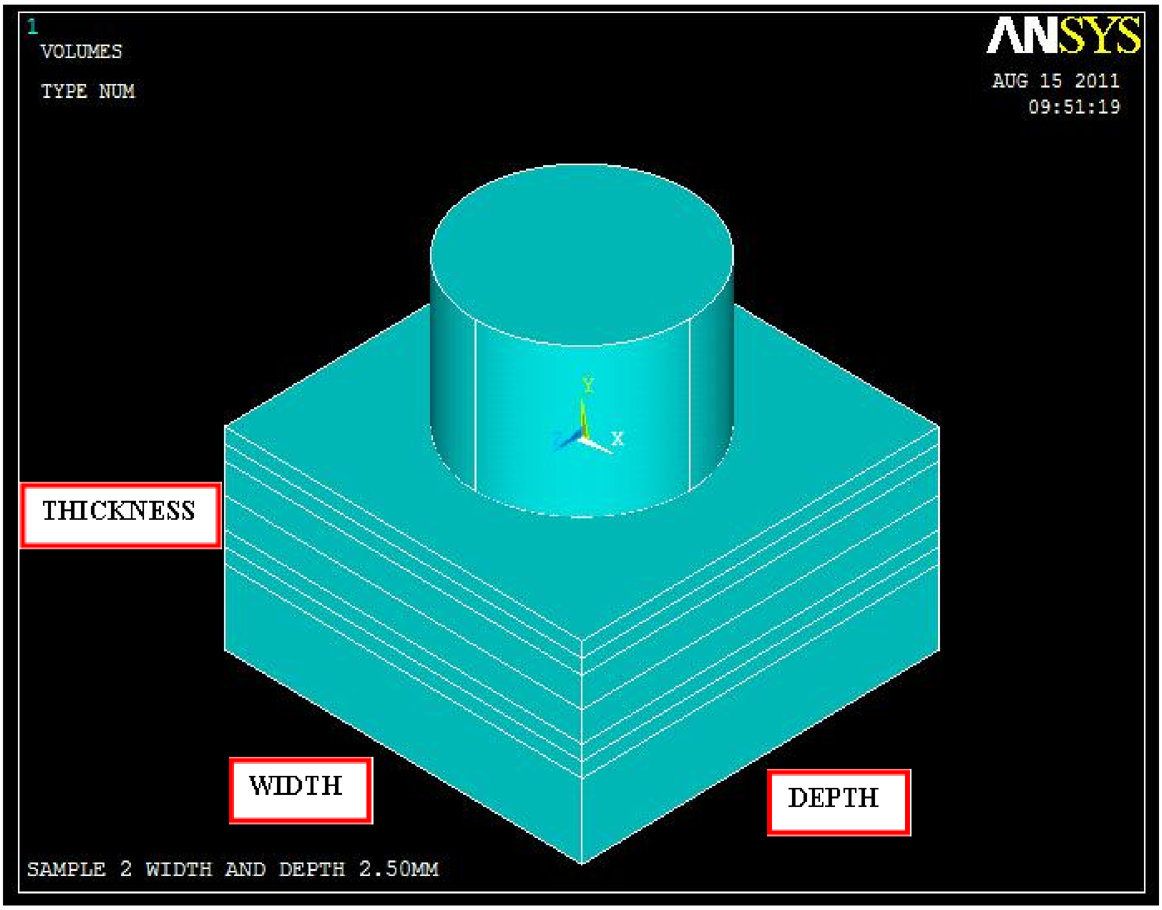

Figure 3.1: The Definition of Width, Depth and Thickness of a Sample Model

3.2 MATERIAL SELECTION

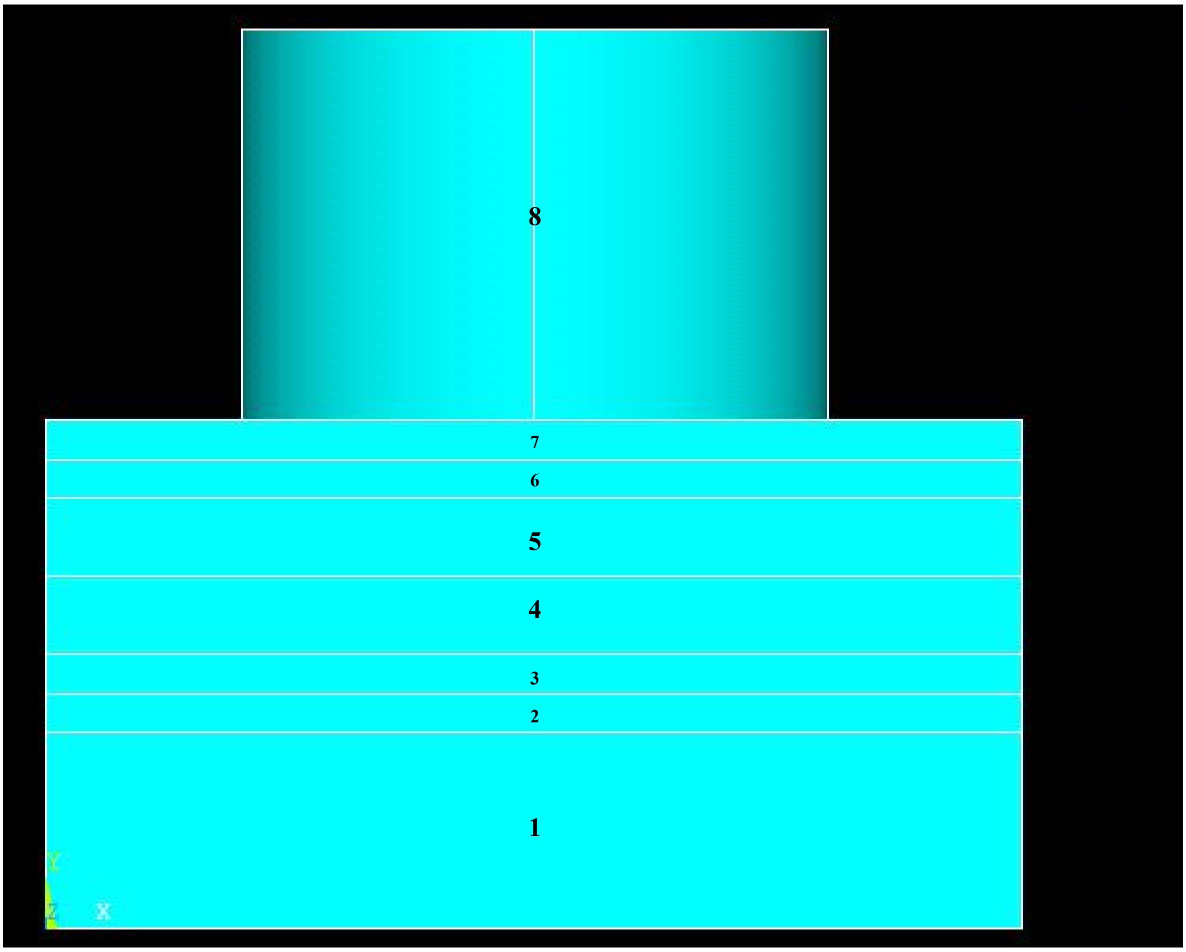

Figure 3.2: The Right View of the Sample Model

The types of material used in this research project are based on the material used by Tuan Zaharinie binti Tuan Zahari in her Doctoral project research. Nevertheless, the types of material used are tabulated in Table 3.1 with refer to the layer numberings as in Figure 3.2.

Table 3.1: Types of Material Used with refer to Figure 3.2

LAYER NUMBERING	TYPE OF MATERIAL
1	Inconel 600
2	Brazing filler BAg-8-Ti
3	Brazing filler BAg-8-Ti
4	Nickel (Ni)
5	Copper (Cu)
6	Brazing filler BAg-8-Ti
7	Brazing filler BAg-8-Ti
8	Sapphire

3.2.1 Material Properties

The following are the properties of the materials used in this research project. The material covered are Inconel 600, brazing filler (BAg-8-Ti), nickel (Ni), copper (Cu), and sapphire. The properties covered are Young's modulus, Poisson ratio, coefficient of thermal expansion (CTE) and thermal conductivity for various temperatures. As for the properties of coefficient of thermal expansion (CTE) and thermal conductivity, mathematical interpolation has been performed in order to obtain the particular values for temperatures of 830^0C, 865^0C and 900^0C as the temperatures are according to the actual brazing temperatures that are currently being carried out by the Doctoral project student. All the values for material properties mentioned are to be configured into the Ansys Mechanical APDL simulation software.

Table 3.2: Material Properties of the Materials Used

MATERIAL	PROPERTIES
Inconel 600	Young's Modulus, E = 164 GPa = 164000MPa Poisson Ratio = 0.29 Thermal conductivity = 28.04 W/m.^{0}C (at 830^{0}C) = 28.6682 W/m.^{0}C (at 865^{0}C) = 29.30 W/m.^{0}C (at 900^{0}C) Coefficient of thermal expansion, CTE = 16.19 µm/m.^{0}C (at 830^{0}C) = 16.295 µm/m.^{0}C (at 865^{0}C) = 16.40 µm/m.^{0}C (at 900^{0}C) Specific heat capacity = 616.1 J/kg.^{0}C (at 830^{0}C) = 622.05 J/kg.^{0}C (at 865^{0}C) = 628.0 J/kg.^{0}C (at 900^{0}C) Density = 8470 kg/m^3 Yield strength (at 0.2% offset) = 283 MPa Composition: *Refer to Appendix A*
Brazing filler (BAg-8-Ti)	Young's Modulus, E = 91.790244 GPa = 91790.244 MPa Poisson Ratio = 0.35 Thermal conductivity = 247.874 W/m.^{0}C (at 27^{0}C) = 247.874 W/m.^{0}C (at 400^{0}C) = 247.874 W/m.^{0}C (at 830^{0}C, 865^{0}C and 900^{0}C) Coefficient of thermal expansion, CTE = 18.6 µm/m.^{0}C (at 27^{0}C) = 18.6 µm/m.^{0}C (at 400^{0}C) = 18.6 µm/m.^{0}C (at 830^{0}C, 865^{0}C and 900^{0}C) Specific heat capacity = 285.17 J/kg.^{0}C (at 27^{0}C) = 285.17 J/kg.^{0}C (at 400^{0}C) = 285.17 J/kg.^{0}C (at 830^{0}C, 865^{0}C and 900^{0}C) Density = 9800 kg/m^3 Yield strength (at 0.2% offset) = 271.0 MPa Composition: 70% Ag – 28% Cu – 2 Ti

Table 3.2: (Continued)

MATERIAL	PROPERTIES
Nickel, Ni (Purity: 99.9%)	Young's Modulus, E = 207 GPa = 207000 MPa Poisson Ratio = 0.31 Thermal conductivity = 74.066 W/m.^{0}C (at 830^{0}C) = 74.836 W/m.^{0}C (at 865^{0}C) = 75.606 W/m.^{0}C (at 900^{0}C) Coefficient of thermal expansion, CTE = 17.81875 µm/m.^{0}C (at 830^{0}C) = 18.0375 µm/m.^{0}C (at 865^{0}C) = 18.25625 µm/m.^{0}C (at 900^{0}C) Specific heat capacity = 578.48 J/kg.^{0}C (at 830^{0}C) = 584.08 J/kg.^{0}C (at 865^{0}C) = 589.68 J/kg.^{0}C (at 900^{0}C) Density = 8900 kg/m^3 Yield strength (at 0.2% offset) = 59.0 MPa
Copper, Cu (Purity: 99.9%)	Young's Modulus, E = 125 GPa = 125000 MPa Poisson Ratio = 0.343 Thermal conductivity = 345.305 W/m.^{0}C (at 830^{0}C) = 343.03 W/m.^{0}C (at 865^{0}C) = 340.755 W/m.^{0}C (at 900^{0}C) Coefficient of thermal expansion, CTE = 23.7718 µm/m.^{0}C (at 830^{0}C) = 24.1506 µm/m.^{0}C (at 865^{0}C) = 24.5294 µm/m.^{0}C (at 900^{0}C) Specific heat capacity = 465.935 J/kg.^{0}C (at 830^{0}C) = 471.01 J/kg.^{0}C (at 865^{0}C) = 476.085 J/kg.^{0}C (at 900^{0}C) Density = 8933 kg/m^3 Yield strength (at 0.2% offset) = 70.0 MPa

Table 3.2: (Continued)

MATERIAL	PROPERTIES
Sapphire (Purity: 99.99%)	Young's Modulus, E = 370 GPa = 370000 MPa Poisson Ratio = 0.220 Thermal conductivity = 5.495 W/m.^{0}C (at 830^{0}C) = 4.705 W/m.^{0}C (at 865^{0}C) = 3.846 W/m.^{0}C (at 900^{0}C) Coefficient of thermal expansion, CTE = 9.3575 µm/m.^{0}C (at 830^{0}C) = 9.445 µm/m.^{0}C (at 865^{0}C) = 9.5325 µm/m.^{0}C (at 900^{0}C) Specific heat capacity = 1248.175 J/kg.^{0}C (at 830^{0}C) = 1256.05 J/kg.^{0}C (at 865^{0}C) = 1263.925 J/kg.^{0}C (at 900^{0}C) Density = 3970 kg/m^3 Yield strength (at 0.2% offset) = 400.0 MPa Composition: α-Al_2O_3

3.2.2 Material Dimensions

All the material dimensions in terms of width, depth and thickness are tabulated in Table 3.3. Again, in the modelling of the sample models, the original width and depth dimension of 25mm is not used but it is instead stepped down to 2.5mm. This means that the ratio of 1:10 is used in the modelling of the sample model for this research project. This is shown in Table 3.3. The purpose of this reason is that the computer used is not able to support the extreme large ratio of thickness to width and depth. Therefore, the width and depth were tried to be stepped down into a different dimension which provide simulation results in a timely manner or simulation settings with less errors or warnings.

Table 3.3: Sample Model Dimensions

Sample No	**1**	**2**	**3**	**4**	**5**	**6**	**7**	**8**	**9**	**10**	**11**	**12**
Sapphire	Diameter = 15 mm, Thickness = 1 mm			Diameter = 20 mm, Thickness = 0.7 mm			Diameter = 20 mm, Thickness = 1 mm			Diameter = 20 mm, Thickness =2 mm		
BAg-8-Ti Filler	Thickness = 0.1 mm											
BAg-8-Ti Filler	Thickness = 0.1 mm											
Copper	Thickness = 0.2 mm											
Nickel	Thickness = 0.2 mm											
BAg-8-Ti Filler	Thickness = 0.1 mm											
BAg-8-Ti Filler	Thickness = 0.1 mm											
Inconel 600	Thickness = 0.05 mm	Thickness = 0.50 mm	Thickness = 1.00 mm	Thickness = 0.05 mm	Thickness = 0.50 mm	Thickness = 1.00 mm	Thickness = 0.05 mm	Thickness = 0.50 mm	Thickness = 1.00 mm	Thickness = 0.05 mm	Thickness = 0.50 mm	Thickness = 1.00 mm
Original Width and Depth	25 mm											
Step Down Width and Depth	2.5 mm											
Ratio of Step Down to Original Width and Depth	1 : 10											

3.3 BRAZING TEMPERATURE DETERMINATION

From all the type of material used, brazing filler BAg-8-Ti is used to determine the brazing temperature of this research project. This is because brazing filler BAg-8-Ti has the lowest in terms of solidus temperature and liquidus temperature, 780°C and 815°C respectively, compared to the other types of material. The brazing filler BAg-8-Ti temperature is required to provide wetting between the interlayers. From the Ag-Cu phase diagram as shown in Figure 3.3, the eutectic point is around 780°C. Therefore, the brazing temperature chosen should be around the eutectic temperature and also above the liquidus temperature. Therefore, the best distribution of brazing temperatures is 830°C, 865°C and 900°C.

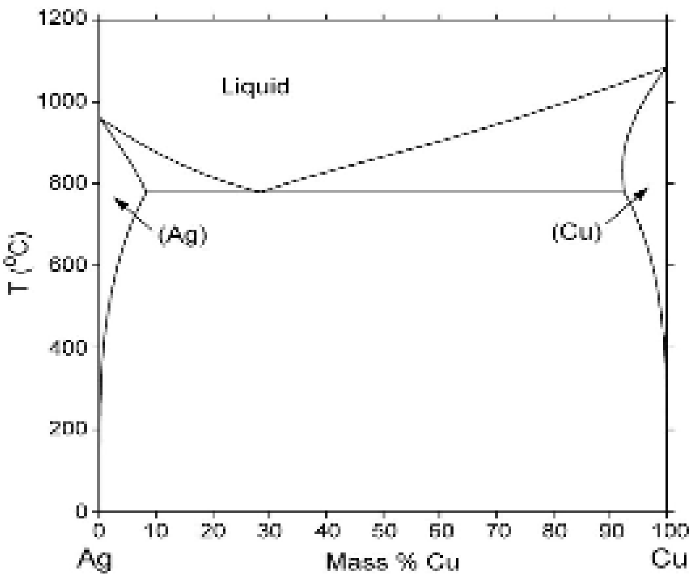

Figure 3.3: Ag-Cu Phase Diagram

(Source: http://www.metallurgy.nist.gov/phase/solder/agcu.html, 2010)

3.4 FRAMEWORK OF THIS RESEARCH PROJECT

The flow chart to display the framework and flow of this research project is shown in Figure 3.4.

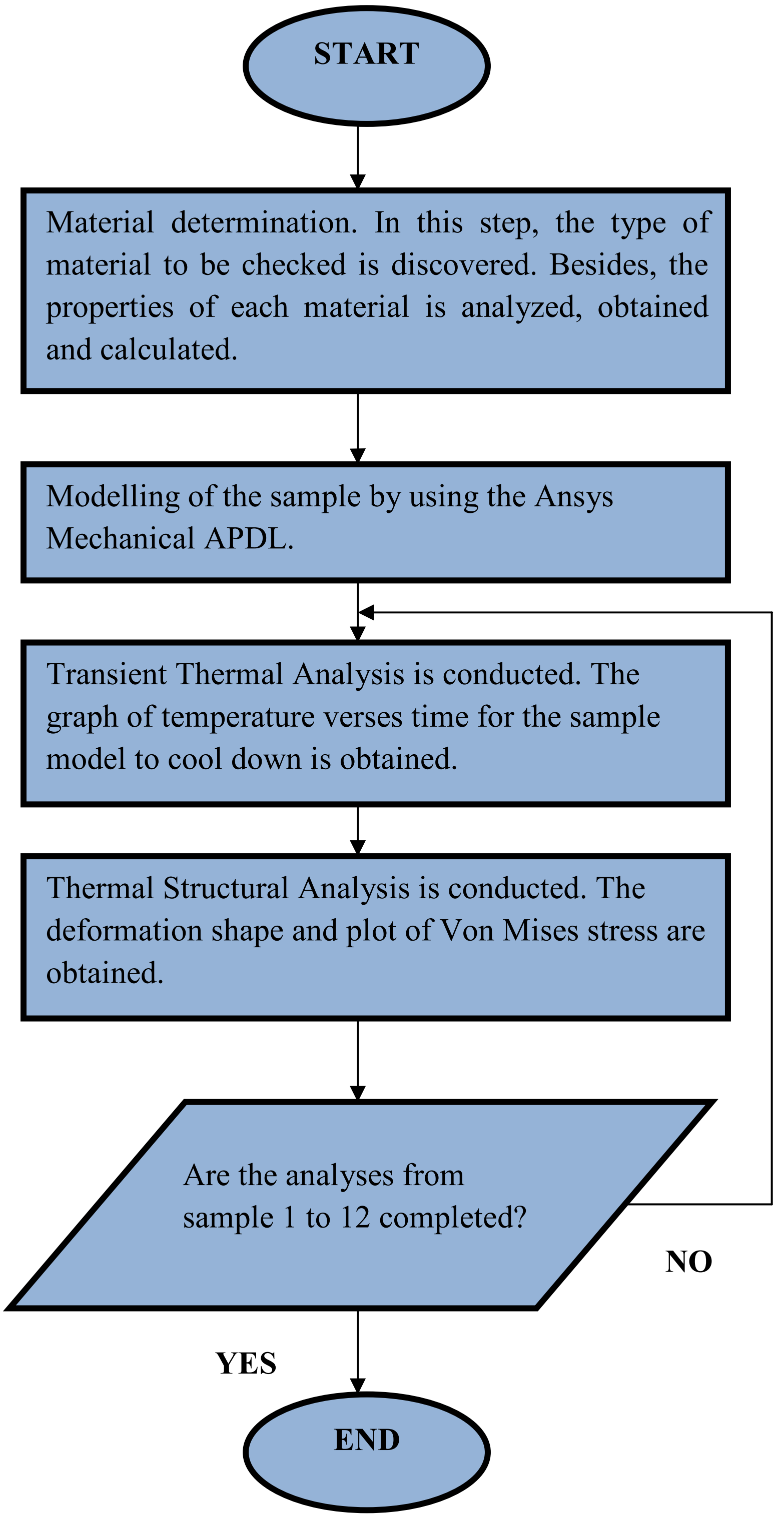

Figure 3.4: The Flow Chart of the Research Methodology

3.5 MODELLING OF SAMPLE

1. *Preprocessor → Modelling → Create → Volumes → Block →By 2 Corners & Z*

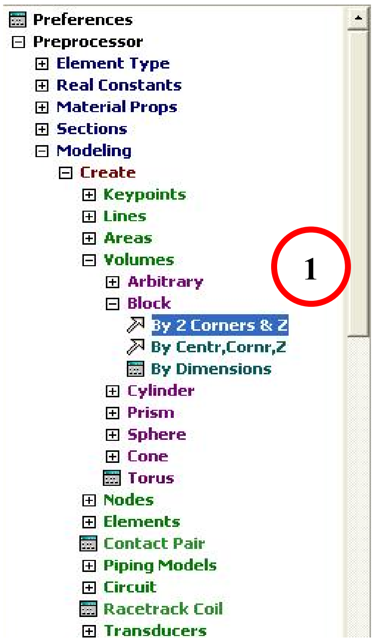

Figure 3.5: Step to Create Volume by Specifying Block by 2 Corners and Z

2. A window as shown in Figure 3.6 will pop up. The particulars are filled up in order to create the first layer. Upon setting the correction dimensions, select OK and the first layer will appear as shown in Figure 3.7.

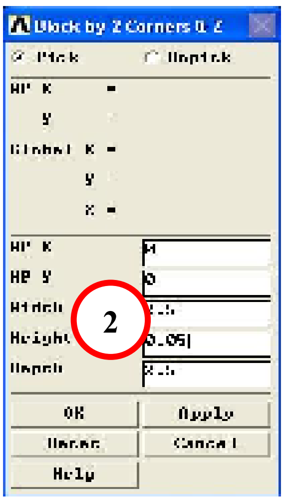

Figure 3.6: Block by 2 Corners and Z Window

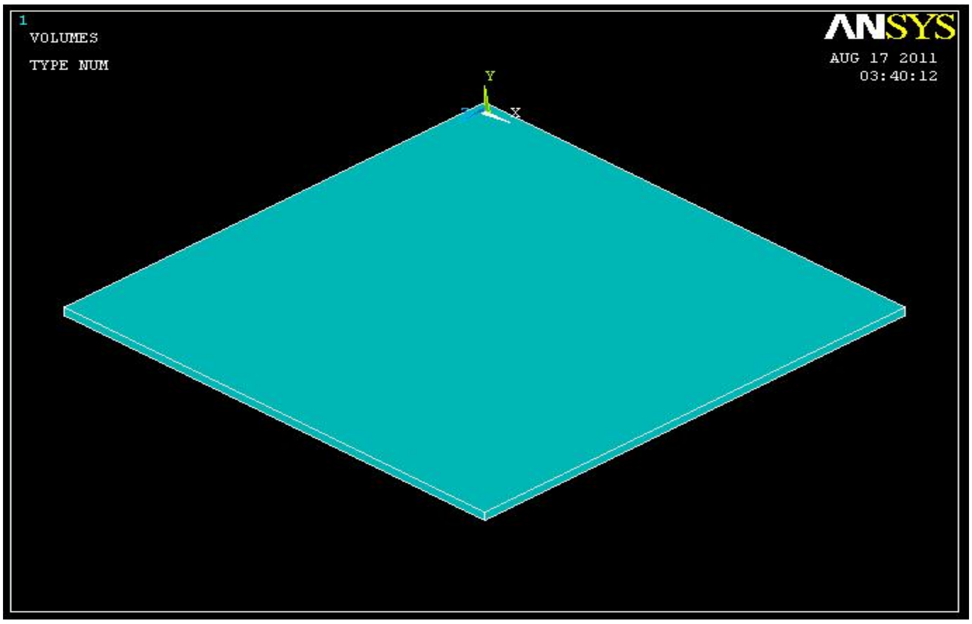

Figure 3.7: Model of the First Layer

3. To create the other layers on top of the first layer the following procedure is observed.

Preprocessor→ Operate → Areas → Along Normal →"Select the top area as shown in Figure 3.9" → Apply → "Enter 0.1 for length of extrusion as shown in Figure 3.11" → OK

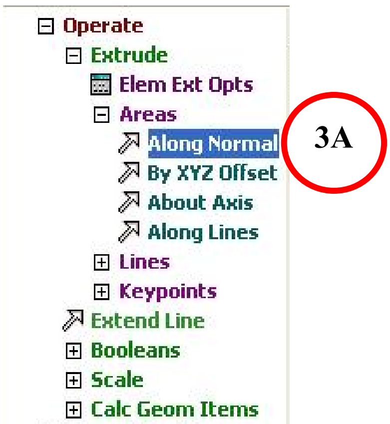

Figure 3.8: Step to Extrude Layer from Areas along Normal

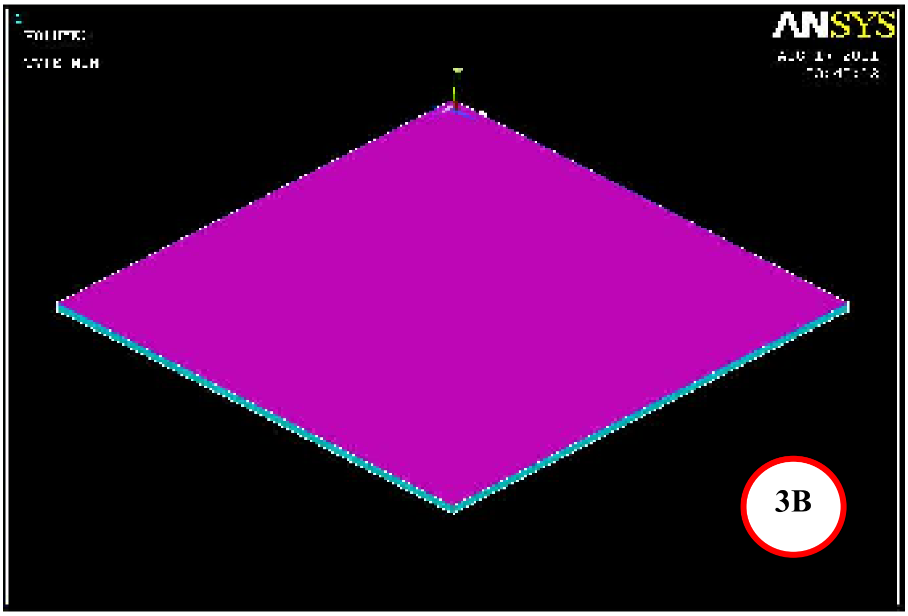

Figure 3.9: Top is Area is Selected to be Extruded

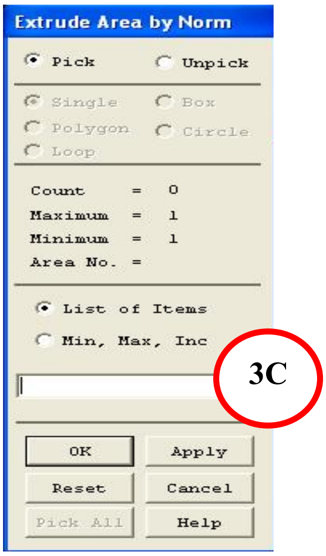

Figure 3.10: Extrude Area by Norm Window

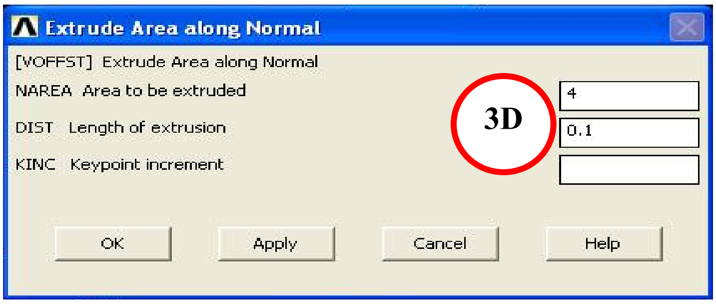

Figure 3.11: Extrude Area along Normal Window

The extruded area will appear as shown in Figure 3.12.

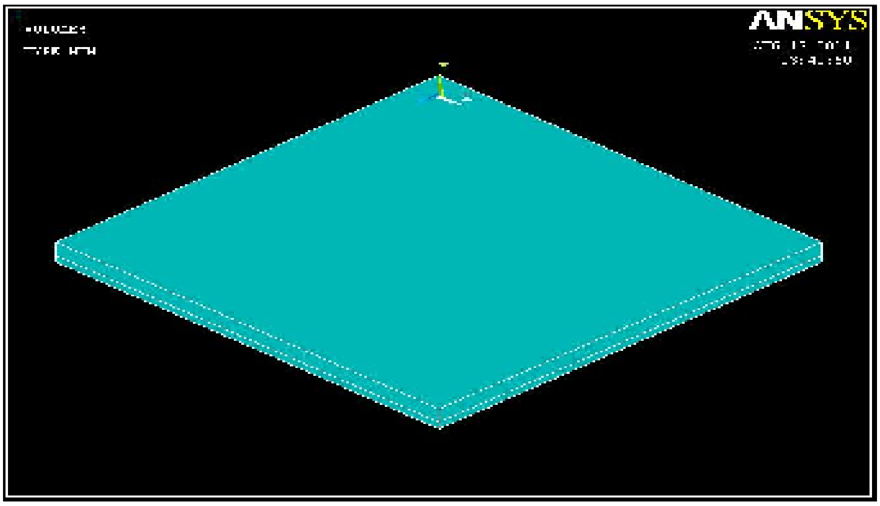

Figure 3.12: Model of the Extruded Layer

4. Step 3 is repeated until all the required layers are modelled. This is as shown in Figure 3.13.

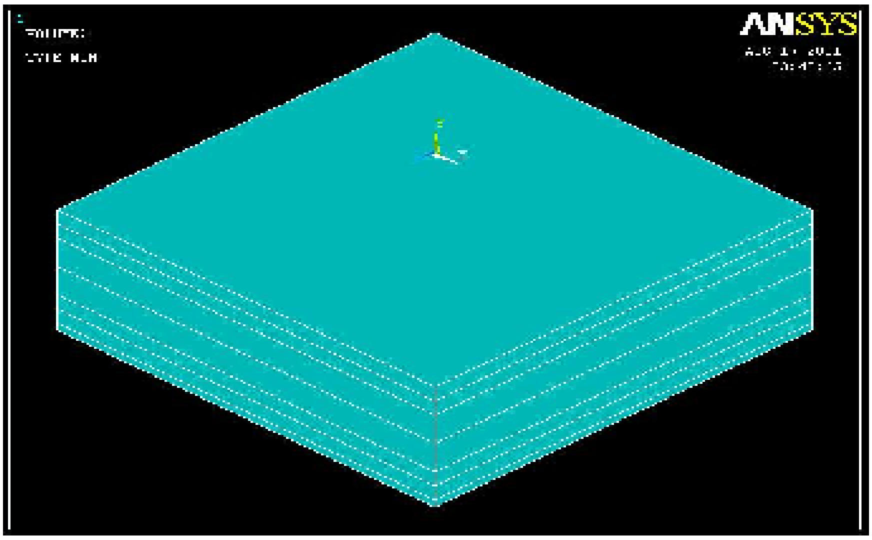

Figure 3.13: Model of the First Seven (7) Layers is Built

5. Keypoints are created in order to an area of circle on the top layer.

Preprocessor→ Modelling → Create →Keypoints→ In Active CS →"Enter all the coordinates for the keypoints required." → OK

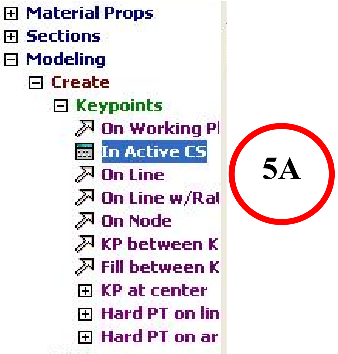

Figure 3.14: Step to Create Keypoints in Active CS

Figure 3.15: Create Keypoints in Active Coordinate System Window

Upon pressing OK, the plot of the keypoints will appear as seen in Figure 3.16.

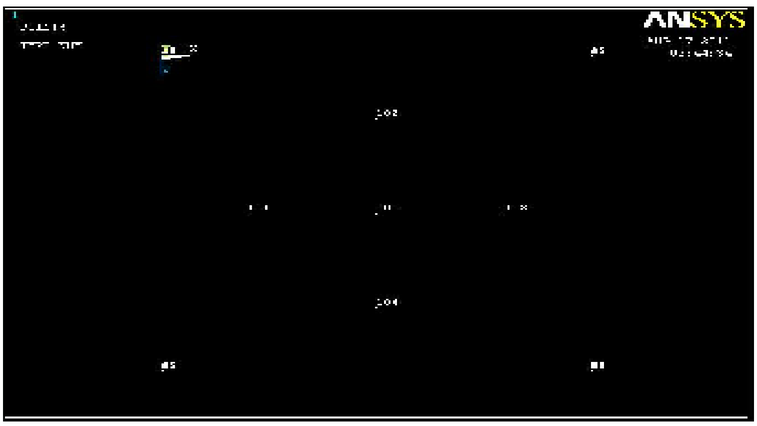

Figure 3.16: Keypoints are Built

6. In order to create circle, the arcs of the circles have to be drawn.

Preprocessor → Modelling → Create → Lines → Arcs → By End KPs & Rad → "Select keypoint 102 and 103." → Apply → "Select keypoint 100 as centre point of the circle." → OK → "Enter the radius of the arc as seen in Figure 3.19." → OK

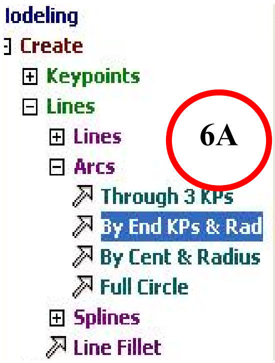

Figure 3.17: Step to Create Arcs by End KPs and Radius

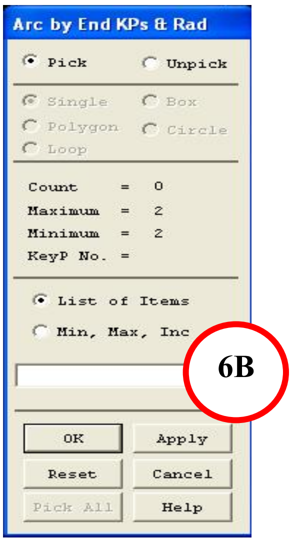

Figure 3.18: Arc by End KPs and Radius Window 1

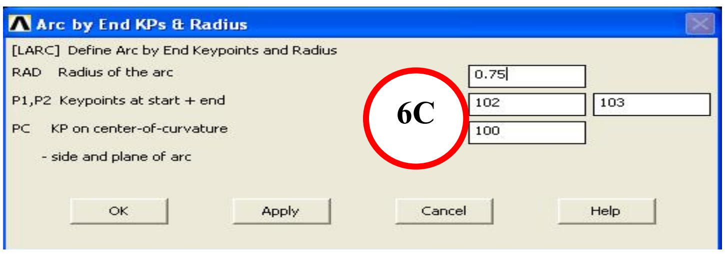

Figure 3.19: Arc by End KPs and Radius Window 2

After all the arcs of a circle have been created, the circle is obtained. This is shown in Figure 3.20.

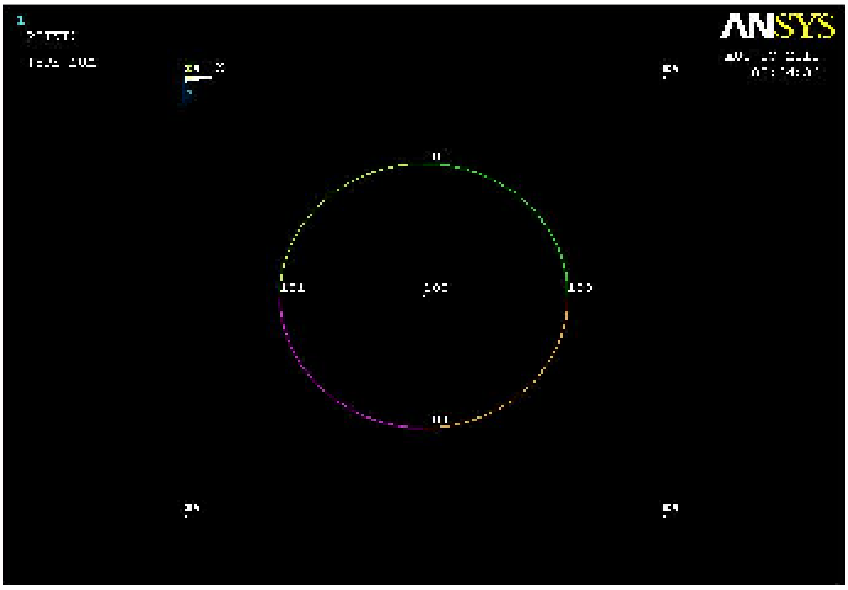

Figure 3.20: Display of the Circle Created

7. In order to create the area of a circle, the following procedure is followed.

Preprocessor→ Modelling → Create → Areas → Arbitrary → By Lines → "Select all the arcs created for the circle modelled." → OK

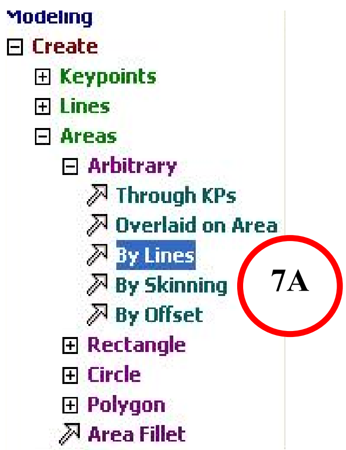

Figure 3.21: Steps to Create Areas by Arbitrary (by Lines)

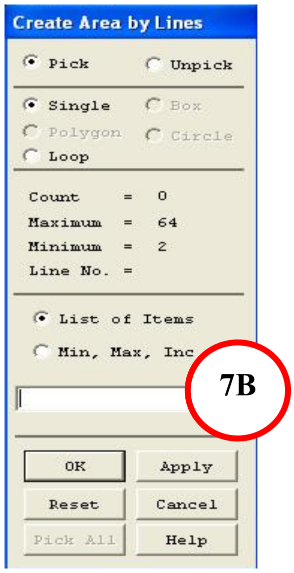

Figure 3.22: Create Area by Lines Window

8. To extrude the area of a circle to become the similar shape of the sapphire, the following procedure is observed.

Preprocessor→ Modelling → Operate → Extrude → Areas → Along Normal → "Select the area that is required to be extruded as shown in Figure 3.24." → OK →"Enter length of extrusion." → OK

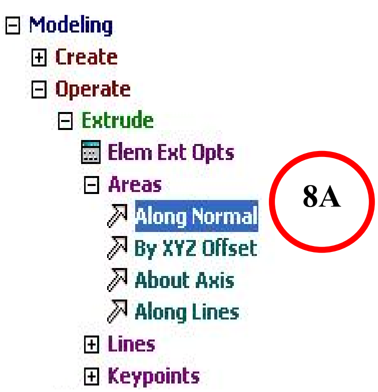

Figure 3.23: Step to Extrude Areas along Normal

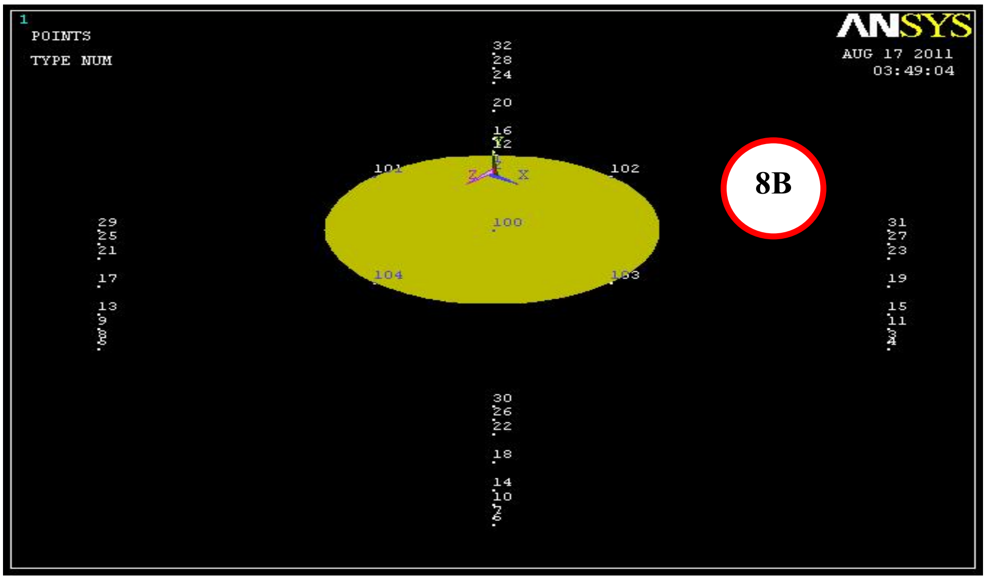

Figure 3.24: Area to be Extruded is Selected

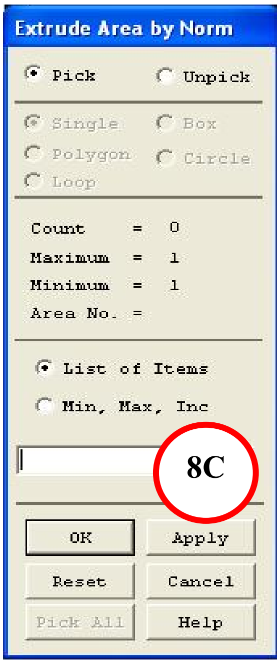

Figure 3.25: Extrude Area by Norm Window

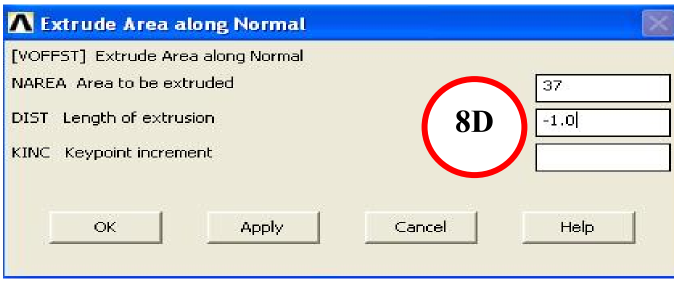

Figure 3.26: Extrude Area along Normal Window

After the extrusion has been done, the model obtained will be as seen in Figure 3.27.

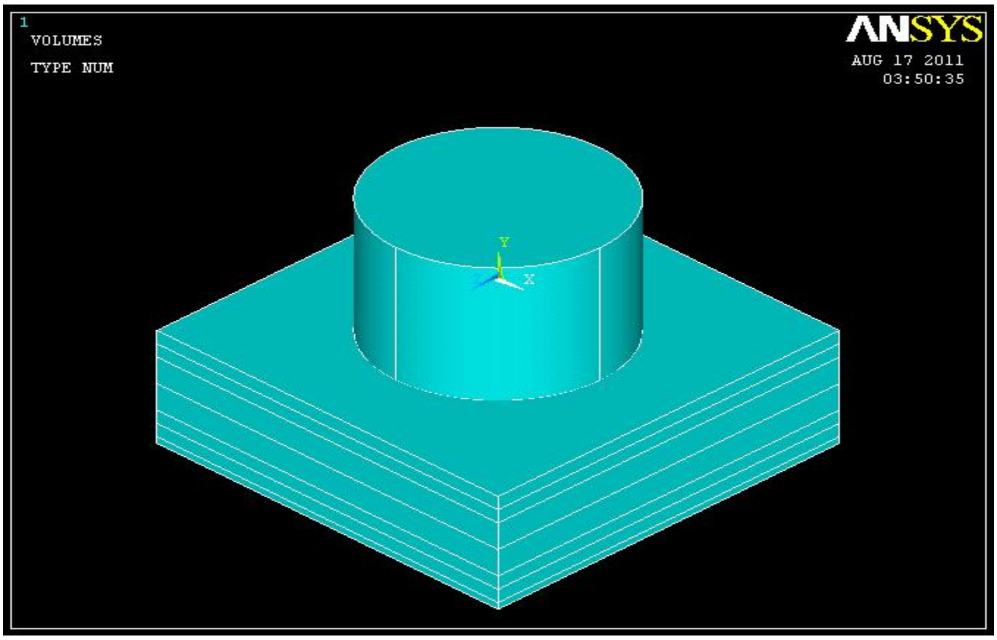

Figure 3.27: Sample 1 Model Built

9. In order to provide a title for the sample model built, the following procedure is observed.

Utility Menu → File → Change Title → "Enter the title as shown in Figure 3.29." → OK

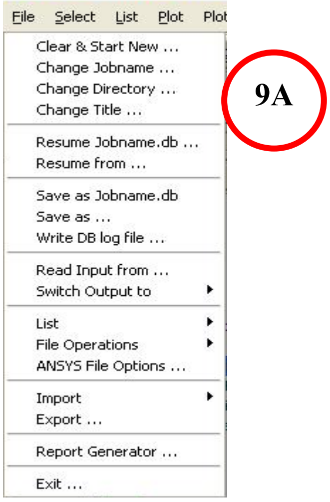

Figure 3.28: Change Title Menu from File Menu

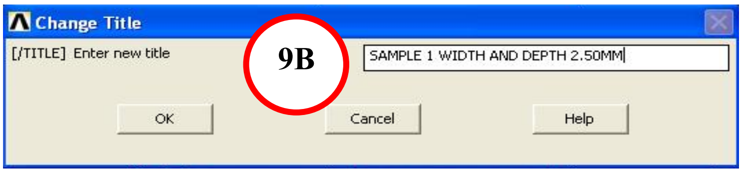

Figure 3.29: Title Labelled

The model with title as shown in Figure 3.30 is obtained.

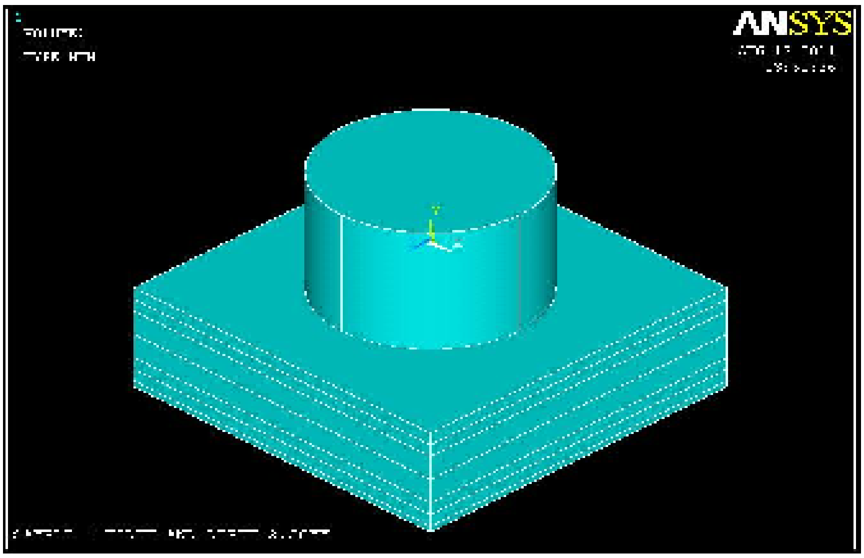

Figure 3.30: Model Sample with Title is Built

3.6 MESHING AND CREATING DB

This part basically is configured for the transient thermal analysis environment.

1. Model of the brazing sample is built.

2. Define the Type of Element.

Preprocessor → Element Type → Add/Edit/Delete → Thermal Mass → Solid → Tet 10node 87 (Solid87)

This procedure is generally shown in Figure 3.31. Nevertheless, the procedure in Figure 3.31 is clearly displayed and enlarged as shown in Figure 3.32, 3.33 and 3.34 respectively.

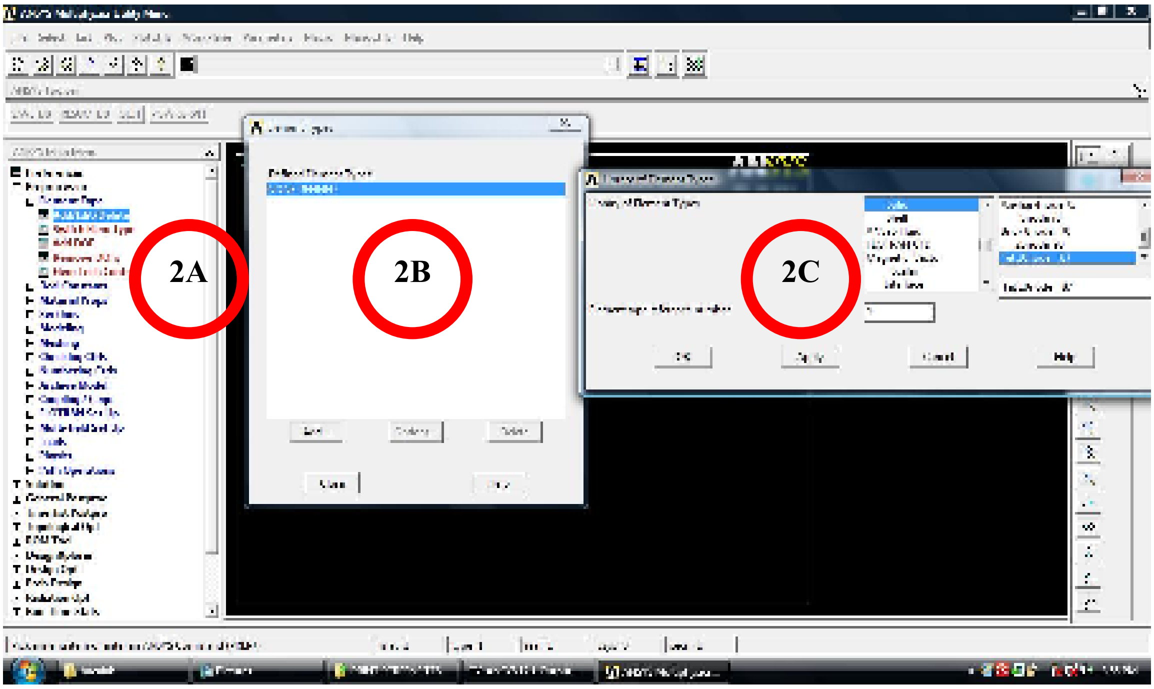

Figure 3.31: Type of Element Setting

Figure 3.32: Element Type Addition Setting

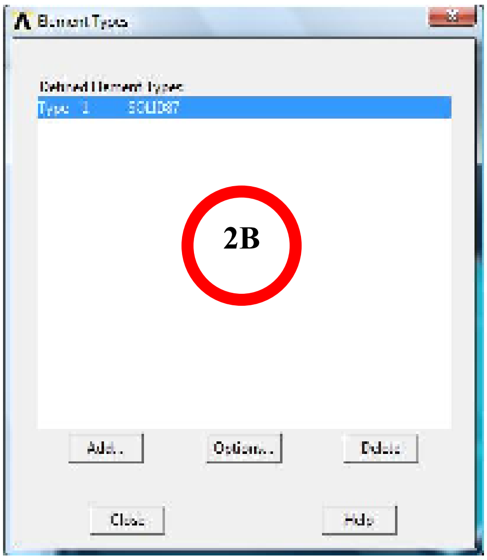

Figure 3.33: Type of Element Setting for Solid87

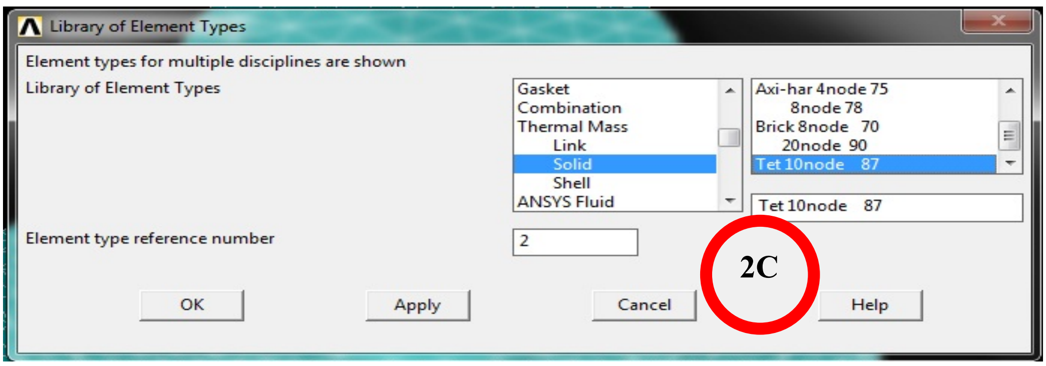

Figure 3.34: Type of Element Setting for Solid87

3. Define Element Material Properties.

(a) The properties for Young's Modulus and Poisson ratio are filled up into the respective properties boxes in EX and PRXY.

Preprocessor → Material Properties → Material Models → Structural → Linear → Elastic → Isotropic

This procedure is shown in Figure 3.35.

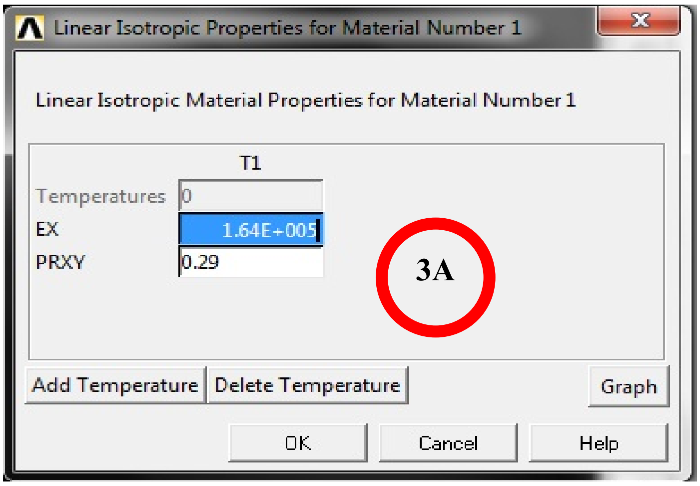

Figure 3.35: Setting for Young's Modulus and Poisson's Ratio

(b) The values for coefficient of thermal expansion for temperature 830^{0}C, 865^{0}C and 900^{0}C are to be filled into the respective columns as shown in Figure 3.36.

Preprocessor → Material Properties → Material Models → Structural → Thermal Expansion → Secant Coefficient

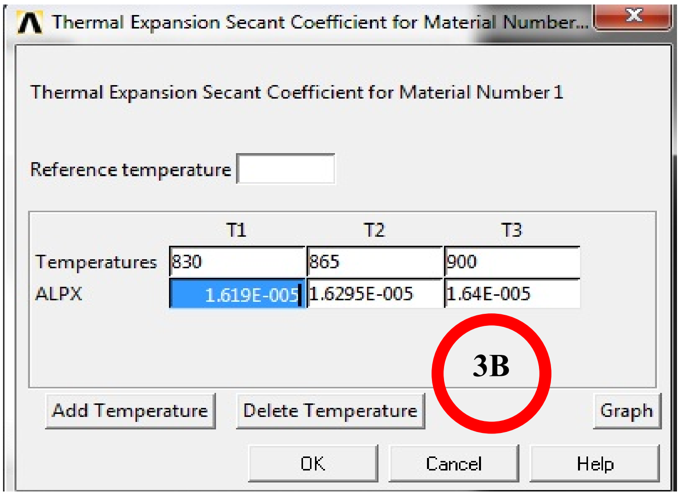

Figure 3.36: Defining Thermal Expansion Coefficient Setting Window

(c) The values for thermal conductivities for temperature 830^{0}C, 865^{0}C and 900^{0}C are to be filled into the respective columns as shown in Figure 3.37.

Preprocessor→ *Material Properties* → *Material Models* → *Thermal* → *Conductivity* → *Isotropic*

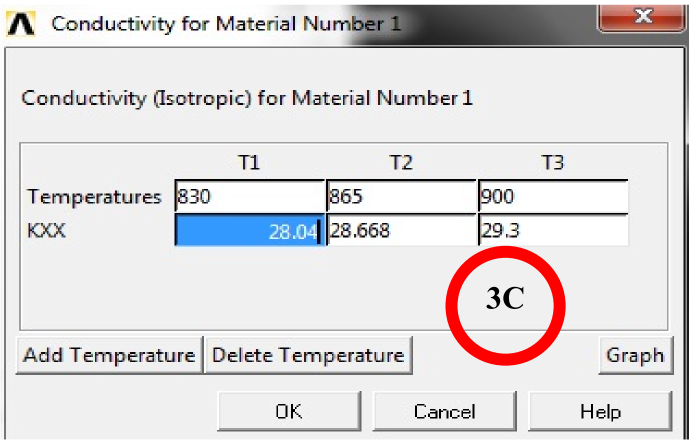

Figure 3.37: Configuration Setting for Thermal Conductivities for 830^{0}C, 865^{0}C and 900^{0}C Brazing Temperatures

(d) The values for specific heat capacities (for temperatures of 830^0, 865^0 and 900^0C) are filled up into the respective properties boxes as shown in Figure 3.38.

Preprocessor→ Material Properties → Material Models → Thermal →Specific Heat

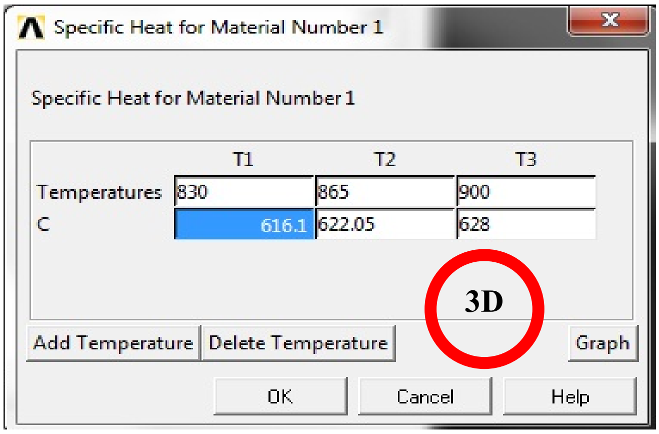

Figure 3.38: Defining Specific Heat for Material Window

(e) The value for density is filled up into the respective properties box as shown in Figure 3.39.

Preprocessor→ Material Properties → Material Models → Thermal →Density

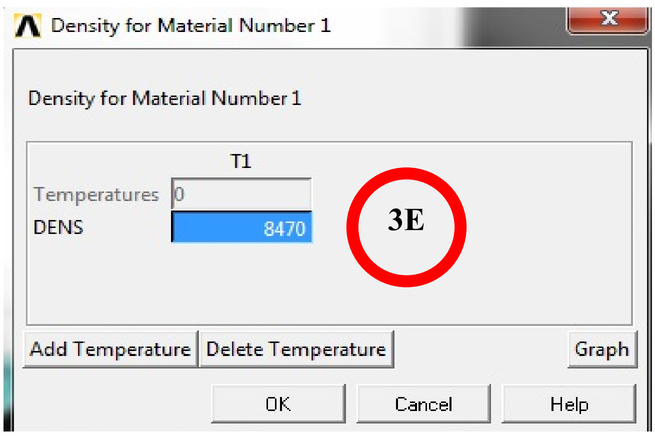

Figure 3.39: Defining Density for Material Window

(f) If there is any other type of material that needs to be clarified, the material model is added. This procedure is shown in Figure 3.40 and 3.41.

Material → NewModel → "Define Material Number" → Ok

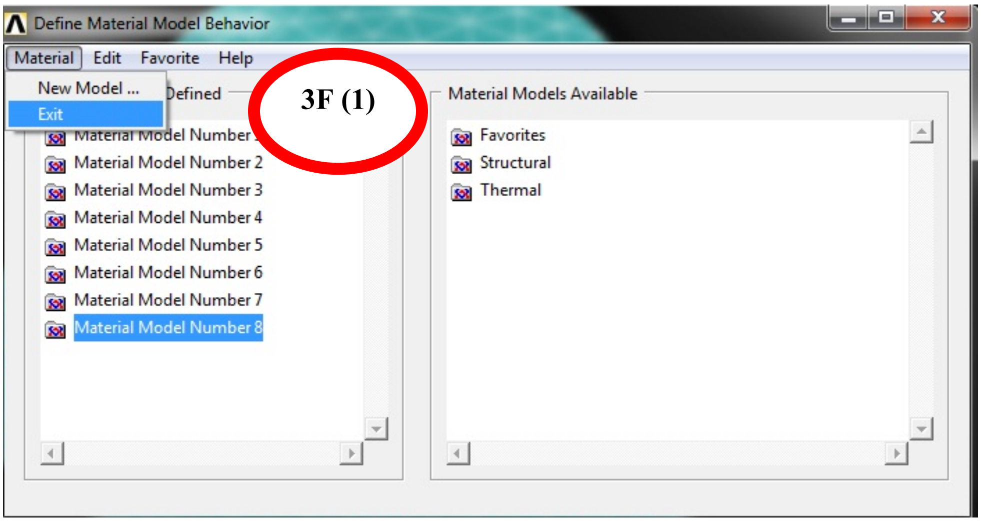

Figure 3.40: Defining Material Model Behaviour Window

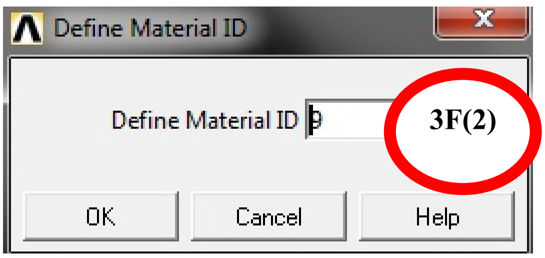

Figure 3.41: Define Material ID Window

After adding the respective material type, the procedures to define the properties of the material like Poisson's ratio, Young's Modulus, coefficient of thermal expansion, density and specific heat capacities are clarified.

4. It is necessary for the model in this research project other to be glued in order that the meshing element type will be distributed equally from one layer to another. This procedure is shown in Figure 3.42 and 3.43. Consequently, the entire material layers in this sample for this research are glued to one another. The gluing of all the volumes together has to be performed so that the areas attached between layers are attached but that the subdivided volumes remain to provide the elements required.

Preprocessor → Modelling → Operate → Booleans → Glue → Volumes → Pick All

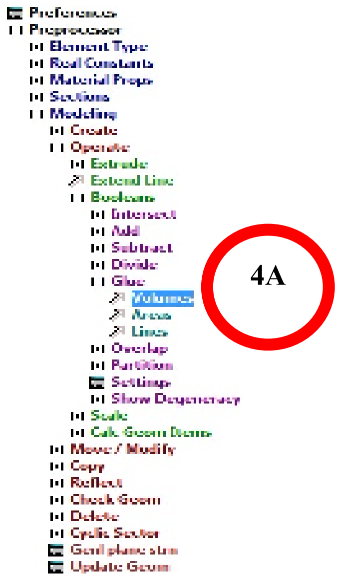

Figure 3.42: Glue Volume Setting

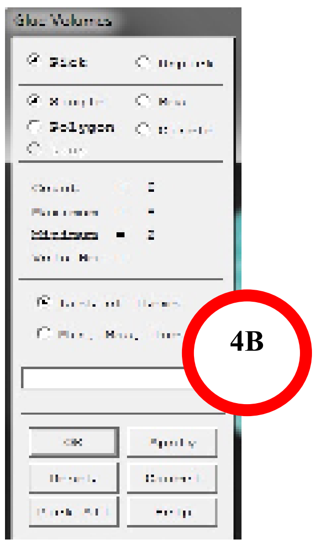

Figure 3.43: Glue Volumes Window

5. Define attribute for the different type of material applied in the research project. This procedure is shown in Figure 3.44 and 3.45.

Preprocessor → Meshing → Mesh Attributes → Picked Volumes → "Pick the respective volume to be given the attribute" → "Select Ok to stop defining other type material or select Apply in order to define any other material."

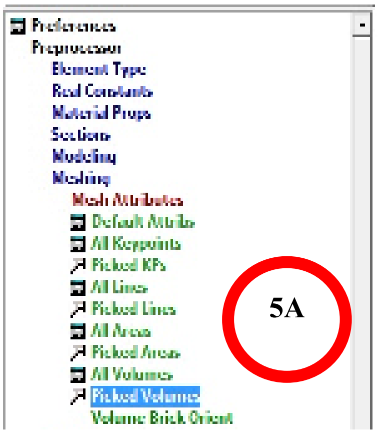

Figure 3.44: Picked Volume to be Meshed Setting

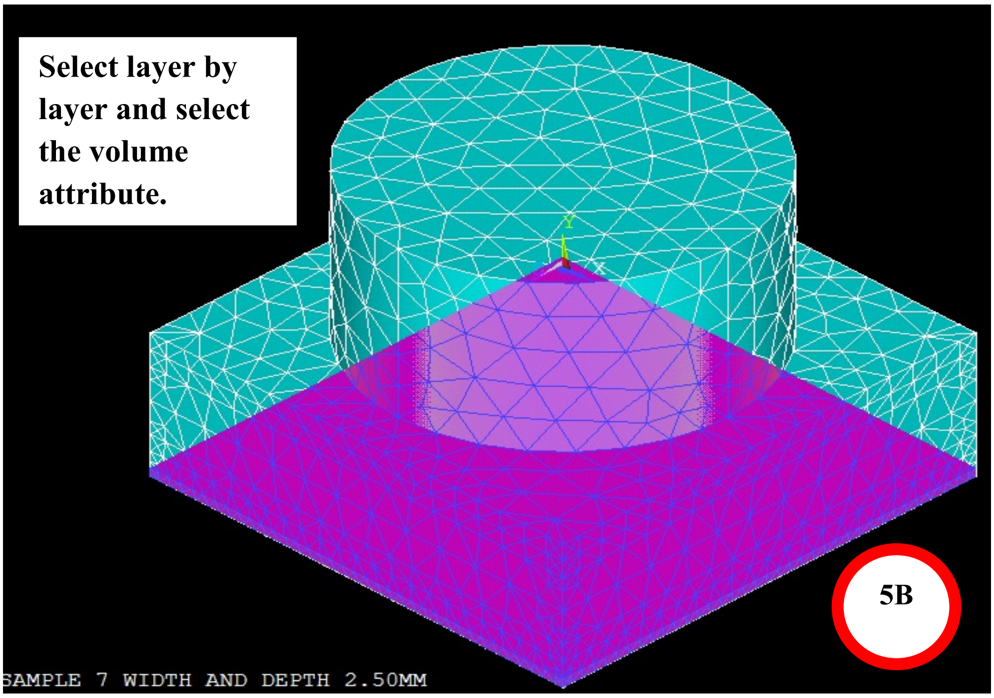

Figure 3.45: Volume Attribute Assignation for Layer by Layer

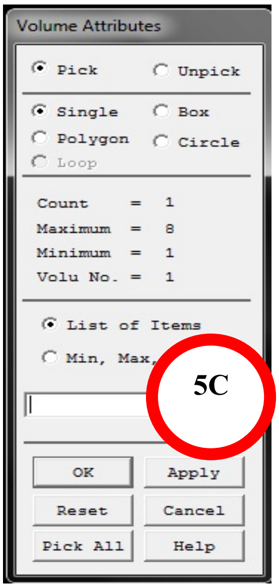

Figure 3.46: Volume Attribitus Window

6. Define meshing for the research sample.

Preprocessor → Meshing → Mesh Tool → "Select the Smart Size according to the requirement and accuracy of the result required." → Mesh → Pick All

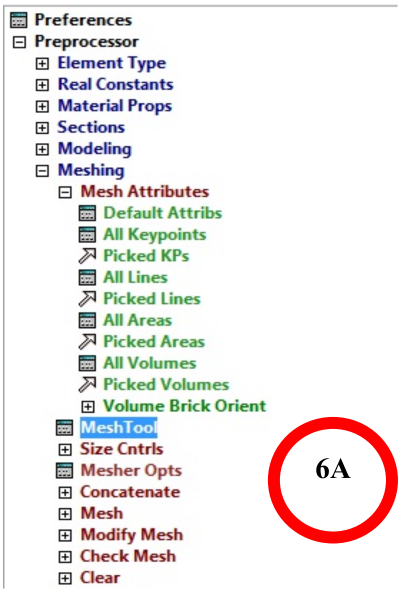

Figure 3.47: Mesh Tool Setting

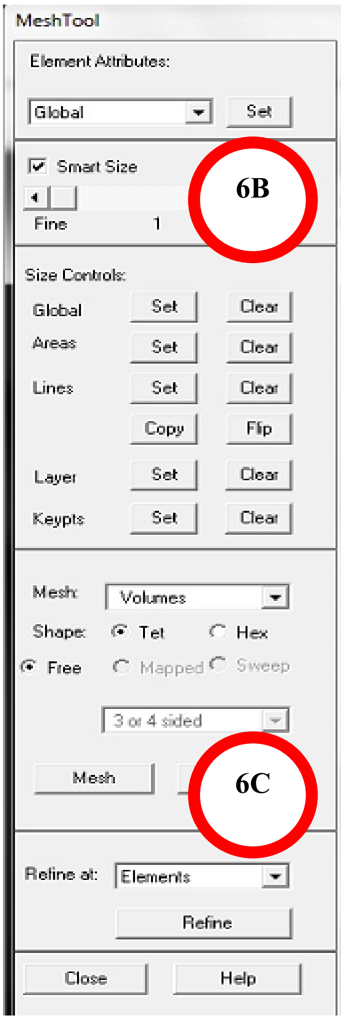

Figure 3.48: Mesh Tool Window

7. Upon obtaining the meshing of the targeted sample, save the database created by selecting Save_DB. Save_DB button is situated at the Ansys toolbar. This is shown in Figure 3.49.

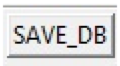

Figure 3.49: SAVE_DB Button

This step is important especially when the thermal structural analysis is carried out, the database of the meshed sample can be called again.

3.7 TRANSIENT THERMAL ANALYSIS SIMULATION SETTING

1. To create a new analysis of transient thermal analysis, the following procedure is observed.

Main Menu → Solution → Analysis Type → New Analysis → "Select Transient for the type of analysis." → Ok → "Select Full for the Solution Method."

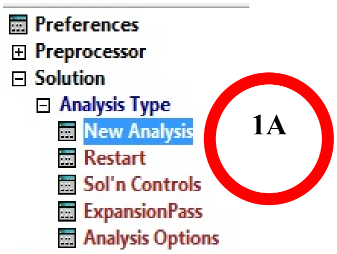

Figure 3.50: New Analysis Setting

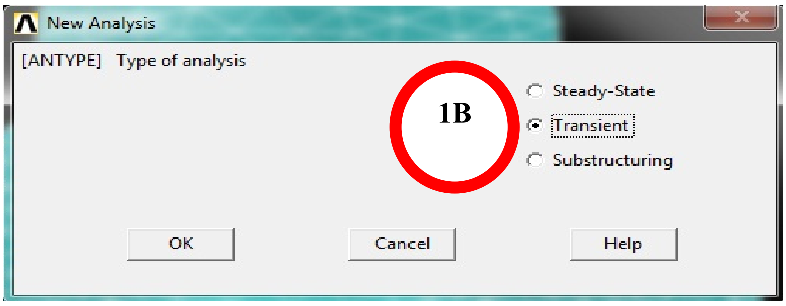

Figure 3.51: New Analysis Selection Window

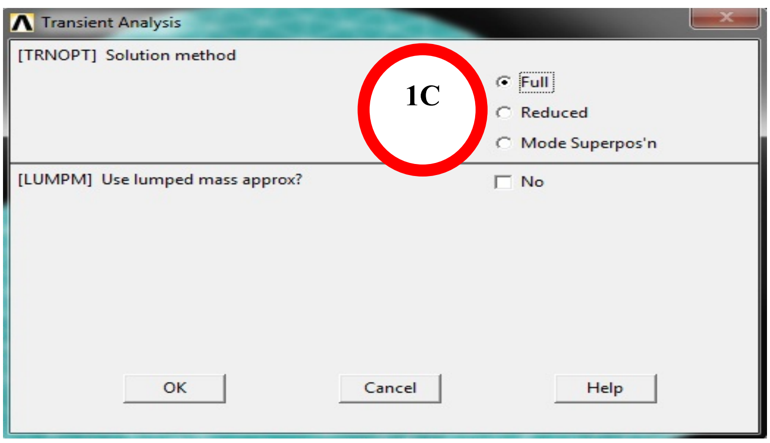

Figure 3.52: Transient Analysis Window

2. Solution control needs to be set also in this transient thermal analysis. The following procedure is observed.

Main Menu → Solution → Analysis Type → Sol'n Controls → "Set the configuration as shown in Figure 3.54." → Ok

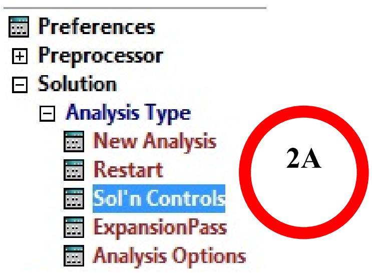

Figure 3.53: Solution Control Setting

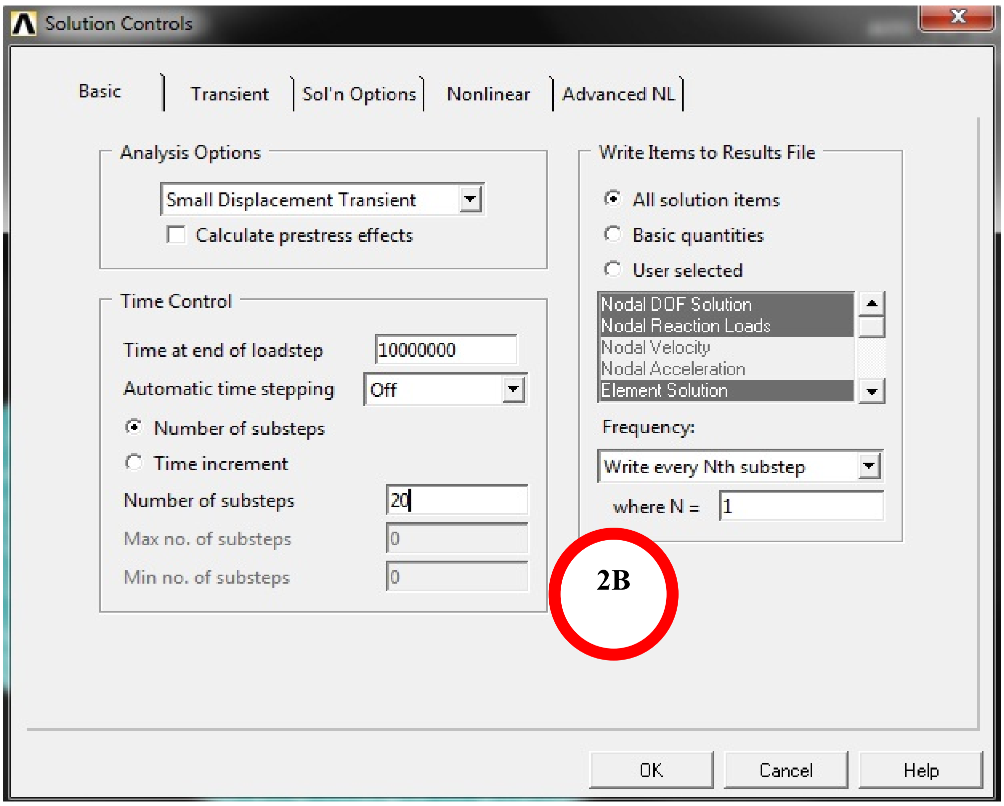

Figure 3.54: Solution Controls Window

3. The temperature on top and below of the sample is applied with the room temperature 27^{0}C so that the heat transfer from one layer to another is observed when the initial condition temperature is set to the brazing temperature of either 830^{0}C, 865^{0}C or 900^{0}C. The following procedure is observed.

Main Menu → Solution → Define Loads → Apply → Thermal → Temperature → On Areas → "Select the top and bottom area." → Ok → "Set the DOFs to be constrained to TEMP while the Load TEMP value is 27."

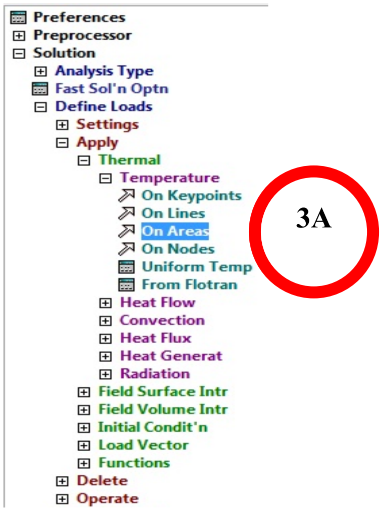

Figure 3.55: Temperature Constraint Applied Setting

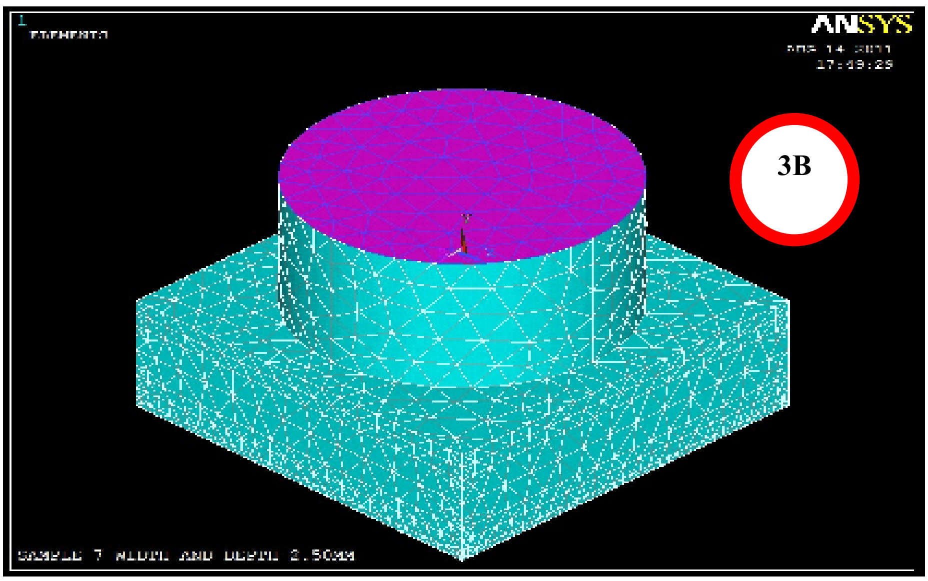

Figure 3.56: Area Selection for the Temperature Constraint Load

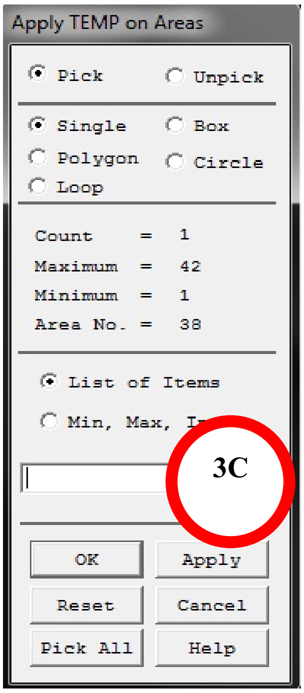

Figure 3.57: Applying Temperature on Areas

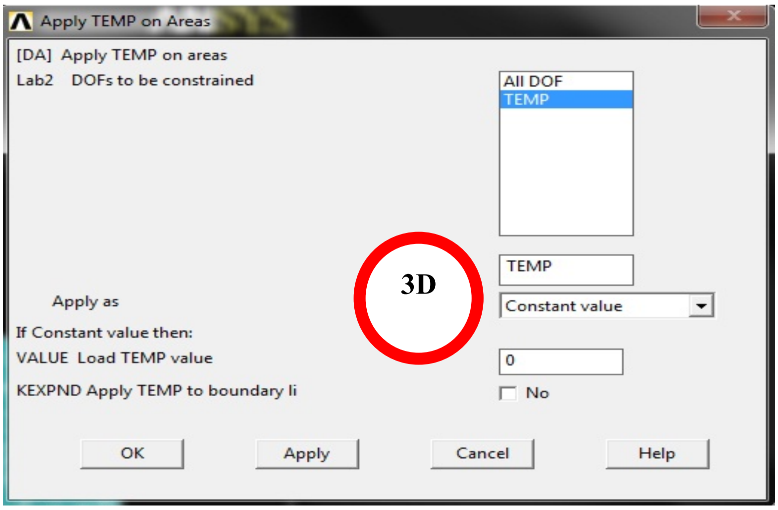

Figure 3.58: Applying Temperature on Areas 2

4. The natural convection need to be applied to sample model. The following procedure is observed.

Main Menu → Solution → Define Loads → Apply → Thermal → Convection → On Areas → "Select all the areas at the side of the sample model to be applied with natural *convection.” → Ok → “Set the value for Film coefficient to 2 while the bulk temperature is 27.”*

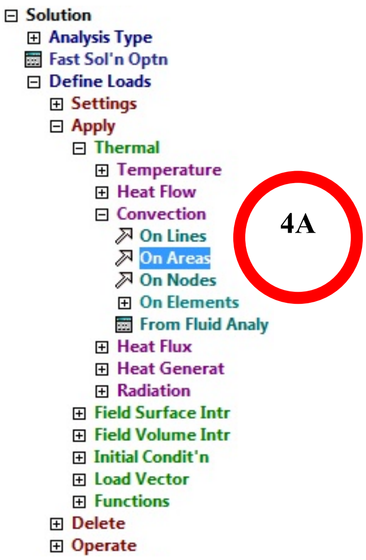

Figure 3.59: Applying Natural Convection Setting

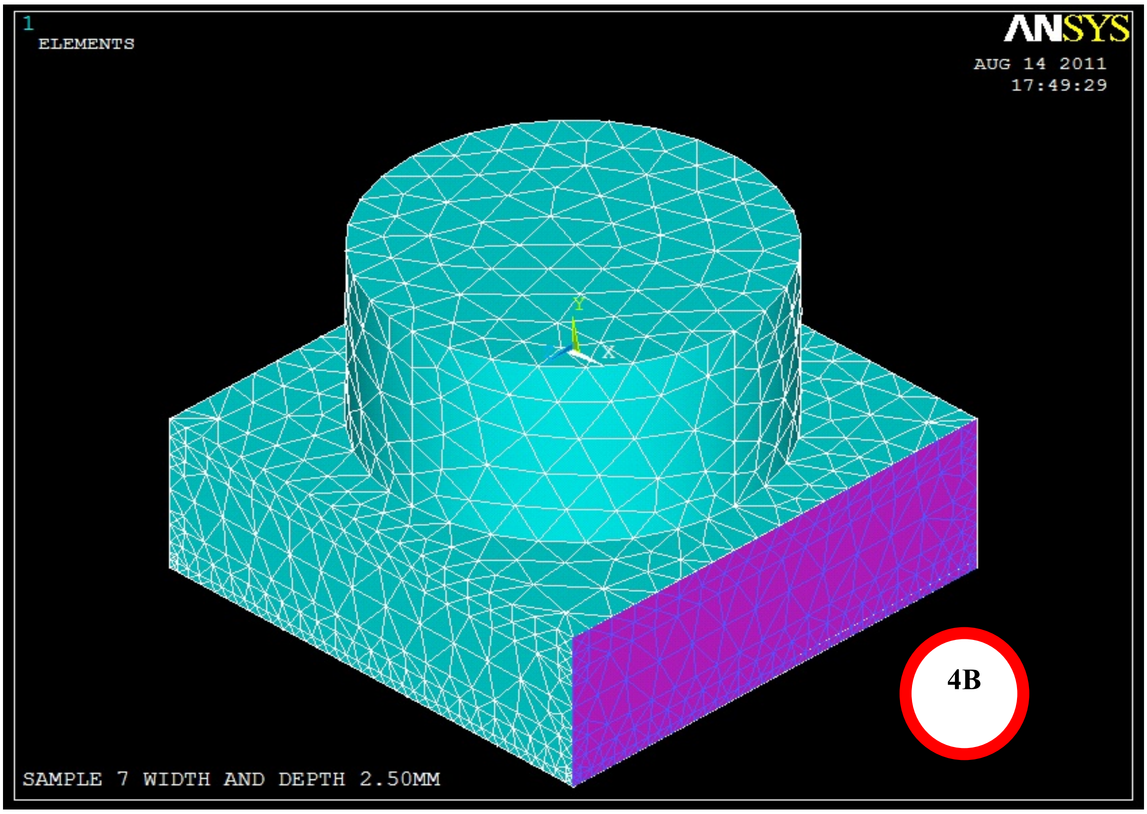

Figure 3.60: Area Selected to Apply Natural (Free) Convection

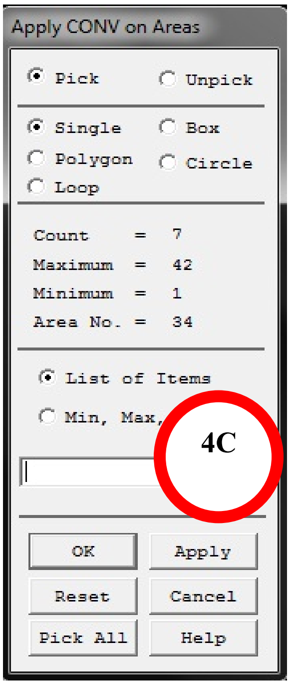

Figure 3.61: Applying Convection on Areas Window

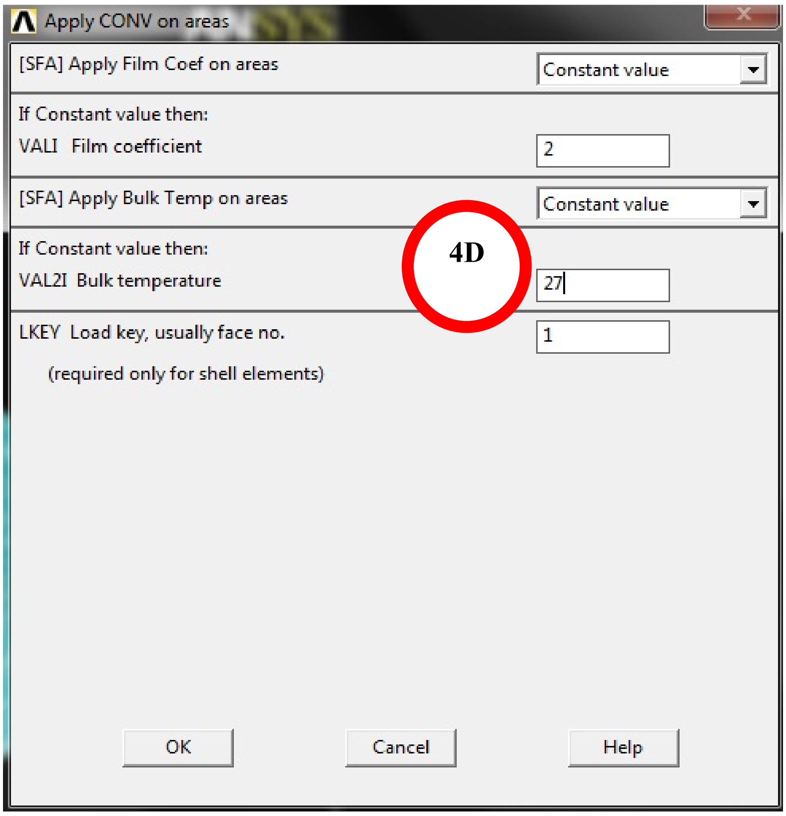

Figure 3.62: Applying Convection on Areas Window 2

5. Set the Heat Generation for the sample model as it is important when cooling down process. Heat generation in this research project can be considered as heat dissipation. The following procedure is observed.

Main Menu → Solution → Define Loads → Apply → Thermal → Heat Generation → On Volumes → "Select Pick All." → OK → "Set the Load HGEN value as -350." → Ok

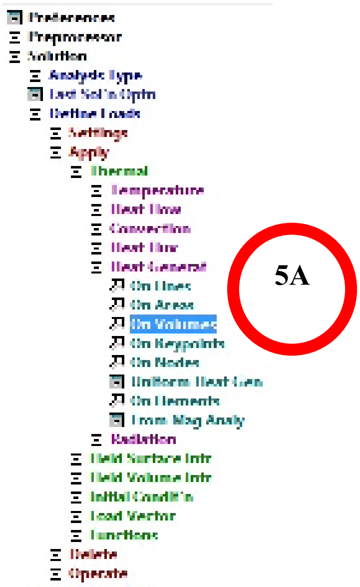

Figure 3.63: Defining Heat Generation on Volumes Step

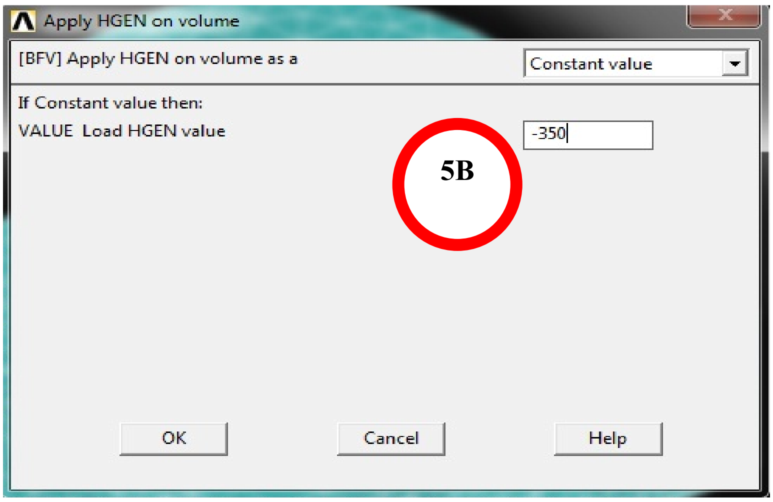

Figure 3.64: Applying Heat Generation Value Window

6. The initial condition of the sample model studied is set. The following procedure is observed.

Main Menu → Solution → Define Loads → Apply → Initial Condit'n → Define → Pick All → OK → "Set DOF to be specified to TEMP while Initial value of DOF is 900." → Ok

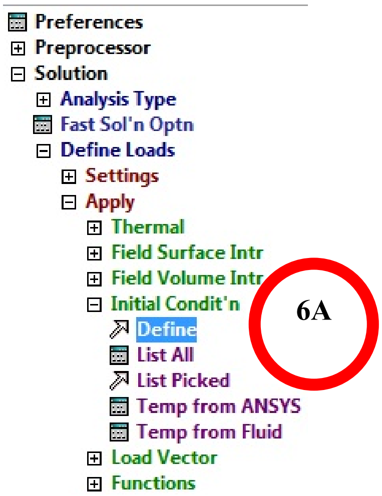

Figure 3.65: Defining Initial Condition Step

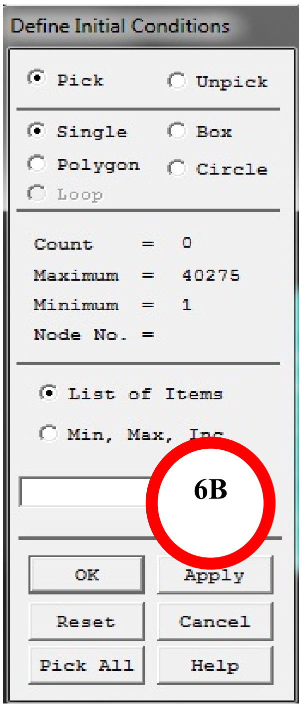

Figure 3.66: Define Initial Conditions Window

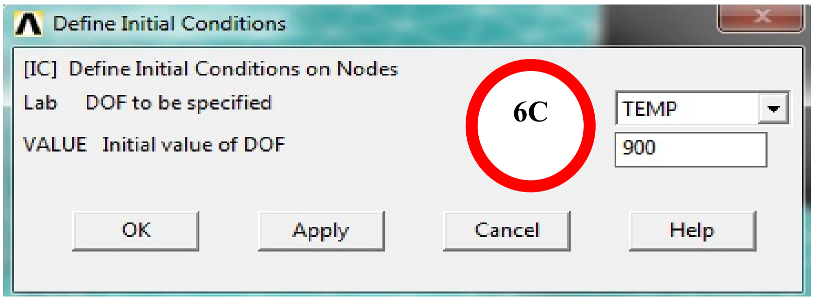

Figure 3.67: Define Initial Conditions Window 2

7. In order to obtain the results required from the settings set, the following procedure is observed.

Main Menu → Solution → Solve → Current LS.

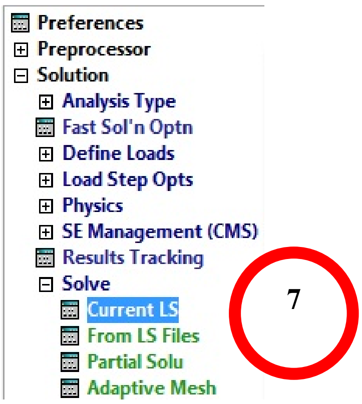

Figure 3.68: Solving Current LS Step

8. Select OK at the Solve Current Load Step window.

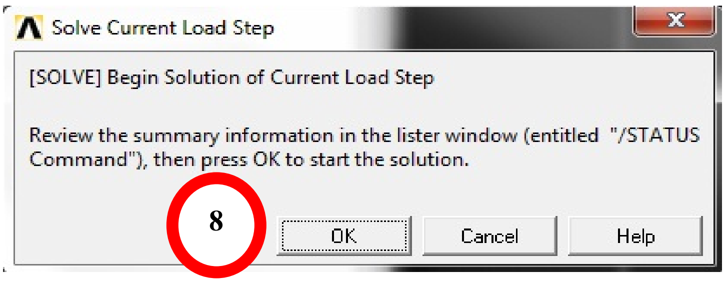

Figure 3.69: Solve Current Load Step Determination

9. Solution can be obtained when the Solution Done message appears.

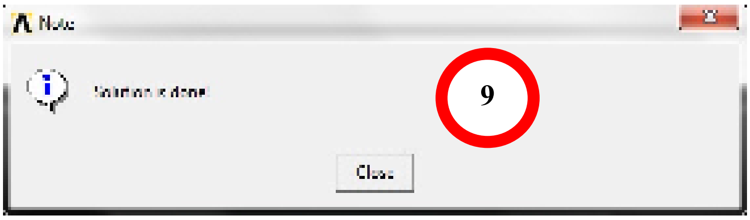

Figure 3.70: Solution Done Message

10. Postprocessing results are required in order to obtain the graph and also the list of temperature over the elapsed time. The following procedure is observed.

Main Menu → General Postproc → Read Results → By Pick → "Choose the necessary pick or the required pick in order to view the results."

11. *Main Menu → General Postproc →Plot results → Contour Plot → Nodal Solu*

12. *TimeHistPostpro → Select*  *→Nodal Solution → DOF solution → Nodal Temperature → OK → "Key in the node of interest, for example, node 8913." → Ok*

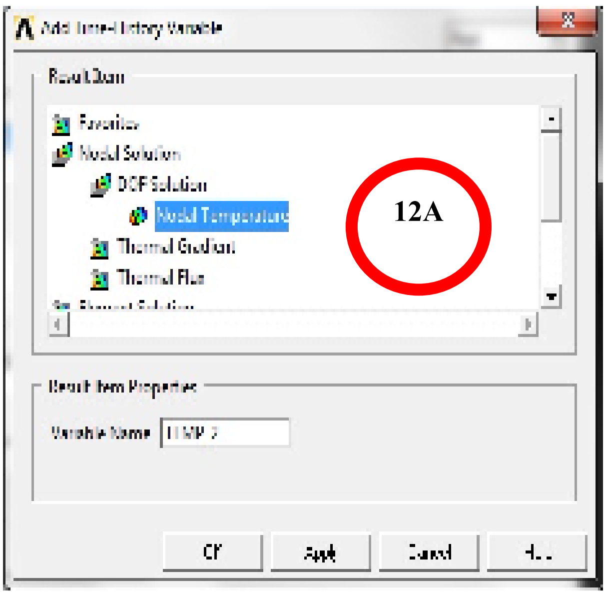

Figure 3.71: Add Time-History Variable Window

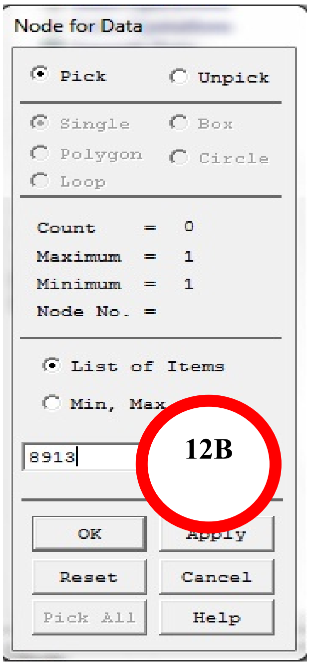

Figure 3.72: Node for Data Window

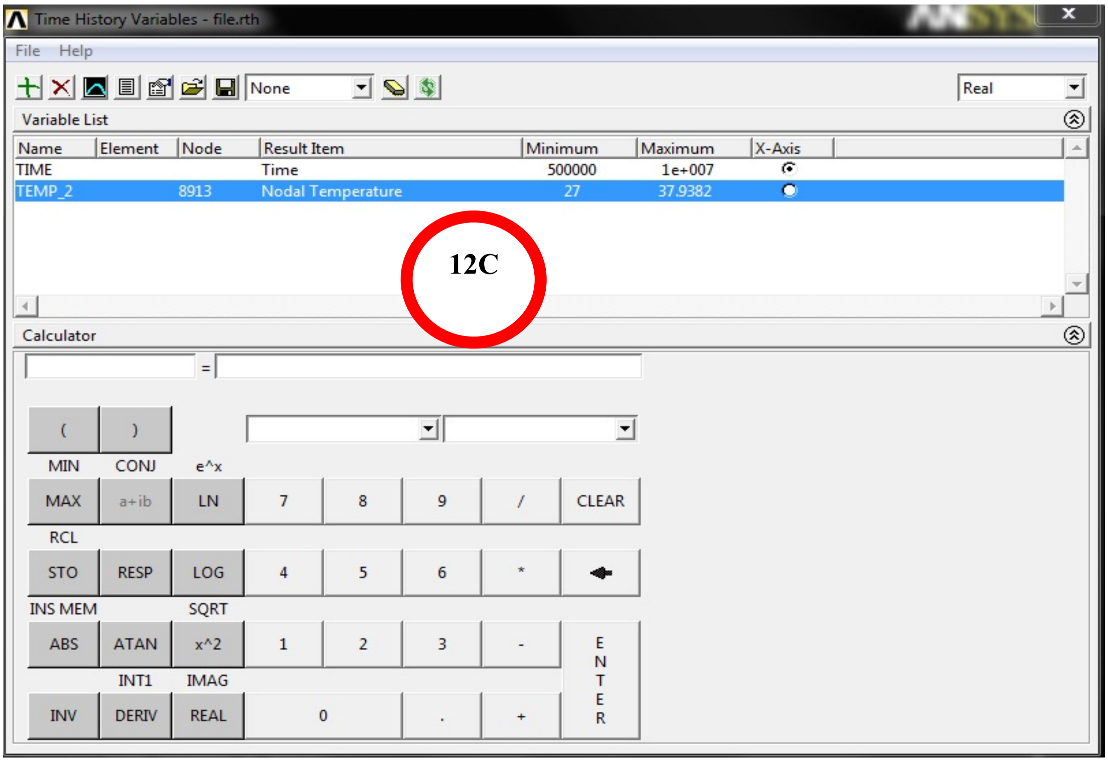

Figure 3.73: Time History Variables Window

13. In order to obtain the list of temperature over the elapsed time, the button  is pressed. The following output list is obtained.

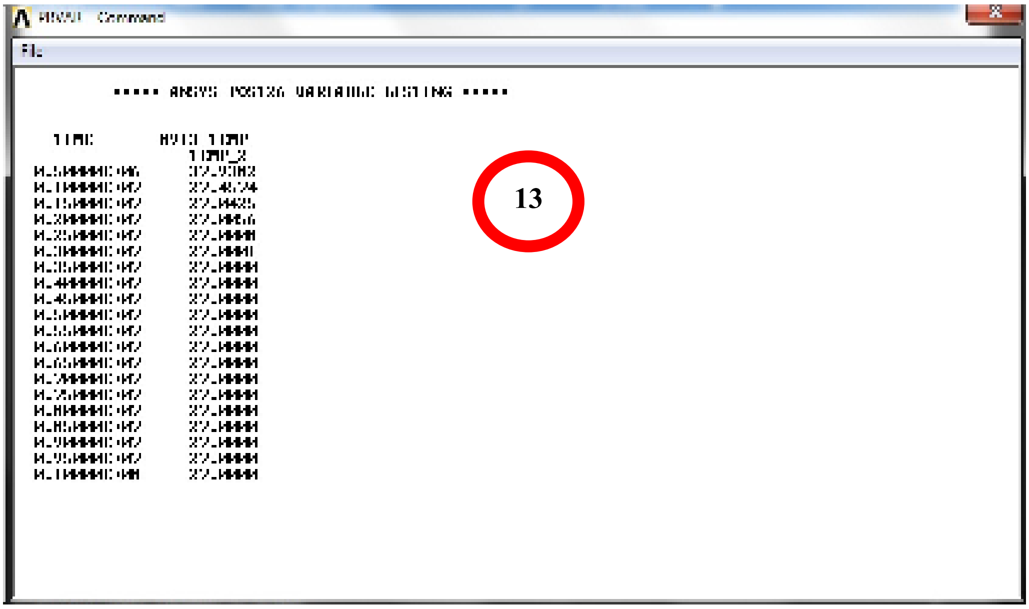

Figure 3.74: List of Temperature over Elapsed Time

14. In order to obtain the graph of temperature against the elapsed time, the button  is pressed. A graph is produced.

15. In the Axes Modifications for Graph Plots window, the X-axis label is changed to TIME while the Y-axis label is changed to TEMPERATURE. Then, select OK. When he mouse is adjusted so that to obtain the label for both x and y axes.

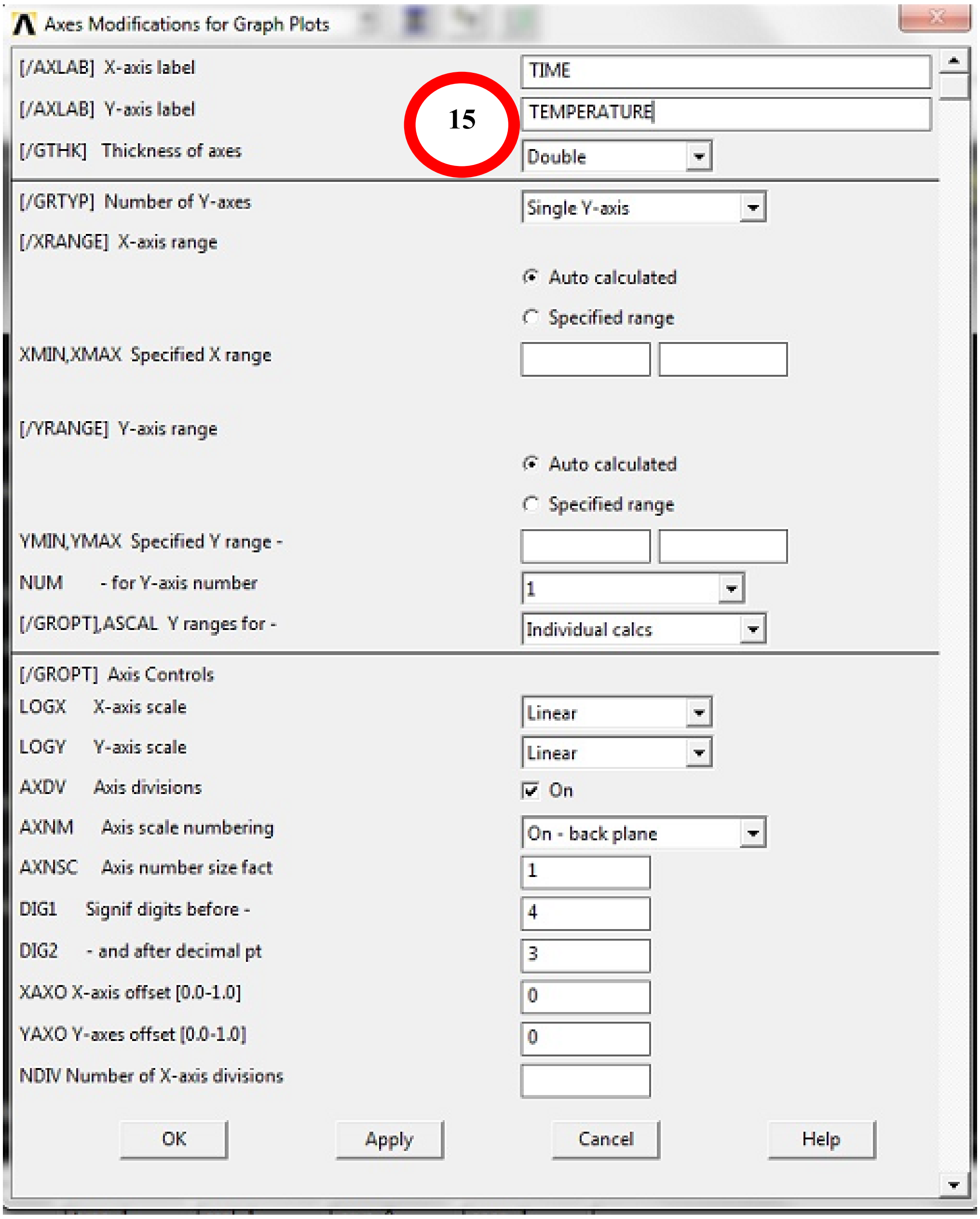

Figure 3.75: Axes Modifications for Graphs Plots Window

3.8 THERMAL STRUCTURAL ANALYSIS SIMULATION SETTING

1. Clear all of the file data that has been set previously in order to perform the thermal structural analysis simulation. This procedure is shown in Figure 3.76.

Utility Menu → File → Clear & Start New

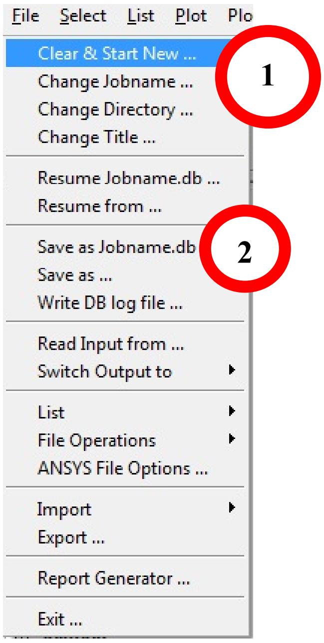

Figure 3.76: Starting a New File DB

2. Choose and call back the necessary db that has been saved previously. This procedure is shown in Figure 3.76.

Utility Menu → File → Resume From....

3. In this thermal structural simulation analysis, the element type of the material has to be redefined. This step is shown in Figure 3.77, 3.78 and 3.79.

Main Menu → Preprocessor → Element Type → Add/ Edit/Delete → Add → Structural Mass library → Solid → 10node 187

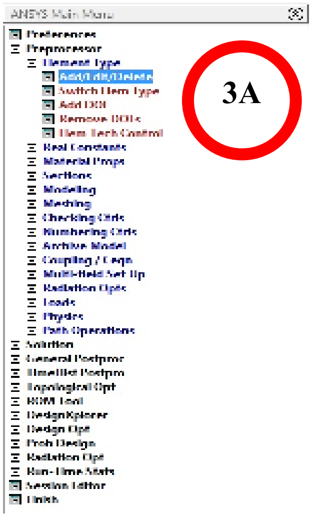

Figure 3.77: Applying Element Type Setting

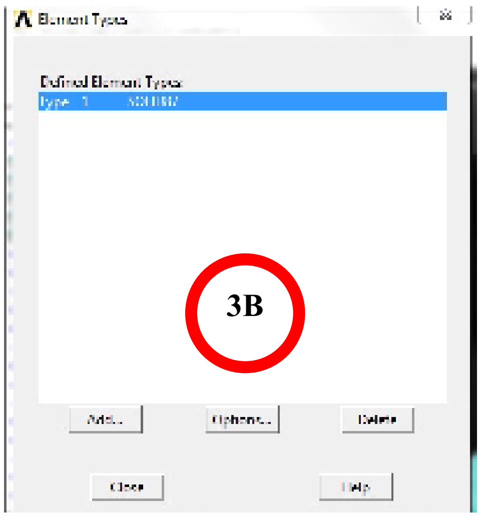

Figure 3.78: Applying Element Type Window

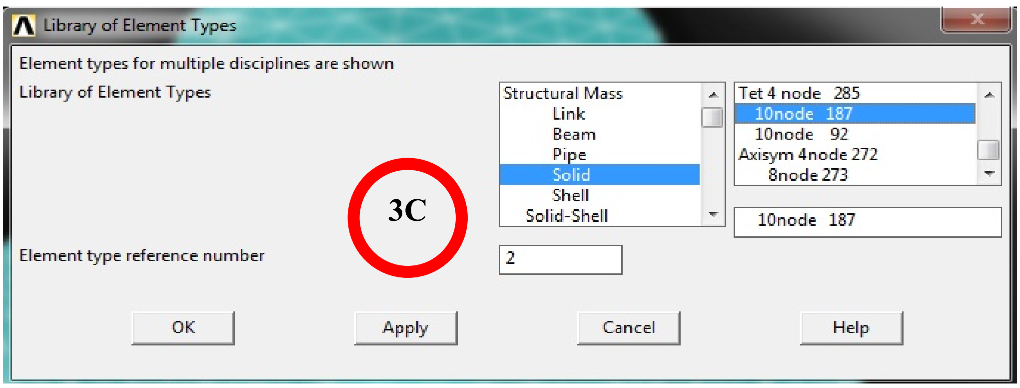

Figure 3.79: Library of Element Types Window

4. Modify the attributes of the sample model element. This procedure is shown in Figure 3.80 and 3.81.

Main Menu → Preprocessor → Modelling → Move/Modify → Elements → Modify Attrib → Pick All

Figure 3.80: Modifying Attributes Setting

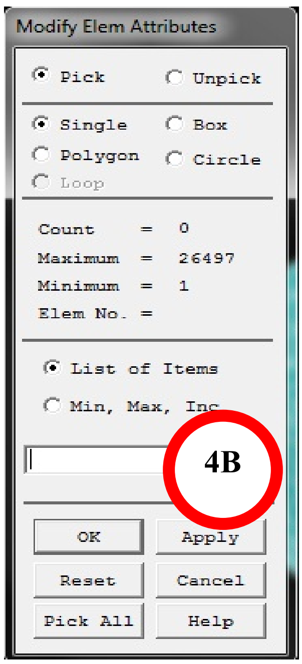

Figure 3.81: Modify Element Attributes Window

In the Modify Elem Attributes window as shown in Figure 3.82, the Attribute to change and New attribute number is changed accordingly. Then, select OK.

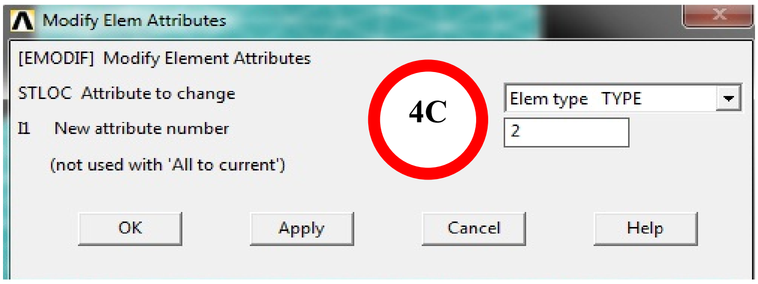

Figure 3.82: Modification of Element Attributes

5. Type of analysis is set and this step is shown in Figure 3.83.

Main Menu → Solution → Analysis Type → New Analysis → Static → OK

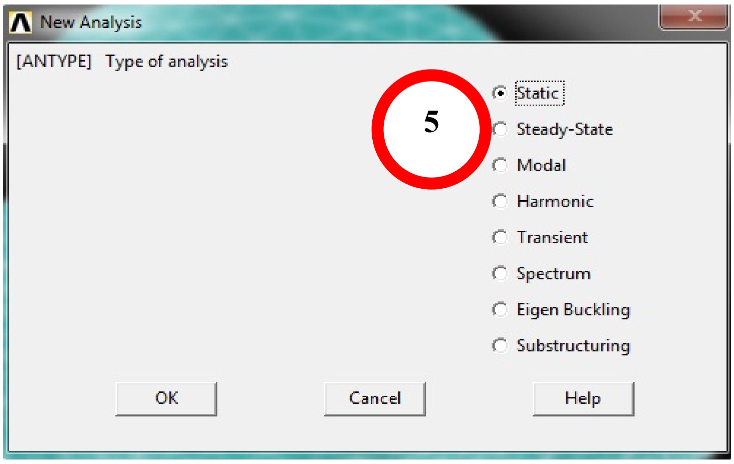

Figure 3.83: New Analysis Setting Window

6. The reference temperature has to be configured so that the results and output obtained will be referred to the reference temperature configured. In this research project, the room temperature of 27^0C is considered as the room temperature. This step is shown in Figure 3.84 and 3.85.

Main Menu → Solution → Define Loads → Settings → Reference Temp

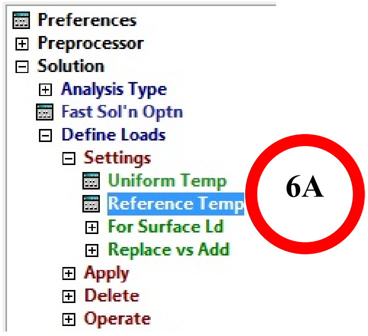

Figure 3.84: Reference Temperature Setting

In the Reference Temperature window, the room temperature of 27^0C is set as shown in Figure 3.85.

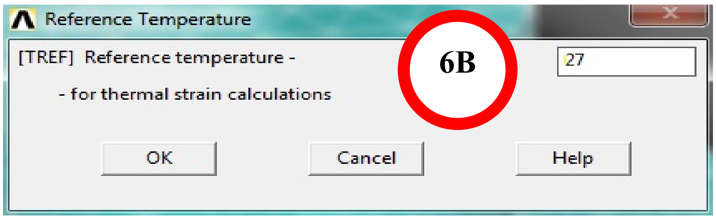

Figure 3.85: Reference Temperature Window

7. The load displacement for this sample model has to be set in this configuration. In this research project, the top are and the bottom area are selected and 0 displacements for all the degree of freedoms is configured. The reason for this setting is that during the experimental brazing process, the top and bottom parts of the sample are clamped properly but not too tight before locating the sample in the brazing furnace. This step is shown in Figure 3.86, 3.87 and 3.88.

Main Menu → Solution → Define Loads → Apply → Structural → Displacement → On Areas → "Select the top and bottom area of the sample." → Ok

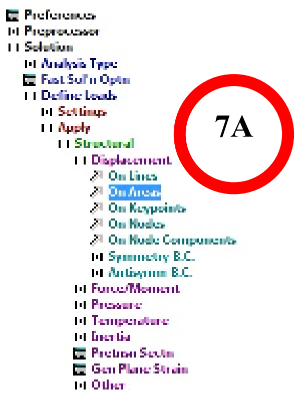

Figure 3.86: Apply Load on Areas

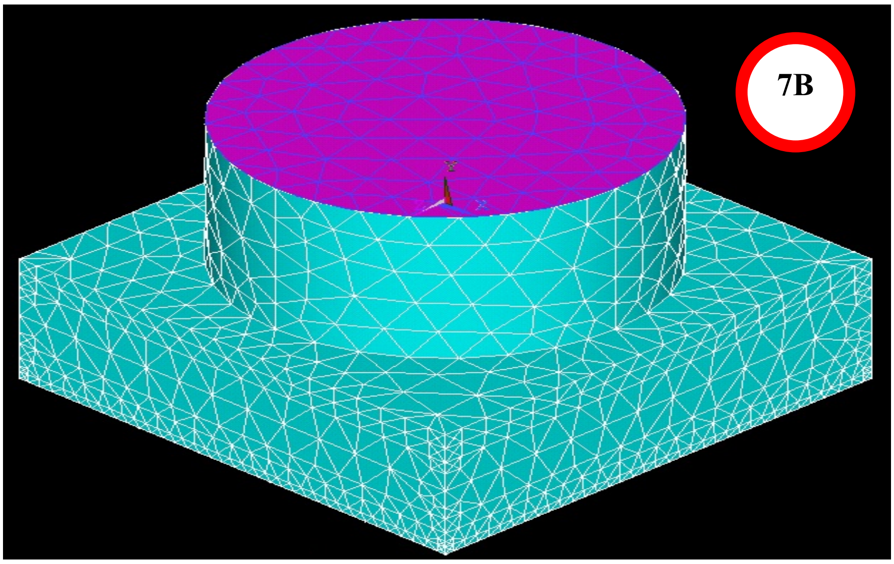

Figure 3.87: Area to be Constrained

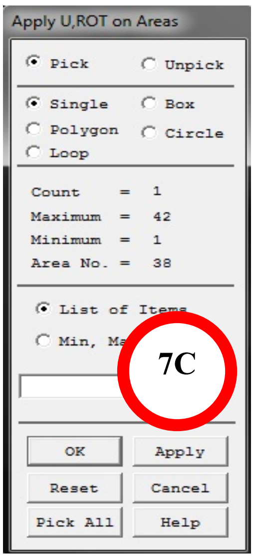

Figure 3.88: Apply on Areas Window

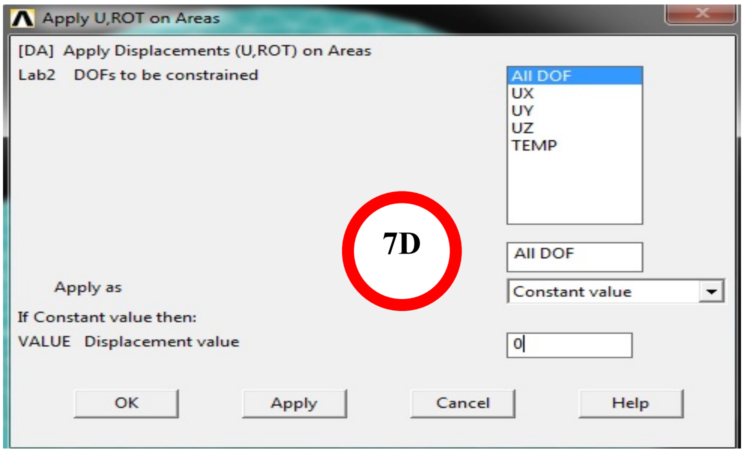

Figure 3.89: Displacements Constraint Window

8. In order to perform the thermal structural analysis, the temperature results from the transient thermal analysis are called. The load step and substep no have to set according to pick set that have been studied in the transient thermal analysis. This is shown in Figure 3.90.

Main Menu → Solution → Define Loads → Apply → Structural → Temperature → From Thermal Analysis → "Set the Load step and substep no." → "Call back the Name of results file which is in rth format." → OK

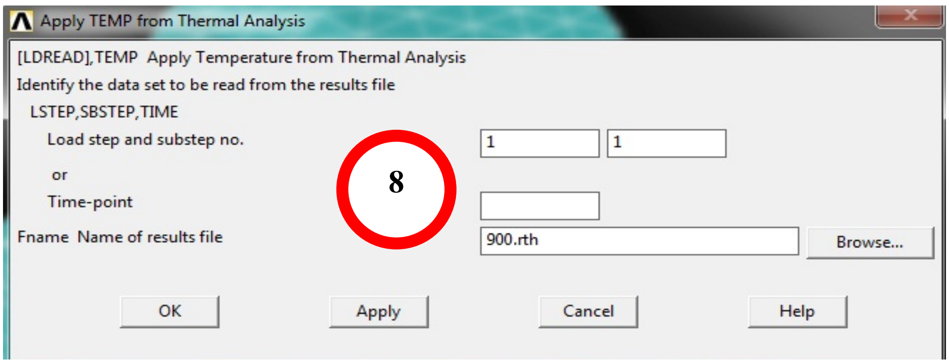

Figure 3.90: Apply Temperature from Transient Thermal Analysis Results

9. Upon configuring all loads and the necessary settings, the solutions are obtained by clicking on the solving the Current LS. This is shown in Figure 3.91.

Main Menu → Solution → Solve → Current LS

The information in the status window is reviewed and checked. Select Ok in order to start the solution process. When the solution is done, the window of solution completion notification is closed.

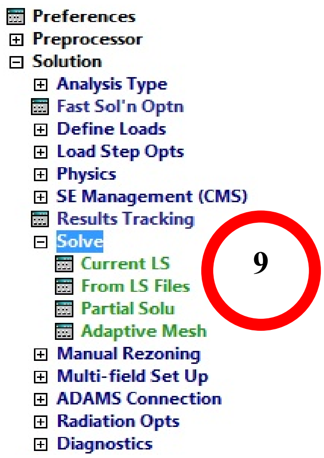

Figure 3.91: Solving Solution Current LS

10. The steps of 8 and 9 are repeated in order to obtain the results for other set of picks.

11. In order to obtain the deformed shape plot, the following settings are configured.

Main Menu → General Postproc → Plot Results → Deformed Shape → "Select Def shape only." → OK

12. In order to obtain the plot of Von Mises equivalent stress results, the following steps are configured.

Main Menu → General Postproc → Plot Results → Contour Plot → Nodal Solu → Stress → Von Mises stress → Ok

13. In order to start another analysis, the step 1 is repeated.

CHAPTER 4

RESULTS AND DISCUSSION

4.1 INTRODUCTION

In this research project, the brazing model sample is modelled according to the dimensions provided by the Doctoral research student. The sample model consists of the following:

(a) Inconel 600

(b) Sapphire

(c) Copper

(d) Nickel

(e) Brazing filler BAg-8-Ti.

The sequence of the arrangement of the brazing sample model is discussed in Chapter 3 Methodology. The brazing sample model is analyzed when it is cooling down from the brazing temperature to room temperature, 27^0C. With refer to Figure 4.1, only the cooling cycle C is analyzed for the residual stress occur due to the high brazing temperature and also the difference of coefficient of temperatures of different types of material. Region A of Figure 4.1 indicates the heating of the sample model until the necessary brazing temperature is achieved. The brazing temperatures suggested are 830^0C, 865^0C and 900^0C. Region B indicates that the brazing process cycle has taken place. The brazing temperature is maintained in the region B. Nevertheless, in this research project, the cooling cycle C is studied and simulated for the residual stress results. This is mentioned in the scope and limitations in Chapter 1.

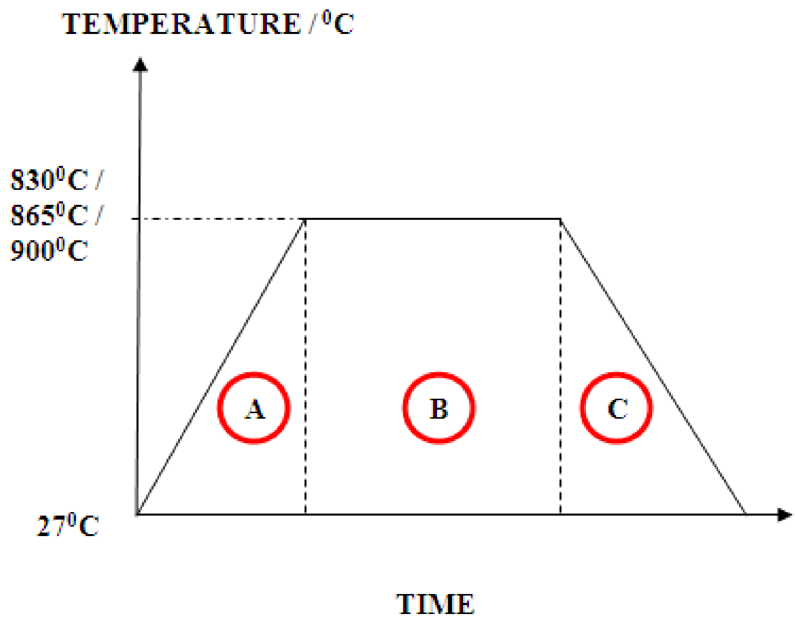

Figure 4.1: Graph of Temperature vs Time in the Brazing Process of Inconel 600 and Sapphire

Upon completing the sample modelling, the model is then configured for its necessary setting in order to visualize the experimental brazing condition. In the transient thermal analysis, the top and bottom area are applied with the temperature of 27^{0}C in order to visualize the cooling process from the brazing temperature. Thus, the initial condition of the sample model is set to the brazing temperature of 830^{0}C, 865^{0}C or 900^{0}C. In the actual brazing experimental, the sample model is placed in the vacuum brazing furnace. Though it is a vacuum condition, the sample model will still experience natural or free convection of h = 2 W/m^2.^{0}C in order for the sample to reduce its temperature from the initial brazing temperature. In another words, the sample model experiences natural convection during the cooling process cycle. Thus, the convection is applied at all the side area of the sample model. Heat generation is also applied in the simulation in order to visualize the actual experimental condition. As for the thermal-structural analysis, the sample model is constrained, at all degrees of freedom, at the top and bottom area of the sample model. This constraint is applied in order to visualize the actual brazing condition whereby the sample model is clamped. Also, the reference temperature has to be set to the room temperature, 27^0C, so that the Von Mises plot and also the deformation shape will be based on the room temperature.

The sample is then simulated for thermal mechanical analysis whereby it is categorised into two analyses. The analyses are transient thermal analysis and thermal-structural analysis. In transient thermal analysis, the heat conduction between interlayer can be observed by studying the heat distribution contour plot. The thermal-structural analysis is subsequently carried out upon completing the transient thermal analysis. In the thermal-structural analysis, the stresses can be observed when the sample model is simulated to cool down to room temperature from the initial brazing temperature condition. The stress distribution can be obtained by referring to Von Mises contour plot. The values indicated are in MPa unit. The values are then compared with the yield strength of each of the material used in this brazing sample model. At room temperature, residual stress is said to have taken place if the stress value in the Von Mises stress exceeds the yield strength of the particular material.

4.2 CONVERGEANCE TEST

The importance on this convergence test is to determine the mesh size control which produce the most accurate result of residual stress.

4.2.1 Comparison in Meshing of the Sample Model

Figure 4.2, 4.3, 4.4, 4.5, 4.6 and 4.7 display the meshing of the sample model. It is noticeable that the meshing element is getting finer as the mesh smart size is getting smaller from mesh smart size of 6 to 1. Likewise, the meshing element is getting coarser as the mesh smart size is getting bigger from mesh smart size of 1 to 6. The fine or coarse of the element smart size used has to be determined by referring to the transient thermal analysis nodal plot.

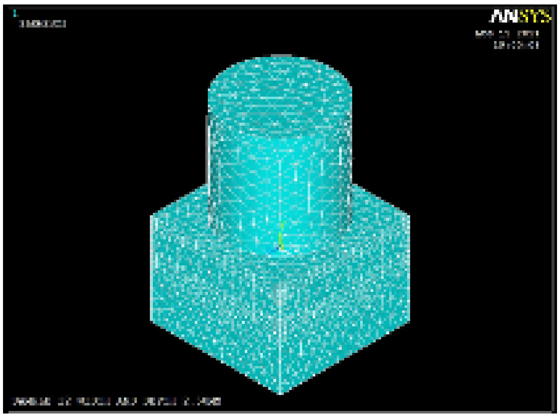

Figure 4.2: Meshing at Mesh Smart Size Control 1

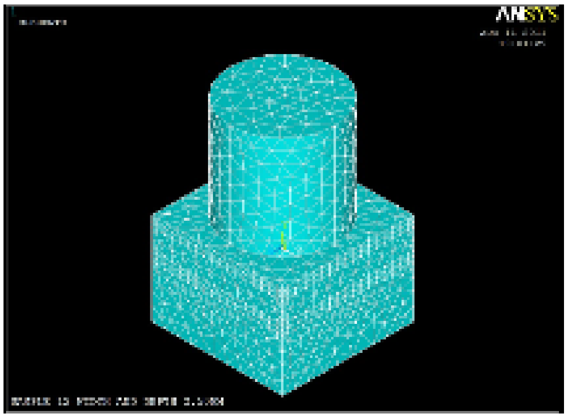

Figure 4.3: Meshing at Mesh Smart Size Control 2

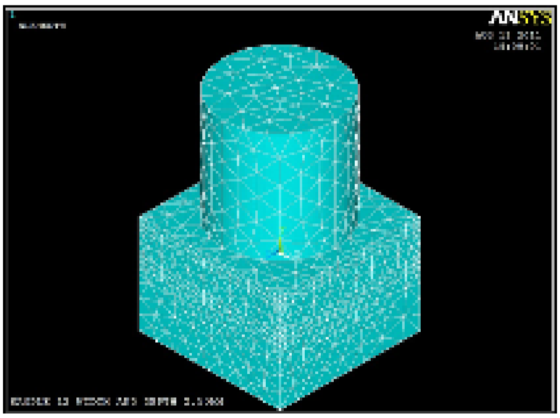

Figure 4.4: Meshing at Mesh Smart Size Control 3

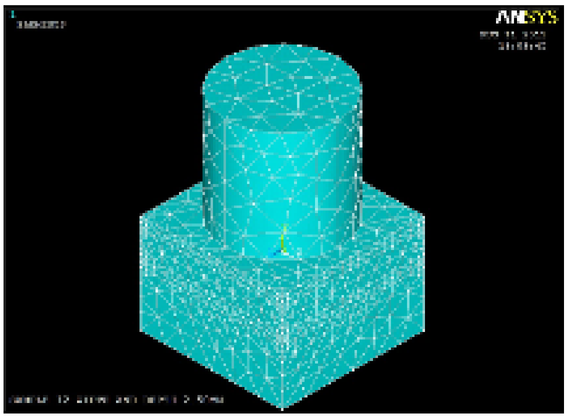

Figure 4.5: Meshing at Mesh Smart Size Control 4

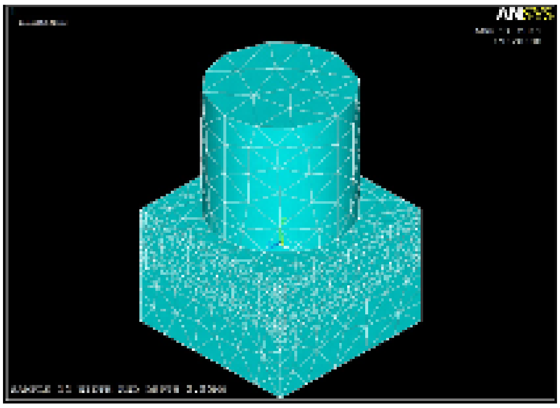

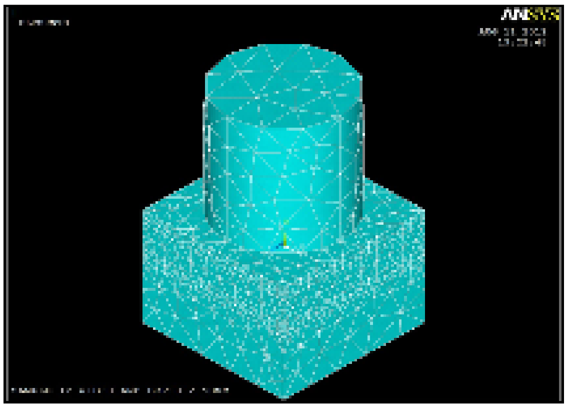

Figure 4.6: Meshing at Mesh Smart Size Control 5

Figure 4.7: Meshing at Mesh Smart Size Control 6

4.2.2 Heat Conduction between Interlayer Nodal Plot

Figures 4.9 to 4.13 display the heat conduction between interlayer nodal plot at meshing smart size control 1, 2, 3, 4, 5 and 6 respectively. It is noticeable that the heat distribution contour is getting rougher as the mesh smart size control is getting coarser. This is due to the size of the meshing element. The finer the mesh smart size, the smoother the heat conduction contour nodal plot. Likewise, the coarser the mesh smart size, the rougher the heat conduction contour nodal plot.

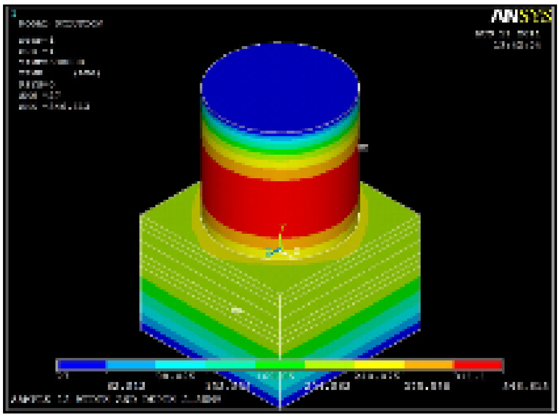

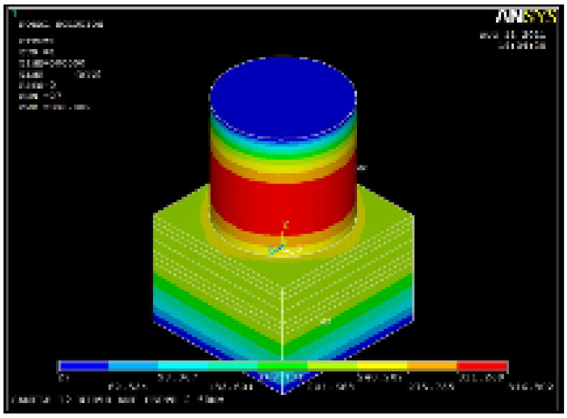

Figure 4.8: Heat Distribution Plot at Mesh Smart Size Control 1

Figure 4.9: Heat Distribution Plot at Mesh Smart Size Control 2

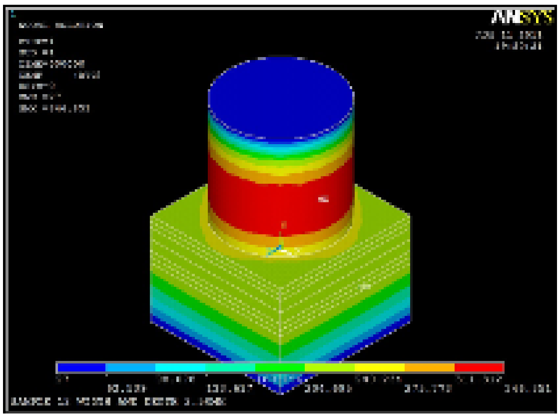

Figure 4.10: Heat Distribution Plot at Mesh Smart Size Control 3

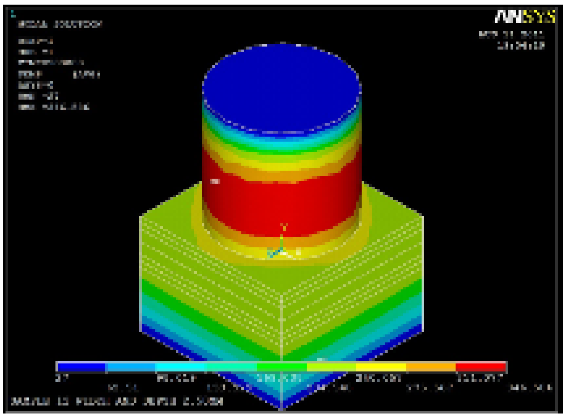

Figure 4.11: Heat Distribution Plot at Mesh Smart Size Control 4

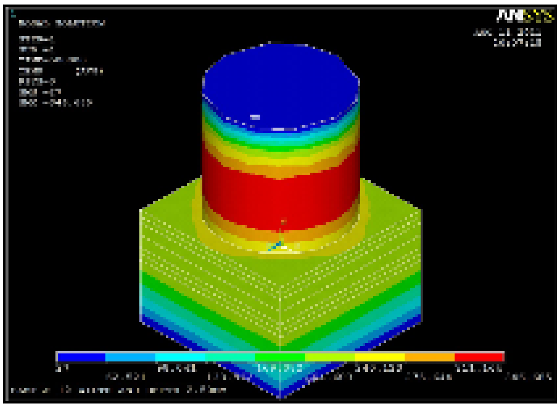

Figure 4.12: Heat Distribution Plot at Mesh Smart Size Control 5

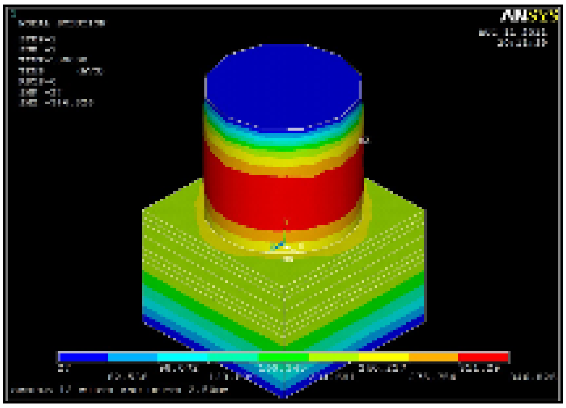

Figure 4.13: Heat Distribution Plot at Mesh Smart Size Control 6

4.2.3 Time for Temperature Decrease to 27^0C (Room Temperature)

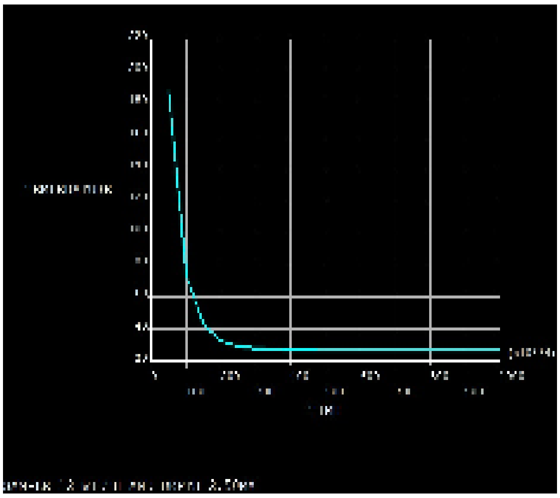

Figure 4.14: Temperature vs Time (In Load Step) Plot for Mesh Smart Size Control 1

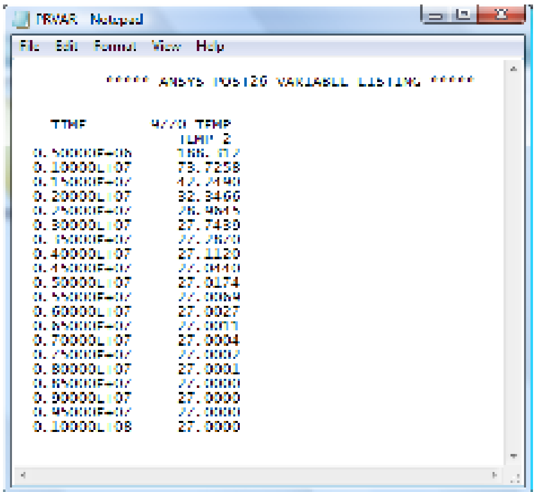

***** ANSYS POST26 VARIABLE LISTING *****

TIME	TEMP 2
[illegible]	[illegible]
0.10000E+07	73.7258
[illegible]	[illegible]
0.20000E+07	32.3466
[illegible]	[illegible]
0.30000E+07	27.7430
[illegible]	[illegible]
0.40000E+07	27.1120
[illegible]	[illegible]
0.50000E+07	27.0174
[illegible]	[illegible]
0.60000E+07	27.0027
[illegible]	[illegible]
0.70000E+07	27.0004
[illegible]	[illegible]
0.80000E+07	27.0001
[illegible]	[illegible]
0.90000E+07	27.0000
[illegible]	[illegible]
0.10000E+08	27.0000

Figure 4.15: List of Time and Temperature for Mesh Smart Size Control 1

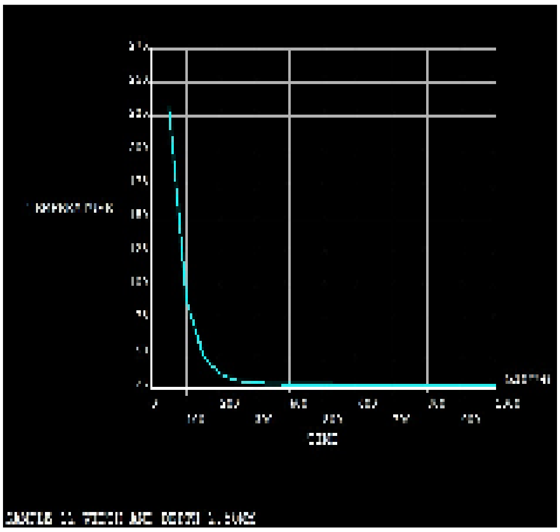

Figure 4.16: Temperature vs Time (In Load Step) Plot for Mesh Smart Size Control 2

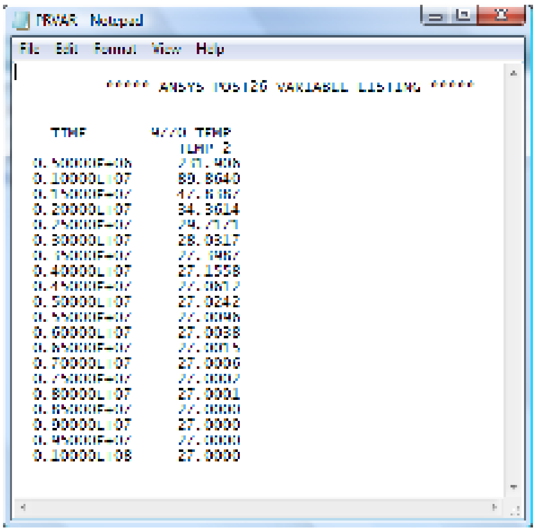

TRVAR - Notepad

File Edit Format View Help

***** ANSYS POST26 VARIABLE LISTING *****

TIME	TEMP 2
[illegible]	[illegible]
0.10000E+07	89.8640
[illegible]	[illegible]
0.20000E+07	34.3614
[illegible]	[illegible]
0.30000E+07	28.0317
[illegible]	[illegible]
0.40000E+07	27.1558
[illegible]	[illegible]
0.50000E+07	27.0242
[illegible]	[illegible]
0.60000E+07	27.0038
[illegible]	[illegible]
0.70000E+07	27.0006
[illegible]	[illegible]
0.80000E+07	27.0001
[illegible]	[illegible]
0.90000E+07	27.0000
[illegible]	[illegible]
0.10000E+08	27.0000

Figure 4.17: List of Time and Temperature for Mesh Smart Size Control 2

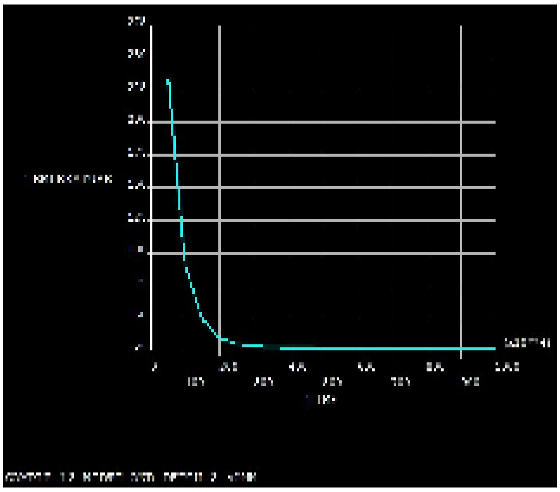

Figure 4.18: Temperature vs Time (In Load Step) Plot for Mesh Smart Size Control 3

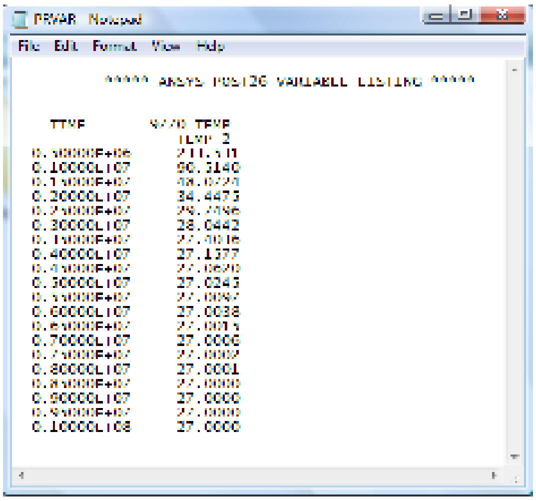

TRVAR - Notepad

File Edit Format View Help

***** ANSYS POST26 VARIABLE LISTING *****

TIME	TEMP 2
[illegible]	[illegible]
0.10000E+07	90.3140
[illegible]	[illegible]
0.20000E+07	34.4473
[illegible]	[illegible]
0.30000E+07	28.0442
[illegible]	[illegible]
0.40000E+07	27.1377
[illegible]	[illegible]
0.50000E+07	27.0243
[illegible]	[illegible]
0.60000E+07	27.0038
[illegible]	[illegible]
0.70000E+07	27.0006
[illegible]	[illegible]
0.80000E+07	27.0001
[illegible]	[illegible]
0.90000E+07	27.0000
[illegible]	[illegible]
0.10000E+08	27.0000

Figure 4.19: List of Time and Temperature for Mesh Smart Size Control 3

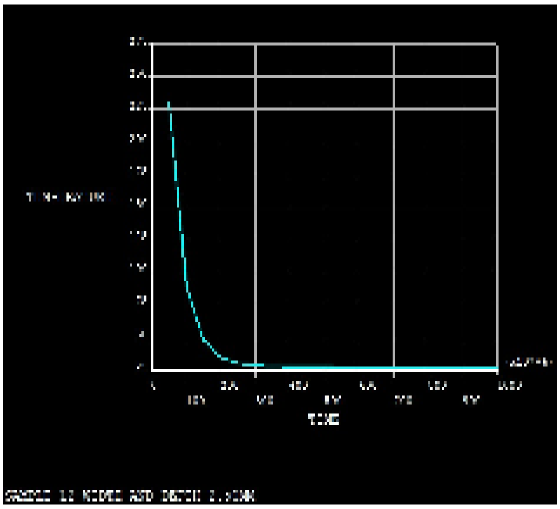

Figure 4.20: Temperature vs Time (In Load Step) Plot for Mesh Smart Size Control 4

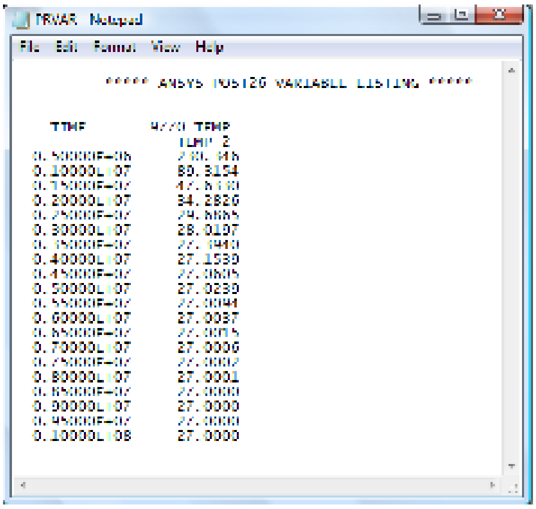

TRVAR - Notepad

File Edit Format View Help

***** ANSYS POST26 VARIABLE LISTING *****

TIME	TEMP 2
[illegible]	[illegible]
0.10000E+07	89.3154
[illegible]	[illegible]
0.20000E+07	34.2826
[illegible]	[illegible]
0.30000E+07	28.0197
[illegible]	[illegible]
0.40000E+07	27.1539
[illegible]	[illegible]
0.50000E+07	27.0239
[illegible]	[illegible]
0.60000E+07	27.0037
[illegible]	[illegible]
0.70000E+07	27.0006
[illegible]	[illegible]
0.80000E+07	27.0001
[illegible]	[illegible]
0.90000E+07	27.0000
[illegible]	[illegible]
0.10000E+08	27.0000

Figure 4.21: List of Time and Temperature for Mesh Smart Size Control 4

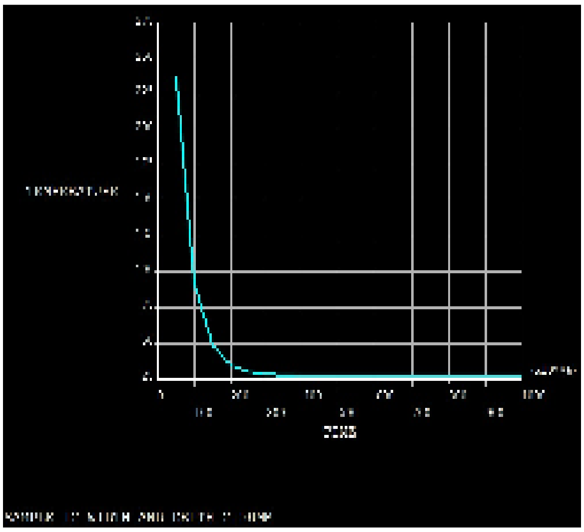

Figure 4.22: Temperature vs Time (In Load Step) Plot for Mesh Smart Size Control 5

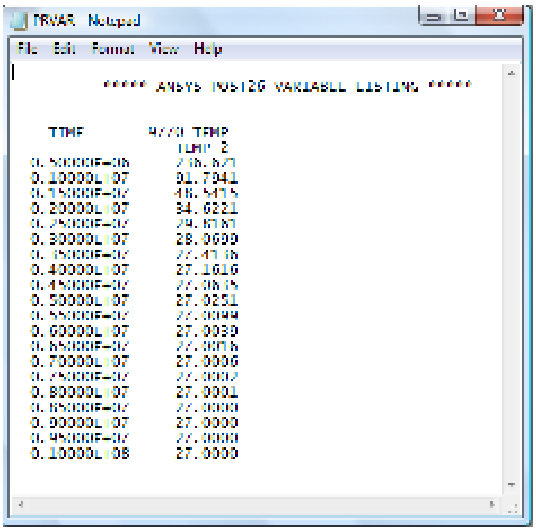

***** ANSYS POST26 VARIABLE LISTING *****

TIME	9770 TEMP TEMP_2
[illegible]	[illegible]
0.10000E+07	91.7941
[illegible]	[illegible]
0.20000E+07	34.6221
[illegible]	[illegible]
0.30000E+07	28.0609
[illegible]	[illegible]
0.40000E+07	27.1616
[illegible]	[illegible]
0.50000E+07	27.0251
[illegible]	[illegible]
0.60000E+07	27.0039
[illegible]	[illegible]
0.70000E+07	27.0006
[illegible]	[illegible]
0.80000E+07	27.0001
[illegible]	[illegible]
0.90000E+07	27.0000
[illegible]	[illegible]
0.10000E+08	27.0000

Figure 4.23: List of Time and Temperature for Mesh Smart Size Control 5

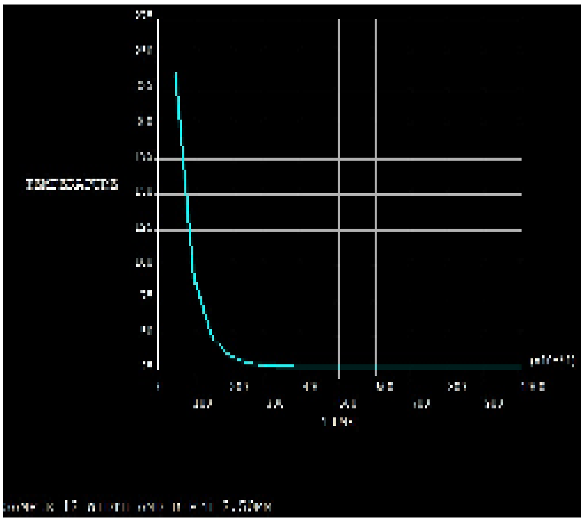

Figure 4.24: Temperature vs Time (In Load Step) Plot for Mesh Smart Size Control 6

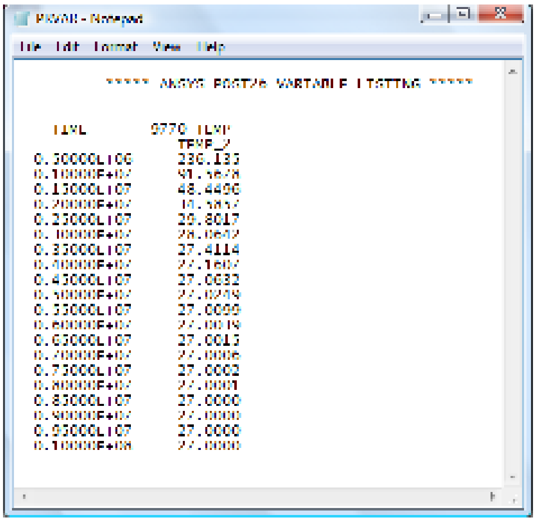

***** ANSYS POST26 VARIABLE LISTING *****

TIME	9770 TEMP TEMP_2
0.50000E+06	236.133
[illegible]	[illegible]
0.15000E+07	48.4496
[illegible]	[illegible]
0.25000E+07	29.8017
[illegible]	[illegible]
0.35000E+07	27.4114
[illegible]	[illegible]
0.45000E+07	27.0632
[illegible]	[illegible]
0.55000E+07	27.0099
[illegible]	[illegible]
0.65000E+07	27.0013
[illegible]	[illegible]
0.75000E+07	27.0002
[illegible]	[illegible]
0.85000E+07	27.0000
[illegible]	[illegible]
0.95000E+07	27.0000
[illegible]	[illegible]

Figure 4.25: List of Time and Temperature for Mesh Smart Size Control 6

Figures 4.15 to 4.29 display the plot of temperature vs time (in load step) for different mesh sizes and its respective list of time and temperature. From Figure 4.15 to 4.19, the time (in load step) to reduce to the room temperature is observed. The figures can be seen in the plot of time (in load steps) to decrease to room temperature vs mesh smart size control as in Figure 4.26.

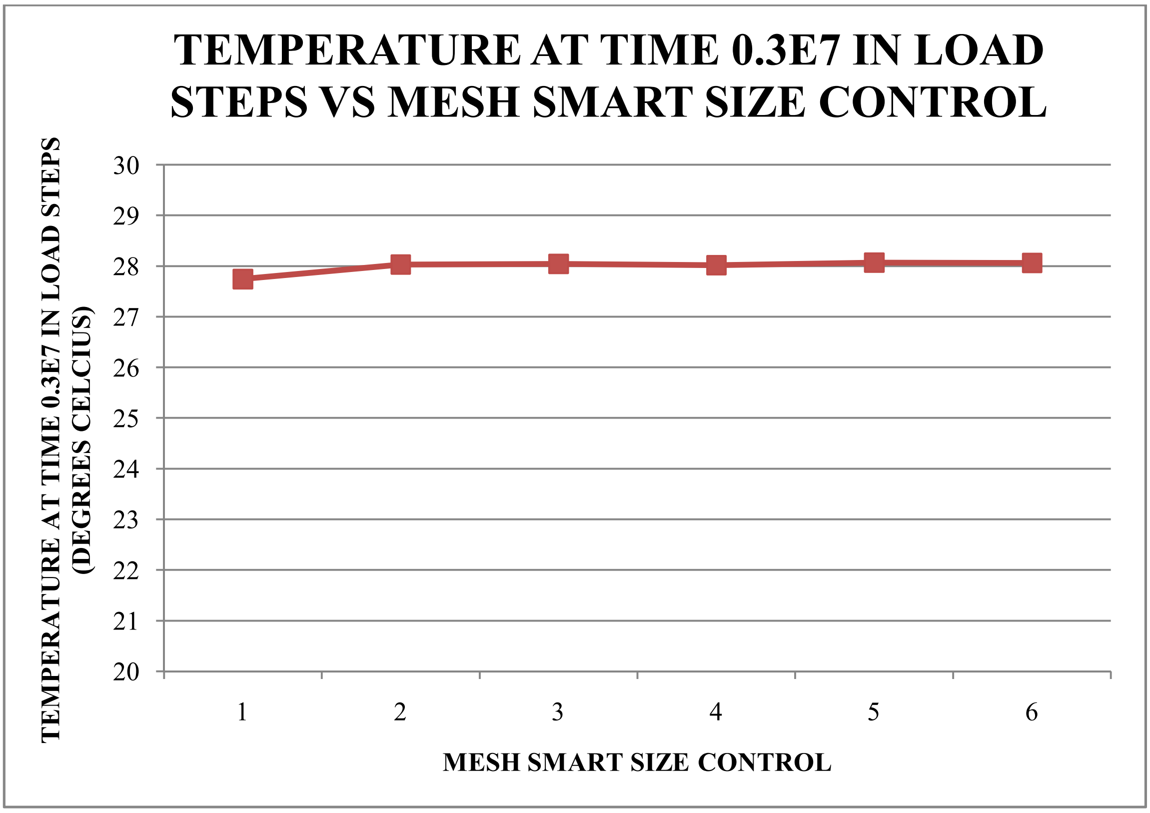

Figure 4.26: Graph of Time (In Load Steps) to Decrease to Room Temperature vs Mesh Smart Size Control

It is noticeable that as the meshing size control is getting courser, the temperature at 0.3 X 10^7 time (in load steps) is getting higher. Likewise, as the meshing size control is getting finer, the temperature at 0.3 X 10^7 time (in load steps) is getting lower. This values of the temperature at 0.3 X 10^7 time (in load steps) can be seen in the list in Figures 4.15, 4.17, 4.19 4.21, 4.23 and 4.25. When the smart size control is getting from fine (1) to coarse (6), the temperatures are 27.7439^{0}C, 28.0317^{0}C, 28.442^{0}C, 28.0197^{0}C, 28.0699^{0}C and 28.0642^{0}C respectively. Therefore, with these results, the mesh smart size control 1 is used throughout this research project.

4.3 SAMPLE 1

(a) 900^0C

It must be taken into consideration that pick 1 and 2 are the properties of temperatures between the brazing temperature of 900^0C to room temperature, 27^0C. On the other hand, pick 3 displays the properties at room temperature, 27^0C.

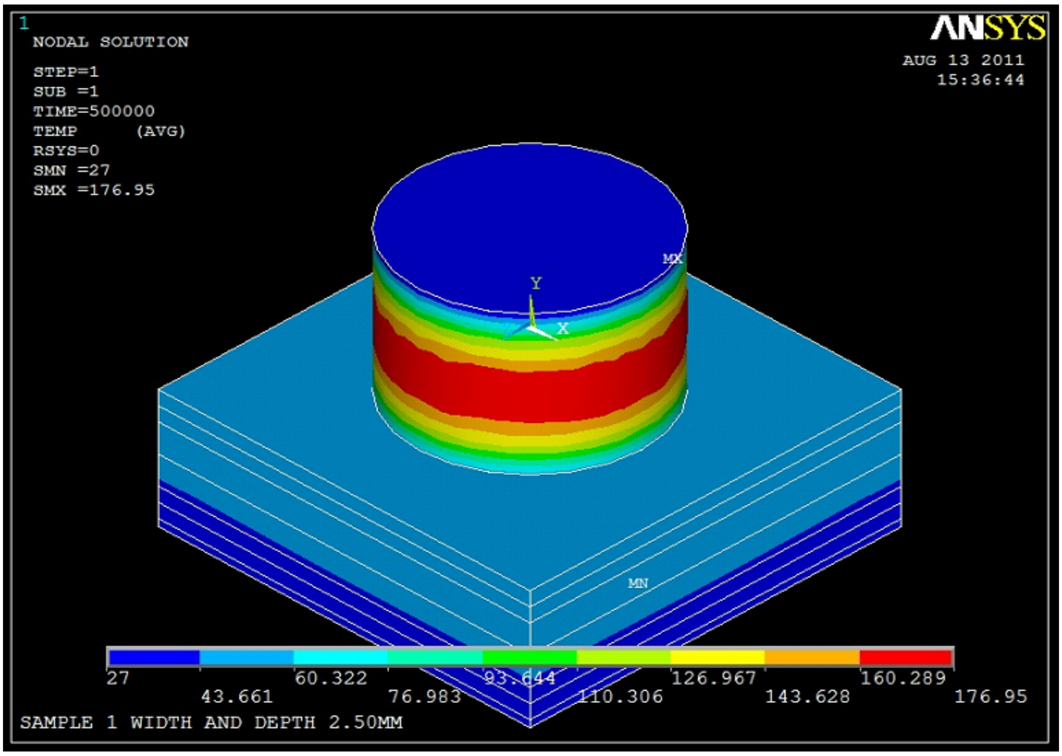

Figure 4.27: Heat Transfer Distribution for Pick 1 (900^0C)

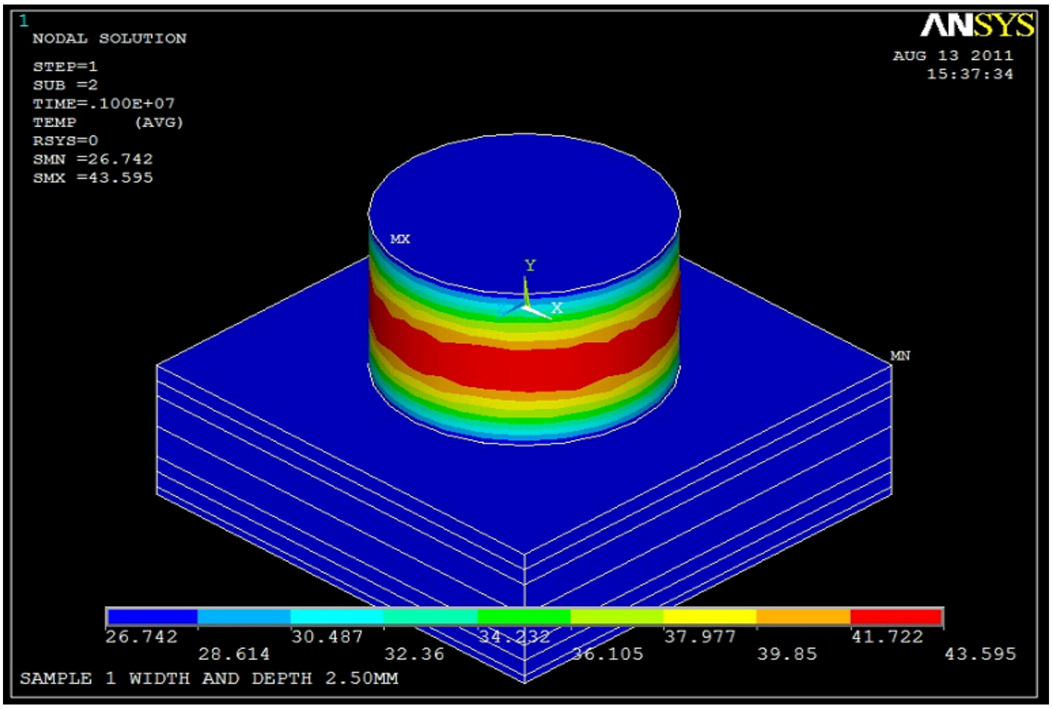

Figure 4.28: Heat Transfer Distribution for Pick 2 (900^{0}C)

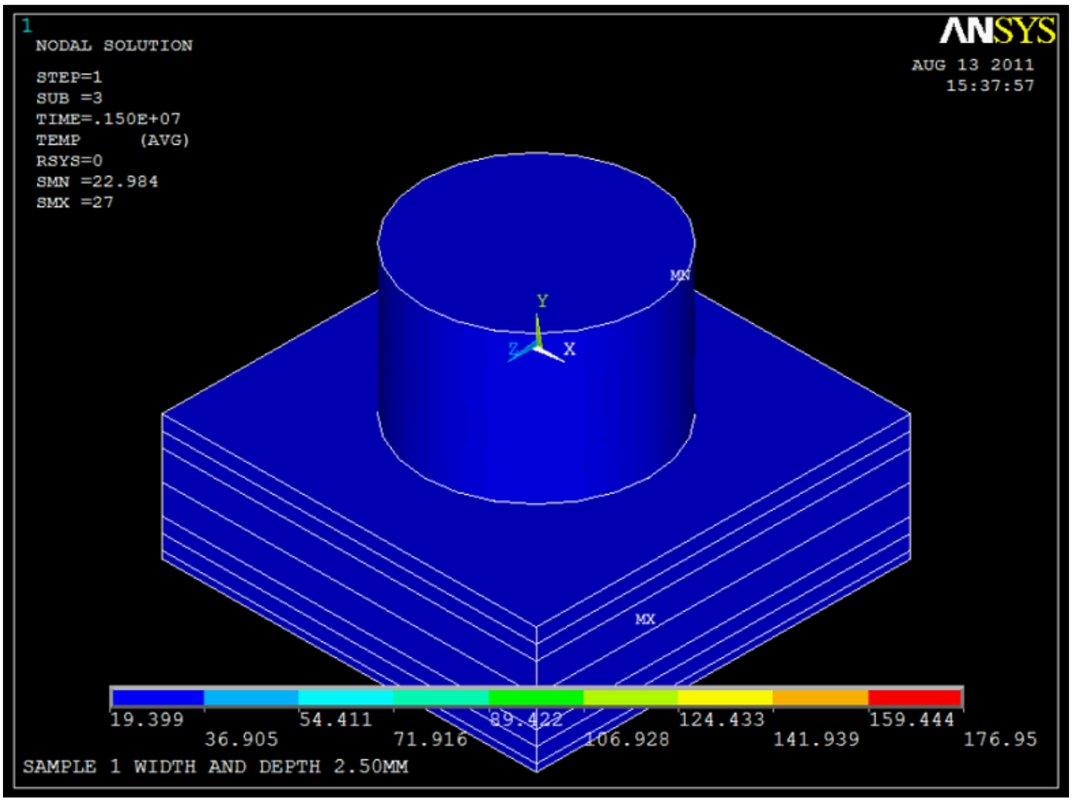

Figure 4.29: Heat Transfer Distribution for Pick 3 (900^{0}C)

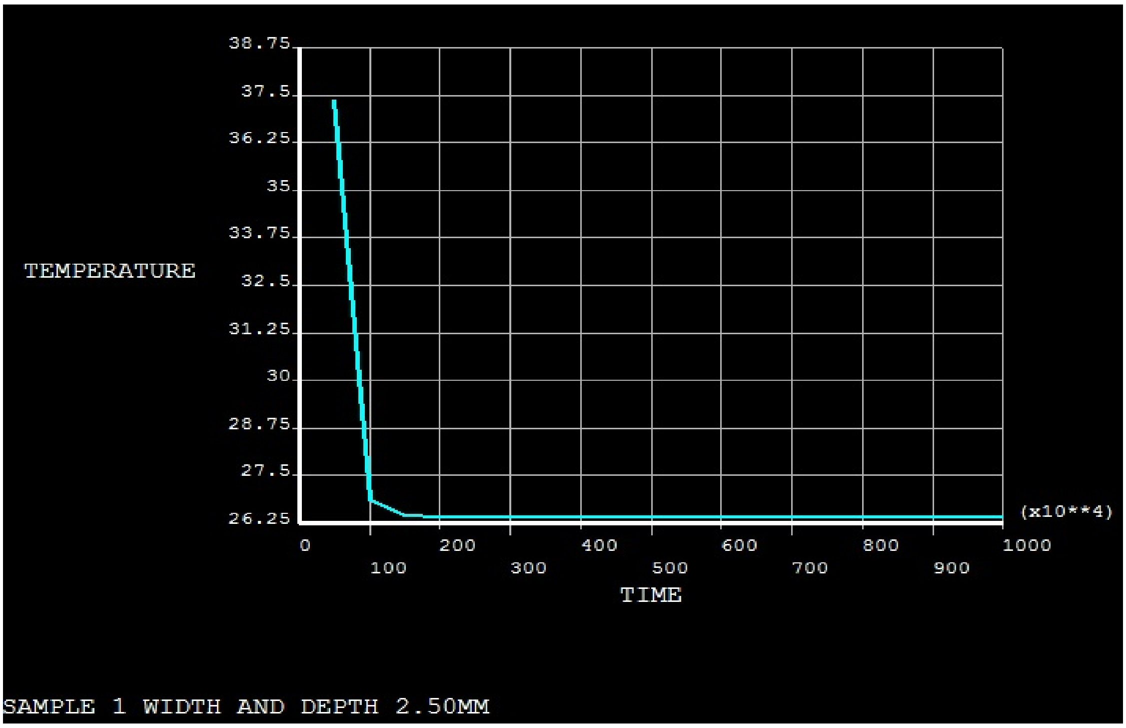

Figure 4.30: Graph of Temperature versus Time, in Load Steps (900^{0}C)

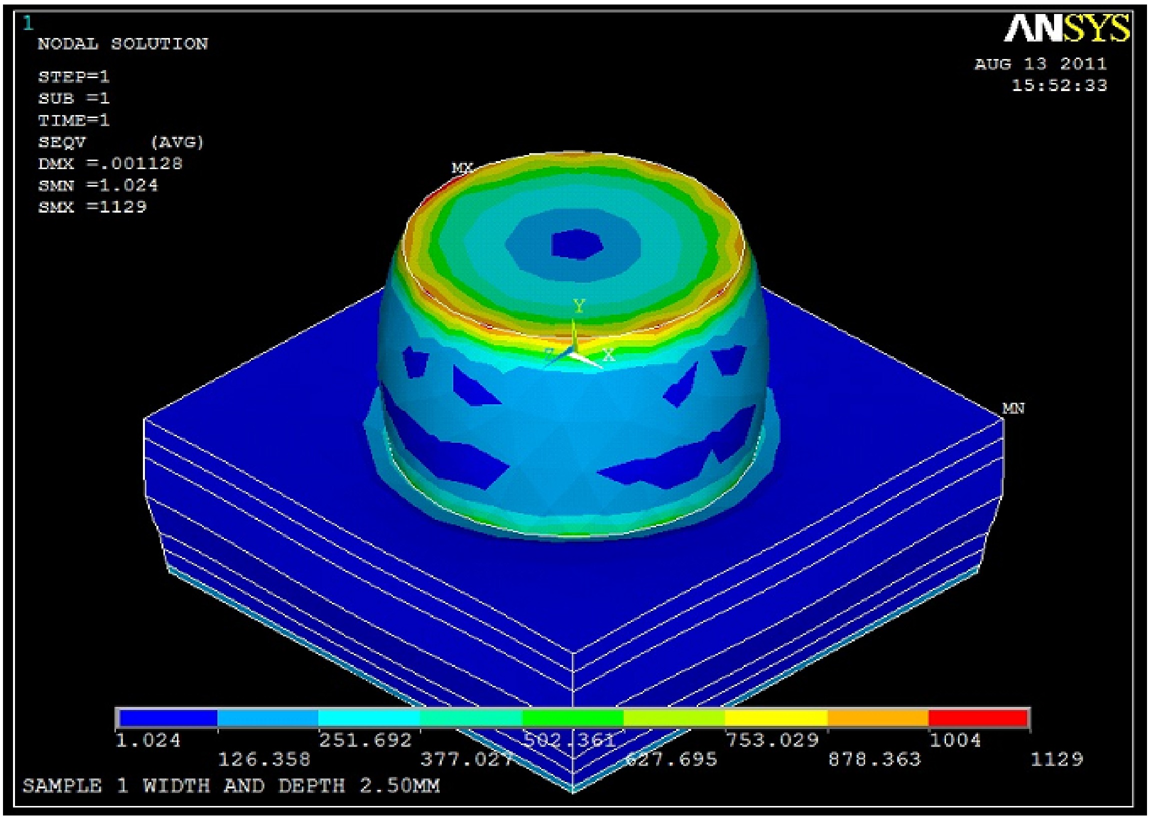

Figure 4.31: Von Mises Stress Distribution Plot for Pick 1 (900^{0}C)

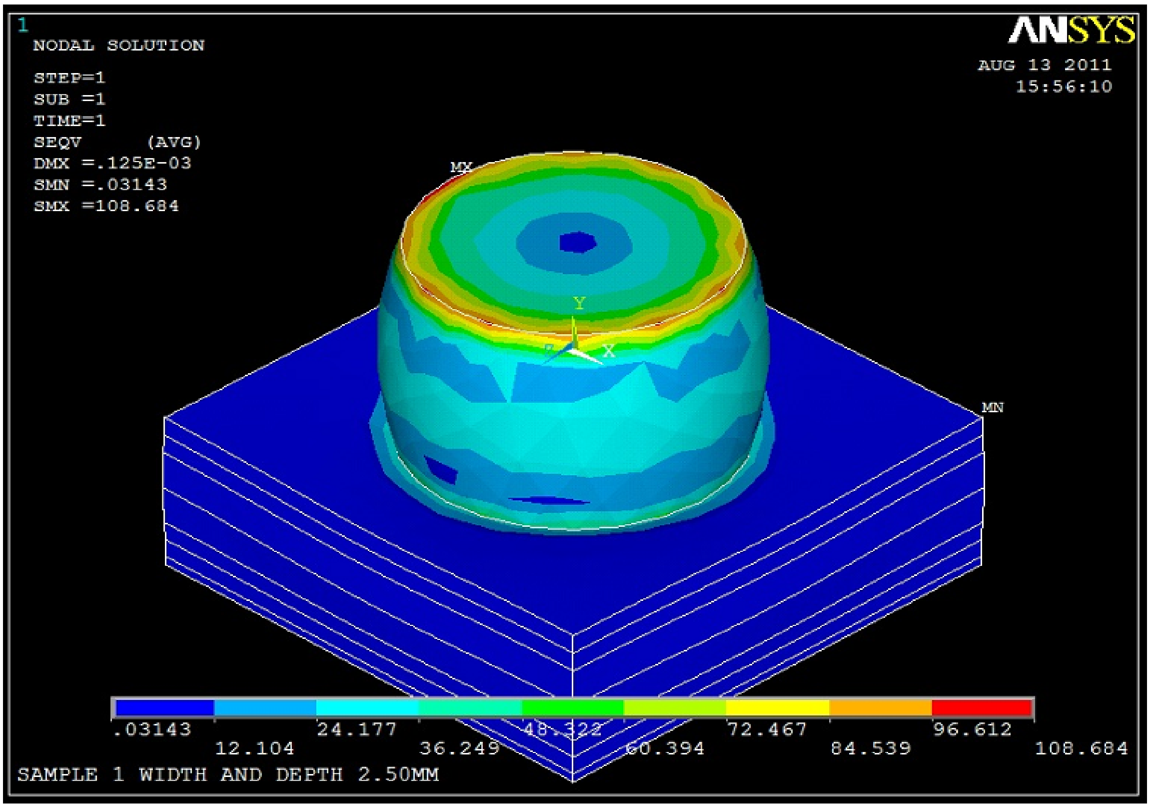

Figure 4.32: Von Mises Stress Distribution Plot for Pick 2 (900^{0}C)

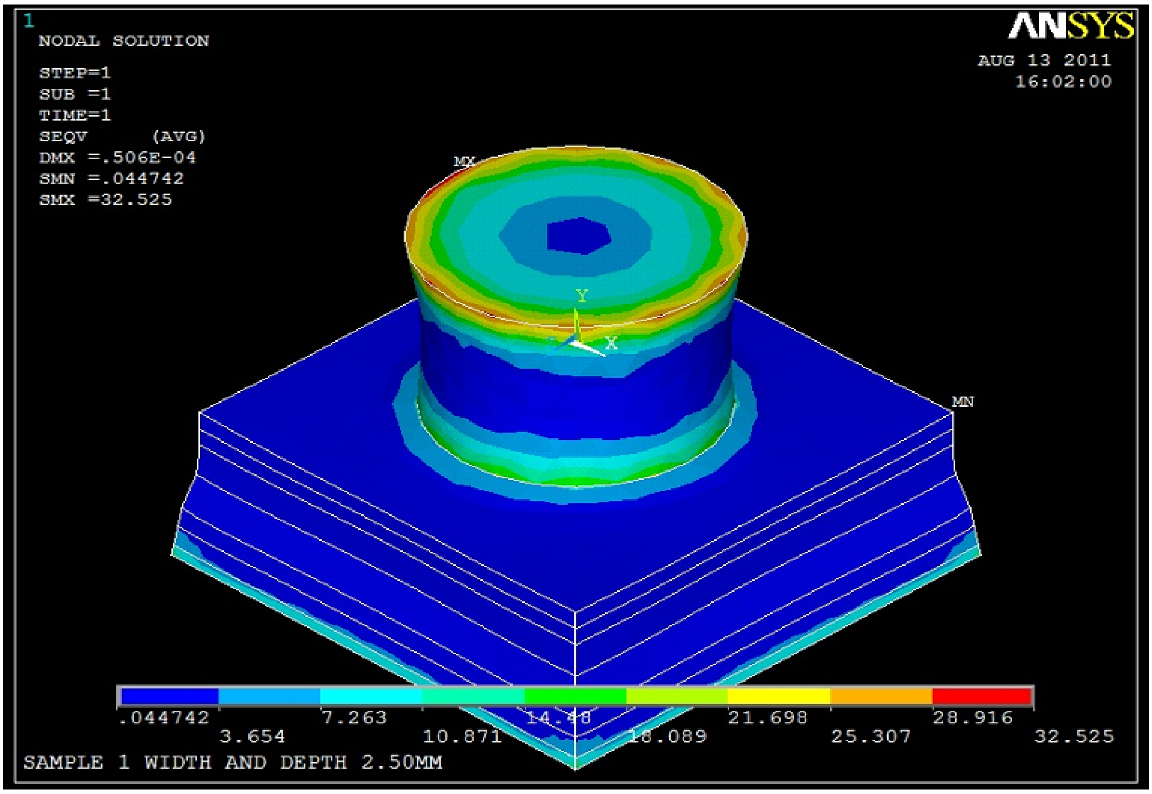

Figure 4.33: Von Mises Stress Distribution Plot for Pick 3 (900^{0}C)

(b) 865^{0}C

It must be taken into consideration that pick 1 and 2 are the properties of temperatures between the brazing temperature of 865^{0}C to room temperature, 27^{0}C. On the other hand, pick 3 displays the properties at room temperature, 27^{0}C.

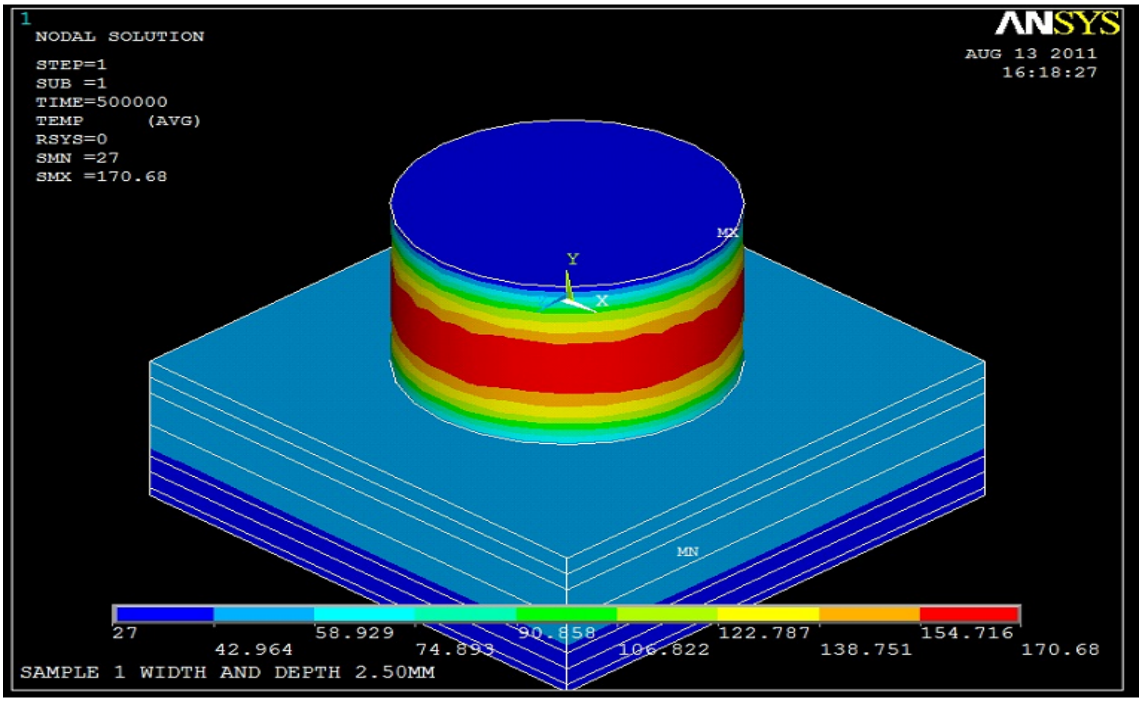

Figure 4.34: Heat Transfer Distribution for Pick 1 (865^{0}C)

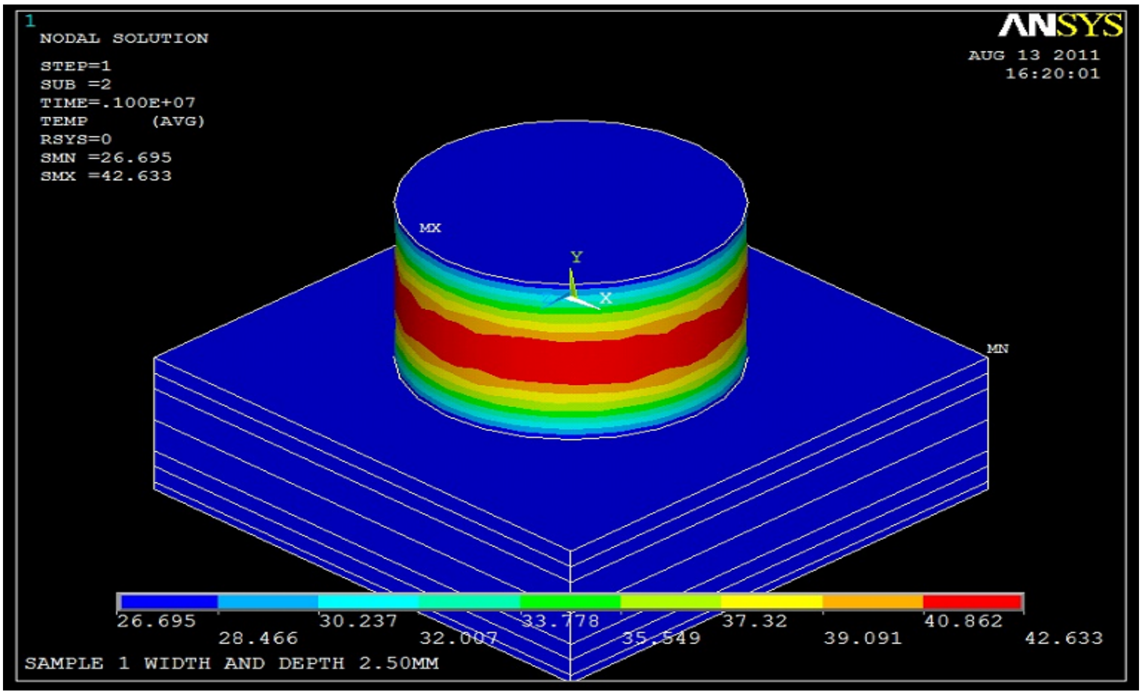

Figure 4.35: Heat Transfer Distribution for Pick 2 (865^{0}C)

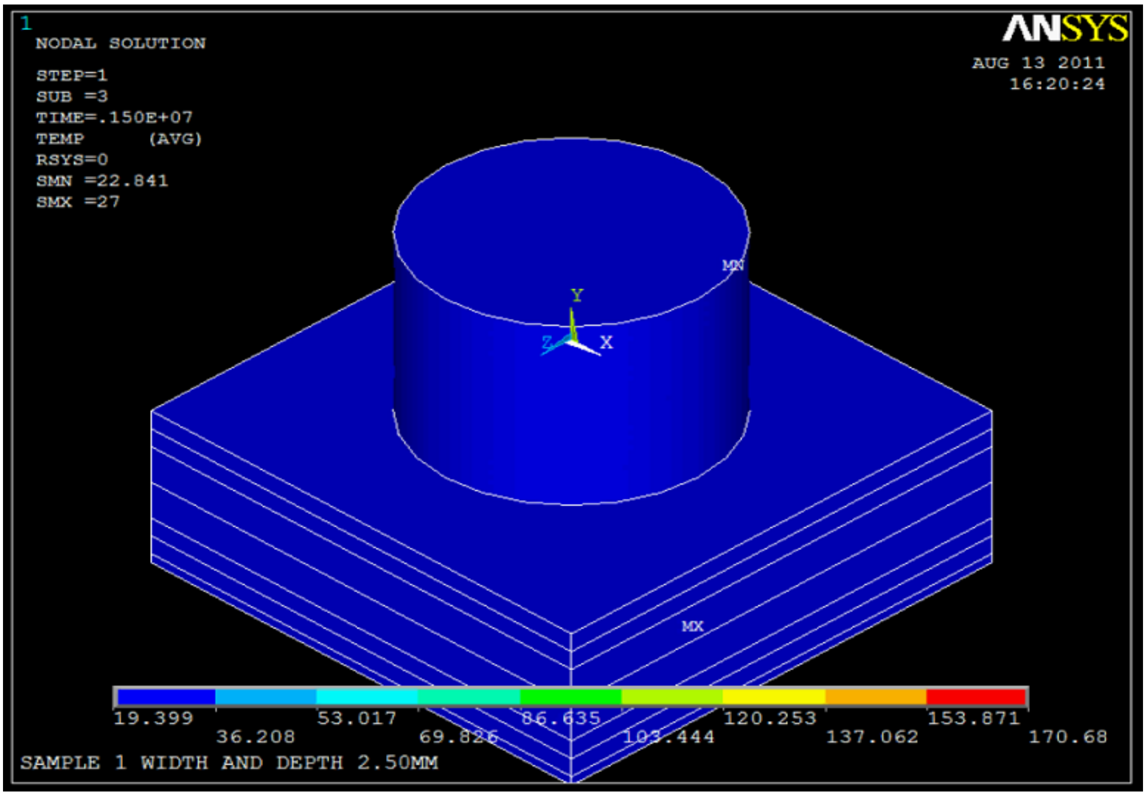

Figure 4.36: Heat Transfer Distribution for Pick 3 (865^0C)

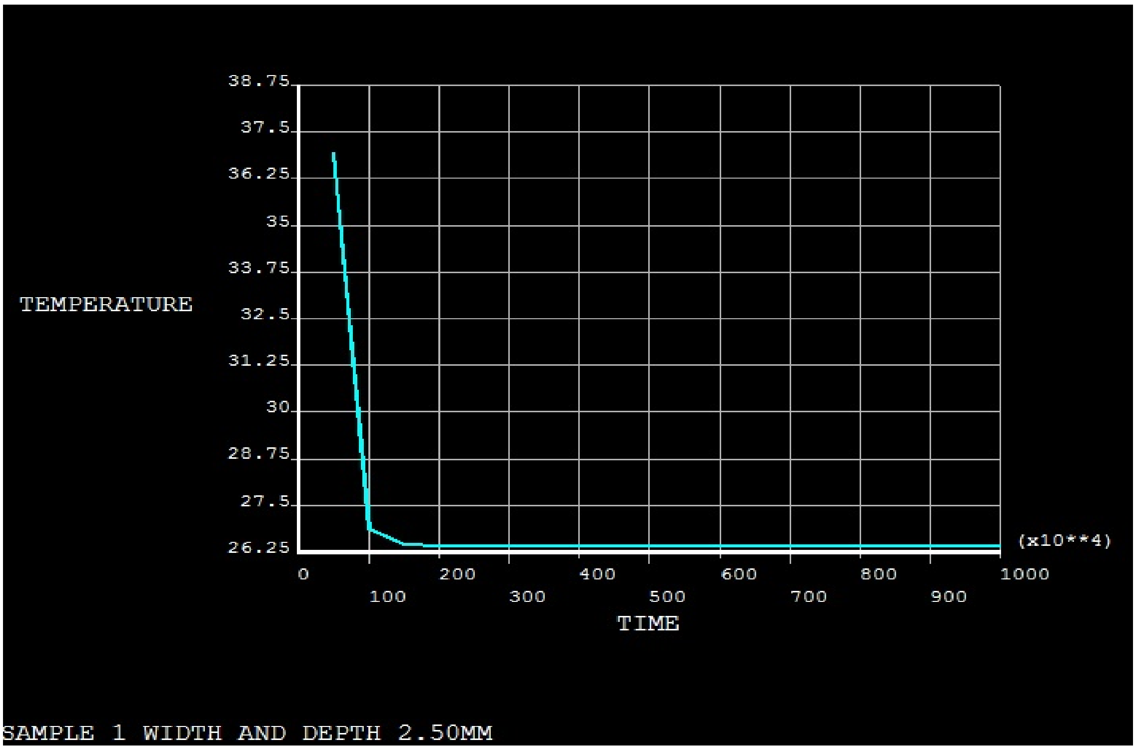

Figure 4.37: Graph of Temperature versus Time, in Load Steps (865^0C)

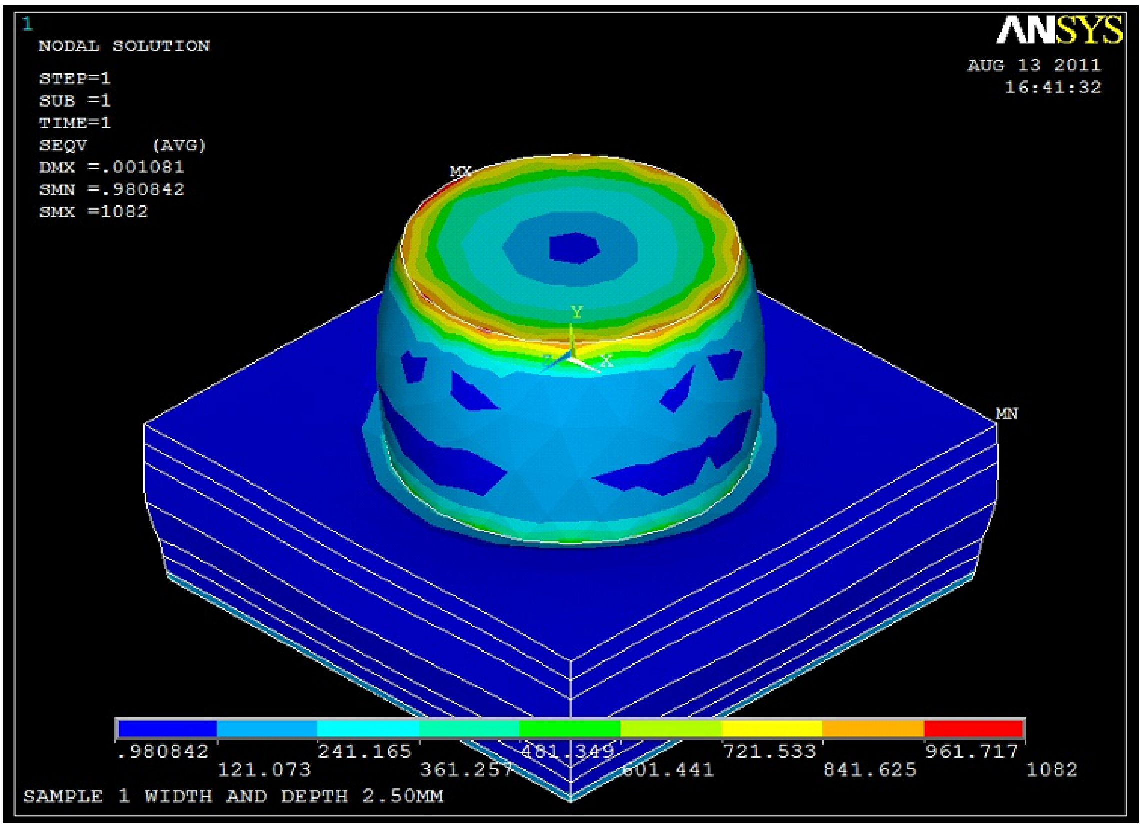

Figure 4.38: Von Mises Stress Distribution Plot for Pick 1 (865^{0}C)

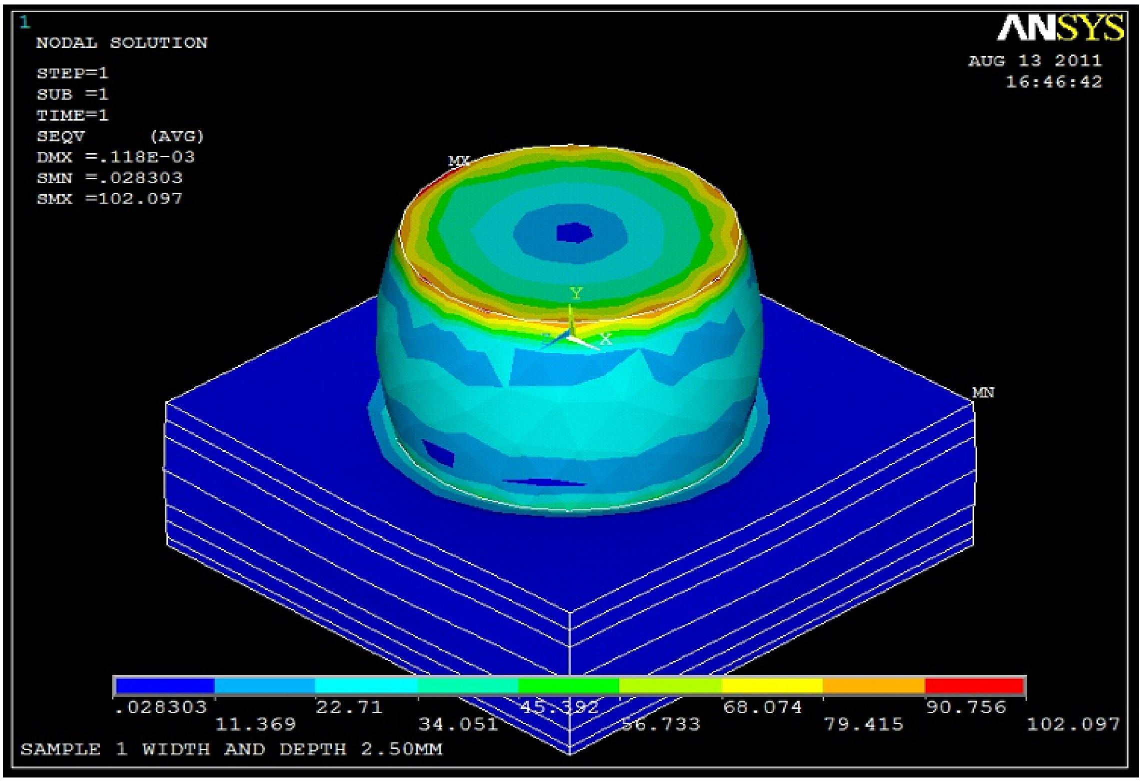

Figure 4.39: Von Mises Stress Distribution Plot for Pick 2 (865^{0}C)

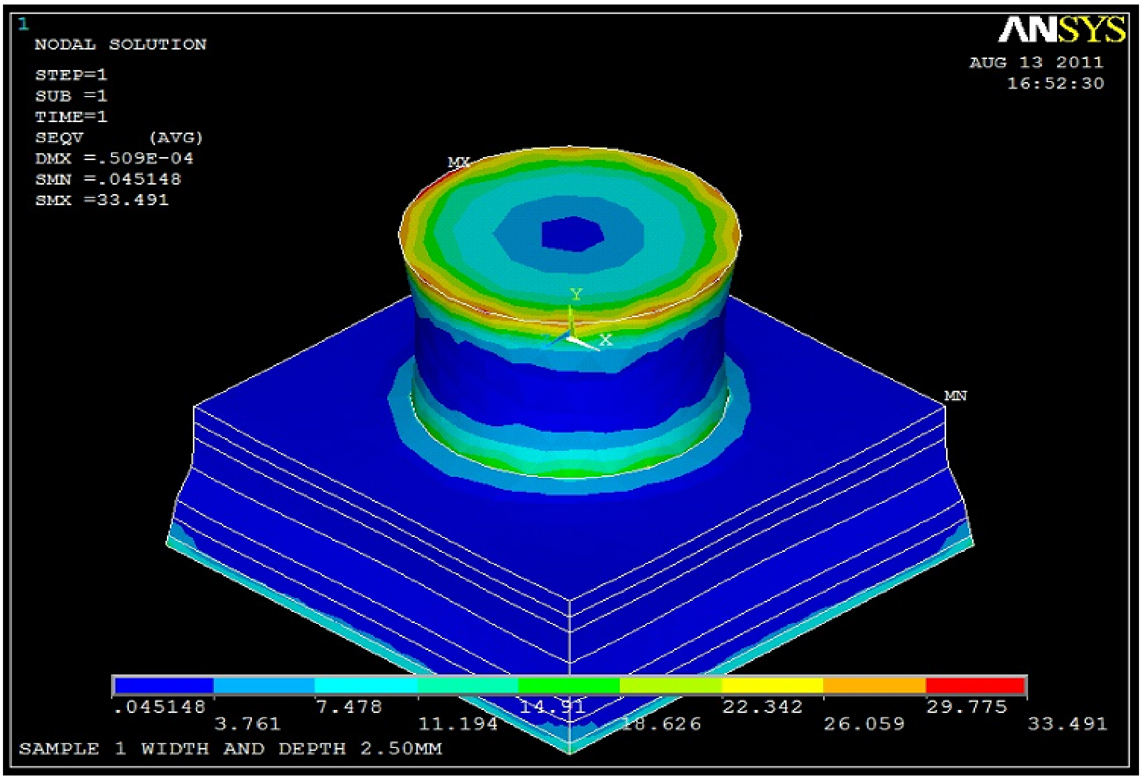

Figure 4.40: Von Mises Stress Distribution Plot for Pick 3 (865^0C)

(c) 830^0C

It must be taken into consideration that pick 1 and 2 are the properties of temperatures between the brazing temperature of 830^0C to room temperature, 27^0C. On the other hand, pick 3 displays the properties at room temperature, 27^0C.

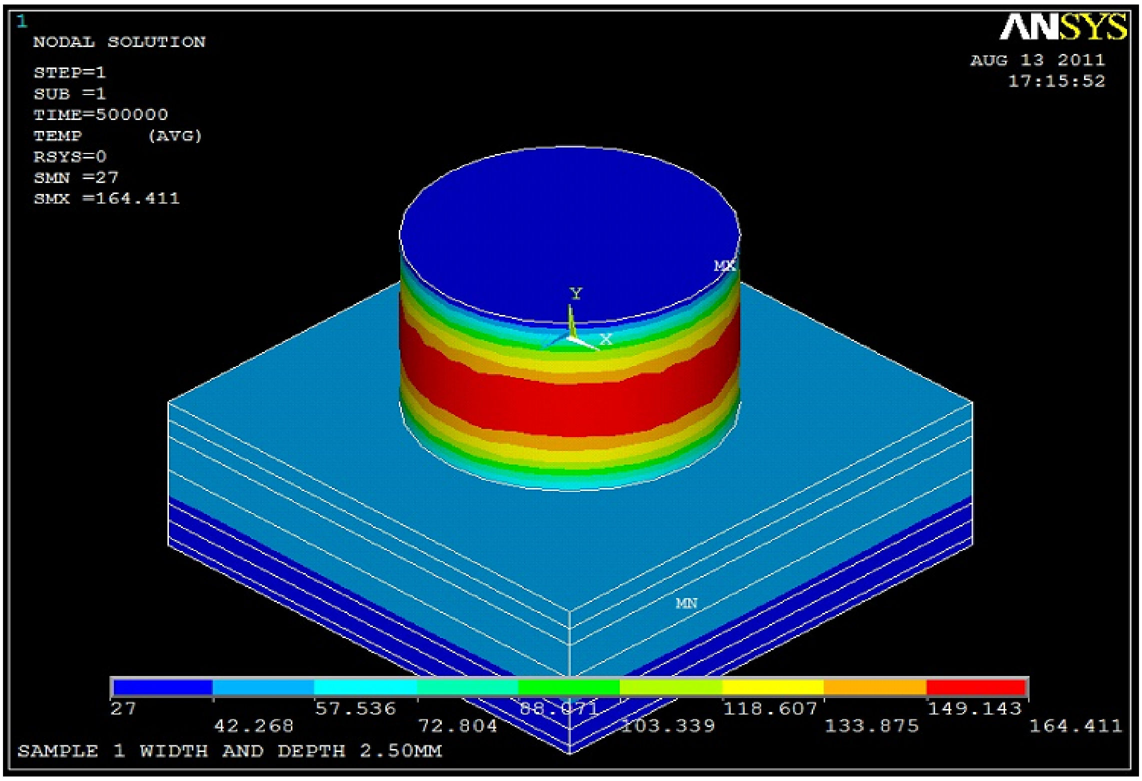

Figure 4.41: Heat Transfer Distribution for Pick 1 (830^0C)

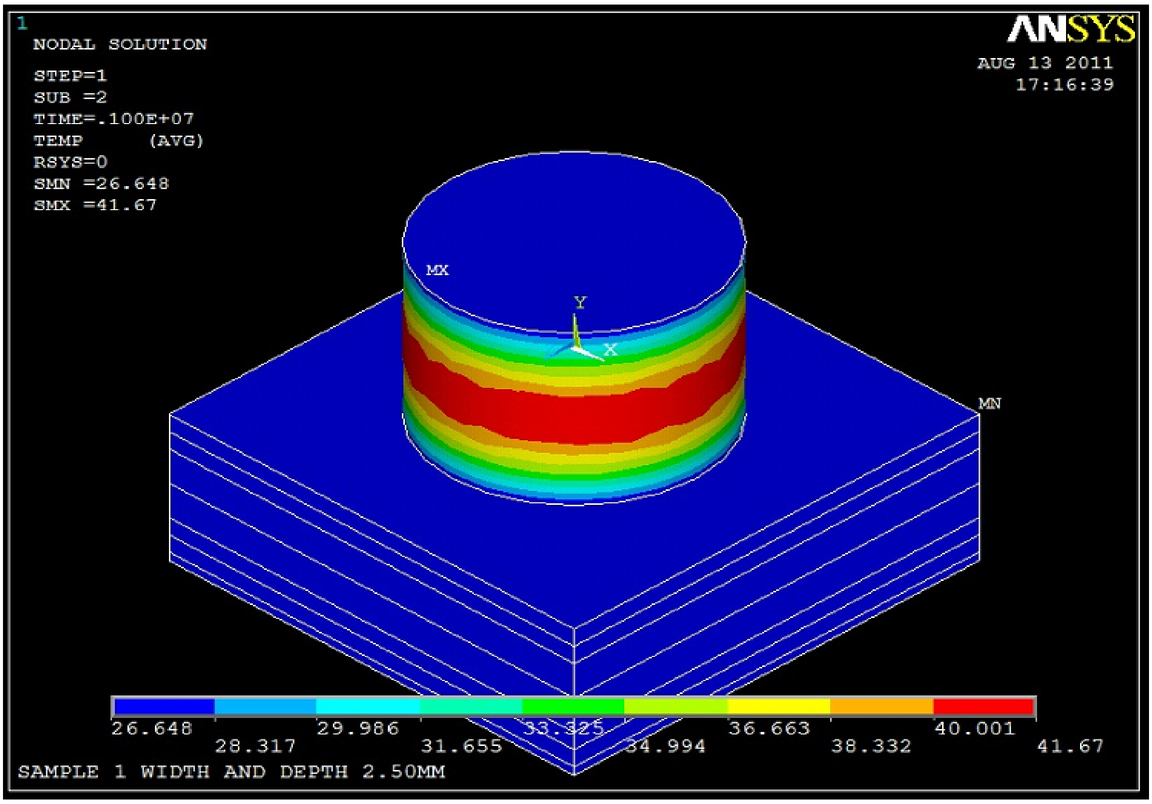

Figure 4.42: Heat Transfer Distribution for Pick 2 (830^0C)

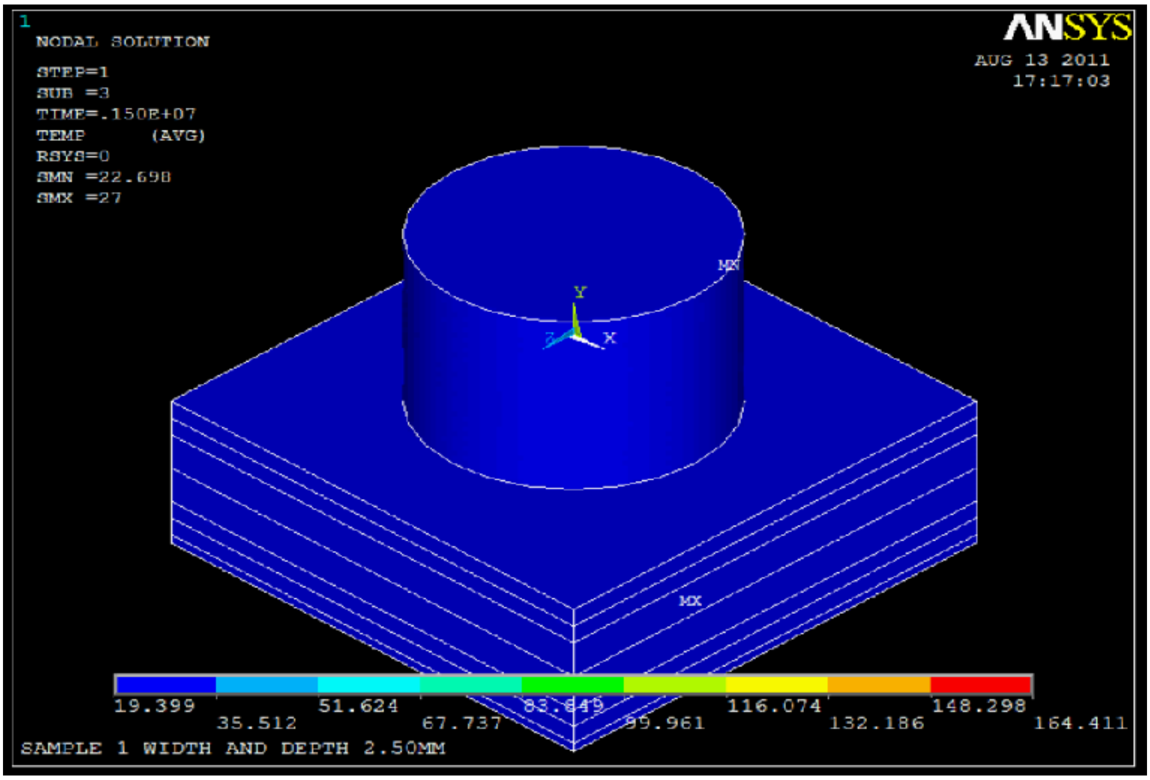

Figure 4.43: Heat Transfer Distribution for Pick 3 (830^{0}C)

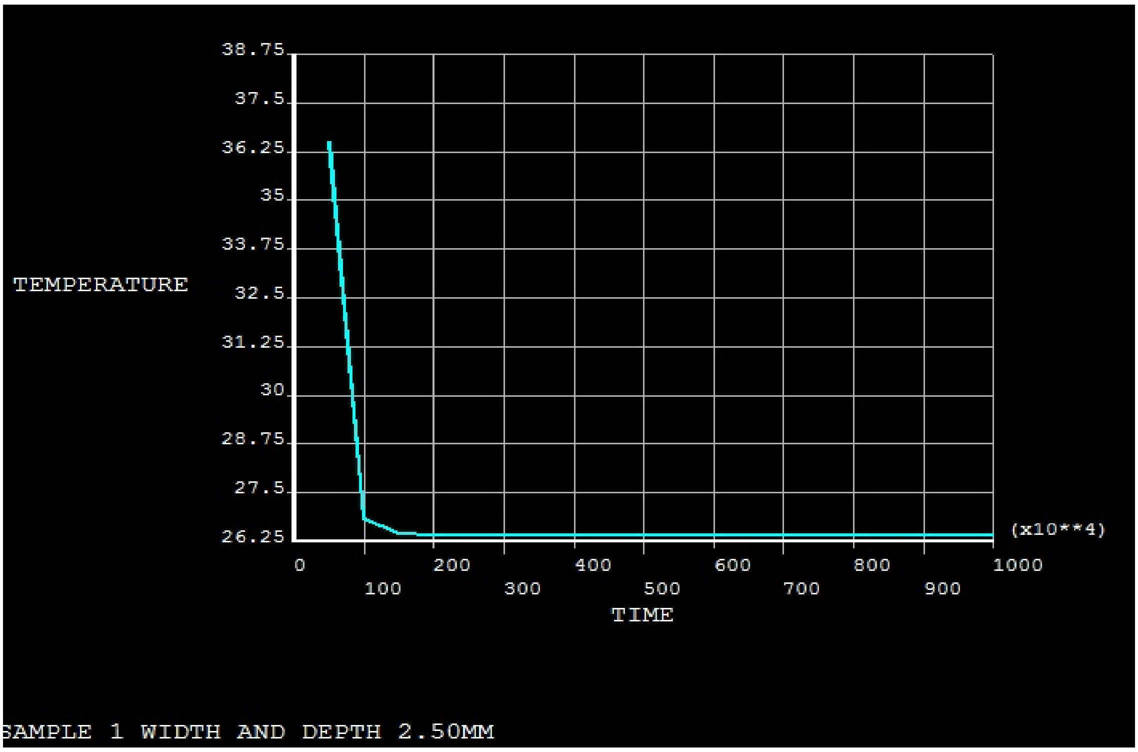

Figure 4.44: Graph of Temperature versus Time, in Load Steps (830^{0}C)

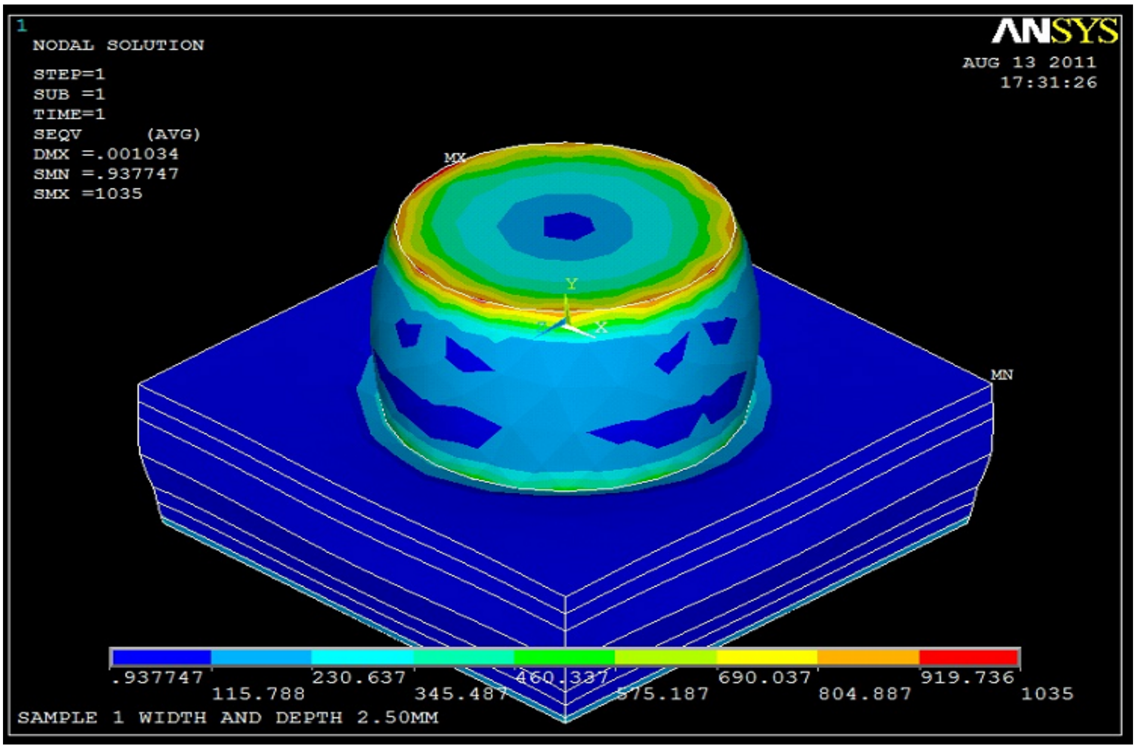

Figure 4.45: Von Mises Stress Distribution Plot for Pick 1 (830^0C)

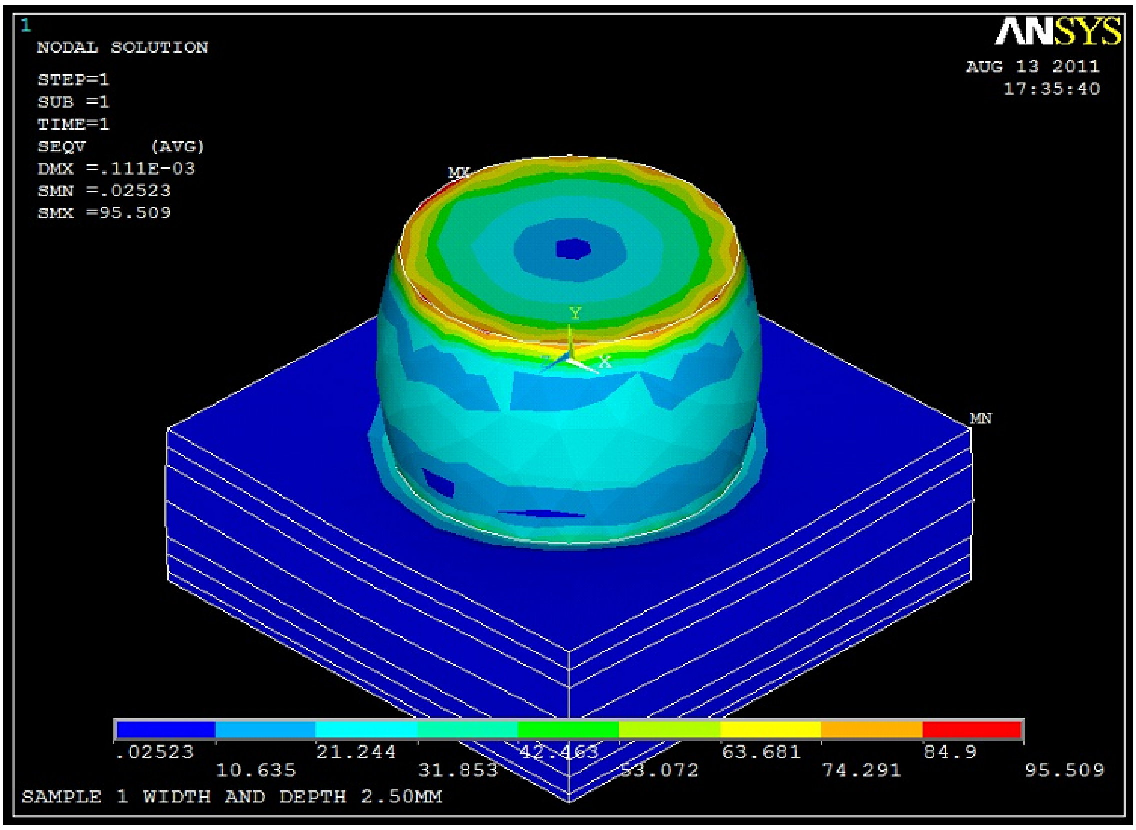

Figure 4.46: Von Mises Stress Distribution Plot for Pick 2 (830^0C)

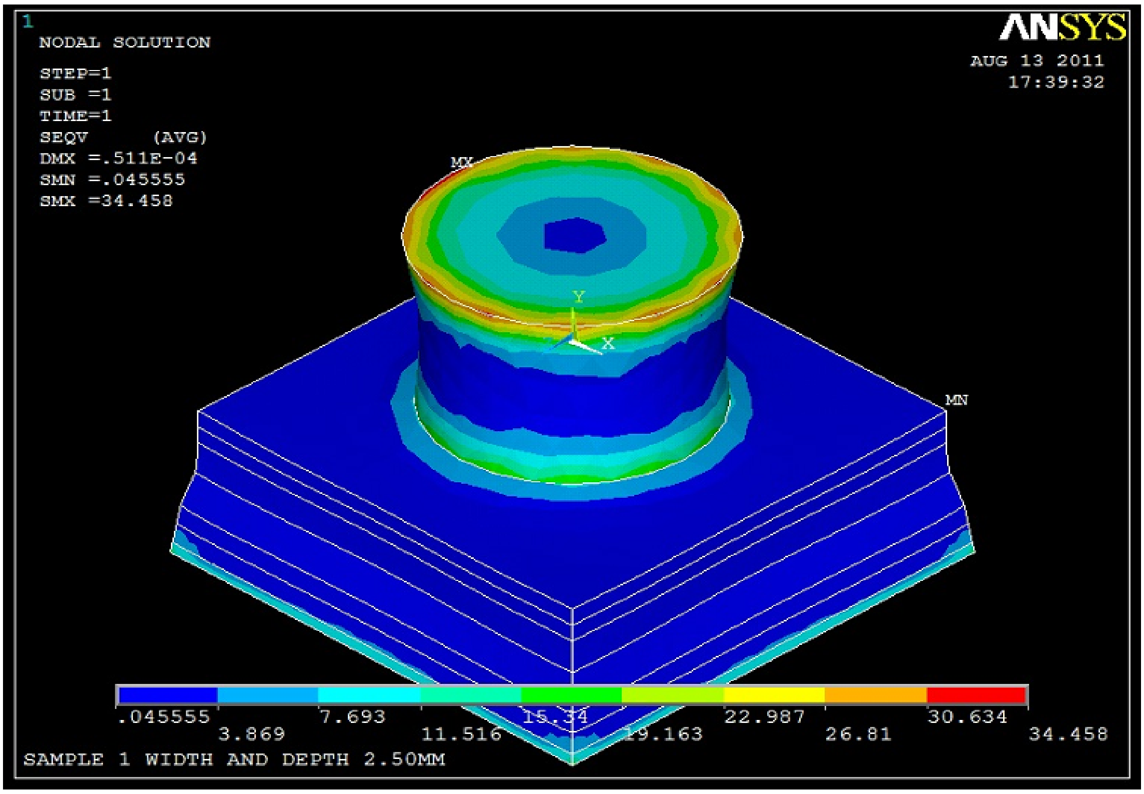

Figure 4.47: Von Mises Stress Distribution Plot for Pick 3 (830^{0}C)

The sample 1 is analyzed from initial brazing temperature of 900^{0}C to room temperature. At pick 1, the sapphire layer has the highest stress distribution of 1004 to 1129 MPa which is higher than the yield strength of sapphire. Also, there is stress from sapphire to the filler of 502.362 to 627.695 MPa which is higher than the yield strength of sapphire. At pick 2, the sapphire layer has the highest stress distribution of 96.612 to 108.684 MPa which is less than the yield strength of sapphire. Also, there is stress from sapphire to the filler of 48.322 to 60.394 MPa which is less than the yield strength of sapphire. At pick 3, the sapphire layer has the highest stress distribution of 28.916 to 32.325 MPa which is less than the yield strength of sapphire. Also, there is stress from sapphire to the filler of 14.48 to 18.089 MPa which is less than the yield strength of sapphire.

The sample 1 is then analyzed from initial brazing temperature 865^{0}C to room temperature. At pick 1, the sapphire layer has the highest stress distribution of 961.717

to 1082 MPa which is higher than the yield strength of sapphire. Also, there is stress from sapphire to the filler of 481.349 to 601.441 MPa which is higher than the yield strength of sapphire. At pick 2, the sapphire layer has the highest stress distribution of 90.756 to 102.097 MPa which is less than the yield strength of sapphire. Also, there is stress from sapphire to the filler of 45.392 to 56.733 MPa which is less than the yield strength of sapphire. At pick 3, the sapphire layer has the highest stress distribution of 29.775 to 33.491 MPa which is less than the yield strength of sapphire. Also, there is stress from sapphire to the filler of 14.91 to 18.626 MPa which is less than the yield strength of sapphire.

The sample 1 is then analyzed from initial brazing temperature 830^0C to room temperature. At pick 1, the sapphire layer has the highest stress distribution of 919.736 to 1035 MPa which is higher than the yield strength of sapphire. Also, there is stress from sapphire to the filler of 460.337 to 575.187 MPa which is higher than the yield strength of sapphire. At pick 2, the sapphire layer has the highest stress distribution of 84.9 to 95.509 MPa which is less than the yield strength of sapphire. Also, there is stress from sapphire to the filler of 42.463 to 53.072 MPa which is less than the yield strength of sapphire. At pick 3, the sapphire layer has the highest stress distribution of 30.634 to 34.458 MPa which is less than the yield strength of sapphire. Also, there is stress from sapphire to the filler of 15.34 to 19.163 MPa which is less than the yield strength of sapphire.

Therefore, the sample 1 with initial brazing temperature 830^0C as the stress obtained is less than the yield strength of sapphire and also the lowest compared to the other stress distribution of 865^0C and 900^0C.

4.4 SAMPLE 2

(a) 900^0C

It must be taken into consideration that pick 1 and 2 are the properties of temperatures between the brazing temperature of 900^0C to room temperature, 27^0C. On the other hand, pick 3 displays the properties at room temperature, 27^0C.

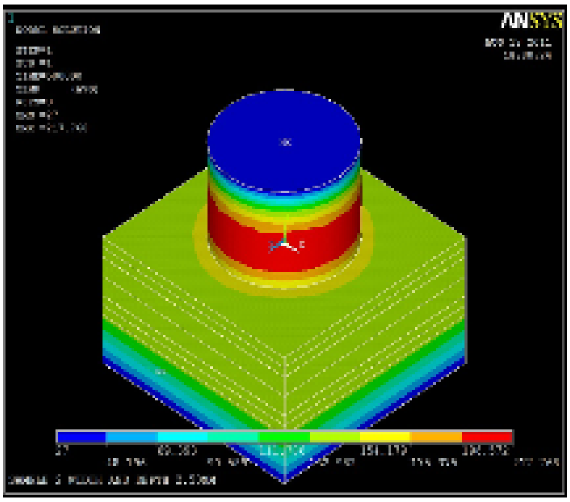

Figure 4.48: Heat Transfer Distribution for Pick 1 (900^0C)

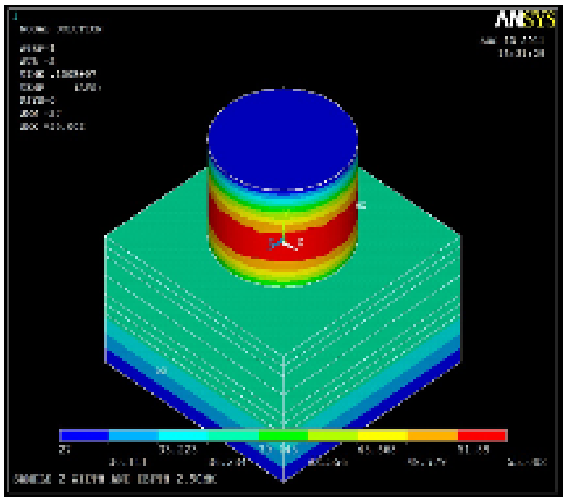

Figure 4.49: Heat Transfer Distribution for Pick 2 (900^0C)

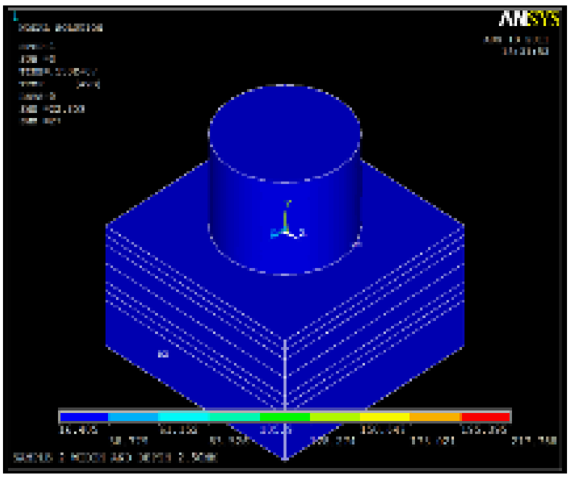

Figure 4.50: Heat Transfer Distribution for Pick 3 (900^0C)

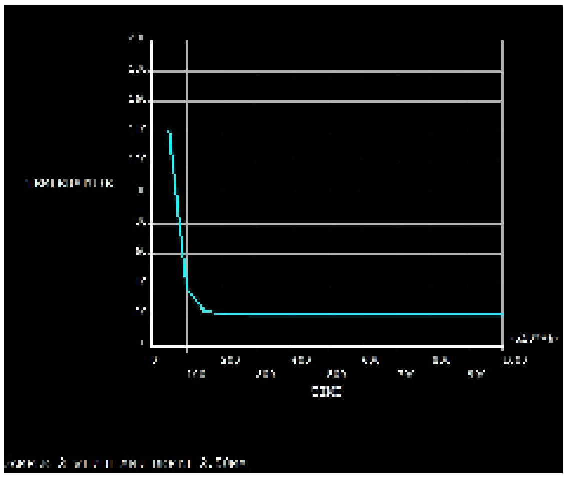

Figure 4.51: Graph of Temperature versus Time, in Load Steps (900^0C)

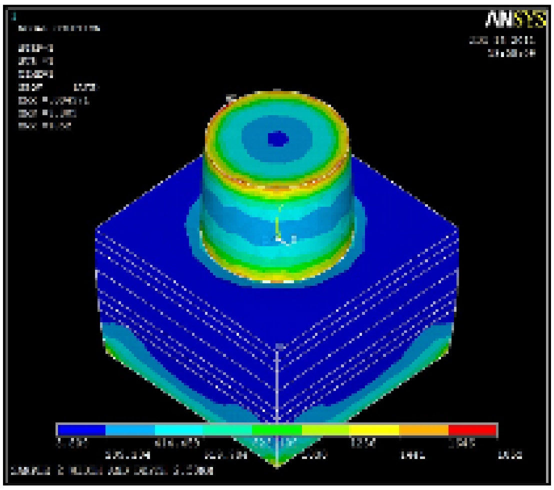
Figure 4.52: Von Mises Stress Distribution Plot for Pick 1 (900^0C)

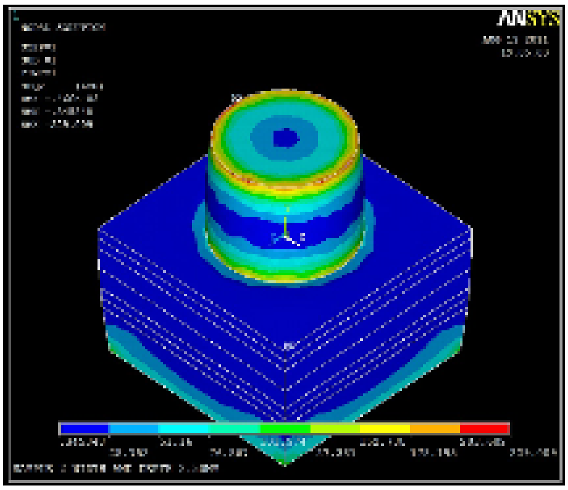
Figure 4.53: Von Mises Stress Distribution Plot for Pick 2 (900^0C)

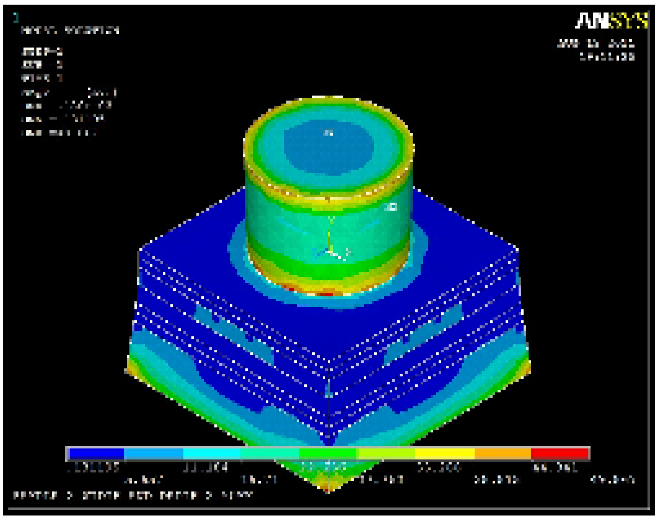
Figure 4.54: Von Mises Stress Distribution Plot for Pick 3 (900^0C)

(b) 865^{0}C

It must be taken into consideration that pick 1 and 2 are the properties of temperatures between the brazing temperature of 865^{0}C to room temperature, 27^{0}C. On the other hand, pick 3 displays the properties at room temperature, 27^{0}C.

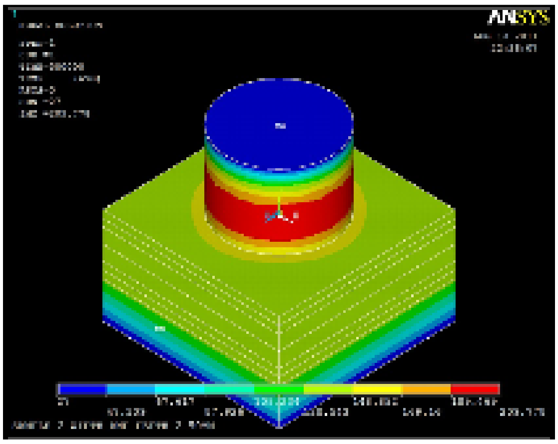

Figure 4.55: Heat Transfer Distribution for Pick 1 (865^{0}C)

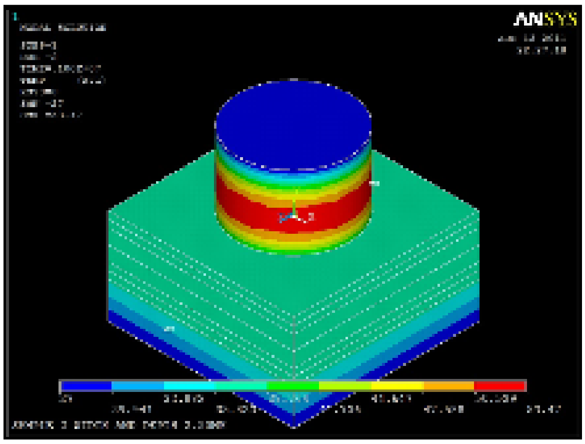

Figure 4.56: Heat Transfer Distribution for Pick 2 (865^{0}C)

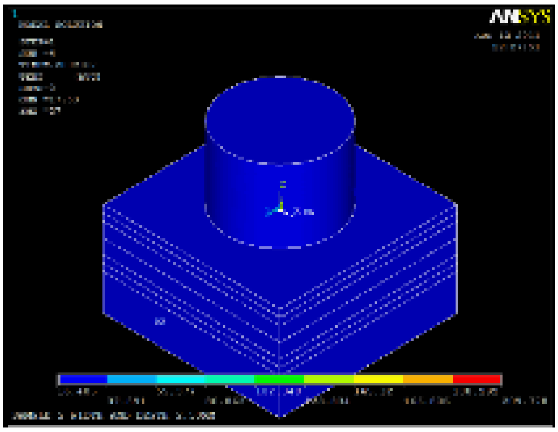

Figure 4.57: Heat Transfer Distribution for Pick 3 (865^{0}C)

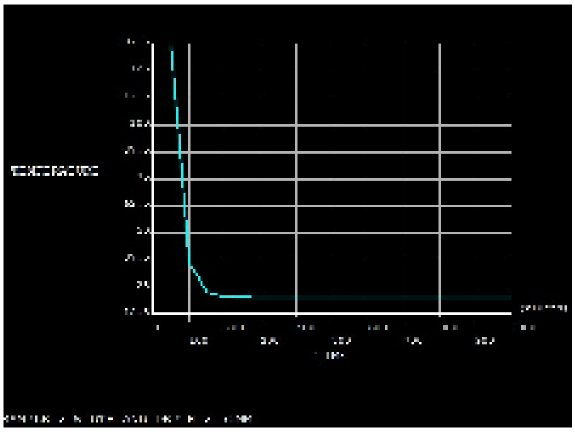

Figure 4.58: Graph of Temperature versus Time, in Load Steps (865^{0}C)

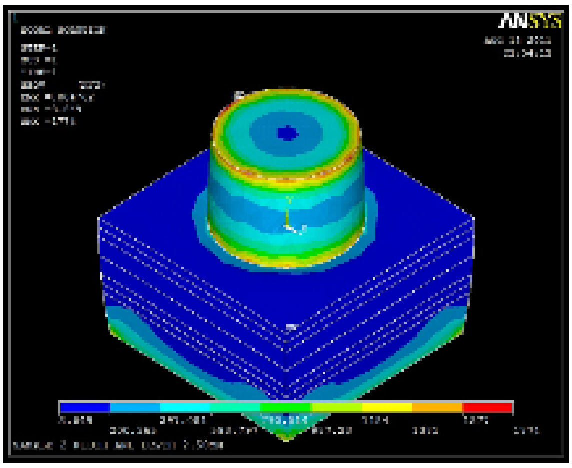

Figure 4.59: Von Mises Stress Distribution Plot for Pick 1 (865^{0}C)

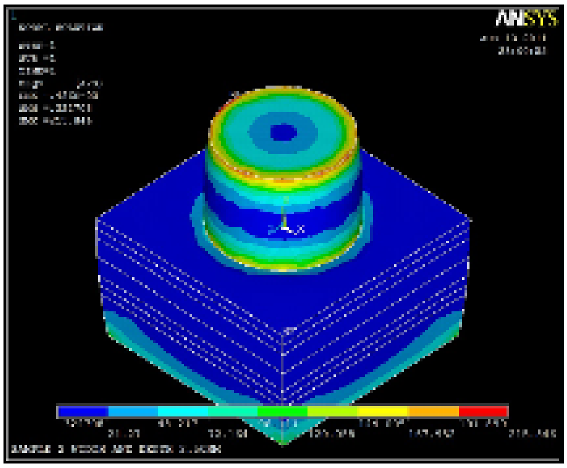

Figure 4.60: Von Mises Stress Distribution Plot for Pick 2 (865^{0}C)

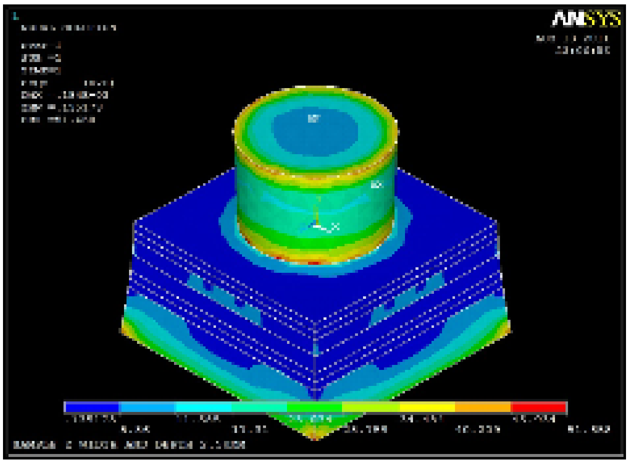

Figure 4.61: Von Mises Stress Distribution Plot for Pick 3 (865^{0}C)

(c) 830^{0}C

It must be taken into consideration that pick 1 and 2 are the properties of temperatures between the brazing temperature of 830^{0}C to room temperature, 27^{0}C. On the other hand, pick 3 displays the properties at room temperature, 27^{0}C.

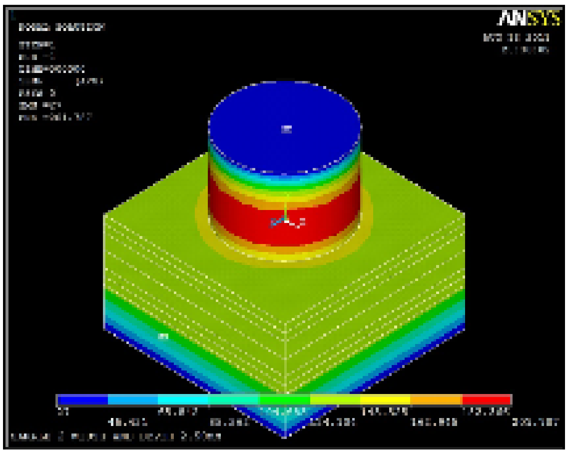

Figure 4.62: Heat Transfer Distribution for Pick 1 (830^{0}C)

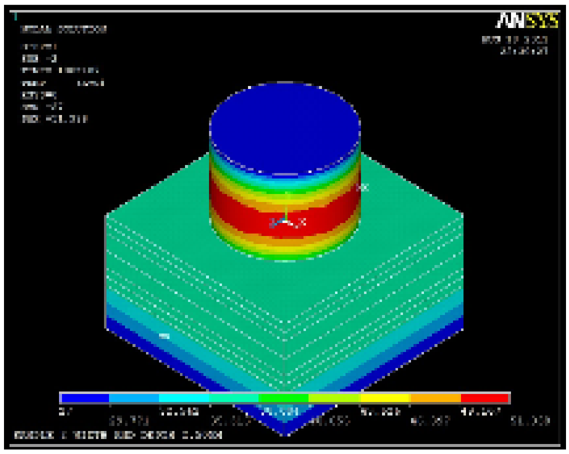

Figure 4.63: Heat Transfer Distribution for Pick 2 (830^{0}C)

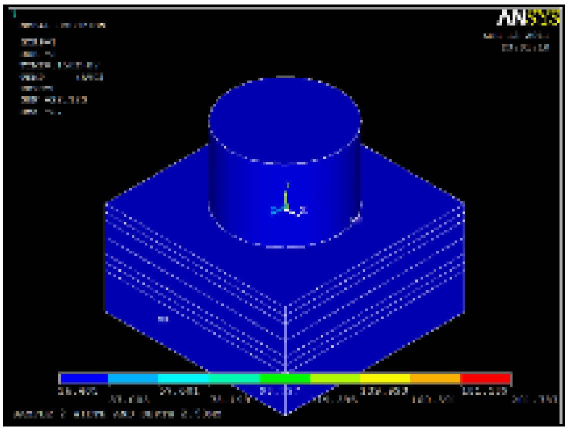

Figure 4.64: Heat Transfer Distribution for Pick 3 (830^{0}C)

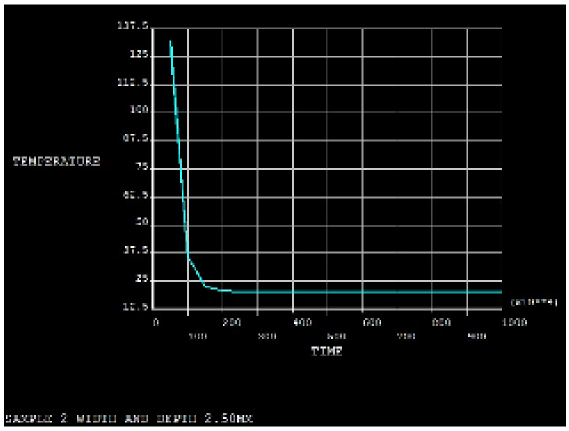

Figure 4.65: Graph of Temperature versus Time, in Load Steps (830^{0}C)

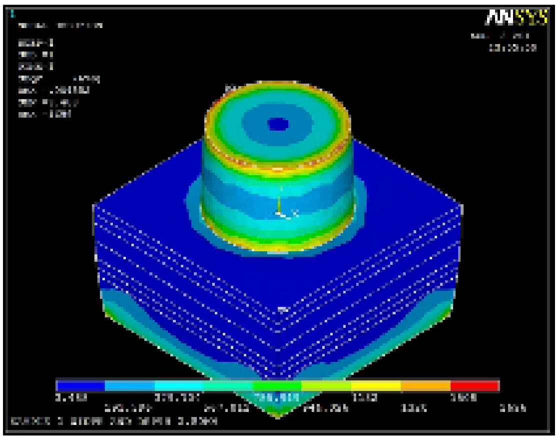

Figure 4.66: Von Mises Stress Distribution Plot for Pick 1 (830^0C)

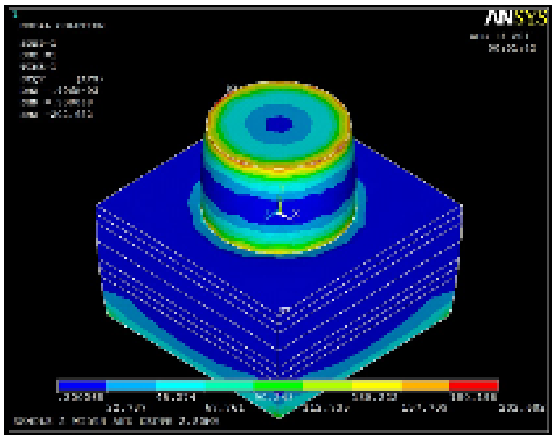

Figure 4.67: Von Mises Stress Distribution Plot for Pick 2 (830^0C)

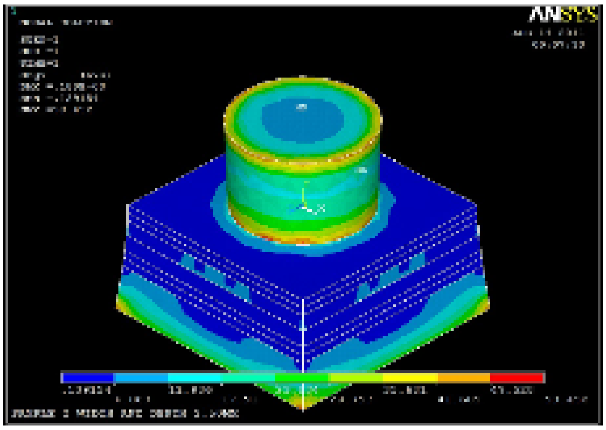

Figure 4.68: Von Mises Stress Distribution Plot for Pick 3 (830^0C)

The sample 2 is analyzed from initial brazing temperature of 900^0C to room temperature. At pick 1, the sapphire layer has the highest stress distribution of 1646 to 1852 MPa which is higher than the yield strength of sapphire. Also, there is stress from sapphire to the filler of 1441.00 to 1646.00 MPa which is higher than the yield strength of sapphire. At the layer of Inconel 600, there is also a high stress of 1030 to 1236 MPa at the edge which is higher than the yield strength of Inconel 600. At pick 2, the sapphire layer has the highest stress distribution of 203.602 to 229.009 MPa which is less than the yield strength of sapphire. Also, there is stress from sapphire to the filler of 152.788 to 178.195 MPa which is less than the yield strength of sapphire. At the layer of Inconel 600, there is also a stress of 101.974 to 127.381 MPa at the edge which is less than the yield strength of Inconel 600. At pick 3, the sapphire layer has the highest stress distribution of 44.341 to 49.867 MPa which is less than the yield strength of sapphire. Also, there is stress from sapphire to the filler of 44.341 to 49.867 MPa which is less than the yield strength of sapphire. At the layer of Inconel 600, there is also a stress of 44.341 to 49.867 MPa at the edge which is less than the yield strength of Inconel 600.

The sample 2 is then analyzed from initial brazing temperature 865^0C to room temperature. At pick 1, the sapphire layer has the highest stress distribution of 1577 to 1774 MPa which is higher than the yield strength of sapphire. Also, there is stress from sapphire to the filler of 1381.00 to 1577.00 MPa which is higher than the yield strength of sapphire. At the layer of Inconel 600, there is also a high stress of 987.23 to 1184 MPa at the edge which is higher than the yield strength of Inconel 600. At pick 2, the sapphire layer has the highest stress distribution of 191.899 to 215.846 MPa which is less than the yield strength of sapphire. Also, there is stress from sapphire to the filler of 144.005 to 167.952 MPa which is less than the yield strength of sapphire. At the layer of Inconel 600, there is also a stress of 96.111 to 120.058 MPa at the edge which is less than the yield strength of Inconel 600. At pick 3, the sapphire layer has the highest stress distribution of 45.934 to 51.658 MPa which is less than the yield strength of sapphire. Also, there is stress from sapphire to the filler of 45.934 to 51.658 MPa which is less than the yield strength of sapphire. At the layer of Inconel 600, there is also a stress of 445.934 to 51.658 MPa at the edge which is less than the yield strength of Inconel 600.

The sample 2 is then analyzed from initial brazing temperature 830^0C to room temperature. At pick 1, the sapphire layer has the highest stress distribution of 1508 to 1696 MPa which is higher than the yield strength of sapphire. Also, there is stress from sapphire to the filler of 1320.00 to 1508.00 MPa which is higher than the yield strength of sapphire. At the layer of Inconel 600, there is also a high stress of 944.026 to 1132 MPa at the edge which is higher than the yield strength of Inconel 600. At pick 2, the sapphire layer has the highest stress distribution of 180.196 to 202.682 MPa which is less than the yield strength of sapphire. Also, there is stress from sapphire to the filler of 135.222 to 157.709 MPa which is less than the yield strength of sapphire. At the layer of Inconel 600, there is also a stress of 90.248 to 112.735 MPa at the edge which is less than the yield strength of Inconel 600. At pick 3, the sapphire layer has the highest stress distribution of 47.528 to 53.452 MPa which is less than the yield strength of sapphire. Also, there is stress from sapphire to the filler of 47.528 to 53.452 MPa which is less than the yield strength of sapphire. At the layer of Inconel 600, there is also a stress of 47.528 to 53.452 MPa at the edge which is less than the yield strength of Inconel 600.

Therefore, the sample 2 with initial brazing temperature 830^0C as the stress obtained is less than the yield strength of sapphire and also the lowest compared to the other stress distribution of 865^0C and 900^0C.

4.5 SAMPLE 3

(a) 900^0C

It must be taken into consideration that pick 1 and 3 are the properties of temperatures between the brazing temperature of 900^0C to room temperature, 27^0C. On the other hand, pick 4 displays the properties at room temperature, 27^0C.

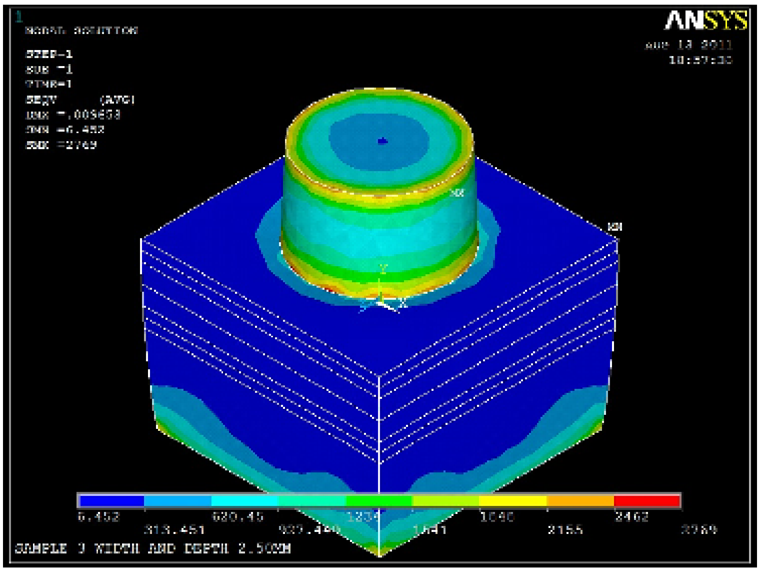

Figure 4.69: Von Mises Stress Distribution Plot for Pick 1 (900^0C)

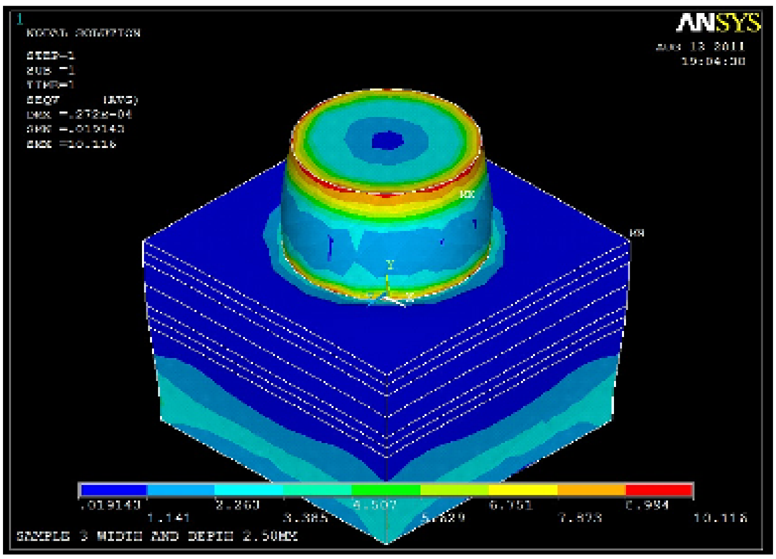

Figure 4.70: Von Mises Stress Distribution Plot for Pick 3 (900^0C)

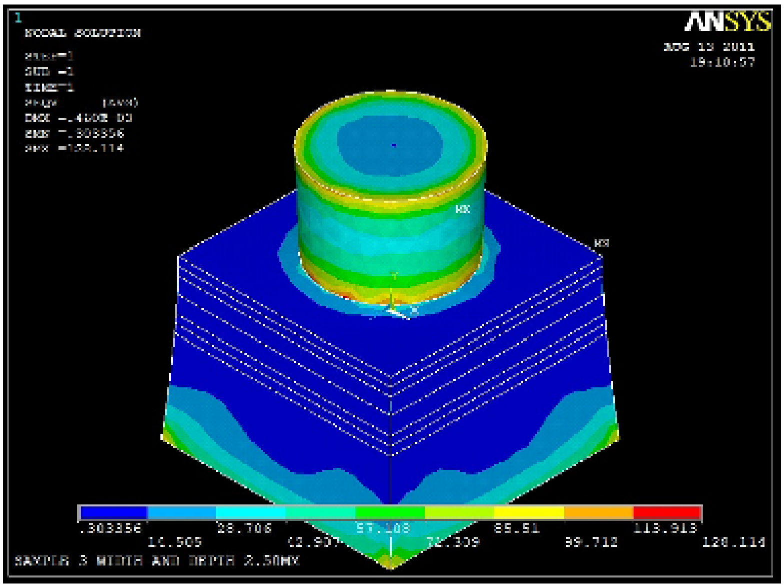

Figure 4.71: Von Mises Stress Distribution Plot for Pick 4 (900^{0}C)

(b) 865^{0}C

It must be taken into consideration that pick 1 and 2 are the properties of temperatures between the brazing temperature of 865^{0}C to room temperature, 27^{0}C. On the other hand, pick 3 displays the properties at room temperature, 27^{0}C.

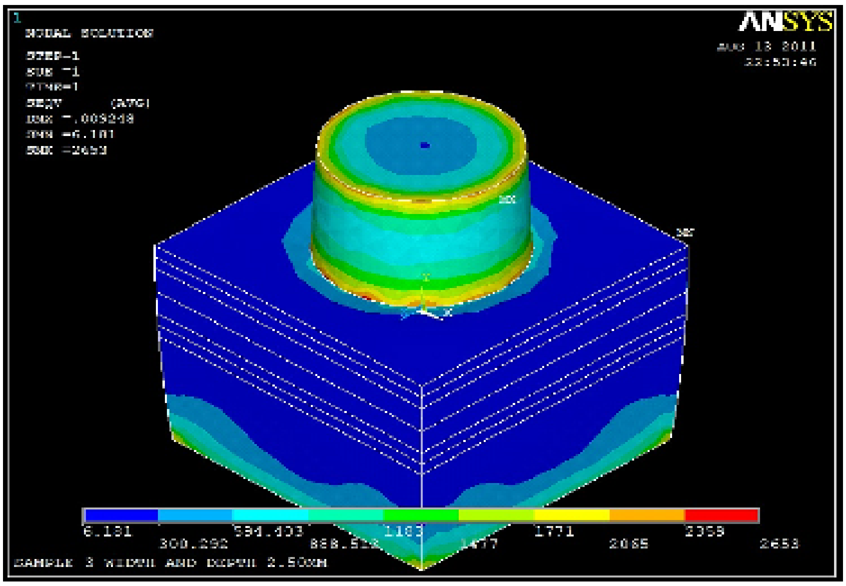

Figure 4.72: Von Mises Stress Distribution Plot for Pick 1 (865^{0}C)

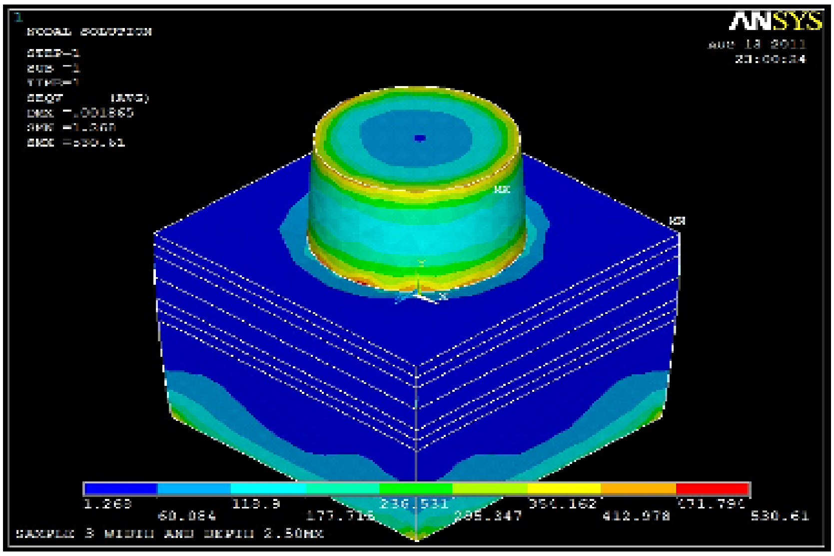

Figure 4.73: Von Mises Stress Distribution Plot for Pick 2 (865^{0}C)

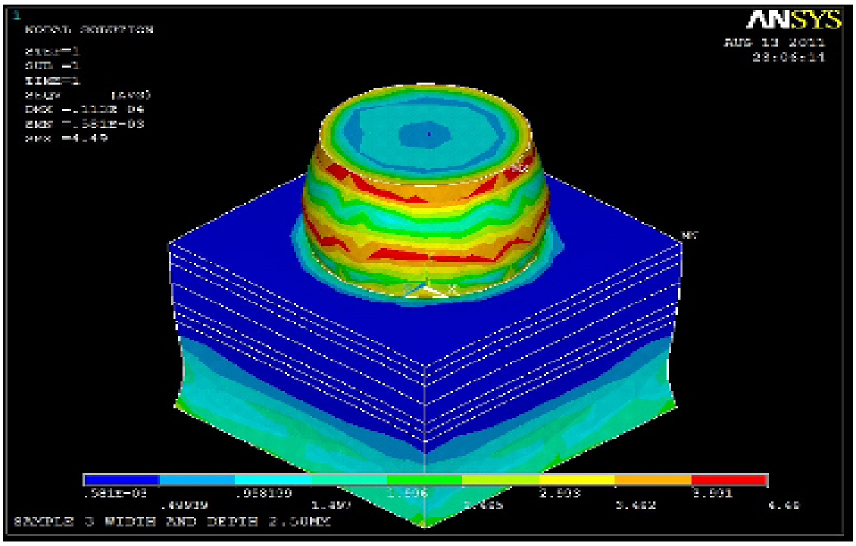

Figure 4.74: Von Mises Stress Distribution Plot for Pick 3 (865^{0}C)

(c) 830^{0}C

It must be taken into consideration that pick 1 and 2 are the properties of temperatures between the brazing temperature of 830^{0}C to room temperature, 27^{0}C. On the other hand, pick 3 displays the properties at room temperature, 27^{0}C.

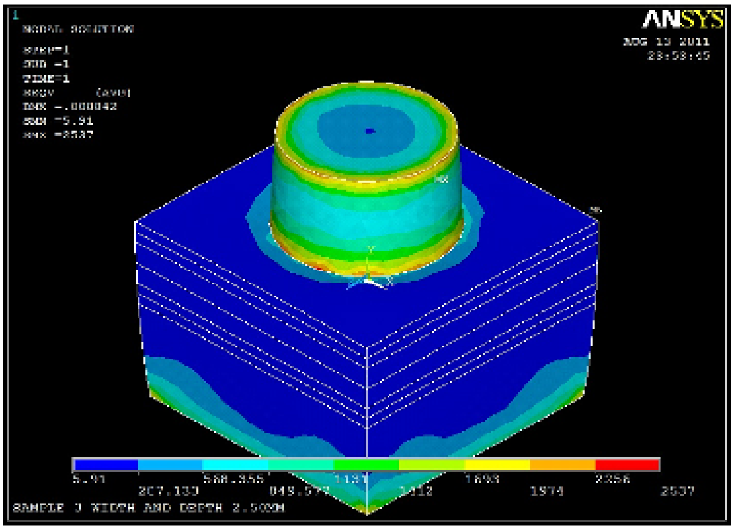

Figure 4.75: Von Mises Stress Distribution Plot for Pick 1 (830^0C)

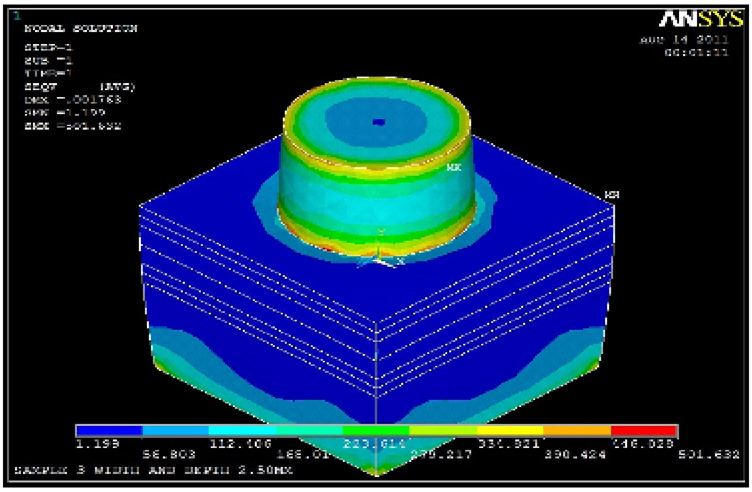

Figure 4.76: Von Mises Stress Distribution Plot for Pick 2 (830^0C)

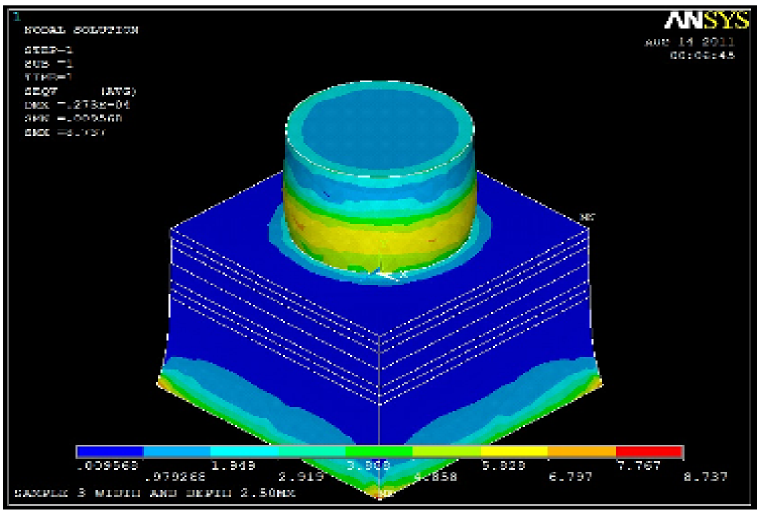

Figure 4.77: Von Mises Stress Distribution Plot for Pick 3 (830^0C)

The sample 3 is analyzed from initial brazing temperature of 900^0C to room temperature. At pick 1, the sapphire layer has the highest stress distribution of 2462 to 2769 MPa which is higher than the yield strength of sapphire. Also, there is stress from sapphire to the filler of 2462.00 to 2769.00 MPa which is higher than the yield strength of sapphire. At the layer of Inconel 600, there is also a high stress of 1841 to 1848 MPa at the edge which is higher than the yield strength of Inconel 600. At pick 3, the sapphire layer has the highest stress distribution of 8.994 to 10.116 MPa which is less than the yield strength of sapphire. Also, there is stress from sapphire to the filler of 8.994 to 10.116 MPa which is less than the yield strength of sapphire. At the layer of Inconel 600, there is also a stress of 1.141 to 2.263 MPa at the edge which is less than the yield strength of Inconel 600 and can be ignored. At pick 4, the sapphire layer has the highest stress distribution of 113.913 to 128.114 MPa which is less than the yield strength of sapphire. Also, there is stress from sapphire to the filler of 113.913 to 128.114 MPa which is less than the yield strength of sapphire. At the layer of Inconel 600, there is also a stress of 85.51 to 99.712 MPa at the edge which is less than the yield strength of Inconel 600.

The sample 3 is then analyzed from initial brazing temperature 865^0C to room temperature. At pick 1, the sapphire layer has the highest stress distribution of 2359 to 2653 MPa which is higher than the yield strength of sapphire. Also, there is stress from sapphire to the filler of 2359.00 to 2653.00 MPa which is higher than the yield strength of sapphire. At the layer of Inconel 600, there is also a high stress of 1477 to 1771 MPa at the edge which is higher than the yield strength of Inconel 600. At pick 2, the sapphire layer has the highest stress distribution of 471.794 to 530.61 MPa which is higher than the yield strength of sapphire. Also, there is stress from sapphire to the filler of 412.978 to 471.794 MPa which is higher than the yield strength of sapphire. At the layer of Inconel 600, there is also a stress of 471.794 to 530.61 MPa at the edge which is higher than the yield strength of Inconel 600. At pick 3, the sapphire layer has the highest stress distribution of 3.991 to 4.49 MPa which is less than the yield strength of sapphire. At the layer of Inconel 600, there is also a stress of 2.495 to 2.993 MPa at the edge which is less than the yield strength of Inconel 600.

Therefore, the sample 3 with initial brazing temperature 900^0C as the stress distribution is more even than the stress distribution of 865^0C and 830^0C.

4.6 SAMPLE 4

(a) 900^0C

It must be taken into consideration that pick 1 and 2 are the properties of temperatures between the brazing temperature of 900^0C to room temperature, 27^0C. On the other hand, pick 3 displays the properties at room temperature, 27^0C.

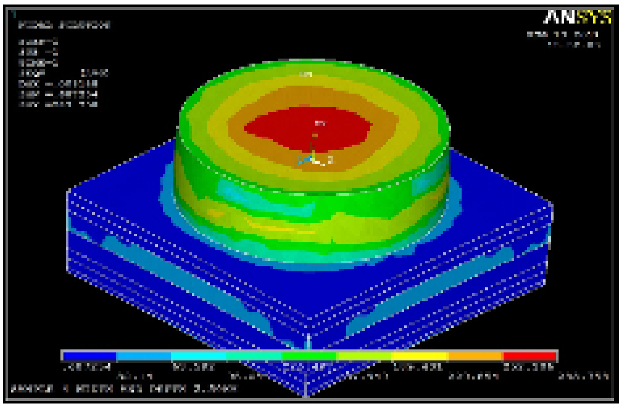

Figure 4.78: Von Mises Stress Distribution Plot for Pick 1 (900^0C)

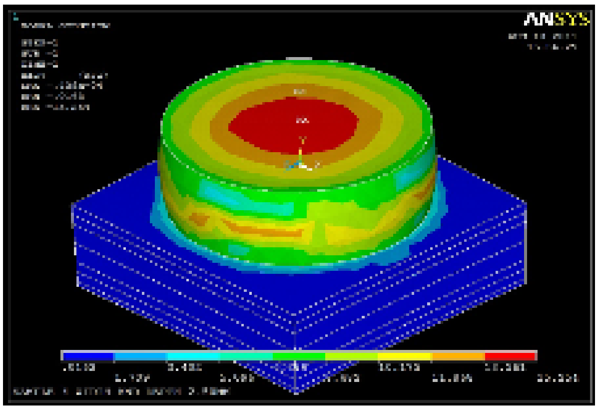

Figure 4.79: Von Mises Stress Distribution Plot for Pick 2 (900^0C)

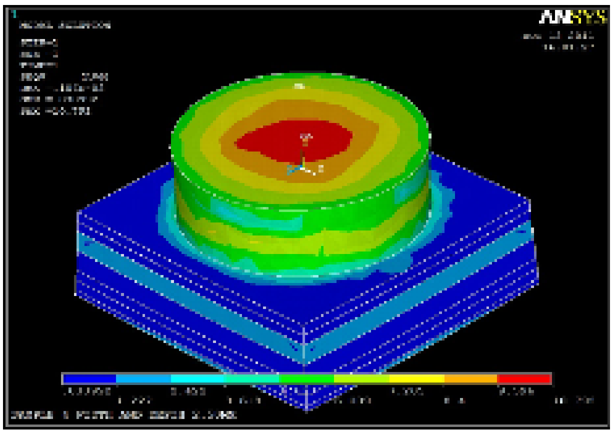

Figure 4.80: Von Mises Stress Distribution Plot for Pick 3 (900^0C)

(b) 865^{0}C

It must be taken into consideration that pick 1 and 2 are the properties of temperatures between the brazing temperature of 865^{0}C to room temperature, 27^{0}C. On the other hand, pick 3 displays the properties at room temperature, 27^{0}C.

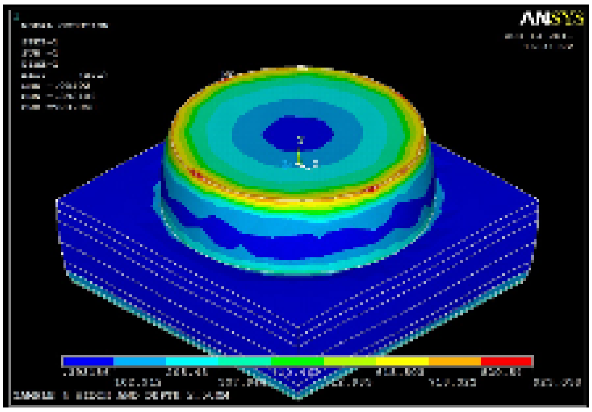

Figure 4.81: Von Mises Stress Distribution Plot for Pick 1 (865^{0}C)

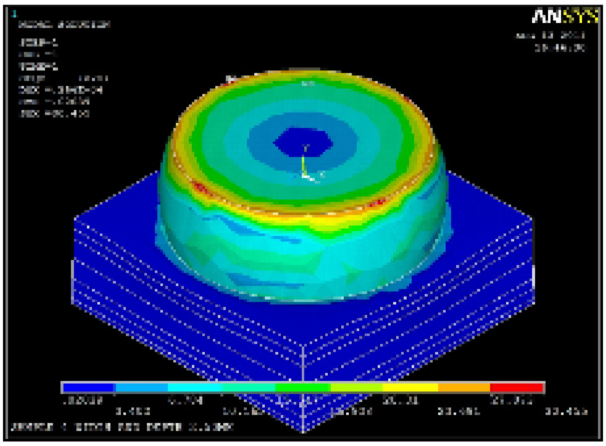

Figure 4.82: Von Mises Stress Distribution Plot for Pick 2 (865^{0}C)

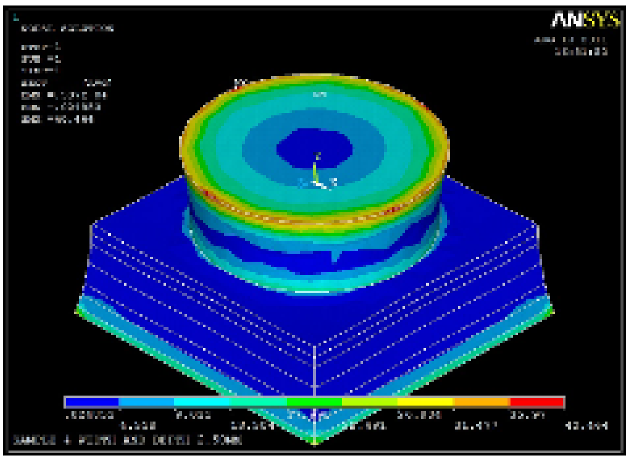

Figure 4.83: Von Mises Stress Distribution Plot for Pick 3 (865^{0}C)

(c) 830^0C

It must be taken into consideration that pick 1 and 2 are the properties of temperatures between the brazing temperature of 830^0C to room temperature, 27^0C. On the other hand, pick 3 displays the properties at room temperature, 27^0C.

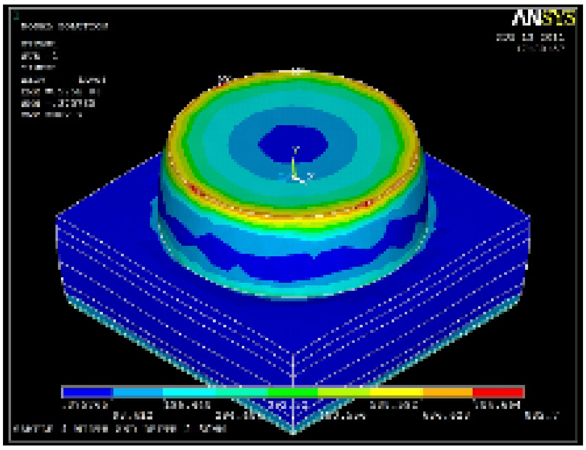

Figure 4.84: Von Mises Stress Distribution Plot for Pick 1 (830^0C)

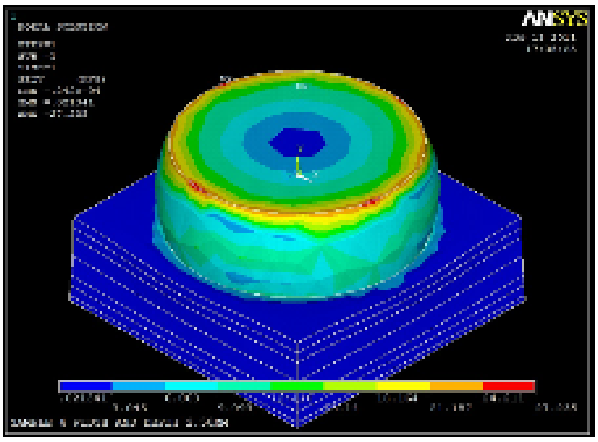

Figure 4.85: Von Mises Stress Distribution Plot for Pick 2 (830^0C)

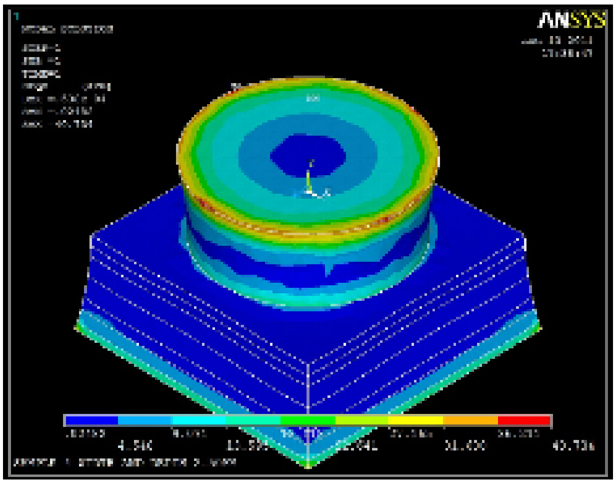

Figure 4.86: Von Mises Stress Distribution Plot for Pick 3 (830^0C)

The sample 4 is analyzed from initial brazing temperature 900^0C to room temperature. At pick 1, the sapphire layer has the highest stress distribution of 252.306 to 283.758 MPa which is less than the yield strength of sapphire. Also, there is stress from sapphire to the filler of 95.044 to 126.497 MPa which is less than the yield strength of sapphire. At the layer of Inconel 600, the stress can be ignored. At pick 2, the sapphire layer has the highest stress distribution of 13.561 to 15.254 MPa which is less than the yield strength of sapphire. Also, there is stress from sapphire to the filler of 11.868 to 13.561 MPa which is less than the yield strength of sapphire. At the layer of Inconel 600, there is also a stress of 5.096 to 6.789 MPa at the edge which is less than the yield strength of Inconel 600 and can be ignored. At pick 3, the sapphire layer has the highest stress distribution of 9.596 to 10.792 MPa which is less than the yield strength of sapphire. At the layer of Inconel 600, there is also a stress of 3.618 to 4.813 MPa at the edge which is less than the yield strength of Inconel 600.

The sample 4 is then analyzed from initial brazing temperature 865^0C to room temperature. At pick 1, the sapphire layer has the highest stress distribution of 820.54 to 923.058 MPa which is less than the yield strength of sapphire. At pick 2, the sapphire layer has the highest stress distribution of 27.073 to 30.455 MPa which is less than the yield strength of sapphire. At pick 3, the sapphire layer has the highest stress distribution of 35.97 to 40.464 MPa which is less than the yield strength of sapphire.

The sample 4 is then analyzed from initial brazing temperature 830^0C to room temperature. At pick 1, the sapphire layer has the highest stress distribution of 784.664 to 882.700 MPa which is higher than the yield strength of sapphire. Also, there is stress from sapphire to the filler of 196.448 to 294.484 MPa which is less than the yield strength of sapphire. At pick 2, the sapphire layer has the highest stress distribution of 24.211 to 27.235 MPa which is less than the yield strength of sapphire. Also, there is stress from sapphire to the filler of 3.045 to 6.069 MPa which is less than the yield strength of sapphire. At pick 3, the sapphire layer has the highest stress distribution of 36.211 to 40.734 MPa which is less than the yield strength of sapphire. At the layer of Inconel 600, there is also a stress of 22.641 to 27.265 MPa at the edge which is less than the yield strength of Inconel 600.

Therefore, the sample 4 with initial brazing temperature 900^0C as the stress obtained is less than the yield strength of sapphire and also the lowest compared to the other stress distribution of 865^0C and 830^0C.

4.7 SAMPLE 5

(a) 900^{0}C

It must be taken into consideration that pick 1 and 2 are the properties of temperatures between the brazing temperature of 900^{0}C to room temperature, 27^{0}C. On the other hand, pick 3 displays the properties at room temperature, 27^{0}C.

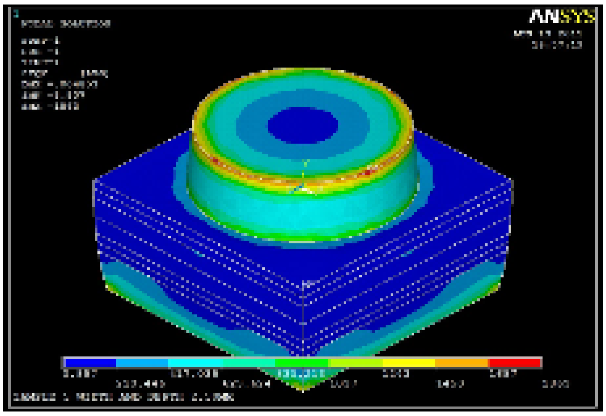

Figure 4.87: Von Mises Stress Distribution Plot for Pick 1 (900^{0}C)

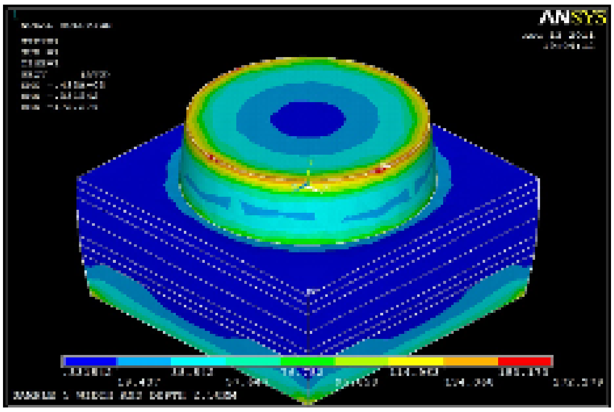

Figure 4.88: Von Mises Stress Distribution Plot for Pick 2 (900^{0}C)

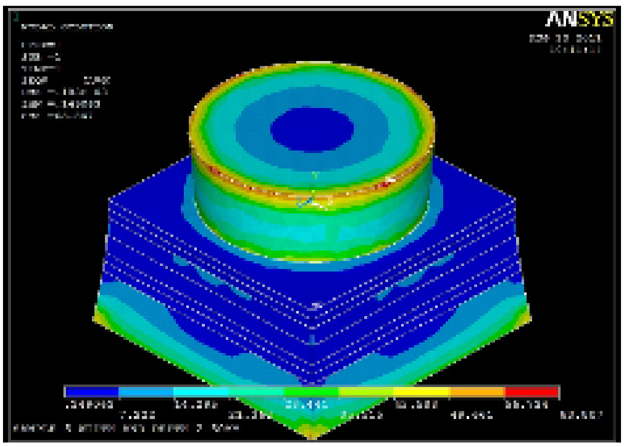

Figure 4.89: Von Mises Stress Distribution Plot for Pick 3 (900^{0}C)

(b) 865^0C

It must be taken into consideration that pick 1 and 2 are the properties of temperatures between the brazing temperature of 865^0C to room temperature, 27^0C. On the other hand, pick 3 displays the properties at room temperature, 27^0C.

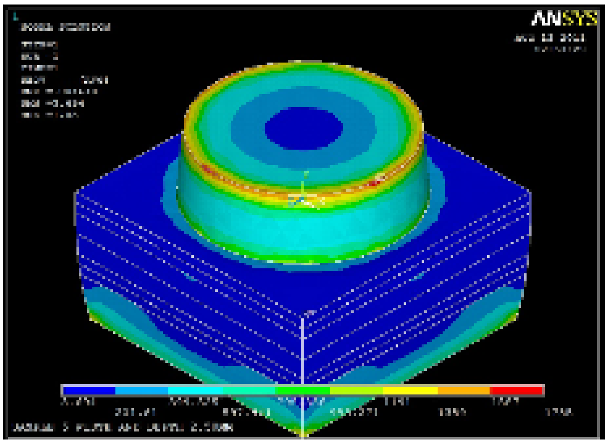

Figure 4.90: Von Mises Stress Distribution Plot for Pick 1 (865^0C)

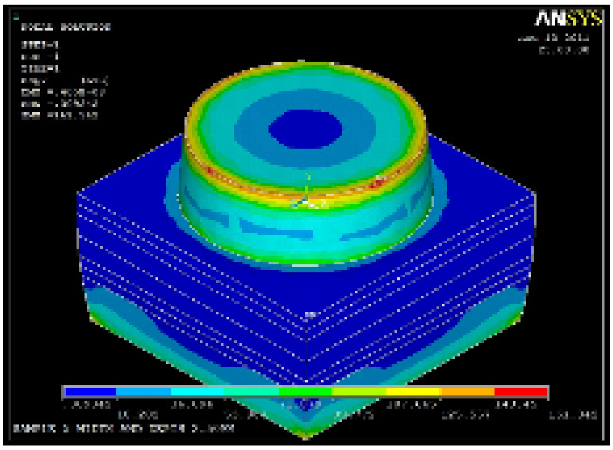

Figure 4.91: Von Mises Stress Distribution Plot for Pick 2 (865^0C)

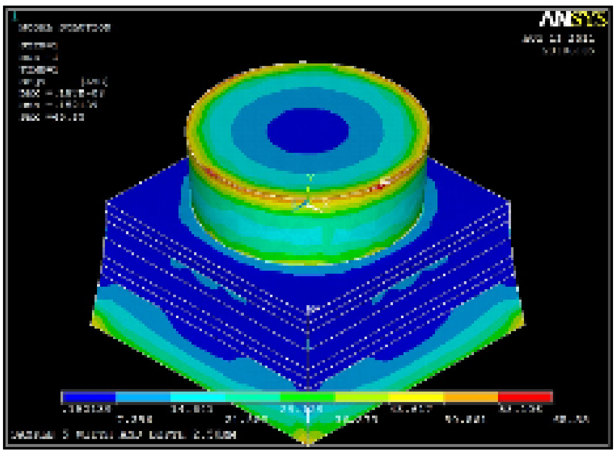

Figure 4.92: Von Mises Stress Distribution Plot for Pick 3 (865^0C)

(c) 830^{0}C

It must be taken into consideration that pick 1 and 2 are the properties of temperatures between the brazing temperature of 830^{0}C to room temperature, 27^{0}C. On the other hand, pick 3 displays the properties at room temperature, 27^{0}C.

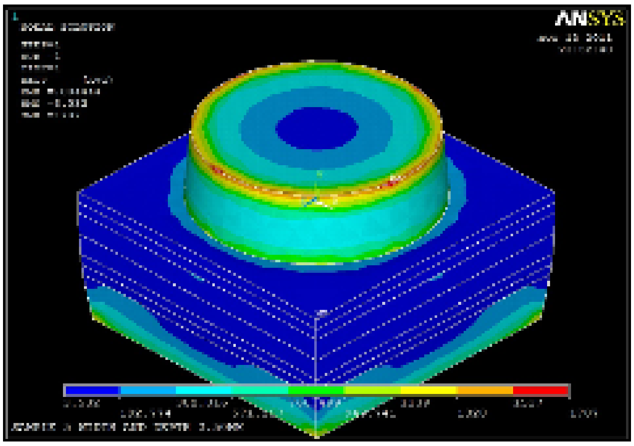

Figure 4.93: Von Mises Stress Distribution Plot for Pick 1 (830^{0}C)

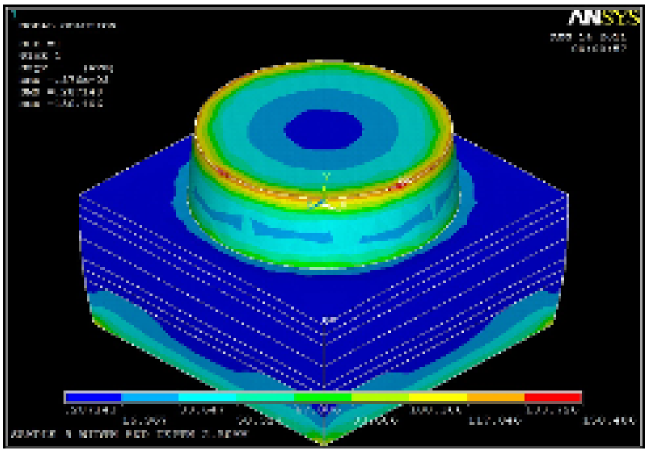

Figure 4.94: Von Mises Stress Distribution Plot for Pick 2 (830^{0}C)

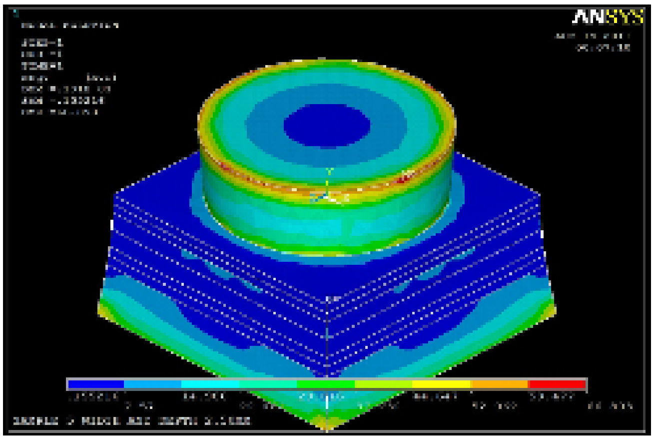

Figure 4.95: Von Mises Stress Distribution Plot for Pick 3 (830^{0}C)

The sample 5 is analyzed from initial brazing temperature of 900^0C to room temperature. At pick 1, the sapphire layer has the highest stress distribution of 1657 to 1863 MPa which is higher than the yield strength of sapphire. Also, there is stress from sapphire to the filler of 1037 to 1243 MPa which is higher than the yield strength of sapphire. At the layer of Inconel 600, there is stress of 1037 to 1243 MPa which is higher than the yield strength of Inconel 600. At pick 2, the sapphire layer has the highest stress distribution of 153.173 to 172.279 MPa which is less than the yield strength of sapphire. Also, there is stress from sapphire to the filler of 95.858 to 114.963 MPa which is less than the yield strength of sapphire. At the layer of Inconel 600, there is also a stress of 95.858 to 114.963 MPa at the edge which is less than the yield strength of Inconel 600. At pick 3, the sapphire layer has the highest stress distribution of 56.734 to 63.807 MPa which is less than the yield strength of sapphire. Also, there is stress from sapphire to the filler of 35.515 to 42.588 MPa which is less than the yield strength of sapphire. At the layer of Inconel 600, there is also a stress of 49.661 to 56.734 MPa at the edge which is less than the yield strength of Inconel 600.

The sample 5 is then analyzed from initial brazing temperature 865^0C to room temperature. At pick 1, the sapphire layer has the highest stress distribution of 1587 to 1785 MPa which is higher than the yield strength of sapphire. Also, there is stress from sapphire to the filler of 993.271 to 1191 MPa which is higher than the yield strength of sapphire. At the layer of Inconel 600, there is stress of 993.271 to 1191 MPa which is higher than the yield strength of Inconel 600. At pick 2, the sapphire layer has the highest stress distribution of 143.45 to 161.342 MPa which is less than the yield strength of sapphire. Also, there is stress from sapphire to the filler of 71.879 to 89.772 MPa which is less than the yield strength of sapphire. At the layer of Inconel 600, there is also a stress of 89.772 to 107.665 MPa at the edge which is less than the yield strength of Inconel 600. At pick 3, the sapphire layer has the highest stress distribution of 58.106 to 65.35 MPa which is less than the yield strength of sapphire. Also, there is stress from sapphire to the filler of 36.373 to 43.617 MPa which is less than the yield strength of sapphire. At the layer of Inconel 600, there is also a stress of 50.861 to 58.106 MPa at the edge which is less than the yield strength of Inconel 600.

The sample 5 is then analyzed from initial brazing temperature 830^0C to room temperature. At pick 1, the sapphire layer has the highest stress distribution of 1517 to 1707 MPa which is higher than the yield strength of sapphire. Also, there is stress from sapphire to the filler of 949.741 to 1139 MPa which is higher than the yield strength of sapphire. At the layer of Inconel 600, there is stress of 949.741 to 1139 MPa which is higher than the yield strength of Inconel 600. At pick 2, the sapphire layer has the highest stress distribution of 133.726 to 150.406 MPa which is less than the yield strength of sapphire. Also, there is stress from sapphire to the filler of 83.686 to 100.366 MPa which is less than the yield strength of sapphire. At the layer of Inconel 600, there is also a stress of 83.686 to 100.366 MPa at the edge which is less than the yield strength of Inconel 600. At pick 3, the sapphire layer has the highest stress distribution of 59.477 to 66.893 MPa which is less than the yield strength of sapphire. Also, there is stress from sapphire to the filler of 37.232 to 44.647 MPa which is less than the yield strength of sapphire. At the layer of Inconel 600, there is also a stress of 44.647 to 52.062 MPa at the edge which is less than the yield strength of Inconel 600.

Therefore, the sample 5 with initial brazing temperature 830^0C as the stress obtained is less than the yield strength of sapphire and also the lowest compared to the other stress distribution of 865^0C and 900^0C.

4.8 SAMPLE 6

(a) 900^0C

It must be taken into consideration that pick 1 and 2 are the properties of temperatures between the brazing temperature of 900^0C to room temperature, 27^0C. On the other hand, pick 3 displays the properties at room temperature, 27^0C.

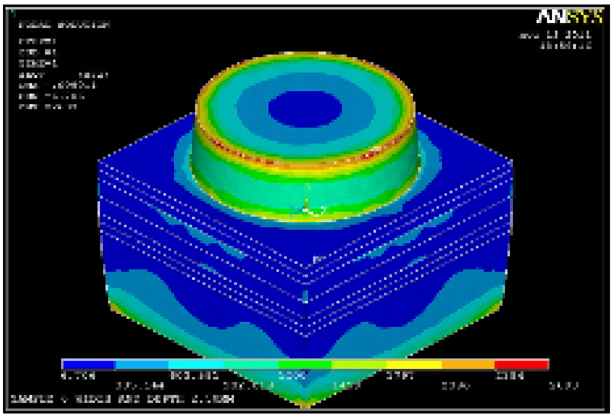

Figure 4.96: Von Mises Stress Distribution Plot for Pick 1 (900^0C)

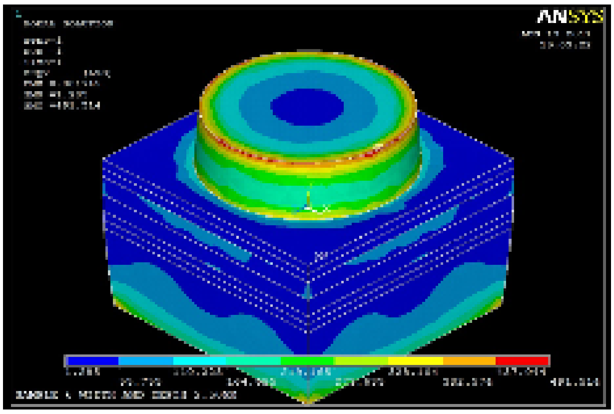

Figure 4.97: Von Mises Stress Distribution Plot for Pick 2 (900^0C)

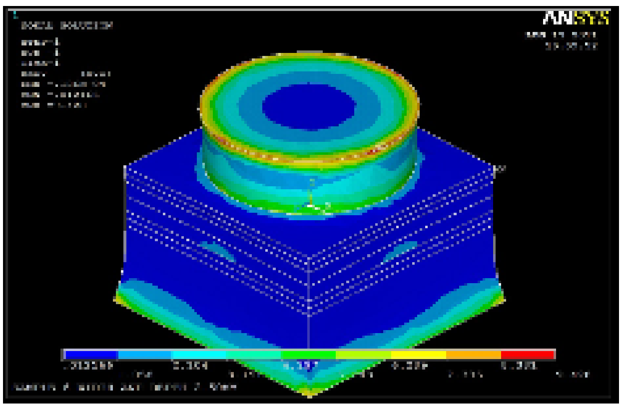

Figure 4.98: Von Mises Stress Distribution Plot for Pick 3 (900^0C)

(b) 865^0C

It must be taken into consideration that pick 1 and 2 are the properties of temperatures between the brazing temperature of 865^0C to room temperature, 27^0C. On the other hand, pick 3 displays the properties at room temperature, 27^0C.

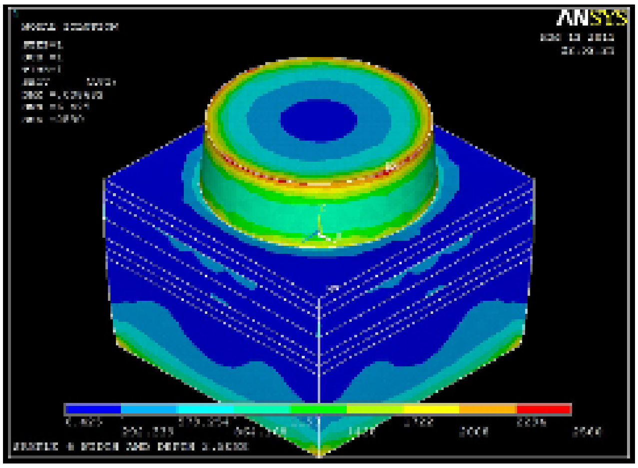

Figure 4.99: Von Mises Stress Distribution Plot for Pick 1 (865^0C)

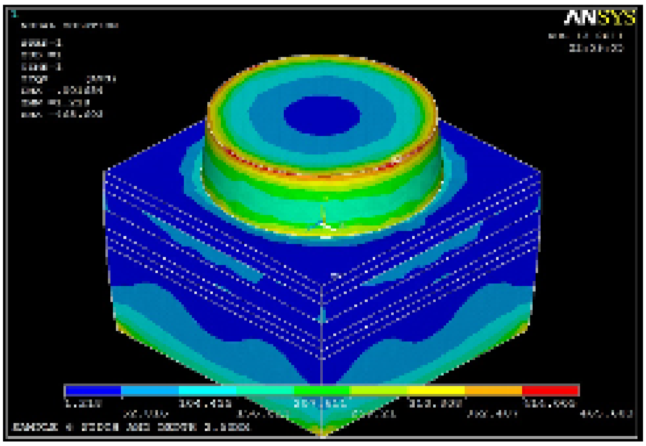

Figure 4.100: Von Mises Stress Distribution Plot for Pick 2 (865^0C)

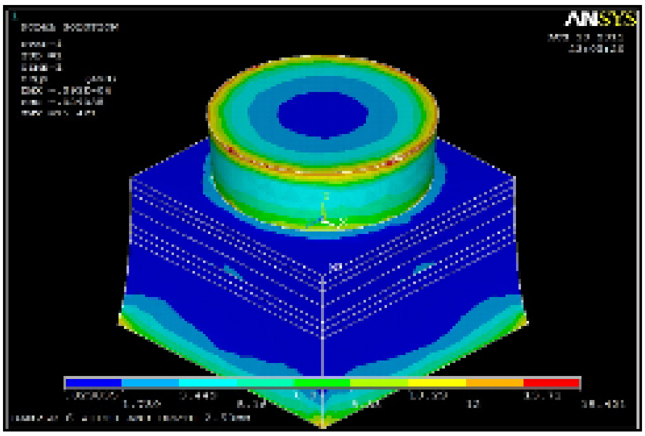

Figure 4.101: Von Mises Stress Distribution Plot for Pick 3 (865^0C)

(c) 830^0C

It must be taken into consideration that pick 1 and 2 are the properties of temperatures between the brazing temperature of 830^0C to room temperature, 27^0C. On the other hand, pick 3 displays the properties at room temperature, 27^0C.

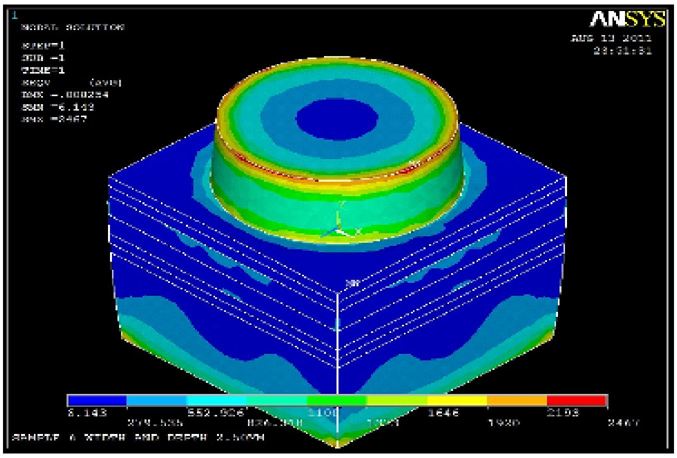

Figure 4.102: Von Mises Stress Distribution Plot for Pick 1 (830^0C)

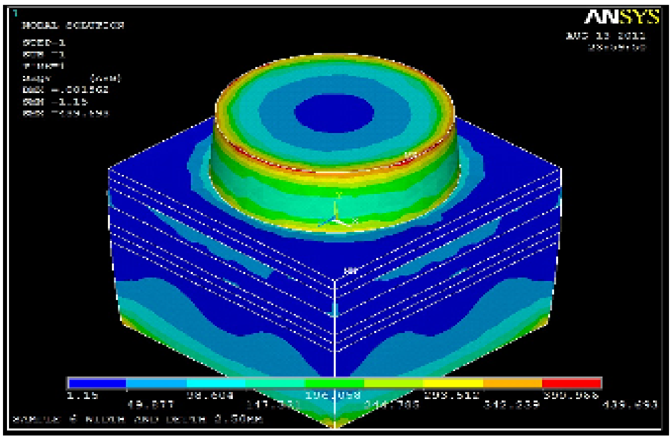

Figure 4.103: Von Mises Stress Distribution Plot for Pick 2 (830^0C)

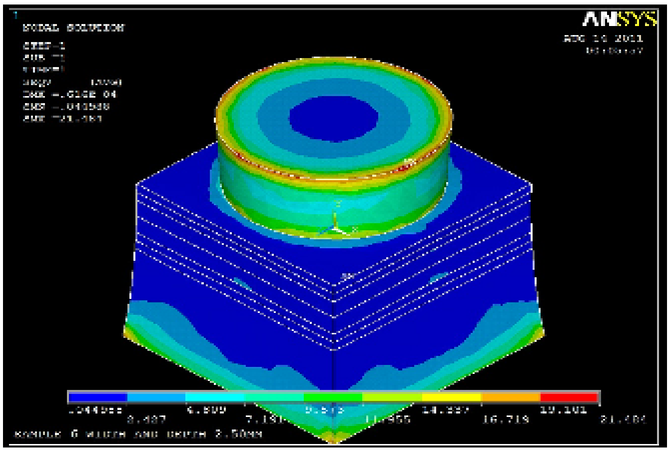

Figure 4.104: Von Mises Stress Distribution Plot for Pick 3 (830^0C)

The sample 6 is analyzed from initial brazing temperature 900^0C to room temperature. At pick 1, the sapphire layer has the highest stress distribution of 2394 to 2693 MPa which is higher than the yield strength of sapphire. Also, there is stress from sapphire to the filler of 1499 to 1797 MPa which is higher than the yield strength of sapphire. At the layer of Inconel 600, there is stress of 1797 to 2096 MPa which is higher than the yield strength of Inconel 600. At pick 2, the sapphire layer has the highest stress distribution of 437.044 to 491.514 MPa which is less or about the yield strength of sapphire. Also, there is stress from sapphire to the filler of 328.104 to 382.574 MPa which is less than the yield strength of sapphire. At the layer of Inconel 600, there is also a stress of 382.574 to 437.044 MPa at the edge which is less than the yield strength of Inconel 600. At pick 3, the sapphire layer has the highest stress distribution of 8.381 to 9.428 MPa which is less than the yield strength of sapphire. Also, there is stress from sapphire to the filler of 5.243 to 6.289 MPa which is less than the yield strength of sapphire. At the layer of Inconel 600, there is also a stress of 6.289 to 7.335 MPa at the edge which is less than the yield strength of Inconel 600.

The sample 6 is then analyzed from initial brazing temperature 865^0C to room temperature. At pick 1, the sapphire layer has the highest stress distribution of 2294 to 2580 MPa which is higher than the yield strength of sapphire. Also, there is stress from sapphire to the filler of 1702 to 2008 MPa which is higher than the yield strength of sapphire. At the layer of Inconel 600, there is stress of 2008 to 2294 MPa which is higher than the yield strength of Inconel 600. At pick 2, the sapphire layer has the highest stress distribution of 414.005 to 465.603 MPa which is higher than the yield strength of sapphire. Also, there is stress from sapphire to the filler of 310.808 to 362.407 MPa which is less than the yield strength of sapphire. At the layer of Inconel 600, there is also a stress of 362.407 to 414.005 MPa at the edge which is higher than the yield strength of Inconel 600. At pick 3, the sapphire layer has the highest stress distribution of 13.71 to 15.421 MPa which is less than the yield strength of sapphire. Also, there is stress from sapphire to the filler of 8.88 to 10.29 MPa which is less than the yield strength of sapphire. At the layer of Inconel 600, there is also a stress of 12.00 to 13.71 MPa at the edge which is less than the yield strength of Inconel 600.

The sample 6 is then analyzed from initial brazing temperature 830^0C to room temperature. At pick 1, the sapphire layer has the highest stress distribution of 2193 to 2467 MPa which is higher than the yield strength of sapphire. Also, there is stress from sapphire to the filler of 1646 to 1920 MPa which is higher than the yield strength of sapphire. At the layer of Inconel 600, there is stress of 1920 to 2193 MPa which is higher than the yield strength of Inconel 600. At pick 2, the sapphire layer has the highest stress distribution of 390.966 to 439.693 MPa which is less than the yield strength of sapphire. Also, there is stress from sapphire to the filler of 293.512 to 342.239 MPa which is less than the yield strength of sapphire. At the layer of Inconel 600, there is also a stress of 342.239 to 390.966 MPa at the edge which is less than the yield strength of Inconel 600. At pick 3, the sapphire layer has the highest stress distribution of 19.101 to 21.484 MPa which is less than the yield strength of sapphire. Also, there is stress from sapphire to the filler of 11.955 to 14.337 MPa which is less than the yield strength of sapphire. At the layer of Inconel 600, there is also a stress of 16.719 to 19.101 MPa at the edge which is less than the yield strength of Inconel 600.

Therefore, the sample 6 with initial brazing temperature 865^0C as the stress obtained is less than the yield strength of sapphire and also the lowest compared to the other stress distribution of 830^0C and 900^0C.

4.9 SAMPLE 7

(a) 900^0C

It must be taken into consideration that pick 1 and 2 are the properties of temperatures between the brazing temperature of 900^0C to room temperature, 27^0C. On the other hand, pick 3 displays the properties at room temperature, 27^0C.

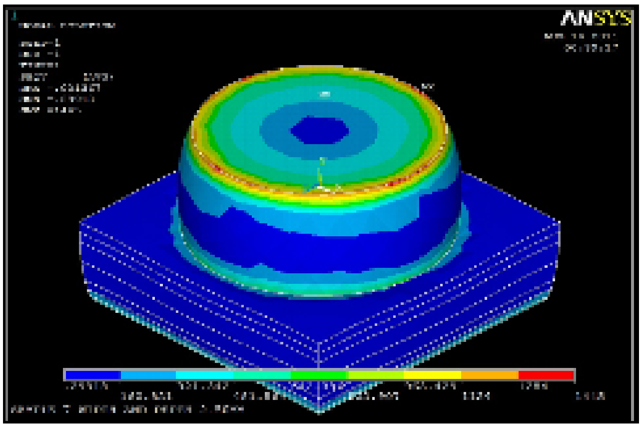

Figure 4.105: Von Mises Stress Distribution Plot for Pick 1 (900^0C)

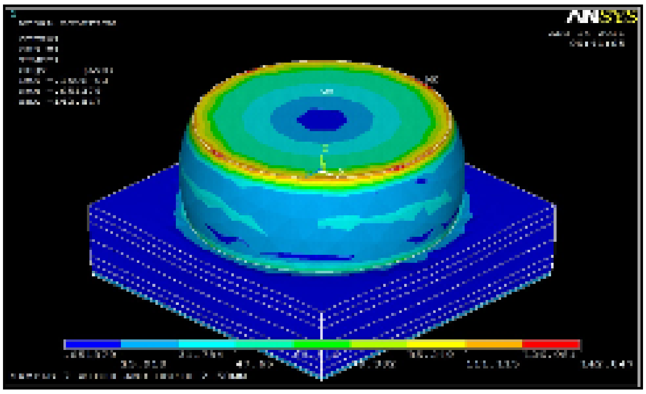

Figure 4.106: Von Mises Stress Distribution Plot for Pick 2 (900^0C)

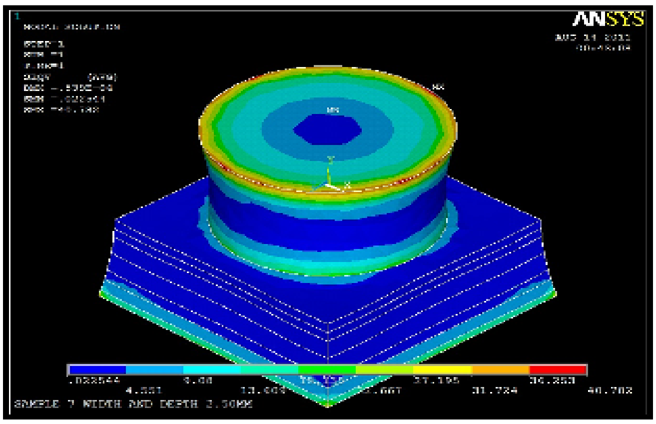

Figure 4.107: Von Mises Stress Distribution Plot for Pick 3 (900^0C)

(b) 865^0C

It must be taken into consideration that pick 1 and 2 are the properties of temperatures between the brazing temperature of 865^0C to room temperature, 27^0C. On the other hand, pick 3 displays the properties at room temperature, 27^0C.

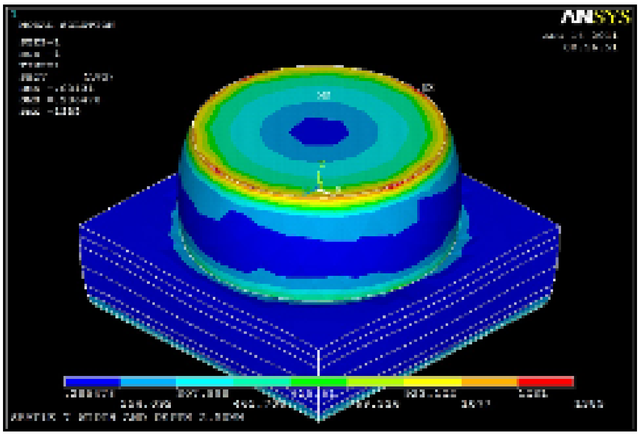

Figure 4.108: Von Mises Stress Distribution Plot for Pick 1 (865^0C)

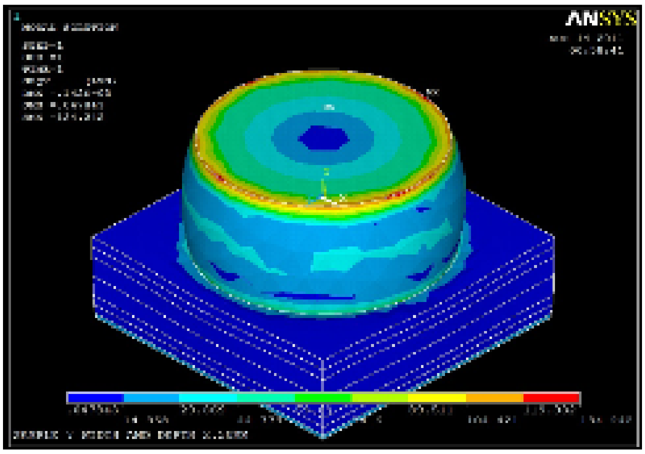

Figure 4.109: Von Mises Stress Distribution Plot for Pick 2 (865^0C)

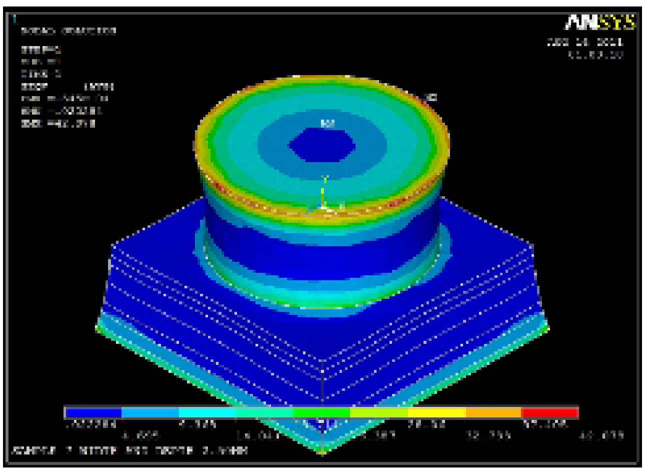

Figure 4.110: Von Mises Stress Distribution Plot for Pick 3 (865^0C)

(c) 830^0C

It must be taken into consideration that pick 1 and 2 are the properties of temperatures between the brazing temperature of 830^0C to room temperature, 27^0C. On the other hand, pick 3 displays the properties at room temperature, 27^0C.

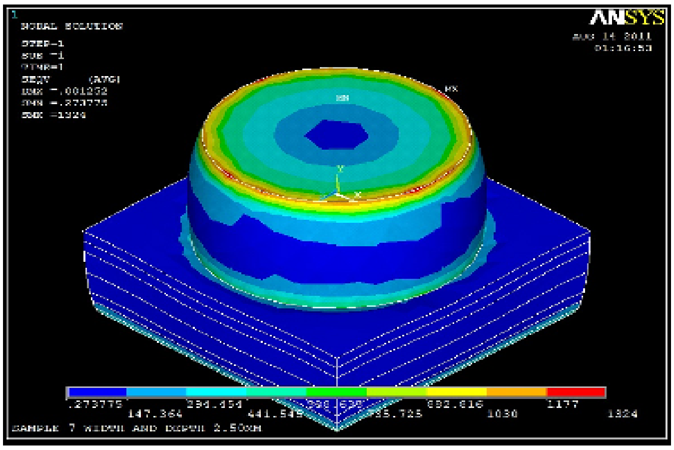

Figure 4.111: Von Mises Stress Distribution Plot for Pick 1 (830^0C)

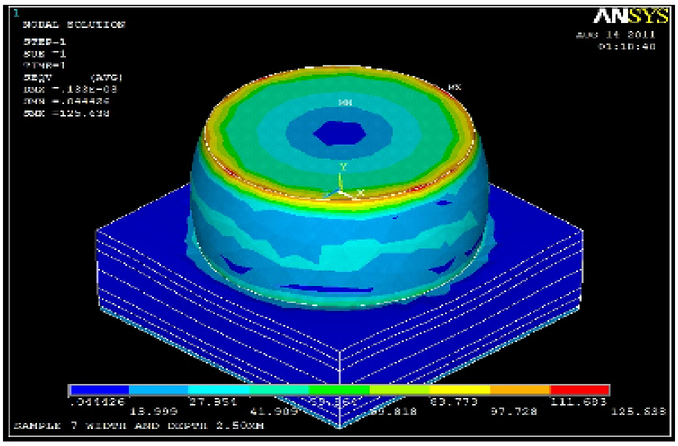

Figure 4.112: Von Mises Stress Distribution Plot for Pick 2 (830^0C)

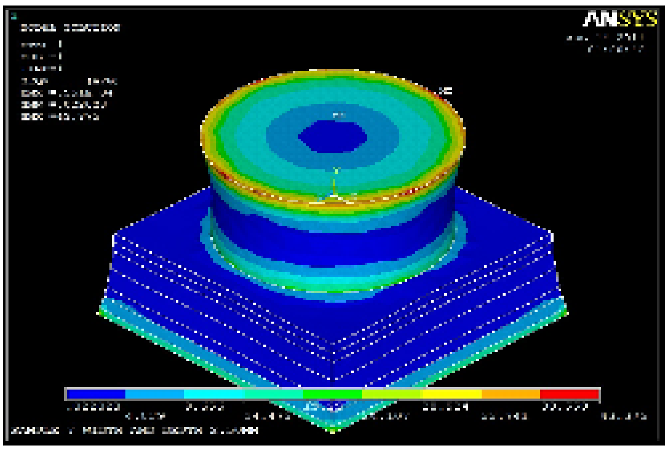

Figure 4.113: Von Mises Stress Distribution Plot for Pick 3 (830^0C)

The sample 7 is analyzed from initial brazing temperature 900^0C to room temperature. At pick 1, the sapphire layer has the highest stress distribution of 1284 to 1445 MPa which is higher than the yield strength of sapphire. Also, there is stress from sapphire to the filler of 481.864 to 642.386 MPa which is higher than the yield strength of sapphire. At the layer of Inconel 600, there is stress of 160.821 to 321.342 MPa which is higher than the yield strength of Inconel 600. At pick 2, the sapphire layer has the highest stress distribution of 126.981 to 142.847 MPa which is less or about the yield strength of sapphire. Also, there is stress from sapphire to the filler of 63.104 to 79.382 MPa which is less than the yield strength of sapphire. At the layer of Inconel 600, there is also a stress of 15.918 to 31.784 MPa at the edge which is less than the yield strength of Inconel 600. At pick 3, the sapphire layer has the highest stress distribution of 36.253 to 40.782 MPa which is less than the yield strength of sapphire. Also, there is stress from sapphire to the filler of 18.138 to 22.667 MPa which is less than the yield strength of sapphire. At the layer of Inconel 600, there is also a stress of 22.667 to 27.195 MPa at the edge which is less than the yield strength of Inconel 600.

The sample 7 is then analyzed from initial brazing temperature 865^0C to room temperature. At pick 1, the sapphire layer has the highest stress distribution of 1231 to 1385 MPa which is higher than the yield strength of sapphire. Also, there is stress from sapphire to the filler of 615.51 to 769.316 MPa which is higher than the yield strength of sapphire. At the layer of Inconel 600, there is stress of 307.898 to 461.704 MPa which is higher than the yield strength of Inconel 600. At pick 2, the sapphire layer has the highest stress distribution of 119.332 to 134.242 MPa which is less than the yield strength of sapphire. Also, there is stress from sapphire to the filler of 59.69 to 74.6 MPa which is less than the yield strength of sapphire. At the layer of Inconel 600, there is also a stress of 14.958 to 29.869 MPa at the edge which is less than the yield strength of Inconel 600. At pick 3, the sapphire layer has the highest stress distribution of 37.405

to 42.078 MPa which is less than the yield strength of sapphire. Also, there is stress from sapphire to the filler of 18.714 to 23.387 MPa which is less than the yield strength of sapphire. At the layer of Inconel 600, there is also a stress of 23.387 to 28.06 MPa at the edge which is less than the yield strength of Inconel 600.

The sample 7 is then analyzed from initial brazing temperature 830^0C to room temperature. At pick 1, the sapphire layer has the highest stress distribution of 1177 to 1324 MPa which is higher than the yield strength of sapphire. Also, there is stress from sapphire to the filler of 588.635 to 735.725 MPa which is higher than the yield strength of sapphire. At the layer of Inconel 600, there is stress of 294.454 to 441.545 MPa which is higher than the yield strength of Inconel 600. At pick 2, the sapphire layer has the highest stress distribution of 111.683 to 125.638 MPa which is less than the yield strength of sapphire. Also, there is stress from sapphire to the filler of 55.864 to 69.818 MPa which is less than the yield strength of sapphire. At the layer of Inconel 600, there is also a stress of 13.999 to 27.954 MPa at the edge which is less than the yield strength of Inconel 600. At pick 3, the sapphire layer has the highest stress distribution of 38.558 to 43.375 MPa which is less than the yield strength of sapphire. Also, there is stress from sapphire to the filler of 19.29 to 24.107 MPa which is less than the yield strength of sapphire. At the layer of Inconel 600, there is also a stress of 24.107 to 28.924 MPa at the edge which is less than the yield strength of Inconel 600.

Therefore, the sample 7 with initial brazing temperature 900^0C as the stress obtained is less than the yield strength of sapphire and also the lowest compared to the other stress distribution of 865^0C and 830^0C.

4.10 SAMPLE 8

(a) 900^0C

It must be taken into consideration that pick 1 and 2 are the properties of temperatures between the brazing temperature of 900^0C to room temperature, 27^0C. On the other hand, pick 3 displays the properties at room temperature, 27^0C.

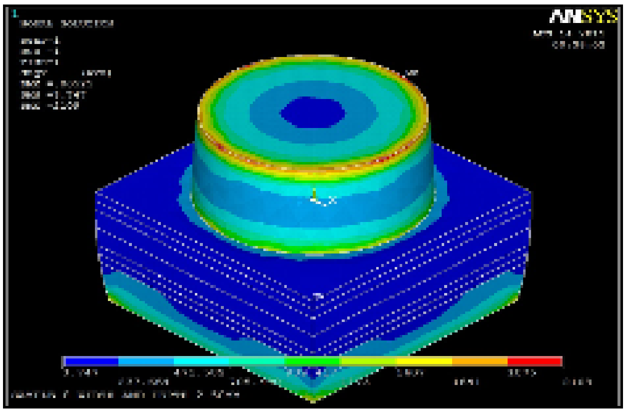

Figure 4.114: Von Mises Stress Distribution Plot for Pick 1 (900^0C)

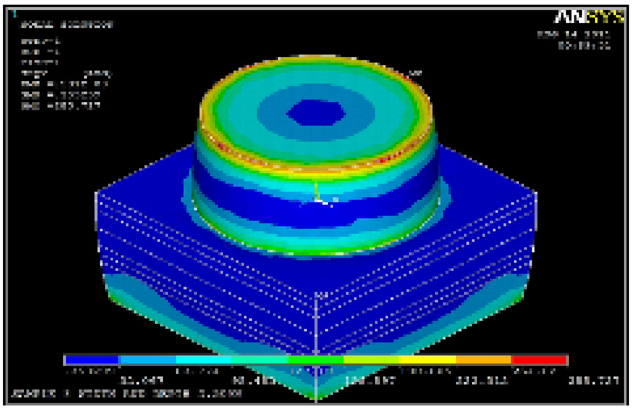

Figure 4.115: Von Mises Stress Distribution Plot for Pick 2 (900^0C)

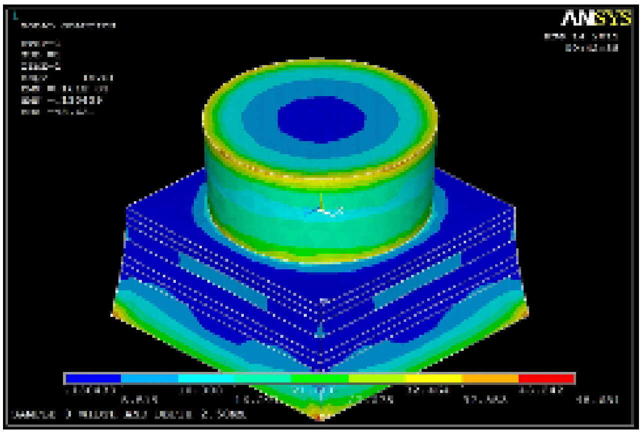

Figure 4.116: Von Mises Stress Distribution Plot for Pick 3 (900^0C)

(b) 865^{0}C

It must be taken into consideration that pick 1 and 2 are the properties of temperatures between the brazing temperature of 865^{0}C to room temperature, 27^{0}C. On the other hand, pick 3 displays the properties at room temperature, 27^{0}C.

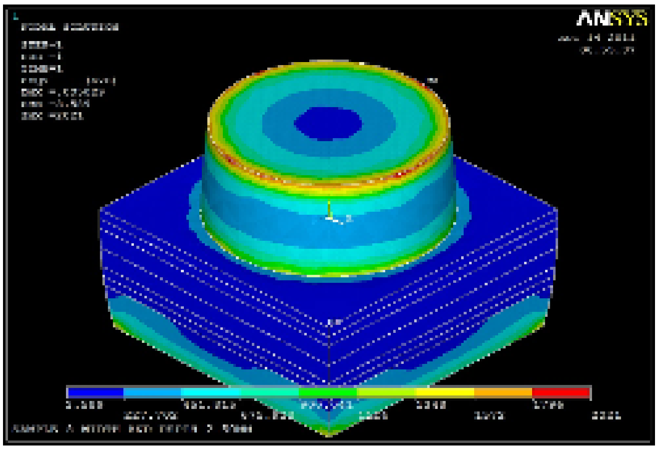

Figure 4.117: Von Mises Stress Distribution Plot for Pick 1 (865^{0}C)

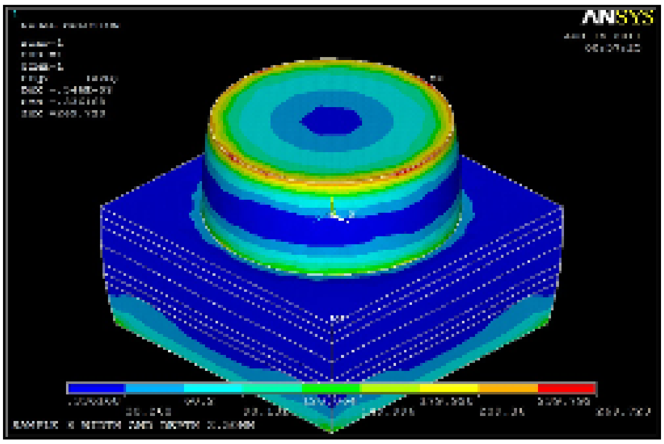

Figure 4.118: Von Mises Stress Distribution Plot for Pick 2 (865^{0}C)

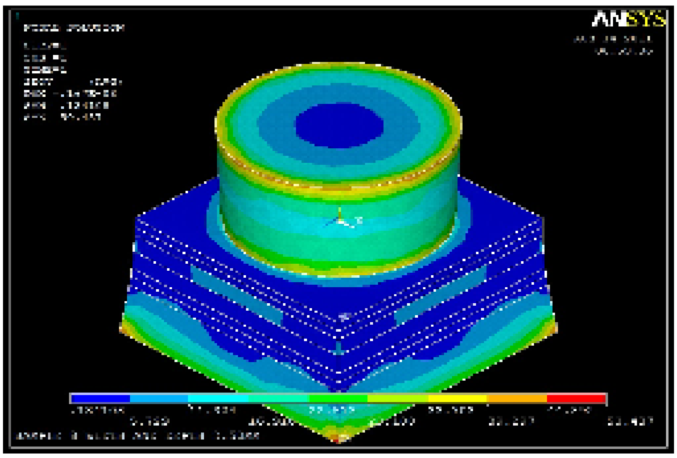

Figure 4.119: Von Mises Stress Distribution Plot for Pick 3 (865^{0}C)

(c) 830^{0}C

It must be taken into consideration that pick 1 and 2 are the properties of temperatures between the brazing temperature of 830^{0}C to room temperature, 27^{0}C. On the other hand, pick 3 displays the properties at room temperature, 27^{0}C.

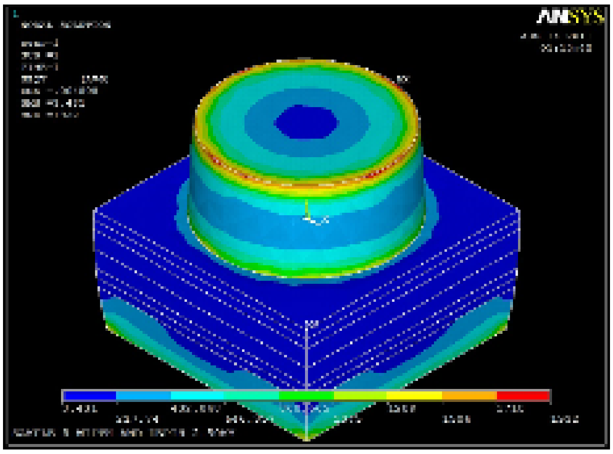

Figure 4.120: Von Mises Stress Distribution Plot for Pick 1 (830^{0}C)

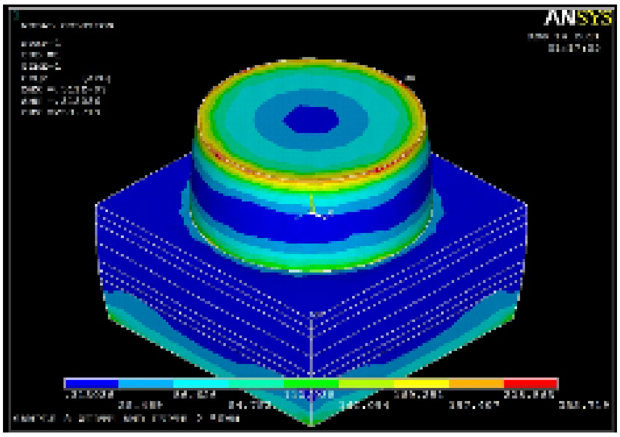

Figure 4.121: Von Mises Stress Distribution Plot for Pick 2 (830^{0}C)

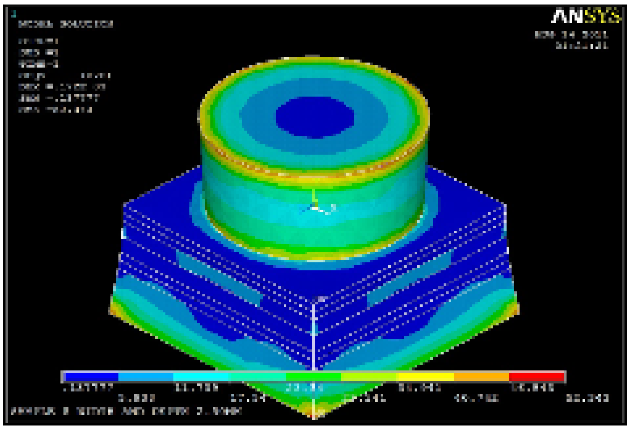

Figure 4.122: Von Mises Stress Distribution Plot for Pick 3 (830^{0}C)

The sample 8 is analyzed from initial brazing temperature 900^0C to room temperature. At pick 1, the sapphire layer has the highest stress distribution of 1875 to 2109 MPa which is higher than the yield strength of sapphire. Also, there is stress from sapphire to the filler of 1407 to 1641 MPa which is higher than the yield strength of sapphire. At the layer of Inconel 600, there is stress of 1173 to 1407 MPa which is higher than the yield strength of Inconel 600. At pick 2, the sapphire layer has the highest stress distribution of 254.02 to 285.727 MPa which is less or about the yield strength of sapphire. Also, there is stress from sapphire to the filler of 156.897 to 190.605 MPa which is less than the yield strength of sapphire. At the layer of Inconel 600, there is also a stress of 127.19 to 158.897 MPa at the edge which is less than the yield strength of Inconel 600. At pick 3, the sapphire layer has the highest stress distribution of 43.242 to 48.631 MPa which is less than the yield strength of sapphire. Also, there is stress from sapphire to the filler of 32.464 to 37.853 MPa which is less than the yield strength of sapphire. At the layer of Inconel 600, there is also a stress of 43.242 to 48.631 MPa at the edge which is less than the yield strength of Inconel 600.

The sample 8 is then analyzed from initial brazing temperature 865^0C to room temperature. At pick 1, the sapphire layer has the highest stress distribution of 1796 to 2021 MPa which is higher than the yield strength of sapphire. Also, there is stress from sapphire to the filler of 1348 to 1572 MPa which is higher than the yield strength of sapphire. At the layer of Inconel 600, there is stress of 1124 to 1348 MPa which is higher than the yield strength of Inconel 600. At pick 2, the sapphire layer has the highest stress distribution of 239.792 to 269.723 MPa which is less than the yield strength of sapphire. Also, there is stress from sapphire to the filler of 149.996 to 179.928 MPa which is less than the yield strength of sapphire. At the layer of Inconel 600, there is also a stress of 120.064 to 149.996 MPa at the edge which is less than the yield strength of Inconel 600. At pick 3, the sapphire layer has the highest stress distribution of 44.892 to 50.487 MPa which is less than the yield strength of sapphire. Also, there is stress from sapphire to the filler of 33.703 to 39.297 MPa which is less than the yield strength of sapphire. At the layer of Inconel 600, there is also a stress of 44.892 to 50.487 MPa at the edge which is less than the yield strength of Inconel 600.

The sample 8 is analyzed from initial brazing temperature 830^0C to room temperature. At pick 1, the sapphire layer has the highest stress distribution of 1718 to 1932 MPa which is higher than the yield strength of sapphire. Also, there is stress from sapphire to the filler of 1075 to 1289 MPa which is higher than the yield strength of sapphire. At the layer of Inconel 600, there is stress of 1075 to 1289 MPa which is higher than the yield strength of Inconel 600. At pick 2, the sapphire layer has the highest stress distribution of 225.563 to 253.719 MPa which is less than the yield strength of sapphire. Also, there is stress from sapphire to the filler of 141.094 to 169.251 MPa which is less than the yield strength of sapphire. At the layer of Inconel 600, there is also a stress of 112.938 to 141.094 MPa at the edge which is less than the yield strength of Inconel 600. At pick 3, the sapphire layer has the highest stress distribution of 46.543 to 52.343 MPa which is less than the yield strength of sapphire. Also, there is stress from sapphire to the filler of 34.941 to 40.742 MPa which is less than the yield strength of sapphire. At the layer of Inconel 600, there is also a stress of 46.543 to 52.343 MPa at the edge which is less than the yield strength of Inconel 600.

Therefore, the sample 8 with initial brazing temperature 830^0C as the stress obtained is less than the yield strength of sapphire and also the lowest compared to the other stress distribution of 865^0C and 900^0C.

4.11 SAMPLE 9

(a) 900^0C

It must be taken into consideration that pick 1 and 3 are the properties of temperatures between the brazing temperature of 900^0C to room temperature, 27^0C. On the other hand, pick 4 displays the properties at room temperature, 27^0C.

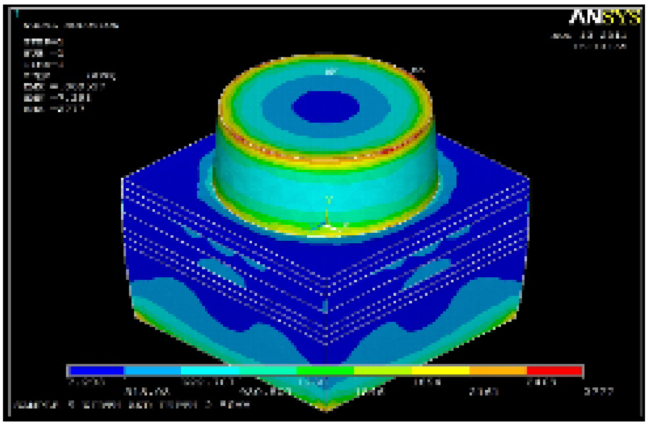

Figure 4.123: Von Mises Stress Distribution Plot for Pick 1 (900^0C)

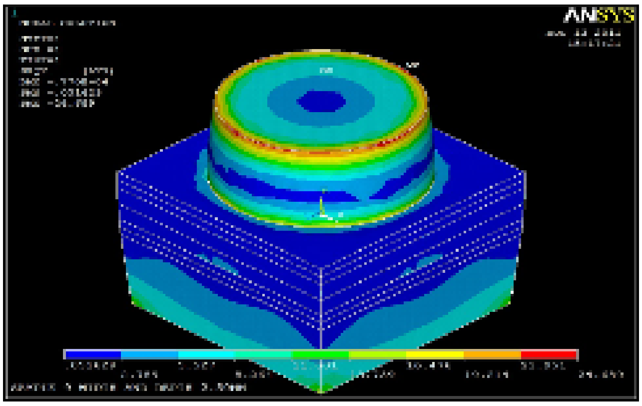

Figure 4.124: Von Mises Stress Distribution Plot for Pick 3 (900^0C)

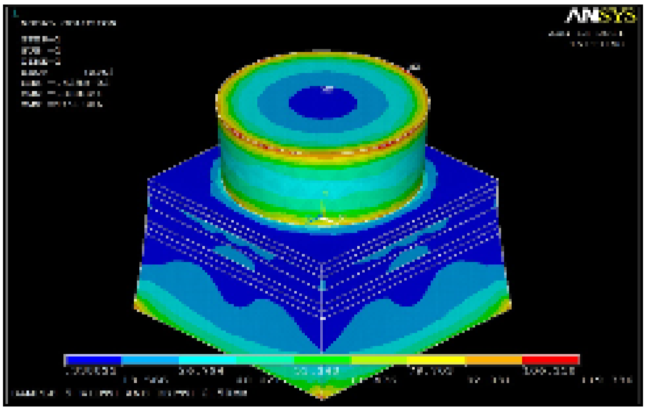

Figure 4.125: Von Mises Stress Distribution Plot for Pick 4 (900^0C)

(b) 865^0C

It must be taken into consideration that pick 1 and 3 are the properties of temperatures between the brazing temperature of 865^0C to room temperature, 27^0C. On the other hand, pick 4 displays the properties at room temperature, 27^0C.

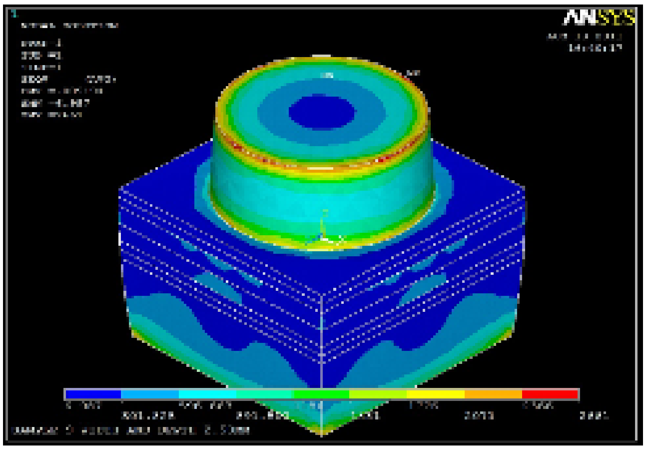

Figure 4.126: Von Mises Stress Distribution Plot for Pick 1 (865^0C)

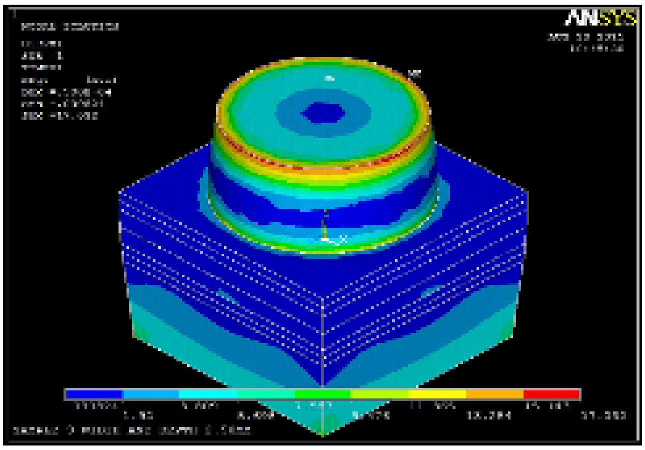

Figure 4.127: Von Mises Stress Distribution Plot for Pick 3 (865^0C)

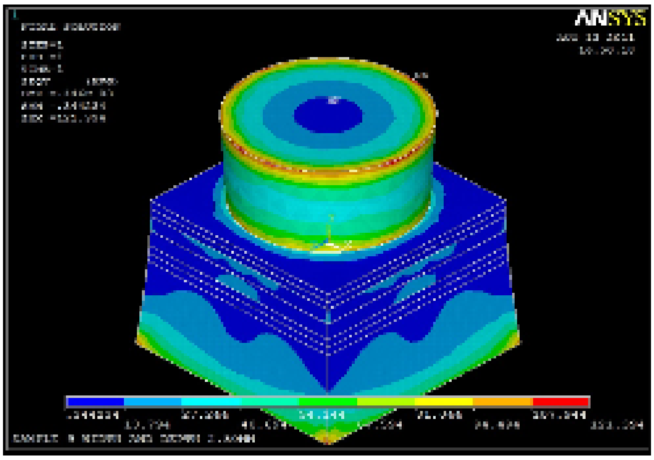

Figure 4.128: Von Mises Stress Distribution Plot for Pick 4 (865^0C)

(c) 830^{0}C

It must be taken into consideration that pick 1 and 2 are the properties of temperatures between the brazing temperature of 830^{0}C to room temperature, 27^{0}C. On the other hand, pick 3 displays the properties at room temperature, 27^{0}C.

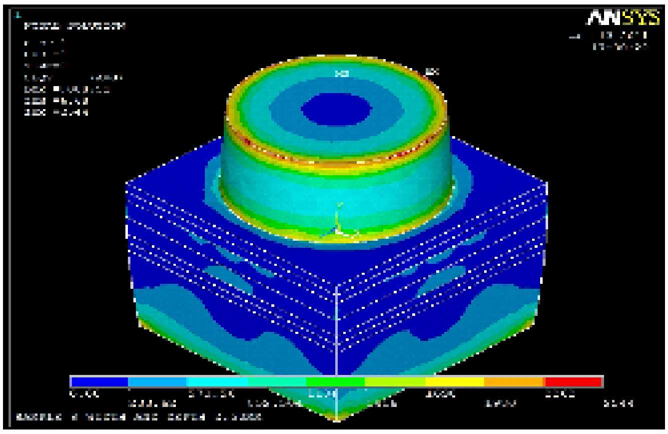

Figure 4.129: Von Mises Stress Distribution Plot for Pick 1 (830^{0}C)

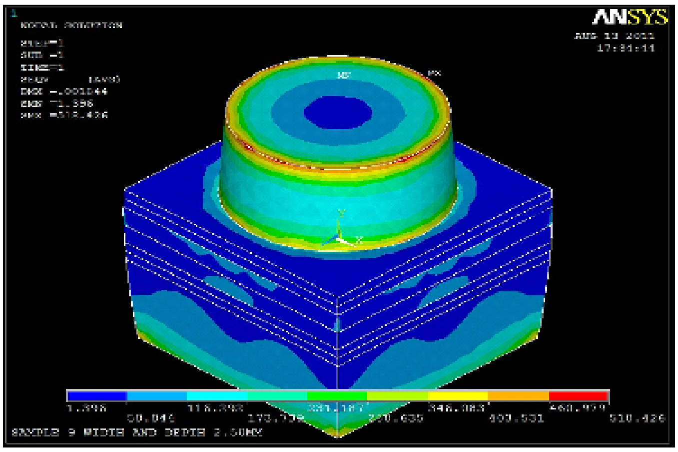

Figure 4.130: Von Mises Stress Distribution Plot for Pick 2 (830^{0}C)

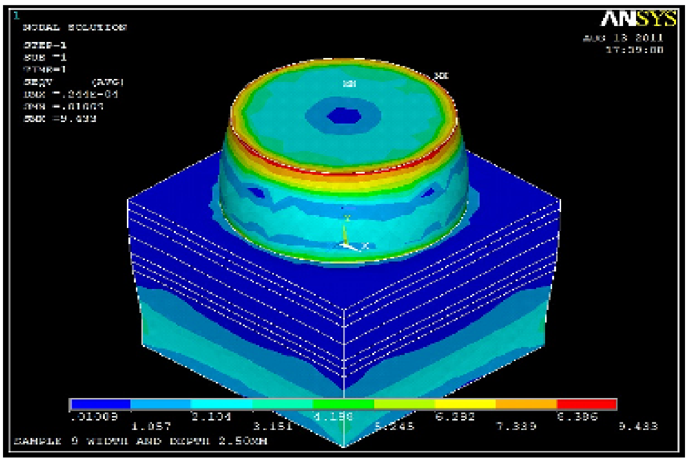

Figure 4.131: Von Mises Stress Distribution Plot for Pick 3 (830^{0}C)

The sample 9 is analyzed from initial brazing temperature 900^0C to room temperature. At pick 1, the sapphire layer has the highest stress distribution of 2469 to 2777 MPa which is higher than the yield strength of sapphire. Also, there is stress from sapphire to the filler of 1854 to 2161 MPa which is higher than the yield strength of sapphire. At the layer of Inconel 600, there is stress of 2161 to 2469 MPa which is higher than the yield strength of Inconel 600. At pick 3, the sapphire layer has the highest stress distribution of 21.951 to 24.689 MPa which is less or about the yield strength of sapphire. Also, there is stress from sapphire to the filler of 13.739 to 16.476 MPa which is less than the yield strength of sapphire. At the layer of Inconel 600, there is also a stress of 13.739 to 16.476 MPa at the edge which is less than the yield strength of Inconel 600. At pick 4, the sapphire layer has the highest stress distribution of 106.158 to 119.386 MPa which is less than the yield strength of sapphire. Also, there is stress from sapphire to the filler of 92.931 to 106.158 MPa which is less than the yield strength of sapphire. At the layer of Inconel 600, there is also a stress of 106.158 to 119.386 MPa at the edge which is less than the yield strength of Inconel 600.

The sample 9 is then analyzed from initial brazing temperature 865^0C to room temperature. At pick 1, the sapphire layer has the highest stress distribution of 2366 to 2661 MPa which is higher than the yield strength of sapphire. Also, there is stress from sapphire to the filler of 1776 to 2071 MPa which is higher than the yield strength of sapphire. At the layer of Inconel 600, there is stress of 2071 to 2366 MPa which is higher than the yield strength of Inconel 600. At pick 3, the sapphire layer has the highest stress distribution of 15.143 to 17.032 MPa which is less than the yield strength of sapphire. Also, there is stress from sapphire to the filler of 9.476 to 11.365 MPa which is less than the yield strength of sapphire. At the layer of Inconel 600, there is also a stress of 5.698 to 7.587 MPa at the edge which is less than the yield strength of Inconel 600. At pick 4, the sapphire layer has the highest stress distribution of 107.944

to 121.394 MPa which is less than the yield strength of sapphire. Also, there is stress from sapphire to the filler of 94.494 to 107.944 MPa which is less than the yield strength of sapphire. At the layer of Inconel 600, there is also a stress of 107.944 to 121.394 MPa at the edge which is less than the yield strength of Inconel 600.

The sample 9 is then analyzed from initial brazing temperature 830^0C to room temperature. At pick 1, the sapphire layer has the highest stress distribution of 2262 to 2544 MPa which is higher than the yield strength of sapphire. Also, there is stress from sapphire to the filler of 1698 to 1980 MPa which is higher than the yield strength of sapphire. At the layer of Inconel 600, there is stress of 1980 to 2262 MPa which is higher than the yield strength of Inconel 600. At pick 2, the sapphire layer has the highest stress distribution of 460.979 to 518.426 MPa which is less than the yield strength of sapphire. Also, there is stress from sapphire to the filler of 346.083 to 423.531 MPa which is less than the yield strength of sapphire. At the layer of Inconel 600, there is also a stress of 403.531 to 460.979 MPa at the edge which is less than the yield strength of Inconel 600. At pick 3, the sapphire layer has the highest stress distribution of 8.386 to 9.433 MPa which is less than the yield strength of sapphire. Also, there is stress from sapphire to the filler of 6.292 to 7.339 MPa which is less than the yield strength of sapphire. At the layer of Inconel 600, there is also a stress of 1.057 to 2.104 MPa at the edge which is less than the yield strength of Inconel 600.

Therefore, the sample 9 with initial brazing temperature 830^0C as the stress obtained is less than the yield strength of sapphire and also the lowest compared to the other stress distribution of 865^0C and 900^0C.

4.12 SAMPLE 10

(a) 900^0C

It must be taken into consideration that pick 1 and 3 are the properties of temperatures between the brazing temperature of 900^0C to room temperature, 27^0C. On the other hand, pick 4 displays the properties at room temperature, 27^0C.

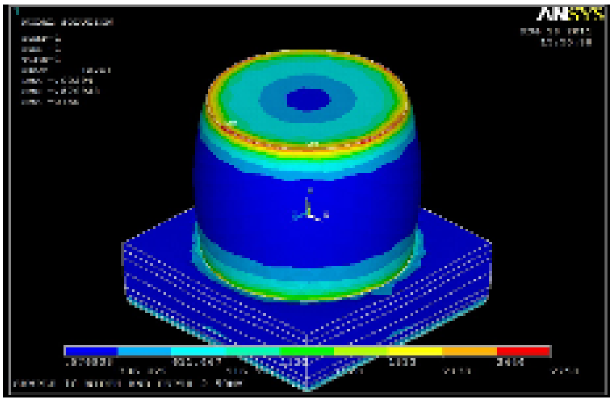

Figure 4.132: Von Mises Stress Distribution Plot for Pick 1 (900^0C)

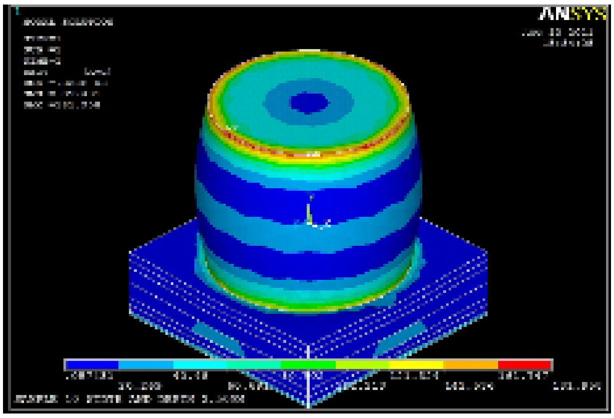

Figure 4.133: Von Mises Stress Distribution Plot for Pick 3 (900^0C)

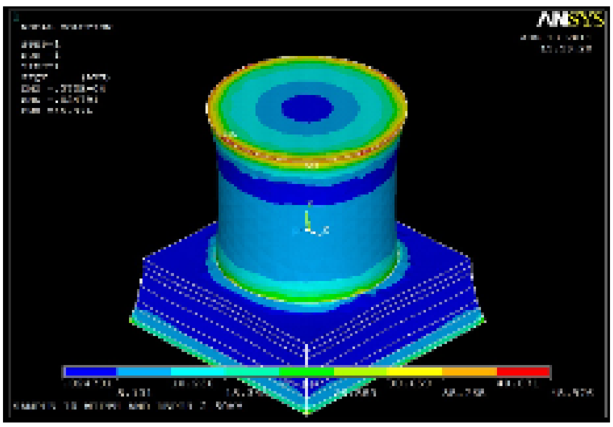

Figure 4.134: Von Mises Stress Distribution Plot for Pick 4 (900^0C)

(b) 865^0C

It must be taken into consideration that pick 1 and 3 are the properties of temperatures between the brazing temperature of 865^0C to room temperature, 27^0C. On the other hand, pick 4 displays the properties at room temperature, 27^0C.

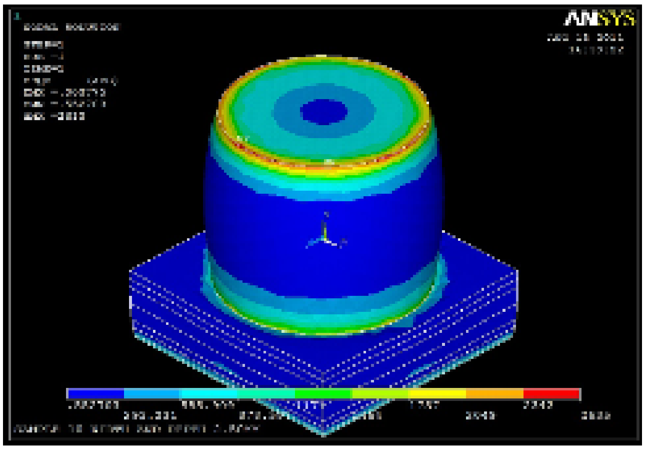

Figure 4.135: Von Mises Stress Distribution Plot for Pick 1 (865^0C)

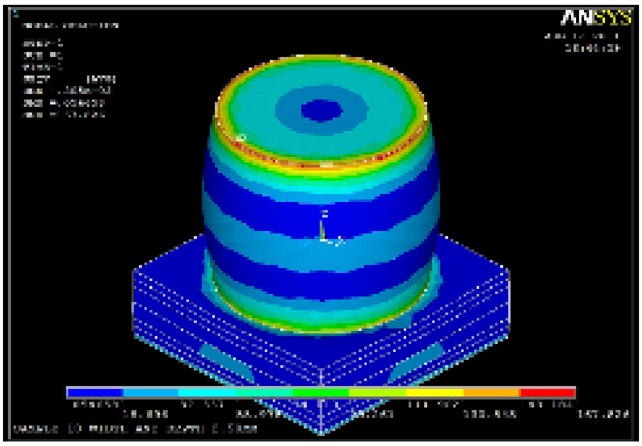

Figure 4.136: Von Mises Stress Distribution Plot for Pick 3 (865^0C)

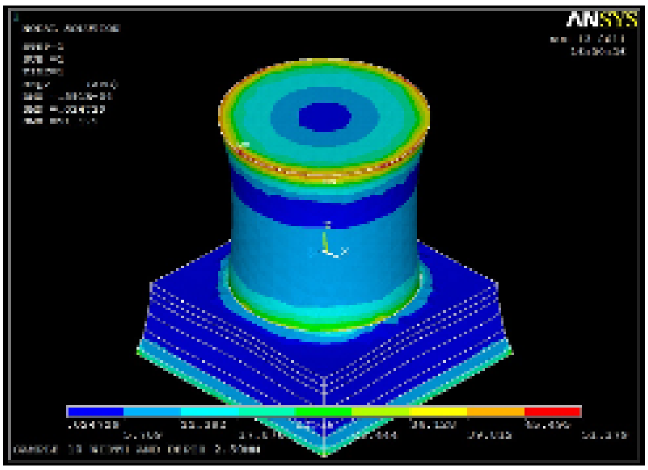

Figure 4.137: Von Mises Stress Distribution Plot for Pick 4 (865^0C)

(c) 830^{0}C

It must be taken into consideration that pick 1 and 3 are the properties of temperatures between the brazing temperature of 830^{0}C to room temperature, 27^{0}C. On the other hand, pick 4 displays the properties at room temperature, 27^{0}C.

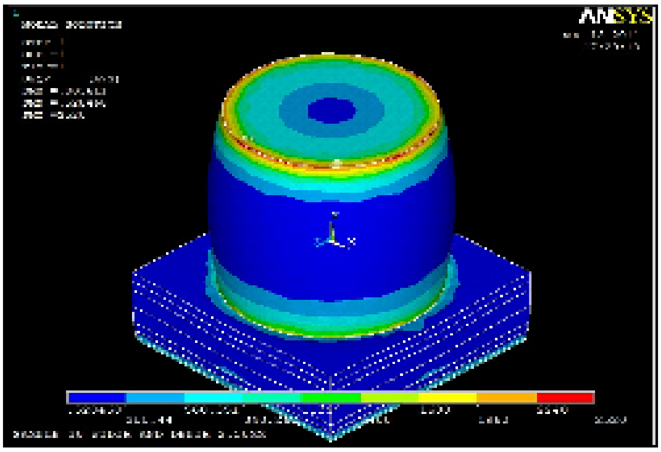

Figure 4.138: Von Mises Stress Distribution Plot for Pick 1 (830^{0}C)

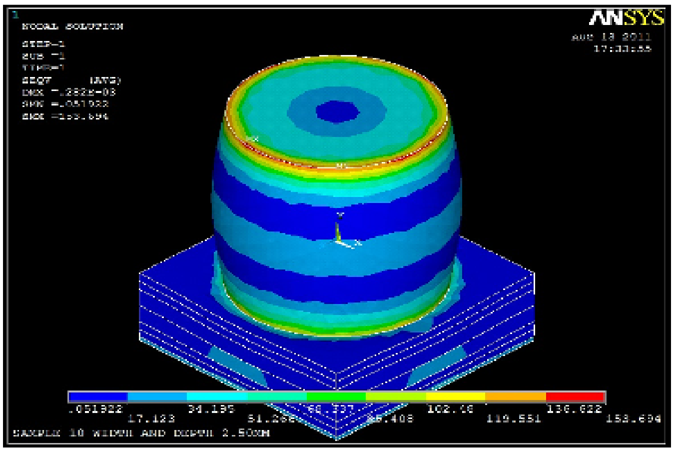

Figure 4.139: Von Mises Stress Distribution Plot for Pick 3 (830^{0}C)

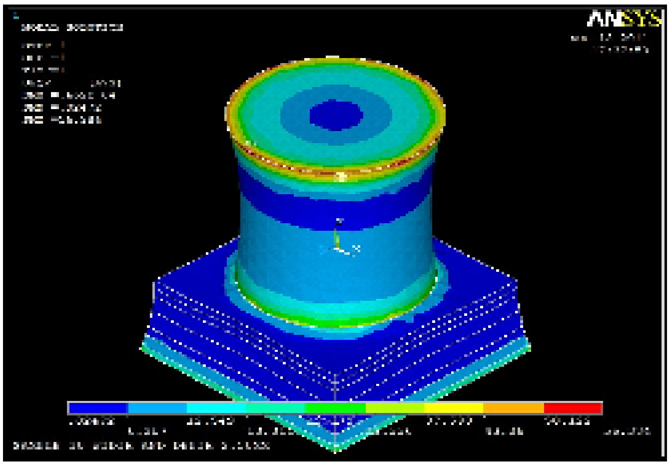

Figure 4.140: Von Mises Stress Distribution Plot for Pick 4 (830^{0}C)

The sample 10 is analyzed from initial brazing temperature 900^0C to room temperature. At pick 1, the sapphire layer has the highest stress distribution of 2444 to 2750 MPa which is higher than the yield strength of sapphire. Also, there is stress from sapphire to the filler of 1528 to 1833 MPa which is higher than the yield strength of sapphire. At the layer of Inconel 600, there is stress of 306.022 to 611.467 MPa which is higher than the yield strength of Inconel 600. At pick 3, the sapphire layer has the highest stress distribution of 161.747 to 181.958 MPa which is less or about the yield strength of sapphire. Also, there is stress from sapphire to the filler of 101.113 to 121.324 MPa which is less than the yield strength of sapphire. At the layer of Inconel 600, there is also a stress of 20.269 to 40.48 MPa at the edge which is less than the yield strength of Inconel 600. At pick 4, the sapphire layer has the highest stress distribution of 40.871 to 45.976 MPa which is less than the yield strength of sapphire. Also, there is stress from sapphire to the filler of 25.553 to 30.659 MPa which is less than the yield strength of sapphire. At the layer of Inconel 600, there is also a stress of 25.553 to 30.659 MPa at the edge which is less than the yield strength of Inconel 600.

The sample 10 is analyzed from initial brazing temperature 865^0C to room temperature. At pick 1, the sapphire layer has the highest stress distribution of 2342 to 2365 MPa which is higher than the yield strength of sapphire. Also, there is stress from sapphire to the filler of 1464 to 1757 MPa which is higher than the yield strength of sapphire. At the layer of Inconel 600, there is stress of 293.231 to 585.909 MPa which is higher than the yield strength of Inconel 600. At pick 3, the sapphire layer has the highest stress distribution of 149.184 to 167.826 MPa which is less than the yield strength of sapphire. Also, there is stress from sapphire to the filler of 93.261 to 111.902 MPa which is less than the yield strength of sapphire. At the layer of Inconel 600, there is also a stress of 18.696 to 37.337 MPa at the edge which is less than the yield strength of Inconel 600. At pick 4, the sapphire layer has the highest stress distribution of 45.495 to 51.179 MPa which is less than the yield strength of sapphire. Also, there is stress from sapphire to the filler of 34.128 to 39.182 MPa which is less than the yield strength of sapphire. At the layer of Inconel 600, there is also a stress of 28.444 to 34.128 MPa at the edge which is less than the yield strength of Inconel 600.

The sample 10 is analyzed from initial brazing temperature 830^0C to room temperature. At pick 1, the sapphire layer has the highest stress distribution of 2240 to 2520 MPa which is higher than the yield strength of sapphire. Also, there is stress from sapphire to the filler of 1400 to 1680 MPa which is higher than the yield strength of sapphire. At the layer of Inconel 600, there is stress of 280.44 to 560.351 MPa which is higher than the yield strength of Inconel 600. At pick 2, the sapphire layer has the highest stress distribution of 136.622 to 153.694 MPa which is less than the yield strength of sapphire. Also, there is stress from sapphire to the filler of 85.408 to 102.48 MPa which is less than the yield strength of sapphire. At the layer of Inconel 600, there is also a stress of 403.531 to 460.979 MPa at the edge which is less than the yield strength of Inconel 600. At pick 3, the sapphire layer has the highest stress distribution of 50.122 to 56.384 MPa which is less than the yield strength of sapphire. Also, there is stress from sapphire to the filler of 31.336 to 37.598 MPa which is less than the yield strength of sapphire. At the layer of Inconel 600, there is also a stress of 5.073 to 31.336 MPa at the edge which is less than the yield strength of Inconel 600.

Therefore, the sample 10 with initial brazing temperature 830^0C as the stress obtained is less than the yield strength of sapphire and also the lowest compared to the other stress distribution of 865^0C and 900^0C.

4.13 SAMPLE 11

(a) 900^0C

It must be taken into consideration that pick 1 and 3 are the properties of temperatures between the brazing temperature of 900^0C to room temperature, 27^0C. On the other hand, pick 4 displays the properties at room temperature, 27^0C.

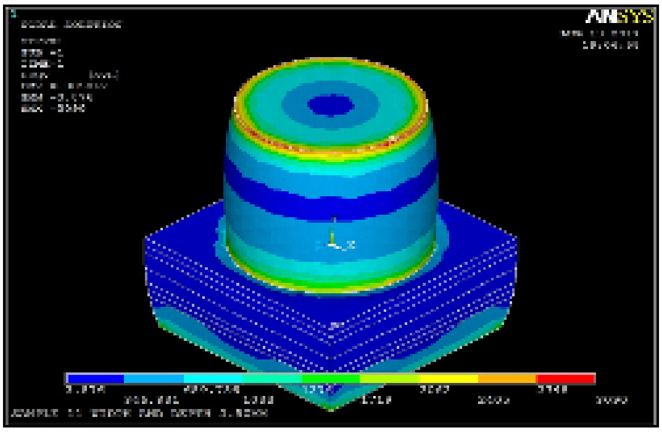

Figure 4.141: Von Mises Stress Distribution Plot for Pick 1 (900^0C)

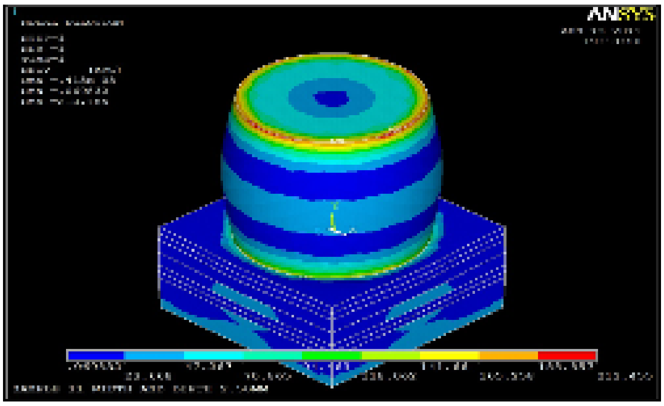

Figure 4.142: Von Mises Stress Distribution Plot for Pick 3 (900^0C)

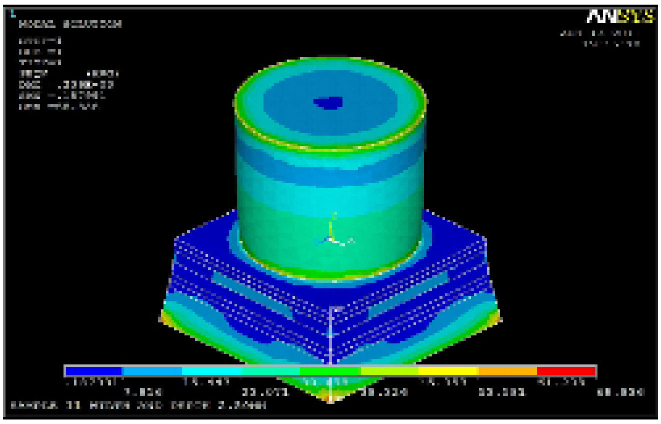

Figure 4.143: Von Mises Stress Distribution Plot for Pick 4 (900^0C)

(b) 865^{0}C

It must be taken into consideration that pick 1 and 3 are the properties of temperatures between the brazing temperature of 865^{0}C to room temperature, 27^{0}C. On the other hand, pick 4 displays the properties at room temperature, 27^{0}C.

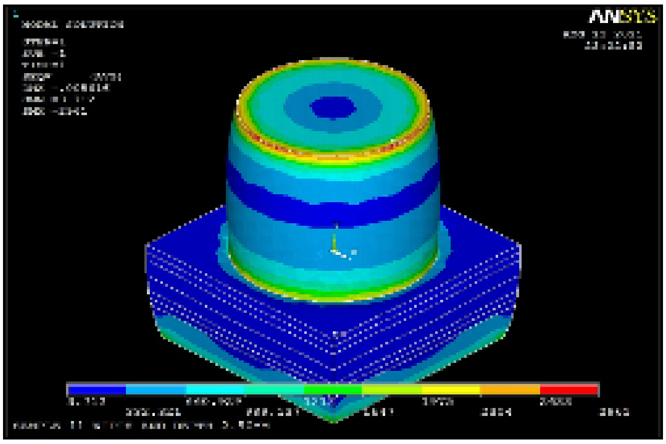

Figure 4.144: Von Mises Stress Distribution Plot for Pick 1 (865^{0}C)

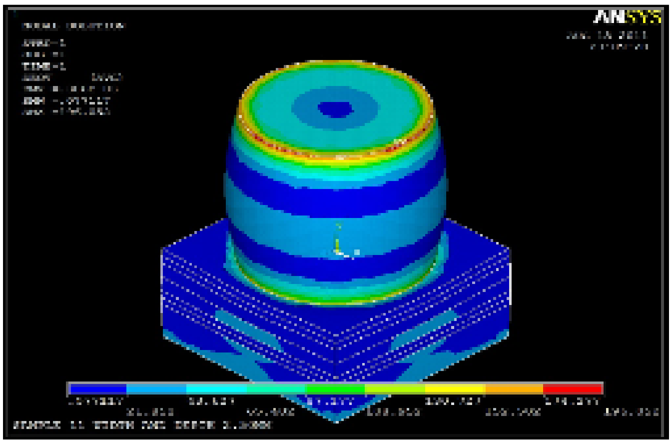

Figure 4.145: Von Mises Stress Distribution Plot for Pick 3 (865^{0}C)

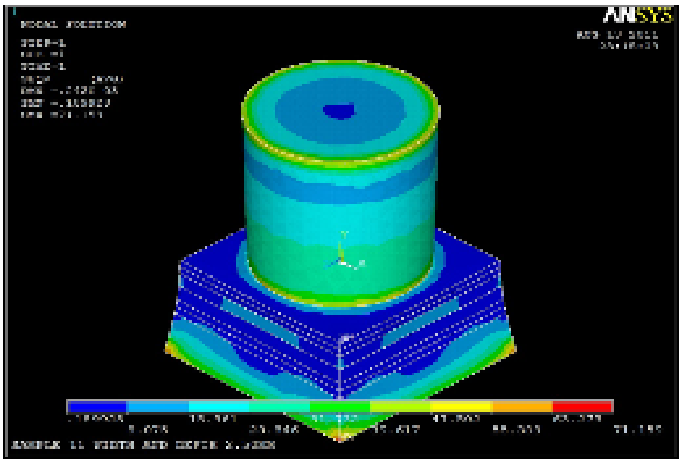

Figure 4.146: Von Mises Stress Distribution Plot for Pick 4 (865^{0}C)

(c) 830^0C

It must be taken into consideration that pick 1 and 3 are the properties of temperatures between the brazing temperature of 830^0C to room temperature, 27^0C. On the other hand, pick 4 displays the properties at room temperature, 27^0C.

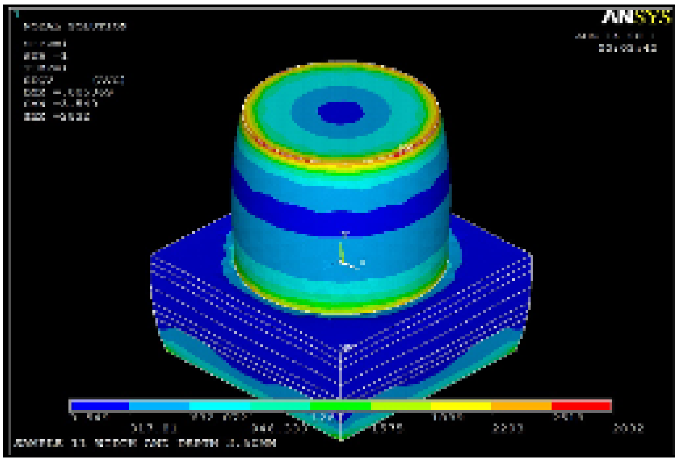

Figure 4.147: Von Mises Stress Distribution Plot for Pick 1 (830^0C)

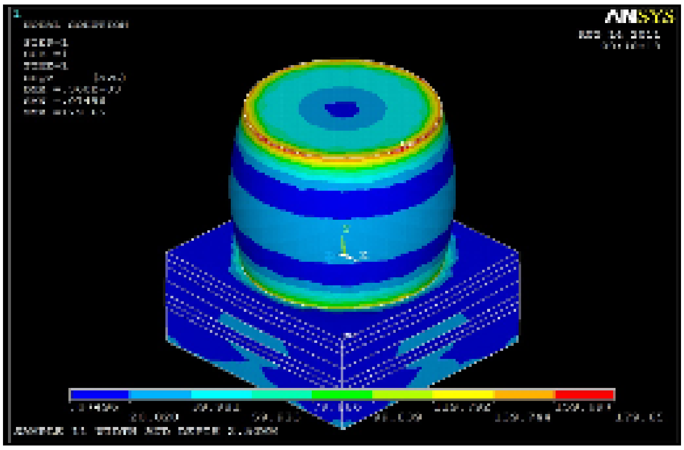

Figure 4.148: Von Mises Stress Distribution Plot for Pick 3 (830^0C)

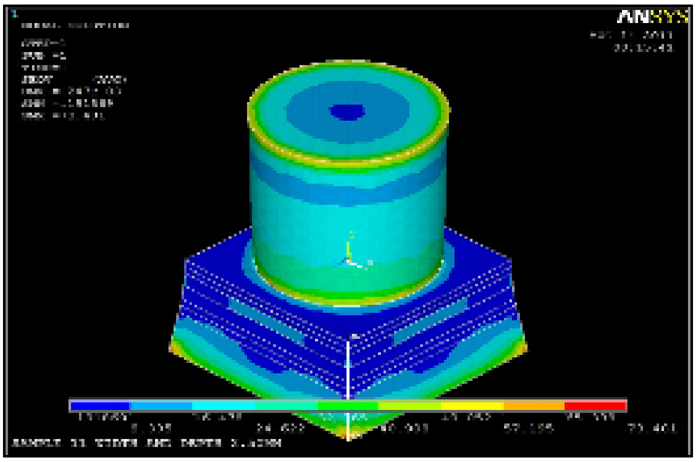

Figure 4.149: Von Mises Stress Distribution Plot for Pick 4 (830^0C)

The sample 11 is analyzed from initial brazing temperature 900^0C to room temperature. At pick 1, the sapphire layer has the highest stress distribution of 2444 to 2750 MPa which is higher than the yield strength of sapphire. Also, there is stress from sapphire to the filler of 1528 to 1833 MPa which is higher than the yield strength of sapphire. At the layer of Inconel 600, there is stress of 306.022 to 611.467 MPa which is higher than the yield strength of Inconel 600. At pick 3, the sapphire layer has the highest stress distribution of 161.747 to 181.958 MPa which is less or about the yield strength of sapphire. Also, there is stress from sapphire to the filler of 101.113 to 121.324 MPa which is less than the yield strength of sapphire. At the layer of Inconel 600, there is also a stress of 20.269 to 40.48 MPa at the edge which is less than the yield strength of Inconel 600. At pick 4, the sapphire layer has the highest stress distribution of 40.871 to 45.976 MPa which is less than the yield strength of sapphire. Also, there is stress from sapphire to the filler of 25.553 to 30.659 MPa which is less than the yield strength of sapphire. At the layer of Inconel 600, there is also a stress of 25.553 to 30.659 MPa at the edge which is less than the yield strength of Inconel 600.

The sample 11 is then analyzed from initial brazing temperature 865^0C to room temperature. At pick 1, the sapphire layer has the highest stress distribution of 2342 to 2365 MPa which is higher than the yield strength of sapphire. Also, there is stress from sapphire to the filler of 1464 to 1757 MPa which is higher than the yield strength of sapphire. At the layer of Inconel 600, there is stress of 293.231 to 585.909 MPa which is higher than the yield strength of Inconel 600. At pick 3, the sapphire layer has the highest stress distribution of 149.184 to 167.826 MPa which is less than the yield strength of sapphire. Also, there is stress from sapphire to the filler of 93.261 to 111.902 MPa which is less than the yield strength of sapphire. At the layer of Inconel 600, there is also a stress of 18.696 to 37.337 MPa at the edge which is less than the yield strength of Inconel 600. At pick 4, the sapphire layer has the highest stress distribution of 45.495

to 51.179 MPa which is less than the yield strength of sapphire. Also, there is stress from sapphire to the filler of 34.128 to 39.182 MPa which is less than the yield strength of sapphire. At the layer of Inconel 600, there is also a stress of 28.444 to 34.128 MPa at the edge which is less than the yield strength of Inconel 600.

The sample 11 is then analyzed from initial brazing temperature 830^0C to room temperature. At pick 1, the sapphire layer has the highest stress distribution of 2240 to 2520 MPa which is higher than the yield strength of sapphire. Also, there is stress from sapphire to the filler of 1400 to 1680 MPa which is higher than the yield strength of sapphire. At the layer of Inconel 600, there is stress of 280.44 to 560.351 MPa which is higher than the yield strength of Inconel 600. At pick 2, the sapphire layer has the highest stress distribution of 136.622 to 153.694 MPa which is less than the yield strength of sapphire. Also, there is stress from sapphire to the filler of 85.408 to 102.48 MPa which is less than the yield strength of sapphire. At the layer of Inconel 600, there is also a stress of 403.531 to 460.979 MPa at the edge which is less than the yield strength of Inconel 600. At pick 3, the sapphire layer has the highest stress distribution of 50.122 to 56.384 MPa which is less than the yield strength of sapphire. Also, there is stress from sapphire to the filler of 31.336 to 37.598 MPa which is less than the yield strength of sapphire. At the layer of Inconel 600, there is also a stress of 5.073 to 31.336 MPa at the edge which is less than the yield strength of Inconel 600.

Therefore, the sample 11 with initial brazing temperature 830^0C as the stress obtained is less than the yield strength of sapphire and also the lowest compared to the other stress distribution of 865^0C and 900^0C.

4.14 SAMPLE 12

(a) 900^0C

It must be taken into consideration that pick 1 and 3 are the properties of temperatures between the brazing temperature of 900^0C to room temperature, 27^0C. On the other hand, pick 4 displays the properties at room temperature, 27^0C.

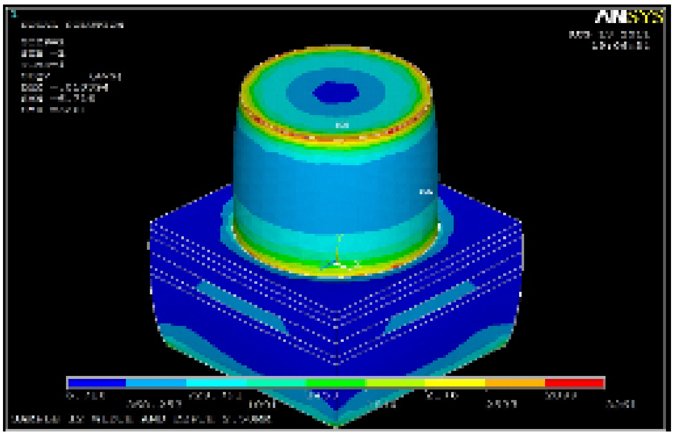

Figure 4.150: Von Mises Stress Distribution Plot for Pick 1 (900^0C)

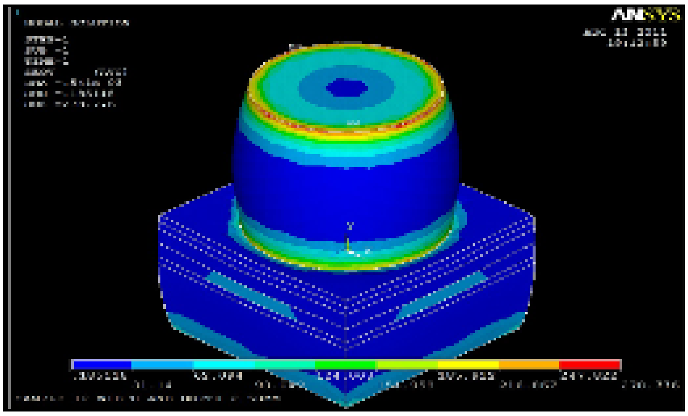

Figure 4.151: Von Mises Stress Distribution Plot for Pick 3 (900^0C)

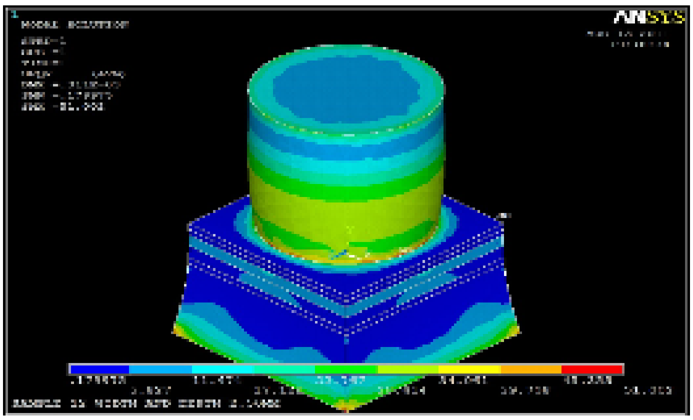

Figure 4.152: Von Mises Stress Distribution Plot for Pick 4 (900^0C)

(b) 865^0C

It must be taken into consideration that pick 1 and 3 are the properties of temperatures between the brazing temperature of 900^0C to room temperature, 27^0C. On the other hand, pick 4 displays the properties at room temperature, 27^0C.

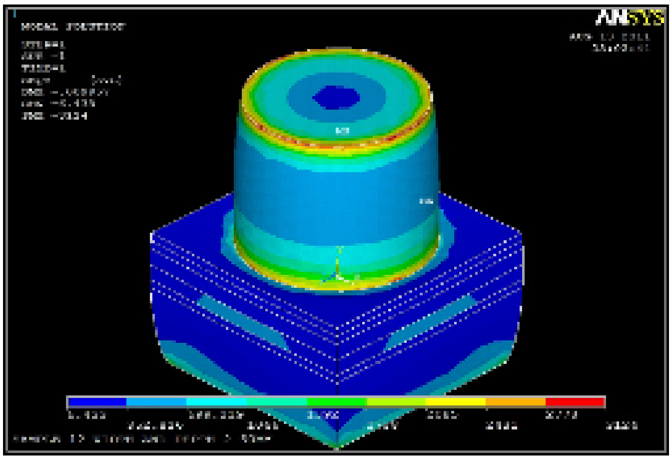

Figure 4.153: Von Mises Stress Distribution Plot for Pick 1 (865^0C)

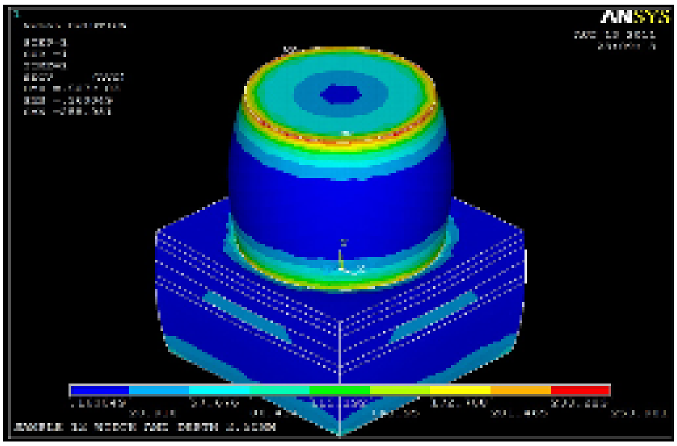

Figure 4.154: Von Mises Stress Distribution Plot for Pick 3 (865^0C)

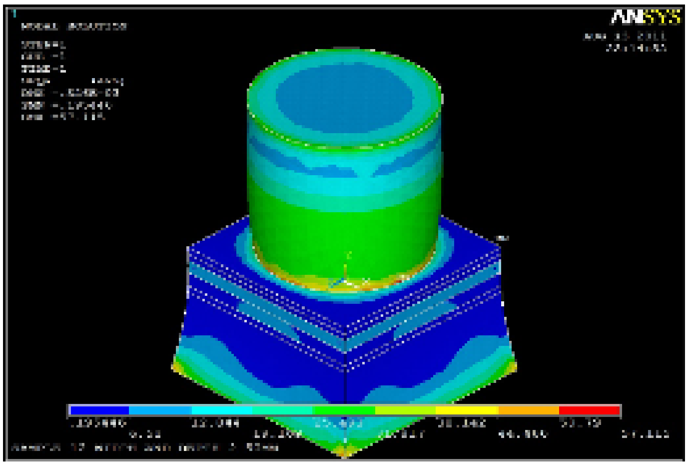

Figure 4.155: Von Mises Stress Distribution Plot for Pick 4 (865^0C)

(c) 830^0C

It must be taken into consideration that pick 1 and 3 are the properties of temperatures between the brazing temperature of 900^0C to room temperature, 27^0C. On the other hand, pick 4 displays the properties at room temperature, 27^0C.

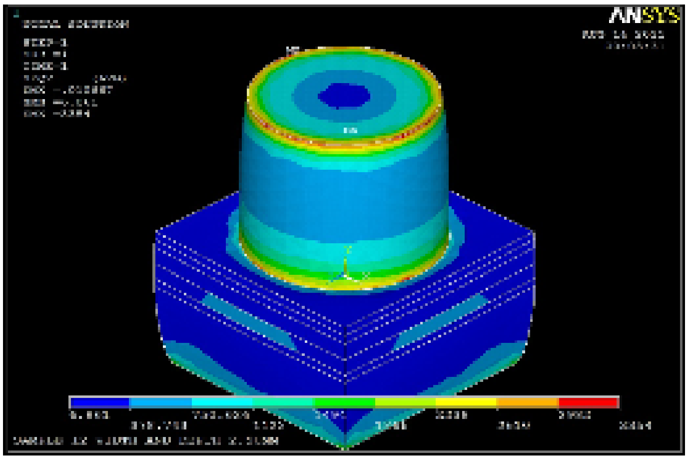

Figure 4.156: Von Mises Stress Distribution Plot for Pick 1 (830^0C)

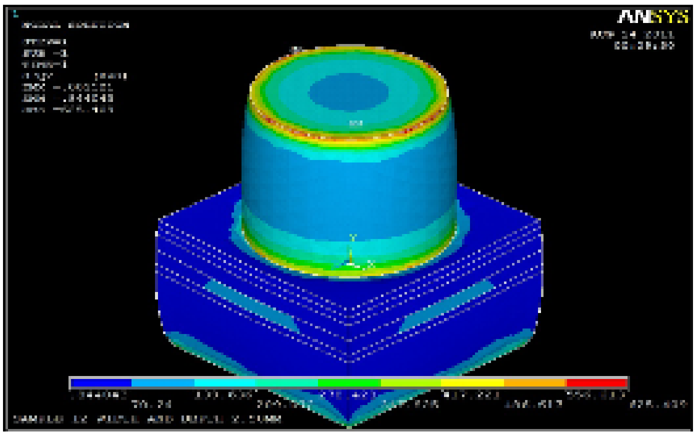

Figure 4.157: Von Mises Stress Distribution Plot for Pick 3 (830^0C)

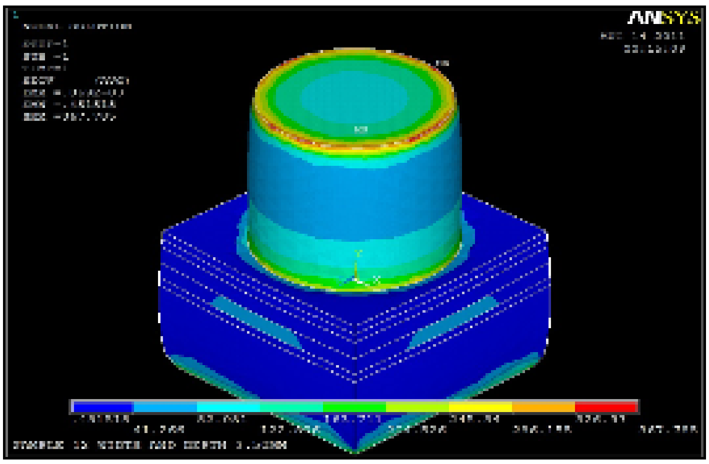

Figure 4.158: Von Mises Stress Distribution Plot for Pick 4 (830^0C)

The sample 12 is analyzed from initial brazing temperature 900^0C to room temperature. At pick 1, the sapphire layer has the highest stress distribution of 2444 to 2750 MPa which is higher than the yield strength of sapphire. Also, there is stress from sapphire to the filler of 1528 to 1833 MPa which is higher than the yield strength of sapphire. At the layer of Inconel 600, there is stress of 306.022 to 611.467 MPa which is higher than the yield strength of Inconel 600. At pick 3, the sapphire layer has the highest stress distribution of 161.747 to 181.958 MPa which is less or about the yield strength of sapphire. Also, there is stress from sapphire to the filler of 101.113 to 121.324 MPa which is less than the yield strength of sapphire. At the layer of Inconel 600, there is also a stress of 20.269 to 40.48 MPa at the edge which is less than the yield strength of Inconel 600. At pick 4, the sapphire layer has the highest stress distribution of 40.871 to 45.976 MPa which is less than the yield strength of sapphire. Also, there is stress from sapphire to the filler of 25.553 to 30.659 MPa which is less than the yield strength of sapphire. At the layer of Inconel 600, there is also a stress of 25.553 to 30.659 MPa at the edge which is less than the yield strength of Inconel 600.

The sample 12 is then analyzed from initial brazing temperature 865^0C to room temperature. At pick 1, the sapphire layer has the highest stress distribution of 2342 to 2365 MPa which is higher than the yield strength of sapphire. Also, there is stress from sapphire to the filler of 1464 to 1757 MPa which is higher than the yield strength of sapphire. At the layer of Inconel 600, there is stress of 293.231 to 585.909 MPa which is higher than the yield strength of Inconel 600. At pick 3, the sapphire layer has the highest stress distribution of 149.184 to 167.826 MPa which is less than the yield strength of sapphire. Also, there is stress from sapphire to the filler of 93.261 to 111.902 MPa which is less than the yield strength of sapphire. At the layer of Inconel 600, there is also a stress of 18.696 to 37.337 MPa at the edge which is less than the yield strength of Inconel 600. At pick 4, the sapphire layer has the highest stress distribution of 45.495

to 51.179 MPa which is less than the yield strength of sapphire. Also, there is stress from sapphire to the filler of 34.128 to 39.182 MPa which is less than the yield strength of sapphire. At the layer of Inconel 600, there is also a stress of 28.444 to 34.128 MPa at the edge which is less than the yield strength of Inconel 600.

The sample 12 is then analyzed from initial brazing temperature 830^0C to room temperature. At pick 1, the sapphire layer has the highest stress distribution of 2240 to 2520 MPa which is higher than the yield strength of sapphire. Also, there is stress from sapphire to the filler of 1400 to 1680 MPa which is higher than the yield strength of sapphire. At the layer of Inconel 600, there is stress of 280.44 to 560.351 MPa which is higher than the yield strength of Inconel 600. At pick 2, the sapphire layer has the highest stress distribution of 136.622 to 153.694 MPa which is less than the yield strength of sapphire. Also, there is stress from sapphire to the filler of 85.408 to 102.48 MPa which is less than the yield strength of sapphire. At the layer of Inconel 600, there is also a stress of 403.531 to 460.979 MPa at the edge which is less than the yield strength of Inconel 600. At pick 3, the sapphire layer has the highest stress distribution of 50.122 to 56.384 MPa which is less than the yield strength of sapphire. Also, there is stress from sapphire to the filler of 31.336 to 37.598 MPa which is less than the yield strength of sapphire. At the layer of Inconel 600, there is also a stress of 5.073 to 31.336 MPa at the edge which is less than the yield strength of Inconel 600.

Therefore, the sample 12 with initial brazing temperature 830^0C as the stress obtained is less than the yield strength of sapphire and also the lowest compared to the other stress distribution of 865^0C and 900^0C.

4.15 COMPARISON OF SAMPLES

All the Von Mises stress of all the samples (from sample 1 to sample 12) are tabulated in Table 4.1. From the simulated Von Mises stress, the stresses are checked and compared with the yield strength of each of the type of material. In this research project, the stress at the last pick usually is selected to be checked and compared with the yield strength of each type of material. If the stress is exceeding the yield strength of the particular material, this means that there is residual stress occurred. Nevertheless, in this simulation research project, all the stresses at the last pick are less than the yield strength of the material used. Therefore, in order to make a conclusion on the best parameter for the experimental project so that there is the least residual stress produced, the lesser the stress at the last pick, the lesser the residual stress is.

From Table 4.1, the stresses are compared for every sample for three different brazing temperatures. The least stress is then selected for each of the sample. The results are then tabulated in Table 4.2.

Table 4.1: The Von Mises Stresses for every Sample of Different Brazing Temperatures

Sample No	1	2	3	4	5	6	7	8	9	10	11	12
At 900^{0}C												
Stress at Pick 1 (MPa)	1004 - 1129	1646 – 1852	2462 – 2769	252.306 – 283.758	1657 – 1863	2394 – 2693	1284 – 1445	1875 – 2109	2469 – 2777	2444 – 2750	2748 - 3090	2899 - 3261
Stress at Pick 2 (MPa)	96.612 - 108.684	203.602 – 229.009	8.994 – 10.116	13.561- 15.254	153.173 – 172.279	437.044 – 491.514	126.981 – 142.847	254.02 – 285.727	21.951 – 24.689	161.747 – 181.958	188.857 – 212.455	247.822 – 278.776
Stress at Pick 3 (MPa)	28.916 - 32.325	44.341 – 49.867	113.913 – 128.114	9.596 – 10.792	56.734 – 63.807	8.381 – 9.428	36.253 – 40.782	43.242 - 48.631	106.158 – 119.386	40.871 – 45.976	45.952 – 54.581	17.121 – 22.767
At 865^{0}C												
Stress at Pick 1 (MPa)	961.717 - 1082	1577 - 1774	2359 - 2653	820.54 – 923.058	1587 - 1785	2294 - 2580	1231 - 1385	1796 - 2021	2366 - 2661	2342 - 2635	2633 - 2961	2778 - 3124
Stress at Pick 2 (MPa)	90.756 – 102.097	191.899 – 215.846	471.794 – 530.61	27.073 – 30.455	143.45 - 161.342	414.005 – 465.603	119.332 – 134.242	239.792 - 269.723	15.143 – 17.032	149.184 – 167.826	174.277 – 196.052	230.223 – 258.980
Stress at Pick 3 (MPa)	29.775 – 33.491	45.934 – 51.658	3.991 – 4.49	35.97 – 40.464	58.106 – 65.35	13.71 – 15.421	37.405 – 42.078	44.892 – 50.487	107.944 – 121.394	45.495 – 51.179	47.502 – 55.388	25.493 – 31.817
At 830^{0}C												
Stress at Pick 1 (MPa)	919.736 - 1035	1508 - 1696	2256 - 2537	784.664 – 882.7	1517 - 1707	2193 - 2467	1177 - 1324	1718 - 1932	2262 - 2544	2240 – 2520	2518 – 2832	2982 - 3354
Stress at Pick 2 (MPa)	84.9 - 95.509	180.196 – 202.682	446.028 – 501.632	24.211 - 27.235	133.726 - 150.406	390.966 – 439.693	111.683 – 125.638	225.563 – 253.719	460.779 – 518.426	136.622 – 152.694	159.697 – 179.65	556.013 – 625.429
Stress at Pick 3 (MPa)	30.634 – 34.458	47.528 – 53.452	6.797 – 7.767	36.211 – 40.734	59.477 – 66.893	19.101 - 21.484	38.558 – 43.375	46.543 – 52.343	8.386 – 9.433	50.122 - 56.384	49.052 – 57.195	326.97 - 367.785

Table 4.2: Comparison Sample by Sample

Sample No	1	2	3	4	5	6	7	8	9	10	11	12
Brazing Temperature (^0C)	900	900	865	900	900	900	900	900	830	900	900	900
Stress at Pick 1 (MPa)	1004 - 1129	1646 – 1852	2359 - 2653	252.306 – 283.758	1657 – 1863	2394 – 2693	1284 – 1445	1875 – 2109	2262 - 2544	2444 – 2750	2748 - 3090	2899 - 3261
Stress at Pick 2 (MPa)	96.612 - 108.684	203.602 – 229.009	471.794 – 530.61	13.561- 15.254	153.173 – 172.279	437.044 – 491.514	126.981 – 142.847	254.02 – 285.727	460.779 – 518.426	161.747 – 181.958	188.857 – 212.455	247.822 – 278.776
Stress at Pick 3 (MPa)	28.916 - 32.325	44.341 – 49.867	3.991 – 4.49	9.596 – 10.792	56.734 – 63.807	8.381 – 9.428	36.253 – 40.782	43.242 - 48.631	8.386 – 9.433	40.871 – 45.976	45.952 – 54.581	17.121 – 22.767

Then, if the samples are compared for every brazing temperature, the results are tabulated in Table 4.3.

Table 4.3: Comparison by Brazing Temperature

Brazing Temperature (^{0}C)	**900**	**865**	**830**
Sample No	**6**	**3**	**3**
Stress at Pick 1 (MPa)	2394 – 2693	2359 - 2653	2256 - 2537
Stress at Pick 2 (MPa)	437.044 – 491.514	471.794 – 530.61	446.028 – 501.632
Stress at Pick 3 (MPa)	8.381 – 9.428	3.991 – 4.49	6.797 – 7.767

Subsequently, if the samples are compared by the same thickness of Inconel 600, the stress results are tabulated in Table 4.4, 4.5 and 4.6. From Table 4.4, the optimum sample will be sample 4 at 900^{0}C. As from Table 4.5, the optimum sample will be sample 8 at 900^{0}C. As from Table 4.6, the optimum sample will be sample 3 at 865^{0}C.

Table 4.4: Comparison by Sample 1, 4, 7 and 10

Sample No	**1**	**4**	**7**	**10**
Brazing Temperature (^{0}C)	900	900	900	900
Stress at Pick 1 (MPa)	1004 - 1129	252.306 – 283.758	1284 – 1445	2444 – 2750
Stress at Pick 2 (MPa)	96.612 - 108.684	13.561- 15.254	126.981 – 142.847	161.747 – 181.958
Stress at Pick 3 (MPa)	28.916 - 32.325	9.596 – 10.792	36.253 – 40.782	40.871 – 45.976

Table 4.5: Comparison by Sample 2, 5, 8 and 11

Sample No	2	5	8	11
Brazing Temperature (^{0}C)	900	900	900	900
Stress at Pick 1 (MPa)	1646 – 1852	1657 – 1863	1875 – 2109	2748 - 3090
Stress at Pick 2 (MPa)	203.602 – 229.009	153.173 – 172.279	254.02 – 285.727	188.857 – 212.455
Stress at Pick 3 (MPa)	44.341 – 49.867	56.734 – 63.807	43.242 - 48.631	45.952 – 54.581

Table 4.6: Comparison by Sample 3, 6, 9 and 12

Sample No	3	6	9	12
Brazing Temperature (^{0}C)	865	900	830	900
Stress at Pick 1 (MPa)	2359 - 2653	2394 – 2693	2262 - 2544	2899 - 3261
Stress at Pick 2 (MPa)	471.794 – 530.61	437.044 – 491.514	460.779 – 518.426	247.822 – 278.776
Stress at Pick 3 (MPa)	3.991 – 4.49	8.381 – 9.428	8.386 – 9.433	17.121 – 22.767

From Table 4.4, 4.5 and 4.6, the best and optimum sample from each group is selected and the results are tabulated in Table 4.7. The best and optimum sample is sample 3 at 865^{0}C.

Table 4.7: Comparison of Sample 3, 4 and 8

Sample No	3	4	8
Brazing Temperature (^{0}C)	865	900	900
Stress at Pick 1 (MPa)	2359 - 2653	252.306 – 283.758	1875 – 2109
Stress at Pick 2 (MPa)	471.794 – 530.61	13.561- 15.254	254.02 – 285.727
Stress at Pick 3 (MPa)	3.991 – 4.49	9.596 – 10.792	43.242 - 48.631

Then, if the samples are compared by the same diameter and thickness of Inconel 600, the results are tabulated in Table 4.8, 4.9, 4.10 and 4.11.

Table 4.8: Comparison of Sample 1, 2 and 3

Sample No	**1**	**2**	**3**
Brazing Temperature (^0C)	900	900	865
Stress at Pick 1 (MPa)	1004 - 1129	1646 – 1852	2359 - 2653
Stress at Pick 2 (MPa)	96.612 - 108.684	203.602 – 229.009	471.794 – 530.61
Stress at Pick 3 (MPa)	28.916 - 32.325	44.341 – 49.867	3.991 – 4.49

Table 4.9: Comparison of Sample 4, 5 and 6

Sample No	**4**	**5**	**6**
Brazing Temperature (^0C)	900	900	900
Stress at Pick 1 (MPa)	252.306 – 283.758	1657 – 1863	2394 – 2693
Stress at Pick 2 (MPa)	13.561- 15.254	153.173 – 172.279	437.044 – 491.514
Stress at Pick 3 (MPa)	9.596 – 10.792	56.734 – 63.807	8.381 – 9.428

Table 4.10: Comparison of Sample 7, 8 and 9

Sample No	**7**	**8**	**9**
Brazing Temperature (^0C)	900	900	830
Stress at Pick 1 (MPa)	1284 – 1445	1875 – 2109	2262 - 2544
Stress at Pick 2 (MPa)	126.981 – 142.847	254.02 – 285.727	460.779 – 518.426
Stress at Pick 3 (MPa)	36.253 – 40.782	43.242 - 48.631	8.386 – 9.433

Table 4.11: Comparison of Sample 10, 11 and 12

Sample No	10	11	12
Brazing Temperature (^{0}C)	900	900	900
Stress at Pick 1 (MPa)	2444 – 2750	2748 - 3090	2899 - 3261
Stress at Pick 2 (MPa)	161.747 – 181.958	188.857 – 212.455	247.822 – 278.776
Stress at Pick 3 (MPa)	40.871 – 45.976	45.952 – 54.581	17.121 – 22.767

The best and optimum sample from Table 4.8, 4.9, 4.10 and 4.11 are then tabulated in Table 4.12.

Table 4.12: Comparison of Sample 3, 6, 9 and 12

Sample No	3	6	9	12
Brazing Temperature (^{0}C)	865	900	830	900
Stress at Pick 1 (MPa)	2359 - 2653	2394 – 2693	2262 - 2544	2899 - 3261
Stress at Pick 2 (MPa)	471.794 – 530.61	437.044 – 491.514	460.779 – 518.426	247.822 – 278.776
Stress at Pick 3 (MPa)	3.991 – 4.49	8.381 – 9.428	8.386 – 9.433	17.121 – 22.767

From Table 4.12, it has been clear that sample 3 with brazing temperature of 865^{0}C produce the least residual stress.

From all the comparisons, it is clear that sample 3 with brazing temperature 865^{0}C has the least residual stress compared to the other samples with different brazing temperatures.

CHAPTER 5

CONCLUSION AND RECOMMENDATIONS

5.1 CONCLUSION

From the simulation analysis results, it can be concluded that sample 3 with the brazing temperature of 865^0C. This is because it has very less stress at room temperature which is 3.991 – 4.49 MPa at the sapphire layer. Also, sample 3 exhibits a uniform heat distribution and heat conduction as this can be seen in the temperature nodal plot during the transient thermal analysis.

5.2 RECOMMENDATIONS

Based on this research project, there are a few suggestions that may improve the results as listed below:

- A cooling down to room temperature process should be visualized in another manner rather applying load and temperature constraint of 27^0C on top and bottom area of the sample model.
- The Von Mises stress should be simulated and studied for the heating process and also the brazing process.
- The deformation of the structure after brazing should be checked and studied.
- Comparison of simulation results should be make in order to confirm and validate the results

BIBLIOGRAPHY

Center, S. C. U. E. D. (2011). Residual Stress. from http://www.dc.engr.scu.edu

E-Lieberman. (1988). Modern Soldering and Brazing techniques. *Business News Publications*.

Flom, A. E. S. a. Y. A. (1997). Brazing of Titanium at Temperatures Below 8000C: Review and Prospective Applications. *Titanium-brazing*.

H. Matsumoto, T. S. a. N. A., KEK, National Laboratory (1996). Low Temperature Brazing technique for accelrators.

He, Y. M., Zhang, J., Sun, Y., & Liu, C. F. (2010). Microstructure and mechanical properties of the Si3N4/42CrMo steel joints brazed with Ag-Cu-Ti + Mo composite filler. [doi: 10.1016/j.jeurceramsoc.2010.07.005]. *Journal of the European Ceramic Society, 30*(15), 3245-3251.

Hwisouck Chang, S.-W. P., Sung-Churl Choi, and Tae-Woo Kim. (2002). Effects of Residual Stress on Fracture Stregth of Si3N4/Satinless Steel Joints With a Cu-Interlayer. *ASM International, 11*.

Kay, W. D. (2000). Ten Reasons to Choose Brazing. *Weld.J.*, 33-35.

Lay, L. (2006). Corrosion Resistance of Technical Ceramics. In Kagakubinran (Ed.).

LiYaJiang, W. J., Chen Maoai and Shen Xiaoqin. (2004). finite element analysis of residual stress in the welded zone of high strength steel. *Bull. Mater. Sci., 27*(2), 127-132.

Mandal, S., Ray, A. K., & Ray, A. K. (2004). Correlation between the mechanical properties and the microstructural behaviour of Al2O3-(Ag-Cu-Ti) brazed joints. [doi: 10.1016/j.msea.2004.06.002]. *Materials Science and Engineering A, 383*(2), 235-244.

P.Incropera, F., Dewitt, D. P., Dewitt, T. L., & Lavine, A. S. (2007). *Introduction to Heat Transfer*: John Wiley & Sons.

Pressure Sensors. (2011). Retrieved 2 May, 2011, from http://www.autoshop101.com/forms/h35.pdf

Ravikumar S. Kurhade, A. P. W. (2004). Finite Element Analysis of Effects of Strain Hardening Rate on Cold Expansion of Fastener Holes. *Ansys Confpaper*.

Schwartz, M. M. (2003). *Brazing* (Second ed.): ASM International The Materials Information Society.

Shigeo Kimura, M. N., Yamatake. (2006). Sapphire Capacitive Pressure Sensor. In Y. Properties (Ed.).

Song, X. G., Cao, J., Wang, Y. F., & Feng, J. C. (2011). Effect of Si3N4-particles addition in Ag-Cu-Ti filler alloy on Si3N4/TiAl brazed joint. [doi: 10.1016/j.msea.2011.03.032]. *Materials Science and Engineering: A, 528*(15), 5135-5140.

T.Shintake, K. K. a. (1996). Allignment issues for C-band Linear Collider. *EPAC*.

Xiong, J. H., Huang, J. H., Zhang, H., & Zhao, X. K. (2010). Brazing of carbon fiber reinforced SiC composite and TC4 using Ag-Cu-Ti active brazing alloy. [doi: 10.1016/j.msea.2009.09.024]. *Materials Science and Engineering: A, 527*(4-5), 1096-1101.

APPENDIX A

Table 1: Limiting Chemical Composition, % in Inconel 600

COMPOSITION	PERCENTAGE OF COMPOSITION (%)
Nickel (plus Cobalt)	72.0 min.
Chromium	14.0 – 17.0
Iron	6.00 – 10.00
Carbon	0.15 max.
Manganese	1.00 max.
Sulphur	0.015 max.
Silicon	0.50 max.
Copper	0.50 max.

(Source: Special Metals Corporation. 2008, Sept 08)

APPENDIX B

Sample of Interpolation Calculation in order to obtain the Thermal Conductivity, coefficient of thermal expansion (CTE) and specific heat capacity.

In this case of nickel material, the specific heat capacities (c_p) obtained are 594 J/kg.^{0}C and 562 J/kg.^{0}C at 927 ^{0}C and 727 ^{0}C respectively. This can be simplified as below:

$$c_p\,(Ni) = 562 \text{ J/kg.}^0\text{C at } 727^0\text{C}$$

$$= 594 \text{ J/kg.}^0\text{C at } 927^0\text{C}$$

The calculations are as below in order to obtain c_p for temperatures of 830^{0}C, 865^{0}C and 900^{0}C.

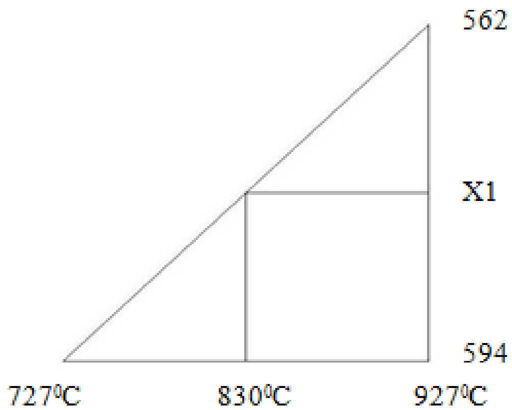

$$\frac{927 - 830}{927 - 727} = \frac{594 - X1}{594 - 562}$$

$$15.52 = 594 - X1$$

$$X1 = 578.48 \text{ J/kg.}^0\text{ C}$$

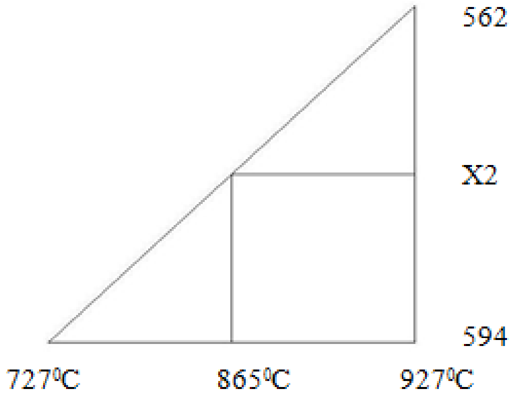

$$\frac{927-865}{927-727}=\frac{594-X2}{594-562}$$

$$9.92 = 594 - X2$$

$$X2 = 584.08\ \mathrm{J/kg.^0\ C}$$

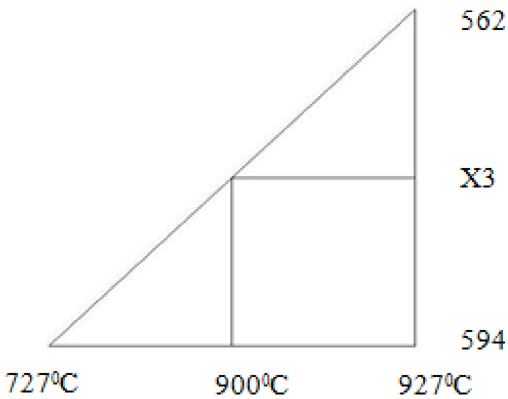

$$\frac{927-900}{927-727}=\frac{594-X3}{594-562}$$

$$4.32 = 594 - X3$$

$$X3 = 584.68\ \mathrm{J/kg.^0\ C}$$

From the calculations above, it can be concluded that the c_p of nickel at temperature of 830^0C, 865^0C and 900^0C:

$$c_p = 578.48\ J/kg.^0C\ (at\ 830^0C)$$

$$= 584.08\ J/kg.^0C\ (at\ 865^0C)$$

$$= 584.68\ J/kg.^0C\ (at\ 900^0C).$$

The same calculation method is used to calculate the thermal conductivity and coefficient of thermal expansion for different types of temperatures.